LONG-TERM PERFORMANCE OF GFRP REINFORCED CONCRETE BEAMS AND BARS SUBJECTED TO AGGRESSIVE ENVIRONMENTS

by

YEONHO PARK

Presented to the Faculty of the Graduate School of

The University of Texas at Arlington in Partial Fulfillment

of the Requirements

for the Degree of

DOCTOR OF PHILOSOPHY

THE UNIVERSITY OF TEXAS AT ARLINGTON

May 2012

ACKNOWLEDGEMENTS

I would like to express my deep gratitude to my advisors, Dr. Ali Abolmaali and Dr. Guillermo Ramirez, for their great commitment to my work and for their supports and cares both on professional and personal levels throughout my study at University of Texas at Arlington. Without their encouragements and great insight, I would not have been able to complete this dissertation. My sincere appreciation also goes to Dr. Shih-Ho Chao, Dr. John H. Matthys and Dr. Wen Chan of committee members for their valuable suggestion and interests.

And, thanks are due to my wonderful beloved wife Hyunjung (Amy) Lim, daughter Chaeyeon (Angela) and son Jaehoon (Alex) for their endless love, understanding and patience. Especially, my study has been possible with Hyunjung's endless love and her constant support. My mother Jungsook Lee and parents-in-laws Youngsoo Lim and Je-eun Yeon are thanked for their guidance, support and love. I sincerely appreciate my brothers Sungho Park and Jinho Park and my sister-in-law Hyunmin Lim for their unconditional love. Finally, I am highly appreciative of my father Dal-hwang Park in heaven.

March 30, 2012

ABSTRACT

LONG-TERM PERFORMANCE OF GFRP REINFORCED CONCRETE BEAMS AND BARS SUBJECTED TO AGGRESSIVE ENVIRONMENTS

Yeonho Park, Ph.D.

The University of Texas at Arlington, 2012

Supervising Professor: Ali Abolmaali

The use of fiber-reinforced polymer (FRP) bars in reinforced concrete (RC) structures has emerged as an alternative to traditional steel reinforcement environments and other applications where steel has shown greater vulnerability. Although the number of analytical and experimental studies on RC beams with FRP reinforcement has increased in recent decades, its long term performance is still questioned in comparison to the traditional steel reinforcement. That is, long-term performance is a much recognized but less-mentioned topic in the field of the reinforced concrete with glass-FRP (GFRP) re-bars. There is a need to validate long-term performance of FRP reinforced concrete structures, and accelerated testing can provide the data for this validation. In order to predict long-term behavior of reinforced concrete with GFRP bars (RC-GFRP), it is critical to determine the effects that long term exposure to the environment can have in degrading the composite materials.

This study presents the results and discussion of an experimental study concerning long-term behaviors of GFRP bars and concrete beams reinforced with GFRP bars after accelerated aging for 300days in an environmental chamber at 115°F(80% relative humidity). The change of

strength/stiffness properties of GFRP bars and concrete beams reinforced with GFRP as compared to steel bars were investigated in this study for various conditioning schemes with the application of sustained loads. Two types (Wrapped surface / Sand-coated surface) of GFRP were used. All beams were clamped in pairs using transverse steel rods at the beam end to simulate cracks typical of those produced by in service conditions. Prior to exposure in the chamber, beams were pre-cracked to simulate the level of cracking seen during service loads. Tensile strength retentions of GFRP bars were tested and considered as the indicator of durability performance. Accelerated aging procedure was conservatively calibrated with the natural weathering data to obtain real time weathering based on the Arrhenius method. Analytical analysis was also conducted to investigate the degradation of strength/stiffness. In addition, not only the change of bond strength between GFRP bars and concrete after aging, but also the durability performance concrete beams with GFRP and steel bars were investigated after exposure to specific accelerated aging conditions(115°F ,RH=80% and 3% saline solution). A non-destructive acoustic emission technique was conducted to assess long-term performances of GFRP bars embedded in real concrete and concrete beams (reinforced with GFRP and steel bars) subjected to temperature, humidity and exposure to saline solution of aging conditions. Both the experimental testing and signal-processing procedures were reported in detail. Various parameters were extracted from the AE received signals and analyzed.

In all cases, results showed not only that the strength and modulus of elasticity of GFRP and steel bars were reduced by the increase of exposure duration to cement-mortar paste at two different temperatures, but also the moment carrying capacities of RC-GFRP beams decreased and the deflections increased as a function of time when exposing in circumstances for accelerated aging. The effects of accelerated aging on the GFRP bars were not critical in terms of bond strength. The AE activity was found sensitive to duration of accelerated aging, type of reinforcement and reinforcement ratio. Acoustic emission technique could provide a useful verification of degradation level of concrete structures reinforced with GFRP and steel rods.

TABLE OF CONTENTS

LIST OF ILLUSTRATIONS

LIST OF TABLES

CHAPTER 1

INTRODUCTION

1.1 General

Numerous reinforced concrete structures are unlikely to reach their expected service life when they are exposed to aggressive environments such as severe climate and de-icing salts [ASCE Report card for America's infrastructure, 2009]. These conditions cause corrosion due to carbonation and/or chlorides. Corrosion is the principal cause of deterioration of conventional reinforced concrete structures. The cost of repairs and restoration in the USA, Canada and in the majority of the European countries constitute a high percentage of the expenditure of these countries on infrastructure. In Canada, it is estimated that more than 40% of all the bridges 40-years old or more and multistory parking garages are structurally deficient mainly due to corrosion caused by de-icing salts and severe climate [Benmokcane, 2005]. According to the ASCE infrastructure report, more than 40% of the 574,729 national bridges inspected are classified as structurally or functionally defective because of the corrosion of steel and the damage from freeze-thaw cycling in the US [Report card for America's infrastructure, 2009].

For many years, there have been many studies on this corrosion issue, and the interest in FRP (Fiber Reinforced Polymer) has arisen recently as a prospective substitute for steel. Careful consideration on potential of FRP rebar to fill the cost and performance needs may suggest appropriate solutions. To reduce corrosion of steel reinforcement, several techniques such as epoxy-coated bars and galvanized steel have been adopted. However, the new techniques have been needed in order to stop corrosion in spite of these efforts. This drawback

directed many researches to the development of new materials such as Fiber-Reinforced Polymer (FRP) for reinforcement. Many investigations carried out during the last two decades have demonstrated that FRP is one of the potential solutions to solve the problem regarding steel corrosion by a replacement of traditional steel re-bars. Especially Glass Fiber Reinforced Polymer (GFRP) has been used and accepted world-widely because of the low cost to performance benefits of glass fiber reinforced polymer. Therefore, the development of reinforced concrete with Glass Fiber Reinforced Polymer (GFRP) bars and their application in infrastructure is gaining considerable interests from the civil engineering field. The reinforced concrete with GFRP bars, designed to replace or supplement conventional reinforcing steel, also provides many advantages including outstanding strength and protection for corrosion under long-term performance exposed to temperature and humidity over time. The predominant advantage of utilizing GFRP reinforcing bars is to take corrosion resistance and durability of composite for steel replacement in concrete under long-term aging. Furthermore, codes and design guide provisions have been recently prepared for the use of FRP bars in concrete structures for bridges and buildings (ACI 440R 2006; CSA 2000; ISIS-Canada 2000).

However, long-term performance is a much recognized but less-mentioned topic in the field of reinforced concrete with GFRP re-bars. There is a need to validate long-term performance of FRP reinforced concrete structures. Accelerated testing can provide the data for this validation. In order to predict long-term behavior of reinforced concrete with GFRP bars (RC-GFRP), it is critical to determine the effects that long term exposure to the environment can have in degrading the composite materials.

1.2 Overview

1.2.1 Benefits of FRP

- Tensile strength greater than steel

- 1/4th weight of steel reinforcement
- Impervious to chloride ion and chemical attack
- Transparent to magnetic fields and radio frequencies
- Electrically and thermally non-conductive

Based on features above, FRP bars appear to be promising alternative to steel reinforcement in concrete structures such as marine structures, parking structures, bridge decks, highway under extreme environments, and structures highly susceptible to corrosion and magnetic fields.

1.2.2 Status

The earliest commercial uses of FRP composite rebar are approximately twenty-five years old. These original applications were for non-magnetic or radio-frequency transparent reinforcements for magnetic resonance imaging (MRI) medical equipment and specialized defense applications [Benmokcane, 2005]. Rebars of FRP composite have emerged as the industry standard for this application. The deteriorating state of the U.S. infrastructure, particularly vehicular highway bridges, caused alternative reinforcements to be considered as recently as the 1990s. Parallel interest in Europe and Japan has helped to make FRP composite rebar an international research topic. One of most important developments is the publication of ACI-440.3R-04. Published to support the ACI 440 design guides, it was understood that these test methods would transition to the more formal ASTM body. The document is available from ACI and provides the practicing engineering with the necessary information to implement these new FRP bars. This transitioning is now occurring and documents such as ASTM D7205 now describe test methods for determining tensile, modulus and strain properties of FRP bars. Several other test methods are also in the process of being printed in the ASTM consensus reviewed format. The Canadian Highway bridge design code of

CSA-S6-06 and Intelligent Sensing for Innovative Structures (ISIS) of the Canadian Network(Design manual No.3) now include provisions which allow for the use of GFRP rebar. Consequently, a number of bridges in Canada are being built on a more routine basis. The largest of these projects to date is the "Floodway Bridge" near Winnipeg. This is a significant bridge structure by any measure but more so due to fact that it was built using the "steel free deck" concept using all GFFRP bars in the concrete above the girders [Nkurunziza et al., 2005].

However, the cost of FRP rebar in $/ft is typically higher than conventional steel rebar yet. Carbon FRP is usually more expensive than GFRP. In general, the cost impact to use GFRP bars in a bridge deck is only raising the cost of the deck by something on the order of 2 to 5% these days. So, it may not be an expensive alternative to utilize GFRP bars and potentially gain many extra years of service life. The cost is $3 to $4/lb (including approx. $1/lb of raw material cost) in case of Glass FRP bar, and Carbon FRP is usually more expensive. (Epoxy coated rebar costs $0.32/lb)[http://www.c-bar.com and http://www.MDAcomposites.org]

1.2.3 Objective of experimental tests

Structural concrete systems reinforced with GFRP rods must have not only sufficient stiffness and strength but also physical and in-service characteristics required in the aggressive environments to resist loads applied to the structures. However, environmental effects including temperature, humidity and chemical solutions are often unavoidable in that these conditions affect the mechanical properties in various ways. The change of material property results in structural degradation of concrete members reinforced with GFRP. It is obvious that the greater the degradation of structures over time, the lower will be their load carrying capacity. However, flexibility of structural design is limited due to the lack of data regarding long-term performances on strength and stiffness of concrete members reinforced with GFRP rods.

This research is an experimental investigation providing data to predict a long-term behavior of concrete beams internally reinforced with GFRP bars. The test program will include

variables such as accelerated exposure time in the chamber, environmental factors of temperature and humidity, types of re-bars and reinforcement ratio. Correlation between natural and accelerated exposure time will be suggested in that the effect of exposure time will have a significant impact on stiffness and strength degradation of specimens. Based on the accelerated aging results, master plots are constructed by accounting for the applied sustained stress on bars. Scope of this research includes testing of 90 tension bars and 72 beams including the unconditioned/conditioned ones. The main objectives of this research are to establish the rate of degradation in strength and stiffness of concrete members reinforced with GFRP bars subjected to saline environment with stress and to evaluate the long-term behaviors of concrete members reinforced with GFRP bars internally.

To detect the source of degradation of specimens after exposure, the acoustic emission (AE) technique will be used along with direct tensile tests of reinforcing bars. Several nondestructive methods have recently been applied to evaluate damage qualifications of structural members. The AE technique, a nondestructive method that is relatively easy to install and is capable of predicting the damage location, is used in this study. Specifically, this study aims to develop an evaluation technique to determine the structural degradation of RC beams reinforced with FRP and steel bars. The AE technique is a method that analyzes the characteristics of elastic waves that are caused by microscopic damage in the concrete member. This technique has been used to assess microscopic damage that is internal to the concrete member and caused by various external loading conditions. AE behavior of concrete beams reinforced with GFRP bars under cyclic loads of various loading stage will be examined by laboratory experiments. The AE monitoring will be able to differentiate each AE source such as the change of AE hit rate, the time history of AE events, first /secondary peak and felicity ratio by applying cyclic loading. The analysis of these AE sources will provide valuable criteria for assessment of degradation of specimens.

1.3 Research significance

It is hard to obtain clear information to predict long-term behaviors of concrete beams reinforced with GFRP bars. The reasons are: (1) many test results were based on a FRP strand test itself as an individual material; (2) combined environmental exposure of temperature and humidity, in particular, were not conducted for the concrete structures internally reinforced with GFRP bars; (3) extensive tests were focused on FRP externally strengthened concrete structures; (4) these tests were based on few test results that were carried out on the early generations of GFRP bars. That means various types of GFRP bars have not been considered.

Therefore, overall objective of this research is to provide unique information by supplementing conditions used in previous investigations. Key features of the test plan include: (1) concrete beams internally reinforced with GFRP bars in terms of not an individual material but structural systems; (2) simultaneous exposures of temperature and humidity; (3) two types of GFRP bars in 72-specimens; (4) test duration of up to 25 years as accelerated aging test; (5) the employment of sustained bending loads during environmental conditionings; (6) comparison of GFRP to steel bars for both accelerated exposures and non-exposures. (7) AE response in association with fiber failure/debonding development and concrete cracking in concrete structures.

The significances of this research for reinforced concrete with internal GFRP bars can be summarized below

- Development of correlation between actual field exposures(natural exposure) and laboratory aging(accelerated aging)
- Test data over extended time period (more than 8-years) up to 25 years based on laboratory aging
- Testing under combined conditions (temperature, humidity and initial stress) at structural level

- Stiffness degradation after comparing with bench-mark models of steel or non-exposures
- Assessment of conservativeness regarding strength/environmental reduction factors adopting ACI 440-1R-06 by using probability methods
- Identifying the characteristics of AE response associated with fiber/matrix failure development in concrete structures.

1.4 Test procedure

Based on the assessment criteria of long-term performances of concrete beams reinforced with GFRP, a test protocol has been identified. A flow chart diagram of the test protocol is shown below in Figure1.1. Conditioning of samples is defined as the combination of environmental exposure and application of a constant sustained load. Each pre-conditioned specimen will be placed in a chamber for the accelerated exposure or an outdoor field for natural weathering. Combined weathering conditions will be introduced by the chamber. The temperature and humidity in the chamber will be increased to 115°F and RH 80%.

Specimens conditioning for prescribed duration will be removed from conditioning fixtures and tested to failure. These should be removed from the conditioning fixtures within two-day of the described time. Specimens will be observed for physical change in appearance and calibrated the crack width by a sustained load. Test should be performed within 24 hours after removal from the exposing fixture. Flexural strength of specimens for each exposure time will be normalized by using the values for non-exposed specimens at the same exposure duration. Also, these data will be used to reveal not only the correlation between the accelerated and real-time exposure but also the reduction effect of stiffness and strength caused by the accelerated environments. Real time field exposure data will be utilized to verify predictions of long-term behaviors by accelerated test.

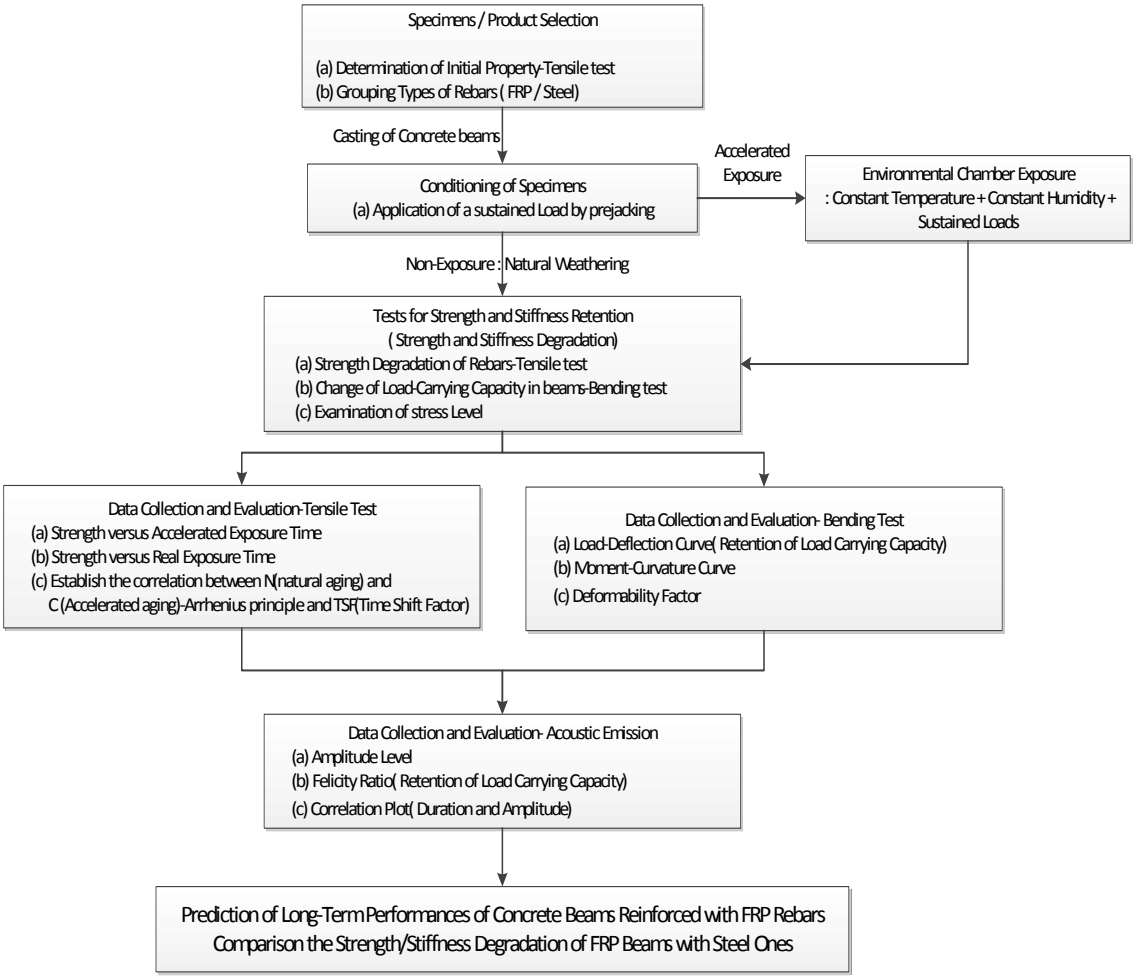

Figure 1.1 Test procedure for long-term behaviors of beams reinforced with GFRP bars

1.5 Organization of the dissertation

This work presents the details of a research. This dissertation is organized into the following sections.

- Chapter 1

  Reasons of emergence of FRP bars in civil engineering are introduced. Then, the research objectives, significances and organization of this dissertation are presented.

- Chapter 2

  The background of the materials aspects of GFRP and steel bars are introduced. Then, flexural design philosophy of GFRP bar reinforced concrete is presented based on the ACI-440-3R.

- Chapter 3

  The literature review related to GFRP bars, flexural design of GFRP bar reinforced concrete members, environmental reduction factors for the tensile strength of GFRP bars in the existing design codes/guidelines and acoustic emission techniques. The limitation of the existing approaches of durability design of GFRP bars is presented and discussed. The outline and contribution of this research are also discussed in this chapter.

- Chapter 4

  The degradation behaviors of GFRP bars subjected to different exposure conditions are investigated. Durability of stand-alone GFRP bars and GFRP bars embedded in cement-mortar paste are evaluated and compared. The critical effects for GFRP bars used as concrete internal reinforcement are identified. In addition, correlation between accelerated aging(C) and natural aging(N) is presented.

- Chapter 5

  Accelerated aging tests are studied on pre-cracked concrete beams conditioned to the environment chamber exposed to 80% relative humidity (RH), 115˚F of temperature and 0.5% salt solution for 100, 200 and 300 days similar to accelerated aging test on GFRP bars mentioned in Chapter 4. The change of load-carrying capacity and stiffness of testes 72-specimens are discussed.

- Chapter 6

  This chapter describes a comparative study of existing deformability models for concrete beams reinforced with GFRP or steel rods by different researchers in recent

years. An empirical modified deformability model has been developed to predict the full range response after accelerated aging.

- Chapter 7

  Characteristics of stiffness/strength degradation and damage propagation in concrete beams reinforced with GFRP and steel after accelerated aging are discussed by acoustic emission (AE) of nondestructive evaluation (NDE).

- Chapter 8

  Conclusions derived for the presented study are summarized in this chapter. In addition, recommendations for future research are also presented.

CHAPTER 2

BACKGROUND OF REINFORCING GFRP / STEEL REBARS

2.1 General

The topics addressed in this study are aimed toward improving the current knowledge for the application of FRP rods in reinforced concrete system as described in the introduction. FRP bars are composed of aligned fibers and resins. Although several types of fiber products such as carbon, aramid and glass are now available for field applications, glass fiber appears to be the most economical reinforcing material. When Glass Fiber Reinforced Polymer (GFRP) reinforcement is used as an internal reinforcement in concrete, tensile strength decreased as a function of time. This is a problem of “durability” under real-life weathering such as alkaline and deicing chemical exposure and mechanical stress cycles. Several studies characterized the parameters influencing the long-term characteristics of GFRP reinforcing bars assessed the mechanism and degree of degradation. In order to conduct accelerated tests for establishing durability of GFRP rods and understanding long-term performance of GFRP internally reinforced concrete members , GFRP bars placed in real concrete and environmental attack(temperature and moisture) are exposed to sustained load simultaneously. In this chapter, strength and stiffness degradation of GFRP bars subjected to environmental attack (physical and chemical aging) are discussed. Not only current knowledge on the durability of FRP bars is reviewed but also the accelerated aging test method and correlation between accelerated aging and real one are also discussed.

2.2 Material aspects of GFRP rods

FRP is a type of composite material. It is also referred to as a structural plastic and has been used in many structural applications such as bridges, tanks, pressure vessels, aircraft, and structures. It is also used for structural repair and strengthening. Composites are well known for having corrosion resistance, high strength-to-weight ratio, and on-site formability. As a result, structural plastics are widely used, especially in corrosive environments and aerospace engineering. FRP can give a wide range of structural properties depending on the types of materials, manufacturing processes, and fiber volume fractions.

2.2.1 Reinforcing fibers

Material stiffness, strengths and the load-carrying capacity are determined relatively easily in isotropic and homogeneous materials such as steel bars [Bank, Composites for construction, 2006]. Unlike steel, however, FRP bars are inhomogeneous and anisotropic materials in nature depending on factors such as fiber volume, type of resin, type of fiber, fiber orientation and quality control. The manufacturing process, the rate of curing and quality control during manufacturing can affect the mechanical characteristics of the bar [Wu, 1990]. Therefore, determination of mechanical material properties of FRP bars should be performed by tests to verifying the material data provided by the bar manufacturers.

The fiber phase of an FRP composite material consists of thousands of individual micrometer-diameter individual filaments. In the large majority of fiber forms used in FRP products for structural engineering, these fibers are indefinitely long and are called continuous. Continuous fibers are used at a relatively high volume percentage (from 20 to 60%) to reinforce the polymer resin: thus the term of fiber-reinforced polymer (FRP). Three fibers are generally used in structural systems such as the glass fiber (the E-glass fiber, the S-glass fiber and the Z-glass fiber), the aramid fiber (the aromatic polyamides, Kevlar 49 fiber) and the carbon fiber (the ultra high-modulus fiber, the high-modulus fiber and the high-strength fiber) [Bank ,2006]. The

fibers may be used separately or as a hybrid of two or three different fibers. Among the various types and mechanical properties of fiber, glass fiber will be discussed in this study.

Glass fiber is the main component in GFRP bars, and it carries the most tensile capacity of the composite bar [Huang, 2010]. Generally, the available glass fibers on the market are E-Glass (Electrical Resistance), S-Glass (High Strength), AR-Glass (Alkaline Resistance), ECR-Glass (Electrical Chemical Resistance). E-Glass fiber is probably the most widely used type of glass fiber due to its good mechanical performance and relatively low price. S-Glass fiber has extreme high tensile strength and stiffness. However, due to its high cost, the S-Glass is often used for special applications such as in the aerospace industry. The other two types of glass fiber, AR-Glass fiber and ECR-Glass fiber, are designed for certain special applications, like chemical exposure or harsh environmental conditions. [Gremel, Commercialization of Glass Fiber Reinforced Polymer (GFRP) Rebar, SEAOH Convention, 1999]. Typically, E-Glass fiber has widely been used because of economic advantage.

Table 2.1 Approximate properties of common grade of glass fiber

Glass designation	Type	Density	Tensile Strength	Tensile Modulus	Max. Elongation
		[g/cm3(lb/in3)]	[MPa (ksi)]	[GPa (ksi)]	%
E-glass	Standard conventional glass	2.57(0.093)	3400(493)	72.5(10.5)	2.5
A-glass	Alkali resistant glass	2.46(0.089)	2760(400)	73(10.6)	2.5
C-glass	Chemical resistant glass	2.46(0.089)	2350(340)	74(10.7)	2.5
S-glass	High strength glass	2.47(0.089)	4600(667)	88(12.8)	3

S-Glass leading to higher temperature performance and strength is three to four times more expensive than E-Glass [Vijay, 1999]. The diameter of an individual glass fiber or filament ranges from approximately 3 to 24 μm (0.00118 to 0.00945 in). The 17- μm (0.0067in) diameter finer is most commonly used for FRP products for structural engineering [Hollaway, 2010]. Approximate properties of common grade of glass fibers are given in Table.2.1.

2.2.2 Polymer resins

The term of polymer resin, or resin simply, is used in the composites industry to refer to the primary polymer ingredient in the non-fibrous part of the FRP material that binds the fibers together. This non-fibrous part is also known as the matrix or binder [Mallick, 1993]. When used in commercial and industrial products a polymer-based material is often known as a plastic and the acronym FRP is also often used to denote a fiber-reinforced plastic [Huang, 2010].

The matrix resin has three important roles; to transfer stress of fiber to other fiber, to bind fibers together and to protect fibers from environment. There are two kinds of polymeric matrices; thermoplastic and thermoset. Matrix materials for most infrastructure applications are thermosetting resins, primarily vinyl ester and polyester due to their reasonable costs [Huang, 2010]. Most composites under development for infrastructure application use E-glass fiber systems, though some use of S-glass, carbon, and aramid fiber is anticipated. Thermosetting polymers are usually made from liquid or semi-solid precursors which hardened irreversibly [Yan, 2005]. Thermoplastic matrices soften or melt upon heating. When the structure of these polymers is investigated, no apparent order among the chain molecules can be observed. They have very high viscosity at their processing temperatures [Mallick, 1993]. Thermoset resins are the most common resin systems used in infrastructure application because of their ease in process and low cost. Various kinds of thermoset-polymer resins have been widely used in structural engineering [Bank,2000]. The vinyl-esters, the epoxies and the polyesters are the thermosetting matrices which are utilized for composite structural members in the civil infrastructure. All are crossed linked. A wide range of amorphous and crystalline polymer materials (an amorphous and a crystalline polymer are those in which there is a random order of their atoms and those in which there is an orderly repeating pattern of their atoms, respectively) can be used to form fibers [Bank ,2006]. Among the various types and mechanical properties of resins, vinyl-esters resin will be discussed in this study. Approximate properties of thermosetting polymer resins are shown in Table.2.2.

Table 2.2 Approximate properties of thermosetting polymer resins (Huang, 2010)

Type	Density	Tensile Strength	Tensile Modulus	Max. Elongation
	[g/cm3(lb/in3)]	[MPa (ksi)]	[GPa (Msi)]	%
Polyester	1.2(0.043)	65(9.4)	4.0(0.58)	2.5
Epoxy	1.2(0.043)	90(13.1)	3.0(0.44)	8.0
Vinyl-ester	1.12(0.041)	82(11.9)	3.5(0.51)	6.0
Polyurethane	varies	71(10.3)	2.9(0.42)	5.9

Vinyl-esters resins have become attractive polymer resins for FRP products for structural engineering due to their good properties, especially their corrosion resistance and their ease of processing [Karbhari et al. 2003]. Today, vinyl-esters resins are used to make the majority of FRP rebars sold in the world and are also used widely in FRP pultruded profiles [Mallick, 1993]. They are generally replacing polyester resins in FRP products in structural engineering because of their superior environmental durability in alkaline environments. A vinyl-esters resin is a hybrid of an epoxy and an unsaturated polyester resin and is sometimes referred to as an epoxy vinyl-ester resin or a modified epoxy resin. Vinyl-esters resin can be filled and pigmented. They have densities from 1.05 to 1.10 g/cm^3 (0.038 to 0.042 lb/in^3) and glass transition temperatures from 40 to 120 °C (100 to 250 °F) [Leslie, 1986]

2.3 Manufacturing methods

Two main manufacturing methods are used to produce FRP composite materials products for use in structural engineering. The one method is an automated industrialized process, developed in the early 1950s, called pultrusion, in which the FRP products are produced in a factory and shipped to construction site for fabrication and installation or erection. The other method is a manual method, known as hand layup or wet layup, in which the FRP product is manufactured in situ at the construction site at the time it is installed [Bank, 2006]. It is original method used to produce fiber-reinforced polymer composites. However, the hand-

layup method as it is used in structural engineering is significantly different from that used in the rest of the composites industry.

Pultrusion is a continuous process of passing continuous fibers through a system [Lesko, 2003]. First, the fibers are soaked in the resin impregnator, and then they are pulled through a heated die. The heated die will remove all the excess resin, and form the shape of the composite as show in Figure.2.1. Because of the continuous molding 10 cycles, the cross section will be the same dimension and will have similar properties along the length of the product. Pultruded composites mainly consist of unidirectional fibers in the pulling direction because continuous fibers are used. However, other mat sheets such as random chopped strand mats can be inserted to improve the properties of the perpendicular direction. Fiber contents can be controlled from 25 to 70 percent by weight. Currently, there are pultruded structural composites available in many shapes like structural steel [Lesko, 2003]. The advantages of this technique are that it is not labor intensive, and the product has a consistent quality.

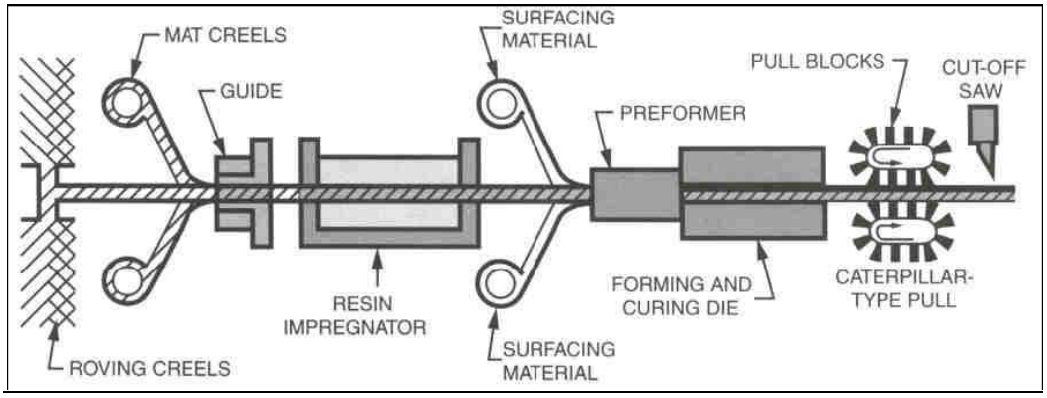

Figure 2.1 Schematic illustration of pultrusion process
(Strongwell Extren DWB Design Guide, 2003)

The pultrusion process is used to manufacturer FRP reinforcing bars, FRP strengthening strips and FRP profiles and is the most cost-competitive method for producing high-quality FRP parts for use in structural engineering [Lesko et al, 2003]

Processing of FRP materials mainly involves the following unit operations;

- Fiber placement along the required orientation
- Impregnations of the fiber with the resin
- Consolidation of the impregnated fivers to remove excess resin ,air and volatiles
- Cure or solidification of the polymer
- Extraction form the mold (If mold would be used)
- Finishing operation

2.4 Mechanical properties of GFRP rebars

GFRP reinforcing bars are well known for linear elastic stress strain response and their high strength to weight ratio. Significant differences exist from one manufacturer to another while all bars exhibit those characteristics. The following sections discuss the different products currently available and their mechanical properties determined from previous testing. Two GFRP products are shown in Figure.2.2 below.

2.4.1 Type -A rebar : ASLAN 100

The Aslan 100 bar is an E-Glass bar, helically wrapped and sand coated partially for enhanced bonding characteristics. The mechanical properties that were determined from Hughes Brothers own internal testing [Colberg, 2007] are shown in Table.2.3. While the modulus of elasticity and the ultimate elongation remained relatively constant over all the diameters tested, the ultimate strength is generally lower for larger bars. One of the main reasons for the inverse relationship of strength and bar size is that the fiber glass is heavily

sensitive to small defects and smaller diameters have a smaller chance of containing or precipitating these defects [Nawy et al. 1971].

Figure 2.2 GFRP and steel bars

Table 2.3 Material properties of ASLAMN 100 (Hughes Brothers Inc.)

	Diameter		Area		Guaranteed Tensile Strength		Ultimate Tensile Load		Tensile Modulus of Elasticity	
Size	(mm)	(in)	(mm^2)	(in^2)	(MPa)	(ksi)	kN	kips	(GPa)	(psi 10^6)
2	6	1/4	31.67	0.049	825	120	26.2	5.89	40.8	5.92
3	10	3/8	71.26	0.110	760	110	54.0	12.1	40.8	5.92
4	13	1/2	126.7	0.196	690	100	87.3	19.6	40.8	5.92
5	16	5/8	197.9	0.307	655	95	130	29.1	40.8	5.92
6	19	3/4	285.0	0.442	620	90	177	39.8	40.8	5.92
7	22	7/8	387.9	0.601	586	85	227	51.1	40.8	5.92
8	25	1	506.7	0.785	550	80	279	62.8	40.8	5.92
9	29	1-1/8	641.3	0.994	517	75	332	74.6	40.8	5.92
10	32	1-1/4	791.7	1.227	480	70	382	85.9	40.8	5.92

2.4.2 Type-B rebar: VROD-HM

The V-ROD-HM bar has vinyl-ester based matrix and sand coated surface fully for enhanced bonding characteristics with E-glass formulation. The mechanical properties of the V-Rod-HM are shown in Table.2.4 below. The properties of this product are relatively similar to those of the ASLAN-100 bars in that the strength decreases with the increase of bar size and. The properties of the V-ROD-HM are significantly higher than that standard ASLAN-100. Two factors contribute to the higher strength, stiffness and elongation at rupture of HM bars. These include higher fiber volume and better quality glass fibers. The V-ROD-HM has much higher glass fiber contents at approximately 80% by weight while ASLAN-100 has 70% minimum per ASTM D2584. While E-glass fibers are used in ASLAN-100, the fiber type in HM bars appear to be the higher grade S type as outlined in Table.2.1. The manufacturer does not provide actual information about the fiber type in HM bars [Johnson, 2009].

Table 2.4 Material properties of V-ROD-HM (Pultrall Inc.)

Description	Units	#4 GFRP	#5 GFRP	#8 GFRP	#10 GFRP
		V•ROD HM	V•ROD HM	V•ROD HM	V•ROD HM
Nominal Tensile Strength	MPa	1450	1439	1260	1060
	ksi	210	209	183	154
Guaranteed Design Tensile Strength	MPa	1300	1259	1130	950
	ksi	188	182	164	138
Nominal Tensile Modulus	GPa	60	64.1	60	60
	ksi	8696	9290	8696	8696
Tensile Strain	%	2.42	2.24	2.10	1.77
Poisson's Ratio		0.26	0.25	0.28	0.28

2.4.3 Other reinforcement products

Some other FRP products are emerging onto the market in addition to the two different types of bars discussed above. Carbodur GFRP rods manufactured by Sika Inc, are also being sold in Canada. Re-Bars DO Brazil have developed new FRP reinforcing bars, one of them being a GFRP bar which is currently undergoing testing. Another emerging product in Europe is

made by a company known as STO Scandinavia which is currently developing CFRP bars, it is unclear whether or not GFRP will follow soon after [Johnson, 2009]. None of these products are dealt with in any detail in this study.

2.5 Steel reinforcement

Concrete has virtually no tensile strength as mentioned above. Concrete structures must therefore be reinforced with a material having a high tensile strength [Parish, 2008]. Since most deteriorating concrete bridges are reinforced with steel reinforcement, standard deformed steel rebar will be the focal existing reinforcing material discussed in this paper. Rebar is hot-rolled from steel with varying carbon content. Almost all new reinforcing bars are made from Grade 60 steel, which means they have the yield strength of 60,000psi.

Table 2.5 Designations, dimensions, and weights of standard U.S. and metric steel reinforcing bars (PCI, 2004)

Imperial Bar Size	"Soft" Metric Size	Weight		Nominal Diameter		Nominal Area		Perimeter (in)
		(lb/ft)	(kg/m)	(in)	(mm)	(in^2)	(mm^2)	
#3	#10	0.376	0.561	0.375	9.525	0.11	71	1.18
#4	#13	0.668	0.996	0.500	12.7	0.20	129	1.57
#5	#16	1.043	1.556	0.625	15.875	0.31	200	1.96
#6	#19	1.502	2.24	0.750	19.05	0.44	284	2.36
#7	#22	2.044	3.049	0.875	22.225	0.60	387	2.75
#8	#25	2.670	3.982	1.000	25.4	0.79	509	3.14
#9	#29	3.400	5.071	1.128	28.65	1.00	645	3.54
#10	#32	4.303	6.418	1.270	32.26	1.27	819	3.99
#11	#36	5.313	7.924	1.410	35.81	1.56	1006	4.43
#14	#43	7.650	11.41	1.693	43	2.25	1452	5.32
#18	#57	13.60	20.284	2.257	57.33	4.00	2581	7.09

Many aged concrete structures are reinforced with Grade 40 (40,000psi) steel, and some are even reinforced with A36 (36,000psi) steel bars. As it is seen in Figure2.2, steel rebar is deformed, or ribbed, so that concrete and steel can develop a solid bond. Steel rebar is available in a variety of sizes. Standard imperial U.S. bars are available in diameters ranging from ⅜” to 2¼” [Parish,2008]. The U.S. designation number represents the diameter of the bar multiplied by 8. For instance, #3 bars are ⅜” in diameter, #7 bars are ⅞” in diameter, and #10

bars are 1¼” in diameter. Both U.S. and metric designations, dimensions, and weights are provided in Table.2.5.

2.6 Flexural design of concrete members reinforced with GFRP bars (ACI.440 Code)

The ACI 440 code states that since GFRP bars are elastic in tension without any ductility rupture, the design of GFRP bar reinforced concrete should be reconsidered. In this section, the flexural design of GFRP bar reinforced concrete in ACI 440.1R-06 will be reviewed in detail.

2.6.1 Flexural behaviors of GFRP bar- reinforced concrete

In case of steel reinforced concrete design, the sections are commonly under-reinforced to ensure the yielding of steel before concrete crushes, thus giving enough warning before failure of the structural member. However, the under-reinforced design approach for GFRP reinforced concrete should be reconsidered because the rupture of a GFRP bar is sudden and catastrophic [ACI440, 2006]. Instead of design based on the rupture of the GFRP reinforcement, design based on concrete crushing produces a flexural concrete member reinforced with GFRP bar that exhibits some plastic behavior before failure. Thus, the concrete crushing failure mode is marginally more desirable for flexural members reinforced with GFRP bars [ACI 440, 2006]. However, both failure modes (GFRP rupture and concrete crushing) are acceptable in the ACI 440 design code. In order to compensate for the lack of ductility, the margin of safety against failure in the 2006 edition of the ACI 440 is specified higher than that used in traditional steel-reinforced concrete design.

2.6.2 Flexural design philosophy of GFRP bar-reinforced concrete

The strength design philosophy states that the design flexural strength at a section of a member must exceed the factored moment (Eq. 2.1).

$$\phi M_n \geq M_u \qquad \text{(Eq.2.1)}$$

Design flexural strength (ϕM_n) refers to the nominal flexural strength of the member (M_n) multiplied by a strength reduction factor(ϕ). Factored moment (M_u) refers to the moments calculated by the use of factored loads as prescribed in ACI 318-11. The computations of the strength of cross sections are performed based on the following assumptions [ACI440-1R, 2006]:

- A plane section before loading remains plane after loading.
- The tensile strength of concrete is ignored.
- Perfect bond exists between concrete and GFRP reinforcement.
- The maximum usable compressive strain in the concrete is 0.003.
- The tensile behavior of GFRP reinforcement is linearly elastic until failure.

With the above assumptions, the nominal flexural strength (Mn) of GFRP bar reinforced concrete member can be determined. As mentioned above, both GFRP rupture failure and concrete crushing failure are acceptable by ACI 440 for design of GFRP reinforced flexural members. Thus, the flexural capacity of the member would be dependent on the failure mode, whether it is governed by concrete crushing or by GFRP rupture [ACI440-1R, 2006].

There are three possible modes of flexural failure of a concrete section reinforced with FRP bars:

- Balanced failure - simultaneous rupture of FRP bars and crushing of concrete;
- Compression failure - concrete crushing while FRP bars remains in the elastic range with a strain level smaller than the ultimate strain; and,
- Tension failure - rupture of FRP bars before crushing of concrete.

The failure mode can be determined by comparing the GFRP reinforcement ratio (ρ_f) with the balanced GFRP reinforcement ratio (ρ_{fb}). If the reinforcement ratio is less than the balanced ratio ($\rho_{fb} > \rho_f$), FRP rupture failure mode governs. Otherwise, ($\rho_{fb} < \rho_f$) concrete

crushing governs. Compression failure is less violent and more desirable than tension failure and is similar to that of an over-reinforced concrete beam with steel reinforcing bars. Tension failure, due to rupture of FRP bars while the strain in the extreme fibers of the compression zone is less than the ultimate compressive strain of the concrete, is sudden. It will occur when the reinforcement ratio is smaller than the balanced failure reinforcement ratio.

In order to ensure the safety of GFRP RC structures under the service lifetime, a strength reduction factor associated with the tensile strength of GFRP bars is incorporated in current design codes/guidelines [JSCE, 1997; CHBDC, 2006; CSA, 2002; ACI 440, 2006], among which the ACI 440 code (Guide for the Design and construction of Structural Concrete Reinforced with FRP Bars, reported by American Concrete Institute Committee 440) is the most practical one. In addition, environmental reduction factors required by various codes and design guidelines are summarized in Table2.6. The guaranteed tensile strength f^*_{fu} cannot be used as the design strength due to the long-term degradation of GFRP bars under services. In ACI 440-1R-06, the design values of the tensile properties are specified as the f^*_{fu} multiplied by an environmental reduction factor C_E, as shown in equations (Eq.2.2) and (Eq2.3).

Table 2.6 Environmental reduction factors by various codes and design guides (Nkurunziza,2005)

Code	ACI 440.1R-03	CAN/CSA-S6-00	JSCE 1997
Properties	Average−3σ	Average −σ	Average −3σ
Reduction due to the environmental degradation	CE 'environmental reduction coefficient' 0.70–0.80	ϕFRP 'strength factor' 0.75	1/γfm 'factor taking the material into account' 0.77
Reduction due to the sustained load	NA	0.8–1.0	NA
Combined reduction due to the environment and sustained load	0.70–0.80	0.60–0.75	0.77
Design limit taking creep into account (0.20 f_{fu})	0.14–0.16	0.60–0.75	⩽0.7

$$f_{fu} = C_E \cdot f^*_{fu} \qquad \text{(Eq.2.2)}$$

$$\varepsilon_{fu} = C_E \cdot \varepsilon^*_{fu} \qquad \text{(Eq.2.3)}$$

Where C_E is environmental reduction factor, f_{fu} is design tensile strength and ε_{fu} is design rupture strain. Note that the effects of temperature are included in the value of C_E.

Figure.2.3 schematically presents the philosophy of the design strength of GFRP bars used as internal concrete reinforcement. It can be seen that the design tensile strength of GFRP bars is less than the guaranteed value, and its value depends on the service conditions.

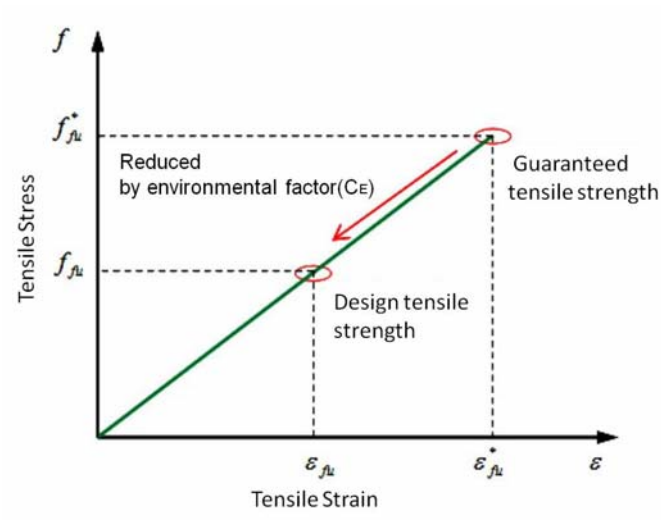

Figure 2.3 Reduced tensile design property of GFRP bars by C_E

2.6.3 Flexural design approach for GFRP bar-reinforced concrete based on failure mode

The design procedure presented in this chapter follows ACI440.1R-06 which is compatible with ACI 318-11.

2.6.3.1 Balanced failure ($\rho_f = \rho_{fb}$)

The balanced failure strain condition occurs when the concrete strain reaches its ultimate value ε_{cu}, while the outer layer of FRP reaches its ultimate strain ε_{frpu}, as shown in Figure.2.4. Because FRP bars do not yield, the balanced ratio of FRP reinforcement is computed using its design tensile strength of f_{fu}. The FRP reinforcement ratio can be computed from Eq.2.4, and the balanced FRP reinforcement ratio can be computed from Eq.2.5. At this

condition, the compressive strain in concrete reaches its ultimate value ε_{cu}=0.003 while the FRP bar reinforcement simultaneously reaches ultimate strain (ε_{frpu}) of FRP bars. From the strain compatibility in the cross-section in Figure2.4, the depth of the compression zone, which is equal to the distance from the extreme outer concrete surface to the neutral axis of the section (c_b) is given in equation 2.6.

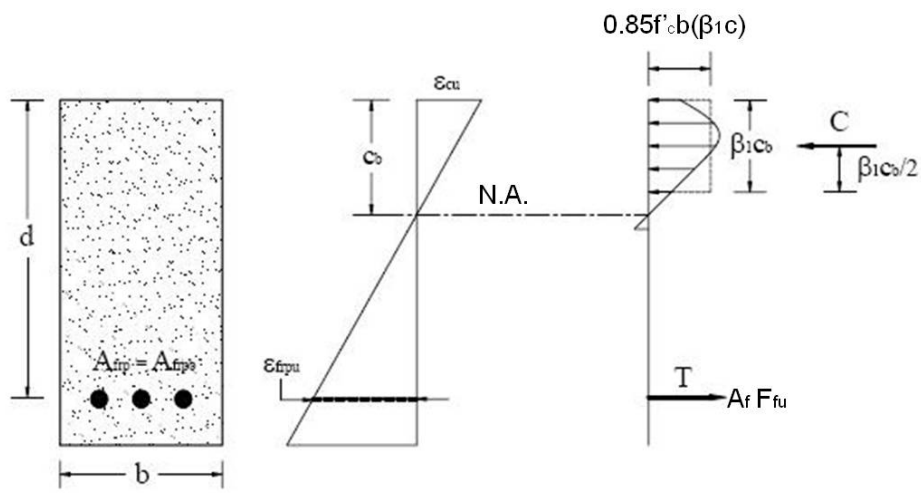

Figure 2.4 Strain and stress distribution in balanced failure condition (ACI440.1R-06)

$$\rho_f = \frac{A_f}{bd} \qquad \text{(Eq.2.4)}$$

$$\rho_{fb} = 0.85\beta_1 \frac{f_c^{'}}{f_{fu}} \frac{E_f \varepsilon_{cu}}{E_f \varepsilon_{cu} + f_{fu}} \qquad \text{(Eq.2.5)}$$

$$C_b = \frac{\varepsilon_{cu}}{\varepsilon_{cu} + \varepsilon_{fu}} d \qquad \text{(Eq.2.6)}$$

2.6.3.2 Over-reinforced failure : Concrete crushing ($\rho_f > \rho_{fb}$)

The failure of the member will be initiated by concrete crushing when $\rho_{fb} < \rho_f$ (and c > c_b) and the stress distribution in the concrete can be approximated with the ACI rectangular stress block. The equilibrium of forces and strain compatibility are shown in Figure.2.5.

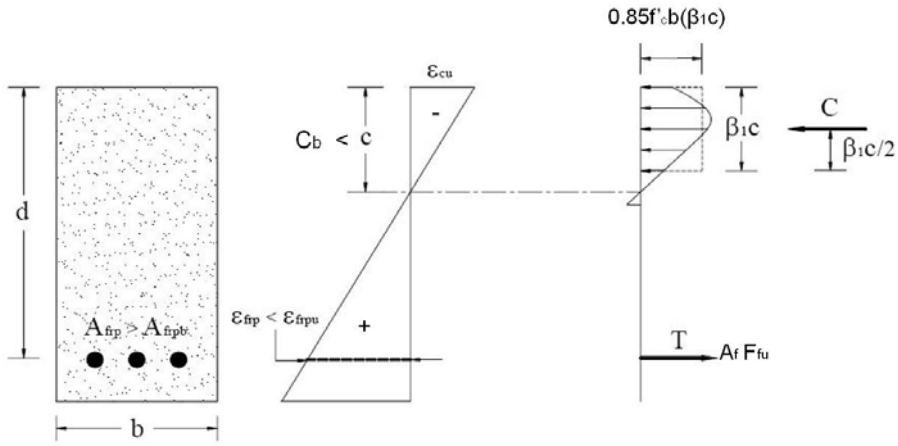

Figure 2.5 Strain and stress distribution in an over-reinforced FRP beam section (concrete crushing)

The nominal moment capacity of the over-reinforced section can be obtained in the given equations below.

$$M_n = A_f f_f (d - \frac{a}{2}) \qquad \text{(Eq.2.7)}$$

$$a = \frac{A_f f_f}{0.85 f_c^{'} b} \qquad \text{(Eq.2.8)}$$

$$f_f = E_f \varepsilon_{cu} \frac{\beta_1 d - a}{a} \qquad \text{(Eq.2.9)}$$

Substituting “a” from equation 2.8 into equation 2.9 and solving for f_f gives the equation.2.10.

$$f_f = (\sqrt{\frac{(E_f \varepsilon_{cu})^2}{4} + \frac{0.85 \beta_1 f_c^{'}}{\rho_f} E_f \varepsilon_{cu}} - 0.5 E_f \varepsilon_{cu}) \leq f_{fu} \qquad \text{(Eq.2.10)}$$

Thus, the nominal flexural strength M_n (Eq. 2.7) can be determined from equation 2.7, 2.8 and 2.10. Alternatively, the nominal flexural strength M_n at a section can be expressed in terms of the GFRP reinforcement ratio ρ_f as given in equation.2.11.

$$M_n = \rho_f f_f (1 - 0.59 \frac{\rho_f f_f}{f_c^{'}}) bd^2 \qquad \text{(Eq.2.11)}$$

2.6.3.3 Under-reinforced failure : FRP rupture($\rho_{fb} > \rho_f$)

when $\rho_f < \rho_{fb}$ (and $c < c_b$), the failure of the member will be initiated by rupture of the FRP rebars in tension before maximum concrete compressive strain (0.003) is reached. The equilibrium of forces and strain compatibility are shown in Figure.2.6

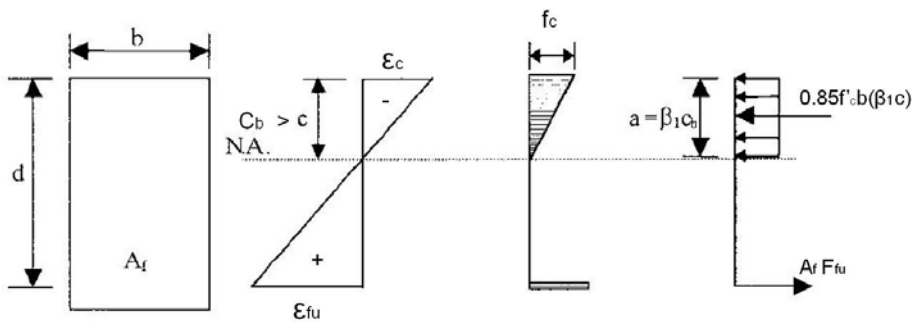

Figure 2.6 Strain and stress distribution in an under-reinforced FRP beam section (FRP-rupture)

In this case, an equivalent stress block would need to be used that approximates the stress distribution in the concrete at the particular concrete compressive strain level reached. The analysis incorporates two unknowns: the concrete compressive strain at failure ε_c and the depth to the neutral axis *c*. In addition, the rectangular stress block factors, α1 and β1, are unknown. The factor α_1 is the ratio of the average concrete stress to the concrete strength. Factor β_1 is the ratio of the depth of the equivalent rectangular stress block to the depth of the neutral axis. The analysis involving all these unknowns becomes complex. ACI 440.1R-06

recommends the simplified and conservative nominal flexural strength at an under-reinforced, singly reinforced rectangular section as shown in equation 2.12.

$$M_n = A_f f_{fu}(d - \frac{\beta_1 c_b}{2}) \qquad \text{(Eq.2.12)}$$

$$c_b = (\frac{\varepsilon_{cu}}{\varepsilon_{cu} + \varepsilon_{fu}})d \qquad \text{(Eq.2.13)}$$

2.6.4 Strength reduction factor for flexure (ACI 440.1R-06)

Because GFRP members do not exhibit ductile behavior, a conservative strength reduction factor should be adopted to provide a higher reserve of strength in the member [ACI, 440.1R-06]. In ACI 440.1R-06, the strength reduction factor for flexure was proposed to be computed by Eq. 2-13, for the purpose of safe design. ACI 318-11 considers a failure tension-controlled whenever the curvature is greater than 0.008/*d* (corresponding to a tensile strain in the steel of 0.005). This indicates that FRP-reinforced beams internally will have larger deflections at ultimate due to the low modulus of elasticity of the reinforcement and that FRP-reinforced beams internally that fail by FRP reinforcing bar rupture will have larger deflections at ultimate than those that fail by concrete crushing. Even though the curvature values of FRP reinforced beams are larger than those of equivalent steel reinforced beams, the committee recommends a φ factor of 0.55 for tension-controlled failure to maintain a minimum reliability index of 3.5. While a concrete crushing failure mode can be predicted based on calculations, the member as constructed may not fail accordingly. For example, if the concrete strength is higher than specified, the member can fail due to FRP rupture. For this reason and to establish a transition between the two values of φ, a section controlled by concrete crushing is defined as a section in which $\rho_f \geq 1.4\rho fb$, and a section controlled by FRP rupture is defined as one in which $\rho_f < \rho_{fb}$.

The strength reduction factor for flexure can be computed by Eq.2.13. This equation is represented graphically by Figure.2.7, and gives a factor of 0.65 for sections controlled by concrete crushing, 0.55 for sections controlled by FRP rupture, and provides a linear transition between the two.

$$\phi = \begin{cases} 0.55 & for \rho_f \le \rho_{fb} \\ 0.3 + 0.25\dfrac{\rho_f}{\rho_{fb}} & for \rho_{fb} < \rho_f < 1.4\rho_{fb} \\ 0.65 & for \rho_f \ge 1.4\rho_{fb} \end{cases} \qquad \text{(Eq.2.13)}$$

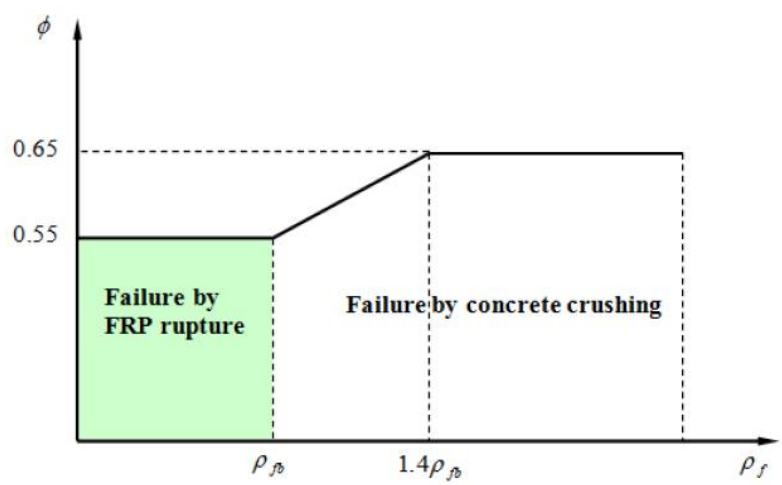

Figure 2.7 Strength reduction factor as a function of the reinforcement ratio (ACI 440.1R-06)

CHAPTER 3

LITERATURE REVIEW

3.1 General

As mentioned in chapter 2, GFRP bars have gained popularity as reinforcement of concrete for their properties of non-corrosion. However, GFRP bars would degrade under certain conditions. Large amount of in-lab research data indicated that GFRP bars undergo physical and chemical changes when they are subjected to harsh environmental conditions, which eventually leads to the degradation of GFRP bars [ACI 440, 2006]. The detrimental environments could be water/moisture, saline solution, alkaline solution, acidic solution, dry-wet cycling, freeze-thaw cycling and elevated temperature [Benmokrane,2005]. Among these environmental conditions, alkaline attack caused the most concern because of the high pH of concrete pore solution [ACI-440, 2006]. The degradation of GFRP bars depends significantly on the exposure conditions. Reduction in tensile strength of GFRP is primarily attributed to the environmental attacks. The following summarize the long-term durability behaviors of GFRP bars [Hollaway, 2010 and ACI-440,2006]:

- GFRP bars undergo the most severe degradation in alkaline solution compared to other exposure solutions.
- The process of degradation of GFRP bars is temperature dependant.
- GFRP bars made of vinyl ester resin have much better aqueous resistance than that of polyester.
- The degradation behavior of GFRP bars exposed to saline solution is similar to that subjected to water.

- GFRP bars undergo more severe degradation when subjected to combination effect of alkaline and sustained load than only alkaline exposure.

Long-term performance of GFRP bars needs to be considered in the design with specific approach other than the existing design of steel reinforced concrete for the purpose of safe design of GFRP bar reinforced concrete.

3.2 Durability

3.2.1 General consideration

Durability has been defined as “its ability to resist cracking, oxidation, chemical degradation, debonding, wear, and/or the effects of a foreign object damage for a specified period of time under the appropriate load and environmental conditions” [Karbhari et al, 2000]. Durability analysis of materials is one of the most important concerns when a new product is being incorporated into industry. Applications of FRP products are increasing as more information about its capabilities and less expensive manufacturing techniques are becoming available. Over last decades, fatigue, creep, cracking, wear and weathering have been performed under non-linear viscoelastic-viscoplastic behavior and environmental degradation in order to investigate the overall degradation mechanism of whole FRP systems [Nelson et al, 1990]. Since the main objective of this study is related to environmental weathering of FRP systems, the other mechanism will not be covered in detail in this review.

The fibers carry the load while the resin transfers the stresses between fibers when a load is applied to the FRP bar. The resin also protects the fibers against the attack of harmful ions coming from the environment, in particular OH-ions of the interstitial solution of the concrete [Mallick, 1993]. As well as interface between its components, degradation of the FRP is a result of the degradation of one or more of them. This complicates the mechanism of degradation of the FRP reinforcement compared to that of traditional steel. If fibers do not deteriorate, the GFRP bars will resist the mechanical load since the mechanical properties of

the GFRP bars are controlled by the fibers [ACI-440R-06, 2006]. If the resin is attacked and deteriorated, the surface of the fibers starts to break, progressing towards the interior of the bar, leading to a reduction in the bar strength. The interface between glass fibers and the resin controls the resistance of the GFRP bars to the alkalis [Uomoto et al. 2004]. The improvement in the strength of the interface bond effectively increases the resistance of the bar to alkalis. The details of the degradation of the GFRP bar components are discussed in the following sections.

3.2.2 Environmental factors affecting properties of FRP bars

There have been many studies on the durability characteristics of the fibers used in the FRP materials. Three most common fiber types (glass, carbon and aramid) have been emphasized for durability tests. Since glass fiber is the most widely used in civil engineering applications, degradation of the glass fiber will be covered in more detail in this reviews. A glass fiber reinforced polymer composite degrades after a prolonged period of service due to the effects of the environment. The causes may involve followings [Sapalidis et al, 1997].

(i) loss of strength in reinforcing fibers due to stress-corrosion

(ii) chemical degradation of matrix material,

(iii) loss of adhesion, and interfacial bond strength degradation of the matrix/fiber interface,

(iv) dependence of the matrix modulus and strength on time and temperature, and

(v) accelerated degradation caused by combined action of temperature and chemical environment

Therefore, understanding the cause of degradation precisely would help in improving the durability of composites. Under everyday service conditions, infrastructures are subjected to a wide range of temperature and moisture yearly. The presence of deicing salts, especially in a bridge, must also be considered as part of the bridge deck service environment. All environmental factors must be considered along with the mechanical loading to which the

composite components will be subjected. Long-term or creep type loading as well as periodic or fatigue-type loading must be considered. The combination of environmental and mechanical loading complicates the durability of FRP composite. Composite properties change over time due to degradation of the resin matrix or the fiber reinforcements, or by breakdown at the fiber/matrix interface. Degradation of organic polymer matrices often manifests molecular rearrangement, with accompanying loss of compounds of low molecular weight [Yan, 2005].

This degradation is accelerated by elevated temperatures and the presence of moisture. Degradation of fiber reinforcements varies with fiber type. Considering the environmental effect on the degradation of FRP, ACI 440 has recommended environmental reduction factors for different fibers depending on their exposure condition. The environmental factors for GFRP are 0.7-0.8 as per their exposure conditions. In this study, the evaluation of GFRP will be done only for conditions of temperature, moisture and alkalinity.

3.2.2.1 Thermal and moisture effect on FRP bars/composites

Due to thermal softening, the elastic modulus and strength of an FRP bar decrease with the increase in temperature when tested at high temperature under sustained load [Mallick, 1988]. In a polymeric composite, the matrix properties are more affected by the increase in the temperature than the fiber properties. The axial mechanical properties -strength and modulus- of a linear composite with fibers oriented at 0° to the load remain unchanged with the increase in the temperature, while the transverse properties are reduced when the temperature approaches the glass transition temperature (T_g). In the short term, an elevation in temperature of between 30 and 40°C does not significantly affect the strength or the elastic modulus of the majority of commercial fibers [Mallick, 1988]. However, prolonged thermal ageing at a high temperature combined with sustained loading can cause deterioration in the properties of the matrix [Uomoto ,2004].

The migration of moisture in FRP composites has been one of the most widely studied subjects during the past several decades. Depending on the type of resin matrix used and surrounding environment, moisture diffuses into composite materials to varying extents and at various rates. This diffusion process occurs at the molecular level. Moisture can be absorbed by capillary uptake along any preexisting crack or interface between the fiber and resin matrix. The effect of moisture on composites is a mass uptake, followed by the plasticization of the matrix and a decrease in the glass transition temperature. Moisture can act as a plasticizer, thus reducing the matrix modulus. The literature has also shown that moisture can increase crack density, which would also have an effect on the modulus [Jungkuist, 2000]. Moisture can attack the fiber during loading causing stress-corrosion cracking. Cracks can form at the fiber–matrix interface, thus decreasing the stress transfer of the composite. The degradation of GFRP bars subjected to water/moisture is often carried out by accelerated ageing tests at different elevated temperatures, in the range of 20-60°C [Bank et al, 1995]. A combination of moisture/water and elevated temperature would accelerate the diffusion of water/moisture into GFRP bars and the reaction rate between water and the constituents of GFRP bars. In the accelerated ageing tests, GFRP specimens were subjected to a variety of exposure conditions for different periods, such as immersion in water at different temperatures and in air with different relative humidity (R.H.) and temperature. The degradation of GFRP bars due to the attacks by water/moisture is often evaluated by the measurements of the retention of tensile strength and elastic modulus of GFRP bars. In some cases, the uptake of water or moisture determined by measuring the weight gain for specimens was utilized to study the rate of water intrusion into the GFRP bars, and then to predict the long-term performance [Karbhari et al., 2003]. Table 4.1 shows the effects of water/moisture on the GFRP bars.

Karbhari et al. (2003) studied the durability of uni-axial, biaxial, and tri-axial nonwoven E-glass fabrics reinforced vinyl ester composites in an aqueous environment. A resin infusion process was used for the fabrication of composites. Samples are immersed in de-ionized water

at 23 °C and 60°C, respectively. Reductions in both tensile strength and tensile modulus were observed. The tensile strength percentage retention is about 30– 60 % after 50 weeks immersion in water at 23 °C and 60°C, while the tensile modulus decreased 10 - 30 % of the control value.

The deterioration of polymer resin matrix in GFRP bars may occur when water molecules act as plasticizers and disrupt Van-der-Waals bonds in polymer chains [Gentry et al,], which causes changes in strength, modulus, toughness and swelling stress in GFRP. The swelling stress leads to polymer matrix cracking, hydrolysis and fiber-matrix de-bonding [Hayes et al., 1998]. The degradation mechanism of GFRP in water/moisture is also summarized as followings:

- The process of degradation of GFRP bars is temperature dependent;
- Water/moisture exposures have less of an effect on the degradation on tensile modulus than that on tensile strength;
- Strength reduction of GFRP bars is directly linked to the water uptake.
- The degradation mechanisms may arise from fiber degradation, resin and/or fiber-matrix interface degradation.

3.2.2.2 Chemical effect on FRP bars

One of the main concerns about the use of GFRP bars in reinforced concrete is the long-term durability in concrete with high pH environments. In order to evaluate the durability of GFRP bars under alkaline exposure, a large number of accelerated ageing tests on stand-alone GFRP bars have been conducted [ACI-440, 2006].

The black area within the GFRP rods in Figure.3.1 represents the area that has been penetrated by the alkali. It can be seen that the alkali penetrated into the GFRP rods with time through the resin matrices. It was proved that the glass fibers in the black area (where alkali is

present) degrade and lose their strength, resulting in the decrease in the overall tensile strength of the GFRP bars [Katsuki and Uomoto, 1995]. This is easy to understand since glass fibers are the main load-carrying constituent in the bar.

Figure 3.1 Rough estimate of alkali penetration in GFRP rods
(Katsuki and Uomoto, 1995)

Table 3-1 presents part of the available data on the strength degradation of GFRP bars under alkaline attacks. From Table.3.1, it can be seen that the pH value of the alkaline solutions ranges from 11.0 to 13.7, and the degradation behaviors can be summarized as follows.

- The alkaline exposures cause significant reduction in tensile strength of GFRP bars.
- GFRP bars undergo more severe degradation under alkaline exposure when compared to the water and saline exposures that discussed above.
- GFRP bars with vinyl ester matrices have better alkaline resistance than that with polyester matrices.

Table 3.1 Durability of GFRP (E-Glass) bars under alkaline solution without sustained stress (Bhise, 2002)

Author	Resin type	Environmental solution	Duration (days)	pH value	Temp. (°C)	Tensile strength reduction (%)	Tensile strength retention (%)
Tannous and Saadatmanesh (1998)	Vinyl ester	Saturated Ca(OH)2	180	12	25	13	87
					60	20	80
Valter Dejke(2001)	Vinyl ester	NaOH 2g/liter KOH 19.6g/liter Ca(OH)2 3.6g/liter water	100	13.7	20	10	90
					40	25	75
					60	35	65
					80	50	50
			200		20	18	82
					40	28	72
					60	45	55
					80	53	47
Coomarasamy (1998)	Vinyl ester	0.6 M KOH 0.2 M NaOH Saturated Ca(OH)2	77	13.5	60	8	92
			175	13.5	60	32	68
Micelli and Nanni (2001)	Polyester	1% NaOH 1.4%KOH 0.16% Ca(OH)2	21	12.6	60	30	70
			42	12.6	60	41	59

3.2.2.3 Effect of chloride on the durability of FRP bars

Wu et al. (2002) carried out an extensive study on the short-term effects of sea water on GFRP composites with E-glass and vinyl–ester resin. Composite specimens were fabricated using wet layup with the application of a vacuum throughout the cure. The reinforcement consisted of two layers of a quadric-axial fabric, laid up symmetrically about the mid-plane with the bias (±45º) plies toward the center, with a resulting fiber weight fraction of between 68 and 69%. Specimens were exposed to the following environments for periods up to 12 months:

- Sea water at 23°C (with the pH of 8.24)
- De-ionized water at 23°C (with a pH of 6.95)
- Synthetic sea water at 23°C (with a pH of 8.24)

Table 3.2 Retention of tensile strength (%) as a function of exposure type and time (Wu et al., 2002)

Exposure Type	Tensile Strength retention (%)					
	Unexposured	Time of Exposure (Months)				
		1	3	6	9	12
Unexposured	100	N/A	N/A	N/A	N/A	N/A
Deionized water	N/A	97.8	96.1	93.9	92.3	88.7
Sea water	N/A	97.5	99.2	93.9	88.7	86.5
Sea water (sealed edges)	N/A	99.2	97.0	96.4	95.0	86.8
Sea water (cycling)	N/A	93.1	100.0	93.4	92.6	91.7
Synthetic sea water	N/A	94.5	96.7	93.7	93.9	87.1

Table3.2 shows the changes in tensile strength of GFRP composites due to the immersion in different aqueous solutions. Exposures to sea water and water result in the reduction of GFRP tensile strength up to 13.5% after 12 months (365 days) immersion at 23°C were observed as shown in Table 3-2. Also it can be found that the strength retentions of GFRP bar under de-ionized water and sea water exposures are approximately the same [Huang,2010].

3.2.2.4 Sustained loading effect on FRP bars

A sustained load has been applied to samples during the conditioning process and has been found to further reduce the composite durability [Hollaway,2001]. The applied stress also has an effect on strength degradation in polymers and polymer composites. Increase of moisture absorption along a path running through a tensile stress field was caused by the residual stresses due to differential thermal expansion of fiber and matrix materials in a composite may cause [Hollaway,2001].

The durability of GFRP bars in concrete beams under sustained loads with three different environmental conditions was investigated [Almusallam et al.,2006]. The sustained beams were designed so that the level of a reasonable sustained load causes a stress equal to

20–25% of its ultimate tensile strength (P_u) in the GFRP bar. The type of GFRP bars was E-glass and vinyl-ester resin with 60% fiber volume fraction. The measured tensile values were used as the reference for the tensile strength of GFRP bars. It can be seen that the retention of tensile strength of GFRP bars was different from each other for stressed and unstressed cases, respectively. The additional effects due to the sustained stress accelerated the degradation rate of GFRP bars in moist concrete, resulting lower tensile strength retention compared to that from un-stressed case. The data for the specimens subjected to a sustained load during conditioning showed that their ultimate tensile strengths were generally lower than those for the corresponding samples which had not been loaded during conditioning especially at higher temperature conditioning.

3.3 Corrosion of steel in concrete

The reduction in the useful service-life of steel reinforced concrete structures is a cause of concern to the construction industry mainly due to reinforcement corrosion [Almusallam,2001]. In normal situations, concrete provides protection to the reinforcing steel. The dense and relatively impermeable structure of concrete provides the physical protection, while the high alkalinity of the pore solution provides the chemical protection. The alkaline compounds, mainly calcium and to a certain extent pottasium and sodium, in the cement contribute to the high alkalinity (pH >13.5) of the pore solution [Pourbaix,1966]

Corrosion of the reinforcing steel bars is caused either due to diffusion of the chloride ions to the steel surface or due to carbonation of concrete. Corrosion of reinforcing steel and the subsequent cracking of concrete due to the ingress of chloride ions to the steel surface is more predominant than that due to carbonation of concrete.

The reduction in the load-carrying capacity of a reinforced concrete member due to reinforcement corrosion is attributed to the combined effect of a decrease in the bond between concrete and/or reduction in the tensile strength of the bars. While some data are available on

the effect of reinforcement corrosion on the bond strength of concrete [Maslehuddin et al 1990], its influence on the mechanical properties of reinforcing steel is scantly investigated. Maslehuddin et al. evaluated the effect of atmospheric corrosion on the mechanical properties of steel bars. However, it should be noted that atmospheric corrosion does not affect the mechanical properties of reinforcing steel as much as its corrosion in concrete. Also, corrosion of reinforcing steel induces cracks in concrete, thereby affecting the integrity of a structural component [Ha et al., 2007]. The degree of reinforcement corrosion and the resulting decrease in the load-carrying capacity of both steel bars and the structural component needs to be evaluated to assess the residual strength of concrete and formulate repair strategies.

In many investigations, the corrosion performance of steel in mortar and concrete was studied and evaluated by some accelerated aging techniques in sodium chloride solutions. Electrochemical techniques such as open circuit potential measurements and anodic polarization studies were carried out as show in Figure.3.2 [Ha et al., 2007].

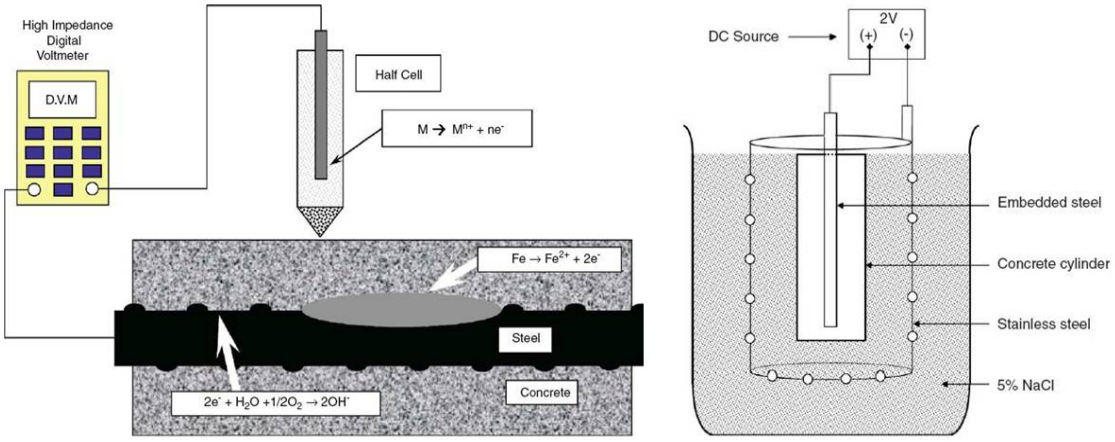

(a) (b)

Figure 3.2 (a) Half-cell potential measurement (b) Set-up for impressed voltage test. (Ha.et al.,2007)

Almusallam et al.(2001) conducted accelerated corrosion test and the test showed that a marginal decrease in the tensile strength of steel bars was noted with increasing degree of reinforcement corrosion when the stress was calculated utilizing the actual area of cross-section. Also, the tensile strength calculated using the actual area of cross-section was more than 600 MPa for bars with as much as 75 to 80% corrosion. However, when the tensile strength was calculated utilizing the nominal diameter, the tensile strength was less than the ASTM A 615 requirement of 600 MPa when the level of corrosion was 12% or more in 6-mm diameter steel bars and 24% or more in the12-mm diameter steel bars. The data on stress-strain characteristics of reinforcing steel bars corroded to varying levels of corrosion indicate a decrease in the ductility of bars with increasing level of corrosion. Furthermore, with increasing levels of corrosion bars failing at low level of yield strain compared to uncorroded steel bars that demonstrate large yielding before failure.

3.4 Accelerated aging tests for long-term performance of FRP bars

The only way to see how durable composite materials are is *accelerated aging test* since 50 - 60 years of performance data is not available for these newly developed materials. There are several proposed prediction models for the residual strength of GFRP bars currently available in the literature. This literature review describes the accelerated tests and resulting changes in the mechanical properties focusing on the effects of environments such as solution exposure and concrete exposures.

3.4.1 Accelerated aging tests of FRP bars- Solution/ water exposure

A critical factor influencing the mechanical deterioration of GFRP bars is the rate at which solution is transported into the GFRP bars. Resin matrix and the interface between them, the diffusion rate of moisture and alkali through the resin matrix is a critical factor influencing the mechanical deterioration of GFRP bars since the longer-term durability performance of GFRP

reinforcement could depend on properties of the fiber [Ceroni et al. 2006]. When a load is applied to the GFRP, the fibers carry the load and the resin transfers the stress to the fibers. The magnitude of deterioration in the strength of GFRP after exposure to alkaline solutions is strongly related to changes in the stress transfer efficiency between fibers and resin matrix [Abbasi and Hogg, 2005].

Litherland et al. (1981) did the tension tests on glass fiber in Portland cement in hot water at temperatures ranging from 20°C to 80°C. They concluded that there is just one chemical reaction controlling the rate of degradation of the fibers over that temperature and developed a method to predict long-term behavior of the composite using the accelerated testing. This methodology was validated by Proctor [1985] on the basis of extensive laboratory testing in correlation with the observations of these glass fiber reinforced cements (GRC) behavior in different climatic conditions over several years.

Katsuki and Uomoto (1995) studied the alkali penetration into the glass fibers of GFRP reinforcement with vinyl-ester resin. In their study, specimens were immersed in 1.0 mol/l aqueous NaOH solutions at 40°C(104°F) to accelerate the deterioration. It was recorded that loss in the tensile strength was up to 60 percent after 120 days of exposure to alkaline solution. To protect the glass from alkali attack, the authors recommended that the thickness of the layer of the resin be controlled.

Micelli and Nanni (2004) performed accelerated aging tests to investigate the residual properties of GFRP bars made of thermoplastic and polyester resin. Specimens fabricated with E-glass fibers and thermoplastic and polyester resins were exposed to simulated pore solution with an average pH of 12.6 at 60°C(140°F). The measured losses in tensile strength of GFRP bars containing polyester resin after 21 and 42 days exposure to alkaline solution were 30 and 40 percent of the ultimate strength. No significant deterioration was reported in the GFRP bars made with thermoplastic resins and immersed in alkaline solution. The authors concluded that the resin properties have an important influence on the durability of GFRP reinforcement, and

polyester resin does not provide sufficient protection from alkali attack and reductions in strength.

Benmokrane et al. (1998) and Nkurunziza et al. (2005) investigated the durability performance of GFRP reinforcement in different environments combined with a range of sustained stresses. Benmokrane et al. (1998) indicated that because two penetration mechanisms of solution in concrete are resin cracking under load and diffusion through the resin matrix, data on the performance of GFRP bars subjected to high alkaline environments at various stress levels is useful for the evaluation of structures containing GFRP reinforcement. For the case of GFRP bars in moist concrete under sustained loads, three types of stress corrosion mechanism were identified [Benmokrane et al. 1998]. These were reported to be stress dominated, crack propagation dominated, and diffusion dominated. It was reported that the applied stresses on the GFRP bars at high temperatures can form cracks in the resin which accelerates the penetration of alkalis through the resin into the glass fibers [Nkurunziza et al. 2005].

3.4.2 Accelerated aging tests of FRP bars- Concrete

It is more important to investigate the deterioration rate of GFRP bars when embedded in actual concrete environments since GFRP reinforcing bars are used as internal concrete reinforcement. Benmokrane et al. (1998), Almusallam (2001), Bakis et al. (2007), and Mufti et al. (2007) performed durability studies of embedded GFRP reinforcing bars in concrete.

Almusallam et al. (2006) investigated the long-term durability behavior of GFRP reinforcement embedded in concrete beams under sustained loads. The type of GFRP bars was of E-glass with modified vinyl-ester polymer with 60 percent volume fraction of E-glass fiber. A total of 36 concrete beams with embedded GFRP reinforcement were immersed in tap and sea water at an elevated temperature of 40°C(104°F) for up to 16 months. Concrete beams immersed in these environments were subjected to loads of 20 to 25 percent of ultimate tensile

capacity. GFRP bars were extracted from the beams and tension tests were performed after 4, 8, and 16 months of exposure. For the 16 month conditioning, reduction in the tensile capacity without loading and with loading was 16.3 and 47 percent in water and 19.6 and 48 percent in sea water, respectively. It is clear that degradation of the GFRP bar was significant when the bars were subjected to sustained loads.

Bakis et al. (2007) investigated the difference in the deterioration rate of GFRP bars between simulated pore solution and actual concrete under loads. GFRP bars made of E-glass and vinyl ester resin were embedded in the concrete beams. After pre-cracking, specimens were placed in four separate environmental conditions for specific conditioning period. After completing sustained loading, the beams were unloaded and subjected to tension tests to measure the residual tensile capacity. Change in tensile strength of bars embedded in concrete beams was 2.5 percent less than the controlled bars that were neither cast in concrete nor loaded. However, reduction in tensile strength of GFRP bars immersed in $Ca(OH)_2$ was nearly 25 percent in one year. It was concluded that reduction in the tensile capacity in real concrete condition is much less than the reduction with simulated pore solution. It was reported that the MOE of the GFRP bars was not significantly affected by the different exposure conditions.

Mufti et al. (2007) conducted an investigation addressing the issue related to the in-situ alkali resistance of GFRP reinforcing bars. Concrete specimens reinforced with GFRP bars were extracted from five different demonstration structures located in North America. GFRP bars made with E-glass and vinyl-ester resin were embedded in concrete for 5 to 8 years and exposed to a wide range of environmental conditions. These samples were extracted from actual structures and sent to different research laboratories to perform analysis on the physical and chemical composition of the bars. All research laboratories concluded that there was no degradation of the GFRP bars embedded in the concrete structures. However, it should be noted that no mechanical tests were conducted to assess potential loss in capacity.

3.4.3 Prediction models from the literatures

There are several prediction models for the residual strength of GFRP bars currently available in the literature. The methodology used for the accelerated ageing tests is based on the Arrhenius principle, which uses high temperature as the accelerating agent for the degradation of the material in a given environment. The Arrhenius empirical model is one of the oldest and most widely used models to predict the time of failure of a material as a function of temperature. Katsuki and Uomoto(1995) reported that the Arrhenius equation offers a good correlation between the temperature and the rate of diffusivity and chemical reaction. This model is shown as follows:

$$t_f = A \times e^{(\frac{\Delta H}{kT})} \qquad \text{(Eq. 3.1)}$$

where t_f is the real time of failure, T the temperature in Kelvin at the time of failure, k the Boltzmann constant (8.617×10^{-5}/K), A the acceleration factor determined graphically from the acceleration tests, and ΔH is the activation energy factor.

Litherland et al. (1981) correlated the data of accelerated ageing tests in the laboratory with the natural ageing of glass fibers in an alkaline environment and have correlated their data with natural weathering samples of about 12 years. The following factors were taken into account in Litherland's method: (1) the annual average temperature was used; (2) no load was applied to the sample; (3) the FRP manufacturing process and the type of resin slow down the fiber degradation. Consequently, a shift factor must be introduced on the time scale when the data are interpreted.

Dejke (2001) used this approach to generate a relative time shift factor(TSF). The time shift method is based on the assumption that the rate of strength retention at different temperatures can be described by the Arrhenius equation. He proposed using the TSF to transform the time in the accelerated test to actual service lives for GFRP reinforcement. The time shift factor (TSF) was proposed as follows:

$$TSF = \frac{t_1}{t_2} = \frac{c/k_1}{c/k_2} = \frac{A \times e^{\frac{-Ea}{RT_2}}}{A \times e^{\frac{-Ea}{RT_1}}} = e^{\frac{E_a}{R}(\frac{1}{T_1} - \frac{1}{T_2})}$$

(Eq.3.2)

Where, T_1 and T_2 are the exposure temperature (in Kelvin) and $t_1$and t_2 are the times required for a certain decrease in some mechanical property at temperatures T_1 and T_2, respectively.

Using Arrhenius' principle, Vijay and GangaRao (1999) proposed a correlation formula between the accelerated ageing in the laboratory and the natural aging on the field. The formula developed for GFRP reinforcements conditioned in aqueous and alkaline solutions is as follows:

$$\frac{N}{C} = 0.098 \cdot e^{0.0558T}$$

(Eq. 3.3)

Where, N is the in-service field performance in day and C is the accelerated exposure age (in day) in the laboratory with the temperature of T. This correlation model was developed for the climatic conditions of Northeastern US, specifically in the state of West Virginia (average annual temperature of 53°F(11.7°C). According to this equation, 104 days of exposure at 140°F(60°C) correspond to 69 years of service life in standard concrete subjected to an annual average temperature of 53°F(11.7°C).

3.5 Research on concrete members reinforced with GFRP rods

Various concrete reinforcement with FRP bars, including Glass, Aramid and Carbon fiber, have been extensively conducted to investigate the strength, serviceability and long-term behaviors. Flexural tests of concrete beams reinforced with FRP reinforcing bars were conducted on investigating whether conventional theory concerning flexural behaviors of beams can be applied to new FRP rebar systems. Results have indicated the possibilities of concrete

beams reinforced with GFRP as the replacement of traditional concrete beams with steel bars even a decade ago [Benmokrane et. al, 1996 and Challal et. al,1996].

The analytical and experimental studies for environmental durability of the FRP material itself for civil infrastructures were reported [Karbhari et.al, 1998 and 2003]. The results of these studies showed not only the relationship between degradation and matrix/fibers interface but also the effects of moisture and alkalis on GFRP bars. That is, these studies demonstrated that the durability of the composites is affected by increase of water temperature and water absorption under the influence of combined moisture and temperature for a short duration. Moreover, the authors also suggested coefficient of reduction dropping strength of the composite materials after short and long terms of exposure.

A correlation formula between accelerated weathering in the laboratory and natural weathering in the field was proposed [Vijay et. al,1999]. An accelerated aging methodology predicted the degradation in the mechanical properties of FRP under the given duration and its relationship with the natural aging. Absolutely, this project was conducted not for FRP re-bars embedded in concrete but for FRP bars them-selves. In aggressive environment, however, FRP will degrade even in the embedded condition providing pre-cracking. This may result in structural degradation on concrete structures reinforcing with GFRP bars. Moreover, studies conducted in United Kingdom showed that the long-term strength of glass fiber reinforced cement (GRC) in any climate can be predicted by using accelerated aging methodology [Litherland et.al, 1981]. This method demonstrated the validity of using accelerated tests with real natural aging of composites to predict long-term behavior. Durability tests of GFRP composites were conducted under the elevated temperatures and environmental exposure as methods to accelerated aging [Porter et.al, 1998]. This study also indicated positive correlation between accelerated aging data and specimens subjected to real time exposure.

To investigate field applications for long-term performance of concrete reinforcement with GFRP bars, flexural test of beams reinforced with GFRP bars was conducted after

exposing those to accelerated and real-time conditionings of up to three-years subjecting to a constant sustained moment [Vijay et.al, 1999]. This project introduced that changes in bar modulus and strength after conditioning are negligible and bar force at onset of free-end slip is not influenced by the duration or the type of conditioning. Similarly, the study approved by ISIS Canada showed that there was no degradation of the GFRP in the concrete of structures exposed to natural environmental conditions for duration of five to eight years.

Although these studies are considered to be important in the evaluation of long-term performance of reinforced concrete with GFRP bars, however, few studies have been reported on the long-term performance of reinforced concrete with GFRP bars subjected to simultaneous sustained loading and aging effects of both temperature and humidity in terms of both stiffness/strength degradation and correlation between accelerated and natural aging.

3.6 Durability of bond performance of GFRP bars

FRP materials are an isotropic and characterized by high tensile strength only in the direction of the reinforcing fiber and the transverse coefficients of thermal expansion (CTE) controlled by the resin is up to three to six times the CTE of the concrete. This anisotropic behavior should affect the bond performance of FRP bars when embedded in concrete and these effects need to be evaluated [Masmoudi et al.2011]. The bond's long-term durability also plays a critical role in the long-term performance of concrete structures using internal FRP reinforcement [Davalos et al, 2008].

Considerable researches have been conducted on the bond behavior of FRP bars in concrete and durability performance of the bond between concrete and FRP bars. The reported results in the literature showed varied bond strengths and behaviors because of differences in material properties of FRP bars and used test methods. Porter and Barnes(1998) found that the pullout bond strength of GFRP bars did not decrease when testing bars embedded in concrete and aged in solutions at a temperature of 60°C. Bakis et al. (1998) showed that, after 28 days of

immersion in a saturated $Ca(OH)^2$ solution at 80 °C followed by 5 days of drying, the ultimate bond strength of GFRP bars embedded in concrete did not decrease, although material degradation of GFRP bars was observed. On the other hand, Robert et al.(2010) reported that the bond strength of GFRP bars decreases as the duration of immersion increases. Even at high temperature (50°C), when the environment is more aggressive, the change in bond strength remained still minor. Recently, the result that conditioning different types of GFRP bars embedded in concrete in water at room temperature and 60 °C reduced the bond by about 20% was found by Davalos et al.(2008).

Even so, the general bond characteristics of FRP bar can be summarized as follows. The durability of bond properties of FRP bars (with surface deformations) is evaluated to be highly influenced by the surface geometry of the bar and transverse properties of the FRP bars [Bakis et al. 1998]. As an economical and simple solution for the evaluation of bond performance, pullout test is widely adopted, but it usually results in un-conservative bond strength values. This is because of the compressive stress induced in the surrounding concrete (usually under tension in practical conditions) and the confining action of reaction plate developed in the test specimen. The splitting of concrete during pullout testing is usually avoided by providing relative large volume of concrete surrounding the bar.

3.6.1 Test method

American Society for Testing and Materials (ASTM) originally developed the standard concentric pull-out test, ASTM C 234, for comparison of different concrete mixtures, not to assess bond strength. When used for the characterization of bond, the concentric pullout test offers the advantage of simplicity but presents two disadvantages:

- The concrete is subjected to compression at the loading face,
- The concrete surrounding the reinforcing rebar tends to split.

Pullout tests were performed on glass and carbon FRP rods embedded in cylinders and prism by Gangarao et al.(1991). The FRP strands made with seven twisted rods showed bond strength values comparable to that of a conventional 7-wire steel strand. Pultruded glass (and some aramid) FRP rods with surface deformation (i.e., helical wrap) were used for pull-out tests from concrete cylinders

The cantilever beam test and the other flexural-type tests solve some of the stress field discrepancies of the concentric pullout tests. Flexural-type complicates the setup as well as the modeling of the phenomenon. Flexural-type tests can be used to determine not only bond strength but also crack width and crack spacing. Flexural-type tests have been used extensively for conventional RC type. In particular, the cantilever beam test has been used recently to evaluate the performance of epoxy-coated steel reinforcement. Vijay et al.(1999) used ribbed and sand-coated glass FRP rods in pullout as well as cantilever-type beam specimens to determine bond properties.

3.6.2 Bond behavior of FRP at environmental aging

Tannous et al. (1998) investigated that an evaluation of tensile strength and moisture content of GFRP rebar placed in corrosive chemical solutions that simulated exposure in the field. Test variables included seven chemical solutions and two matrix materials (polyester and vinyl-ester). Results showed that the vinyl ester showed lower diffusivity and better resistance to chemical attack than polyester and the degree of deterioration depends on the constituents materials and the quality control in the manufacturing process.

Hamidah et al. (2007) investigated water and alkali absorption of AFRP rebar in aggressive solutions. They noticed weight change and scanning electron microscope of specimen placed in acid and alkali solution and water. The results showed that AFRP rebar is durable in alkaline and water and degradation occurs due to swelling of the rebar.

Long-term durability of GFRP rebar with vinyl-ester resin was investigated by Nishizaki et al. (2002). They studied the effects of water and moisture on the durability of bare GFRP rebar at various temperatures. Cracks shown on the surface of the GFRP and the weight of the materials decreased were observed as the results. Also, bending strength of the GFRP was found to be reduced.

Effect of environmental conditioning on bond properties of GFRP rebar to concrete was also studied by Bank et al.(1998). They performed pullout test of embedded GFRP rebar specimen in order to measure changes in bond properties. Test variables included different surface type of GFRP rebar (round, deformed, helically wrapped and sand coated bar) and two matrix materials (poly-ester and vinyl-ester). Environmental conditioned specimen submerged in a tank of water for 14 days, 84 days at 80℃. The conclusion of this study was that a good correlation has been found between material degradation and the decrease in bond strength and stiffness properties of GFRP rebar. Both the poly-ester and the vinyl-ester matrix bars showed polymer resin degradation [Moon, 2005]. However, not only the degradation was much more severe in the case of polyester resins, but also radial and circumferential cracking in the resin matrix is seen in all bars.

3.7 Deformability and ductility

Conventional definition of ductility is based on its capacity to absorb energy without critical failure and is generally related to the amount of inelastic deformation taking place before complete failure [Park et al, 1975]. Ductility can be expressed quantitatively as the ratio of the total deformation at failure to the deformation at the elastic limit because conventional steel reinforced beams have a distinct elastic and inelastic phase of deformation before and after yielding of steel. Ductility is an important attribute of materials in that visible deformations can occur if the loads become too large, thus providing an opportunity to take remedial action before fracture occurs. This is particularly important for the performance of structures in high seismic

regions where structures must undergo large cyclic displacement without structural collapse [Priestley et al,1996]. Because of its significance, ductility must be quantified. The conventional ductility factors are often mathematically defined below:

$$\mu_{\phi} = \frac{\phi_u}{\phi_y} or \mu_{\theta} = \frac{\theta_u}{\theta_y} or \mu_{\Delta} = \frac{\Delta_u}{\Delta_y} \qquad \text{(Eq.3.4)}$$

where μ is the ductility index, ϕ is the curvature, θ is the rotation and Δ is the deflection. The subscript y stands for yield and u stands for ultimate. Thus, μ_{Δ} would be the ratio of deflection at ultimate to the deflection at yield [Naaman et al ,1995].

Unlike steel, however, FRP material is brittle in nature with linearly elastic behavior up to failure although it has advantages such as corrosion resistance, high-strength, non-conductivity and light weight. This way of estimating ductility is inappropriate for concrete structures reinforced with FRP because the behavior of them is linear until failure. Since concrete flexural beams reinforced with FRP exhibit also substantial deformation prior to failure despite the fact that FRP does not yield unlike steel, the term of deformability was introduced by researchers as a means of assessment of ductility that occurs before failure. It is for this reason that many researchers and design codes have suggested other measures which are collectively referred to as pseudo-ductility measures. Bakis et al. (2001) in their paper on GFRP in concrete structures identified that the major measure of pseudo-ductility is the deformability index. The index is a ratio of the ultimate deflection and the service deflection and the same can be done with curvatures as well.

Ductility of a GFRP reinforced beam depends on uniform elongation of FRP bars at different locations as compared with localized steel bar yielding, confinement effect, uniform crack location and spacing in the case of FRP reinforced concrete beams, the bond between bar and concrete, the plastic hinge formation in concrete and frictional force development along diagonal and wedge cracks [Vijay et al, 2001]. To understand the energy absorption in GFRP reinforced concrete sections, load versus deflection of each beam under progressive loading

and unloading in five to seven cycles was noted with each cycle resisting a higher load than the previous cycle. Relative to previous cycles, an increase in the amount of energy absorption was observed during final cycle of loading in a compression failure. DFs for compression failures were observed to be in the range of 6.70 to 13.90, whereas for tension failures, the ratios were observed to be in the range of 5.80 to 6.78. These values may differ with extremely low or high reinforcement ratios [GangaRao et al, 2001]

3.7.1 Energy based approaches

Naaman and Jeong introduced an energy-based deformability index (the Naaman Index) to compute the ductility index of μ_e for beams reinforced or prestressed with FRP tendons as seen in Eq.3.4.

$$\mu_e = 0.5(\frac{E_T}{E_{el}} + 1) \qquad \text{(Eq. 3.4)}$$

Where E_T is the total energy which is area under load-deflection curve and E_{el} is the elastic energy which is area of the triangle formed at the failure load by a line with the weighted average slope of S as illustrated in Figure.3.3. It is suitable for beams with steel as well as FRP reinforcement, thus providing a common basis for comparison.

Grace proposed four parameters in equation 3.5 in order to account for the influence of type of reinforcement (main bars and stirrups), failure mode of the beam, modulus of elasticity and failure strength of the reinforcement on the slope S.

$$S = \alpha\beta\gamma \frac{E_f}{E_s} \frac{f_y}{f_{ds}} \frac{P_1 S_1 + (P_2 - P_1) S_2 + (P_3 - P_2) S_3}{P_3} \qquad \text{(Eq.3.5)}$$

where, α is stirrup factor (GFRP=0.95), β is failure mode factor (Compressive factor=1.0), γ is factor that depends on the type of reinforcement(GFRP=4.0), E_f is FRP modulus of elasticity, E_s is steel modulus of elasticity, f_y is steel yield strength and f_{ds} is design strength of FRP. The

above energy-based deformability index is dependent on the ratio of total energy to the elastic energy at the failure state of a beam.

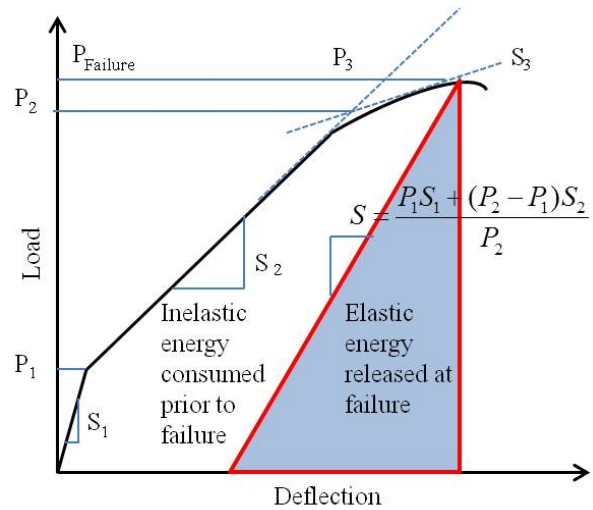

Figure 3.3 Ductility index by Naaman and Jeong

3.7.2 Moment and deformation based approaches

The moment-deformation based model (the Jaeger index) was introduced by Jaeger et al. taking into account the strength effect of moment as well as the curvature (or deflection) effect on the ductility. For the deformability of the Jaeger index, margin between the service stage and the ultimate stage reflect the ductility. Moment and curvature at ultimate state are used as well as the moment and curvature at service state. The service limit stage corresponds to the value at concrete compressive strain of 0.001 considered as the beginning of inelastic deformation of concrete top compression fiber.

$$\mu_E = \left(\frac{\varphi_u}{\varphi_{0.001}}\right) \times \left(\frac{M_u}{M_{0.001}}\right) \qquad \text{(Eq. 3.6)}$$

Where M_u and φ_u are the moment and curvature at ultimate stage; $M_{0.001}$ and $\varphi_{0.001}$ are the moment and curvature at service stage respectively.

Subsequently Zou introduced a deformability index for FRP prestressed concrete beams (the Zou Index) defined in terms of both a deflection factor and a moment factor [Au et al.,2008]. The deflection factor is the ratio of the deflection at failure to that at first cracking, while the moment factor is the ratio of the ultimate moment to the cracking moment. The Zou deformability index Z appears as

$$Z = \mu_E = \left(\frac{\Delta_u}{\Delta_{cr}}\right) \times \left(\frac{M_u}{M_{cr}}\right) \qquad \text{(Eq. 3.7)}$$

3.7.3 Deflection based approach

Abdelrahman et al. (1995) established a deformability model based on deflection for beams prestressed by FRP tendons. This Abdelrahman deformability index (the Abdelrahman Index) $A_b$is expressed as the ratio of the maximum Δ_u corresponding to the failure or maximum load to the equivalent Δ_1 of the uncracked section at a load equal to the ultimate load [Au et al.,2008].

$$A_b = \frac{\Delta_u}{\Delta_1} \qquad \text{(Eq. 3.8)}$$

Figure3.4 shows the equivalent deflection Δ_1 and failure deflection Δ_u. According to Abdelrahman et al.(1995) , this definition overestimates ductility for prestressed concrete beams with steel. This method represents the bilinear elastic deformation of beams pre-stressed by FRP and is different from the traditional ductility evaluation in terms of the inelastic deformation of the system prior to collapse [Au et al.,2008].

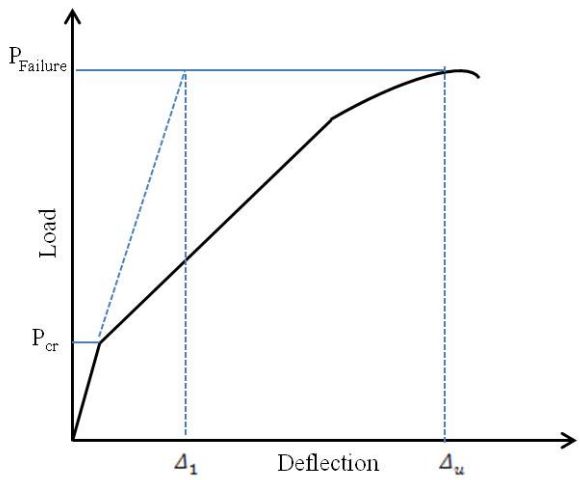

Figure 3.4 Equivalent deflection Δ_1 and failure deflection Δ_u

For example, the moment-curvature and load-deflection of the GA3-5-300 specimen plots are shown below in Figure. 3.5. The deflection under service load levels was estimated at concrete compressive strain of 0.001 considered as the beginning of inelastic deformation of concrete top compression fiber.

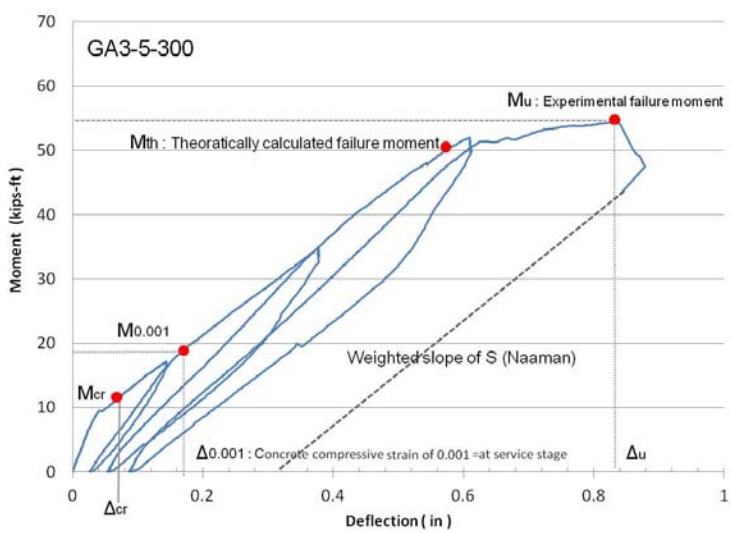

Figure 3.5 Load-deflection curve for deformability indices

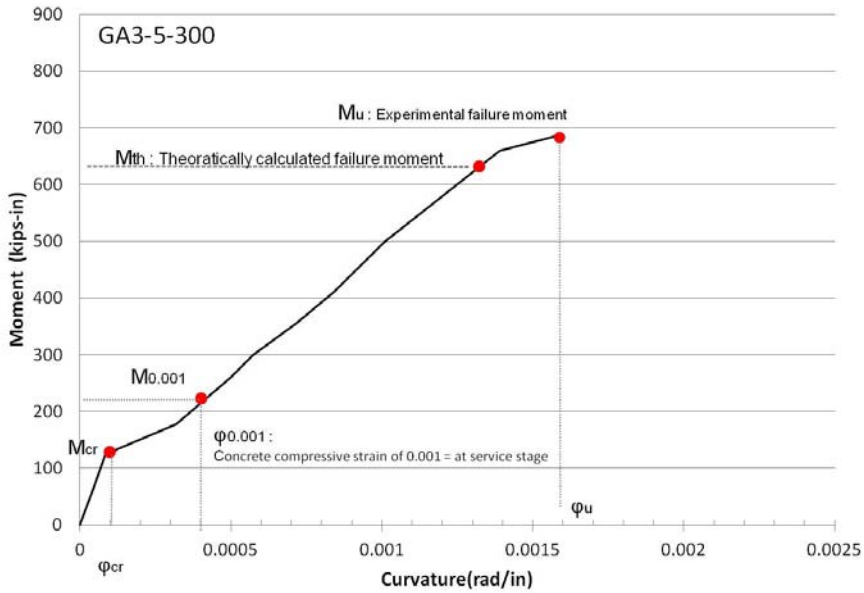

Figure 3.6 Moment-curvature curve for deformability indices

3.8 Acoustic emission

Every structure or component in the real world always has some imperfections and can be damaged by exposure under chemical or mechanical attack. Chemical attack such as deicing salt and alkaline environment usually occurs in concrete beams reinforced with GFRP and steel bars. It can take the form of permeation, chemical changes, and dissolution of rebars. The permeation in FRP can cause blisters, swelling, debonding, and softening of resin. The chemical changes can cause softening of the resin or cracking at the surface. The dissolution removes the resin, and leaves fibers hanging down from the laminate [Niesse and Ahluwalia, 2001]. FRP material and steel are very sensitive to environmentally induced degradation in terms of environmental aging. Temperature and moisture can degrade the resin. The effect includes changing the color, initial softening and later hardening of resin [Niesse and Ahluwalia, 2001].

The damages and imperfections in a structure may or may not be harmful or visible. Therefore, nondestructive inspection (NDI) or nondestructive evaluation (NDE) or nondestructive testing (NDT) can be performed to ensure that structures can be safely operated for a certain period of time. In general, the roles of NDT are to help detect, locate, and evaluate the significance of the flaws in in-service structures [Atitavas,2002]. Recently several nondestructive methods have been applied to investigate damage levels of structural components. The AE technique, a nondestructive method that is relatively easy to install and is capable of predicting the damage location, is used in this study.

AE is defined as "the class of phenomena whereby transient elastic waves are generated by the rapid release of energy from localized sources within a material, or the transient waves so generated" [ASTM E1316 and Atitavas, 2002]. Acoustic emission is generated by the material itself, unlike other types of stress wave nondestructive testing techniques such as impact echo and ultrasonic, which require external input sources [Atitavas,2002]. Depending on the type of material, the source of AE can be generated from many phenomena of the materials. For example, AE sources can be from dislocation movements, cracks, fractures, and even corrosion in case of metals. In concrete, micro-cracking and macro-cracking as well as debonding or movement of reinforcement can cause emissions [Carey ,2002]. For composites, AE comes from matrix cracking, delamination, debonding of the matrix from the fibers, fiber breakage, and fiber pullout [Fowler, 1979]. In addition to internal acoustic emission sources, external noise (background noise) such as mechanical rubbing, wind, air hoses, and moving trucks can create elastic waves, which interfere with the genuine data [Atitavas,2002]. These background noises have to be prevented or filtered out before the AE data is analyzed [Bray and Stanley, 1997]. Definitions and Terminologies of acoustic emission signatures will be mentioned in Chapter 8.

3.8.1 Acoustic emission applications

The acoustic emission technique has been recently used to evaluate the integrity of a structure since AE is emitted from a structural damage/imperfection earlier than from unflawed material. The time of flight of the stress wave can also be used to identify the location of the source [Promboon, 2000]. Not only acoustic emission has been used to investigate many types of structures such as bridges, pressure vessels and storage tanks, but also has been used with a variety of material such as steel, concrete, composites. As a result, AE standards have been established and developed. The advantage of AE is that it is a global method rather than a local method meaning that the technique monitors a large area of the structure, rather than a small local area. As a result, the monitoring can be done within a short period of time and, is not labor intensive [Atitavas, 2002].

3.8.2 Research on acoustic emission signatures

Mirmiran et al.(2000) carried out the acoustic emission response of concrete beams reinforced with GFRP under bending. The FRP-RC beams emitted higher activity and peak amplitude than their steel-RC counterparts. They also had lower felicity ratios, showed higher activity at each load drop, and emitted signals even during the unloading process. These characteristics were attributed to the lower stiffness, larger deflections, and brittleness of FRP re-bars, as well as their lower bond strength with concrete.

Chen et al.(1992) investigated the acoustic emission activity in (1) FRP bars of different size under direct tension (2) bonding behavior between FRP bars and concrete (3) reinforced concrete beams under bending. In this research, crack initiation and crack propagation due to bending load were monitored for acoustic emission activity and compared with visual observations. Monitoring AE activity was a viable method of determining active crack growth in RC beams was determined. It was indicated that the AE events versus time (or load) relationship can tell us the unusual events occurring inside a structure. Different AE results were

obtained from the same kinds of bars. They also reported that the AE technique could be useful in detecting the time and the stress intensity of de-bonding between the FRP re-bars and concrete.

In the experiments at the University of Texas at Austin on carbon fiber composite pipes, Ramirez et al.(1983) showed that AE hits with amplitude of 40-60 dB and duration of 2,000-10,000 microseconds were from delamination, whereas lower amplitude events were from matrix cracking. It was also found that the carbon fiber composites gave more 100 dB hits than the glass fiber composites, from which they concluded that the carbon fiber's diameter is smaller than the glass, it is believed that amplitude is more related to the stiffness of the strand than to its size. In addition, the waveform of the hits were recorded and they showed that delamination can be associated with low amplitude, long duration, and frequency, while fiber breakage yielded high amplitude, short duration, and a wide range of frequencies.

The Kaiser effect has been applied as to know the initial stress condition of rock materials [Yoshikawa et al, 1989], Based on the Kaiser effect, it was proposed the Felicity ratio, which can show the damage quantitatively in tank structures [Fowler, 1986]. The felicity ratio was established because of the following fact. The Kaiser effect can only hold in the stable condition of the materials. As progress the internal instability, the Kaiser effect is gradually breaking down. As a result, AE activity starts to be observed even under lower stress than that of the maximum stress experienced. The Felicity ratio is defined as;

$$\text{Felicity ratio} = \frac{P_{AE}}{P_{1st}} \qquad \text{(Eq.3.9)}$$

where P_{AE} is a stress at which AE activity starts to generate, and P_{1st} is the maximum stress. The Felicity ratio becomes equal to or larger than one in an intact or stable state, while in a damaged condition it reveals smaller one. When damage occurs in a structure under an applied load, there will be some energy release. Part of this energy is transformed into the acoustic

emission. Thus, the energy of the hits is directly related with the severity of the damage [Bray and Stanley, 1997]. Therefore, signal strength has become an important parameter for AE applications. As the load increases, more damages occurred, and the graph of cumulative signal strength versus load generally shows the rise of the curve [Atitavas,2002].

Yun et al.(2010), in this study, the applicability of acoustic emission techniques to monitor damage evolution in reinforced concrete beams strengthened in flexure with carbon fiber reinforced polymer (CFRP) sheets is investigated. From the results of this study, the signal characteristics – event, amplitude versus frequency, and amplitude versus duration – show clear differences in the different loading stages, depending upon the active damage mechanism. The b-value is correlated to the fracture process of the RC beams bonded with CFRP sheets and the degree of localization of damage. The AE technique is a useful nondestructive technique for monitoring the behavior of RC beams that are externally reinforced in flexure with CFRP sheets.

Sagar et al.(2011) carried out the experimental tests of notched three point bend specimens (TPB) under crack mouth opening displacement (CMOD) control at a rate of 0.0004 mm/s. Acoustic emissions were simultaneously monitored during the fracture process. It was observed that AE energy could be related to fracture energy. An experimental study was done to understand the behavior of AE energy with parameters of concrete like its strength and size. In this study, AE energy was used as a quantitative measure of size independent specific fracture energy of concrete beams and the concepts of boundary effect and local fracture energy were used to obtain size independent AE energy from which size independent fracture energy was obtained.

CHAPTER 4

TENSILE TESTS: CORRELATION OF ACCELERATED AND NATURAL AGING OF GFRP/ STEEL BARS

4.1 General

GFRP composites are simple and economical structural materials for rehabilitating deteriorating infrastructure facilities, and for reinforcing the new construction. However, it has been reported that glass fibers are known to degrade not only in the presence of water, acidic but also when placed contact with cements used in concrete. Degradation in alkaline solution is most severe. Therefore, commercial use of GFRP products is seriously hindered by lack of field or experimental data and lack of understanding of durability aspects under long-term weathering such as alkaline and deicing chemical exposure and sustained loading of live loads.

Objective of this study is to perform accelerated aging tests for establishing durability of GFRP bars and understanding long-term behavior of GFRP reinforced concrete members, including strength and stiffness degradation rates due to physical and chemical aging. In this chapter, results of accelerated aging of GFRP bars embedded in real concrete exposed to specific humidity level, temperatures and sustained stress are presented. Aging results are calibrated using natural weathering data obtained by other researchers [Litherland,1981 and Vijay, 1999]. Steel reinforcement is covered as a benchmark specimen of traditional one.

4.2 Materials

Two types of FRP bars were used in this study. ASLAN 100 provided by Hughes Brothers Inc. and VROD-HM by Concrete Protection Inc. were selected on the basis of wide applications of their products and studies reported in various publications. ASLAN 100 is a vinyl

-ester Matrix GFRP Rebar(E-glass fiber) with helically wrapped surface and binding material of VROD-HM(E-glass fiber formulation) is composed of vinyl-ester resin formulation with a sand coating that promotes bond adhesion of bar to concrete. ASLAN 100 is widely often used in industry while VROD-HM is a new product in development. Table.2.3 and Table.2.4 in chapter 2 show material aspects and properties provided by their manufacturers.

In the part of concrete mixtures, Table.4.1 shows the mix-design and 28-days compressive strength of the concrete.

Table 4.1 Concrete mix design (lbs /yr^3)

	W/Cm*	Portland Cement (Type- II)	Fly-ash	Coarse-aggregates (3/4 in)	Fine-aggregates	Water	Water reducing admixture	28-days, compressive strength (psi)
Mix	0.48	451	113	1750	1455	268	8	4000

* Notes : W/Cm= water to cementitious materials ratio

4.3 Accelerated conditioning

Accelerated test methods which widely used to predict the durability of FRP reinforcement in concrete is to immerse bars in alkaline solutions, and then test the mechanical properties. Many studies have shown the validation of this method to accelerate the aging of FRP bars. However, it has been reported that a pure alkaline solution is a more aggressive condition than that of real concrete. [Dejke,2001]. Moreover, the accelerated test method of immersion in alkaline solutions cannot explain the neutralization of concrete by increasing of exposure duration.

In this study, specimens have been subjected to not alkaline solution but real concrete of cement mortar paste. Fabrication procedures of tensile specimens for accelerated aging conditioning are shown in Figure.4.1. Figure.4.1 (a) shows the fabrication of tensile specimens casted into concrete with the clear cover of 1in. Concrete cover as protection of reinforcement

against weather and the other effect is measured from the concrete surface to the outermost surface of the reinforcement to which the cover requirement applies.

Figure 4.1 (a) Fabrication of tensile specimens embedded in cement mortar paste
(b) Initial cracks (c) Simulation of the chemical environment (saline)
(d) Sustained loading at Chamber and steel grip based on ASTM D7205

According to the ACI 318-11, concrete cover for reinforcement shall not be less than 1-½ in for No. 5 bar and smaller ones in the case that concrete exposed to earth or weather as shown in Figure.4.1 (a). The clear cover of 1 in was used to expose into harsh conditions.

With respect to cracking, Vedalakshmi et al.(2008) concluded that load-induced cracking does affect the corrosion initiation of the reinforcement in structural concrete and it is almost certain that the corrosion initiates at the cracked sections of reinforced concrete structural members. To make the specimens exposed to penetration of chlorides, humidity and temperature as harsh environmental conditions, initial cracking of concrete cover was adopted with same sizes at service loading level compared with flexural tests of beams. According to the data of prototypes, the crack widths of beam specimens covered in chapter 5 were observed from 0.004 to 0.007in at service loading level assumed as $0.25P_u$, where P_u is the calculated load-carrying capacity of the beam. The factor of 0.25 is based on the normal loads carried by a structural concrete member under service condition [Tan et al, 2009]. In order to simulate initial crack of 0.005in before exposing in the saline solution (3%) and accelerated aging chamber, preloading was conducted by MTS-100kips. By using a portable microscope and high resolution handheld microscope (the Proscope), the cracks were measured as shown in Figure.4.1 (b). Figure.4.1(c) shows that, after simulating cracks, salt solution consisting of 3% sodium chloride and 97% tap water was used for chemical conditioning of de-icing salt. This solution with chloride ion (Cl^-) concentration of 1.23mol/L was to simulate concrete pore solution contaminated with chloride ions from deicing salts. Moreover, the aging was accelerated by using two different constant temperatures of 115˚F(46˚C:average outdoors temperature in DFW from August to September) and 79˚F(26˚C: average outdoors temperature in North Texas from January to December). For specimens placed in the weathering chambers (Chamber A: 79°F and RH=80% / Chamber B: 115°F and RH=80%), the sustained bending loads were used during environmental conditionings. It was shown in Figure.4.1 (d). The sustained loads to cause the same strain in beam specimens at service level were 192lbs (8-concrete bricks) with the 500με of strain. The conditioned specimens were exposed for 100, 200 and 300 days in the chambers. After exposing, the concrete was removed to make tensile specimens based on ASTM D7205.

4.4 Mechanical tensile test

To evaluate the durability performance of FRP bars, unconditioned and conditioned specimens were tested for tensile strength. The above mechanical properties described in chapter 2 have been selected on the basis of the following considerations. FRP bars embedded in concrete should meet two basic requirements: (1) the tensile strength must be enough to carry the desired tensile force (Chapter 4); (2) the bond strength between FRP bar and concrete must be sufficient to transfer the load (Chapter 5).

The test methods for tensile properties of FRP bar can be observed in ACI 440.1R-06-Section.8 [ACI 440, 2008], ASTM D3916 and ASTM D7205/7205M. However, an adequate testing grip should be used in that stress concentration in and around anchorage on the tensile test specimen makes the determination of FRP strength complicated in order to avoid premature failure. In ASTM D3916, an aluminum alloy grip adaptor is suggested to avoid localized premature failure due to the low transverse strength of FRP bars. However, a few published reports showed the an aluminum alloy grip adaptor suggested in ASTM D3916 was difficult to adopt in some cases where the tensile strength is high and the transverse strength is relatively low [Chen, 2007]. According to ASTM D7205/7205M, the ratio of free length between the anchors and the effective bar diameter should be not less than 40 times to avoid effect of the free length on the tensile strength of bars. A schematic diagram of the tension test specimen is shown in Figure 4.2. The internal diameter of the grips was greater than the external diameter of the bar to be tested. The steel tubes were filled with expansive cement grout (SHEP-ROCK) as the anchor filler materials. SHEP-ROCK is a scientifically formulated non-metallic pourable anchoring cement and grout. It is rapid setting, expansive and a non-shrink hydraulic cement with controlled expansion. It was self- leveled when mixed with water to a pourable consistency. Its controlled expansion grips the material to be anchored, locking it into place. The material properties of it are described in Table 4.2 below.

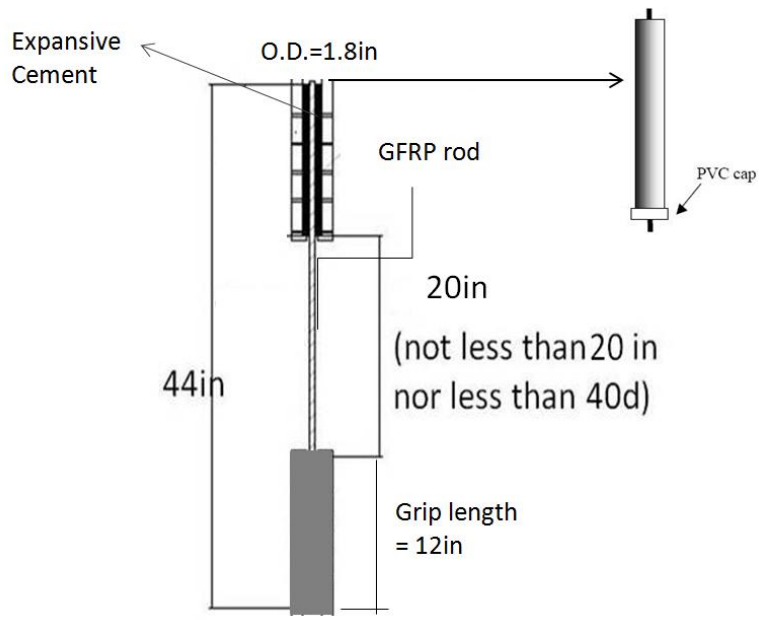

Figure 4.2 Schematic diagram of a tension test specimen

A minimum of 24 hours curing time was allowed for the resin to set before the specimens were tested. Length of the grips was based on the diameter of the bars tested as shown in Table 4.3.

Table 4.2 Technical data of the expansive cement grout : (SHEP-ROCK)

Technical data	Description
Initial Set	17 minutes at 75 degrees
Final Set	45 minutes at 75 degrees
Expansion	0.30%
Compressive Strength (ASTM C 109, Air Cured):	
1 day	10,920 psi
7 days	11,060 psi
Pullout Strength : (1 inch diameter bolt anchored in 1.5 inch diameter hole)	
3 days	35,650 psi

The free length between the anchors should be not less than 15in (380mm) nor less than 40 times the effective bar diameter (d). Table.4.3 gives different specimens tested for tension in this research. The test was carried out in a Material Testing System (MTS) machine

with the loading rate of 0.2in/min (0.0033in/sec). The loading time for the test was 2–4 min for GFRP Bars.

Table 4.3 Length of steel grips used for tension tests (ASTM D7205)

Internal diameter of the test specimens (in)	Minimum length of steel tube grip (in)	Minimum free length of specimens (in)
0.375(#3)	12	15
0.500(#4)	15	20
0.625(#5)	15	25
0.750(#6)	18	30

After the specimens were exposed in the accelerated aging conditions, the GFRP and steel bars were tested in tension to evaluate their mechanical properties. The mechanical properties of the GFRP and steel bars were evaluated using an Universal Testing Machine (MTS and Baldwin) of 400kips capacity. A purpose-built extensometer was utilized to measure the elongation in the bar as shown in Figure 4.3. A linear variable displacement transducer (LVDT) was installed to verify the elongation of the sample. Because of the potential for a large amount of slip between the jaws of the machine and the couplers to occur at the high loads required for failure, the LVDT was also used to calibrate the jack position readings. Subsequent tests on used strain gauges instead of LVDTs as they proved to be more accurate in determining the elongation of the bars. The load and elongation data were recorded using a computerized data acquisition system (Vishay DAQ) at pre-determined load intervals till failure of the specimen occurred. The data so generated were utilized to plot stress and strain diagrams for each of the tested specimens. The stress-strain diagrams were utilized to determine the yield and ultimate strength of the GFRP and steel bars. The elongation, due to the applied load, was measured after the completion of the tensile test and it was expressed as a percentage of the original gauge length. The tensile tests were conducted on both non-conditioned (as control specimens) and conditioned GFRP/steel bars so that the influence of

accelerated aging conditions on the tensile properties of GFRP and steel bars could be assessed.

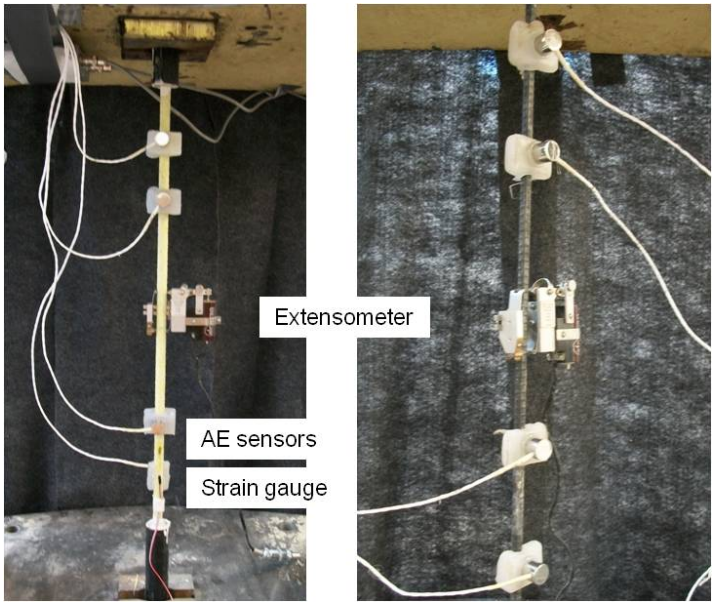

Figure 4.3 Experimental setup for tensile strength test

4.5 Tensile test results

4.5.1 Failure mode

Chen (2007) investigated that small white blister were observed on the external surface of GFRP bar after exposure into alkaline solutions with different temperatures (40 and 60 °C). Similarly, whitening was observed in both types of GFRP rebars casted in cement mortar paste after environmental exposures as shown in Figure 4.4. Figure 4.4 also shows the corrosion level of steel bars exposed to environmental conditions in chambers

Tensile tests were performed on the No.3 GFRP bars (Type-A and Type-B: diameter =3/8 in) and steel bars to obtain the ultimate tensile strength, modulus of elasticity and the stress-strain behavior. Tests were performed on plain specimens, unconditioned but incased in cement mortar paste (natural exposed specimens) and conditioned and incased specimens for 79°F(26°C) and 115°F(46°C). All tensile test specimens of GFRP rods exhibited fiber rupture in

the gauge length. This confirmed that the alignment of the rods and grip system used worked successfully. The modulus of elasticity was measured by taking the gradient of the linear relationship between stress and strain. The strength was defined as the maximum load divided by the initial cross section of the rod.

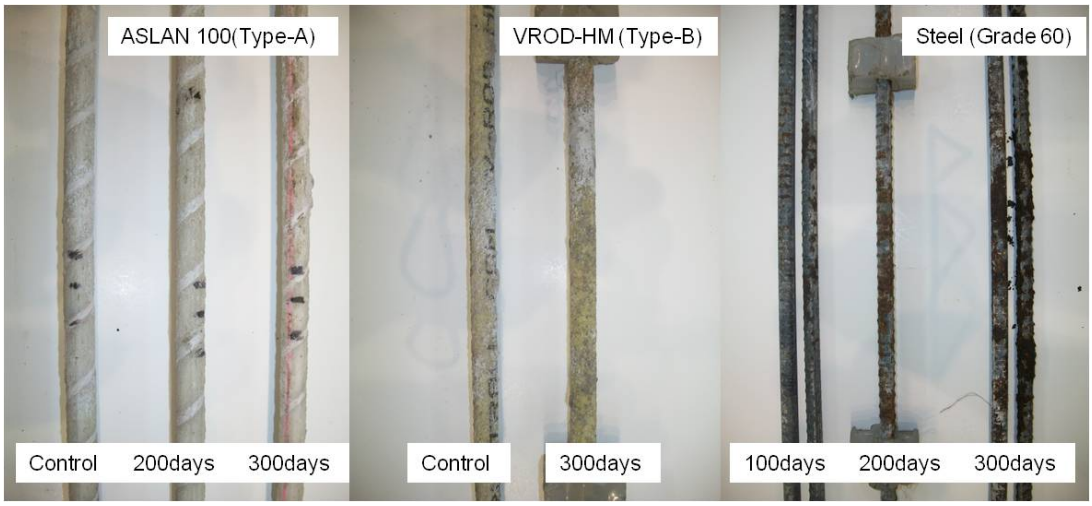

Figure 4.4 Visual inspection of surfaces of rebars after accelerated aging

The tensile stress–strain diagrams for all environmental exposures and all test temperatures were linear to failure with failure being a sudden catastrophic rupture while steel bars generally exhibited a very linear stress–strain relationship up to a well defined yield point. and the curve typically decreases slightly because of hardening after the yield point. The failure of both type of GFRP bars were accompanied by the separation of fibers and the rupture of the fiber bundle with spiral pattern(Type-A : ASLAN 100) and linear pattern(Type-B:VROD-HM) as shown in Figure 4.5. Similar tensile failure mode of GFRP bars was also observed by Micelli and Nanni(2004) and Chen(2007). The failure modes of conditioned specimens were not changed. However, less violent failures with more delamination of fibers were observed.

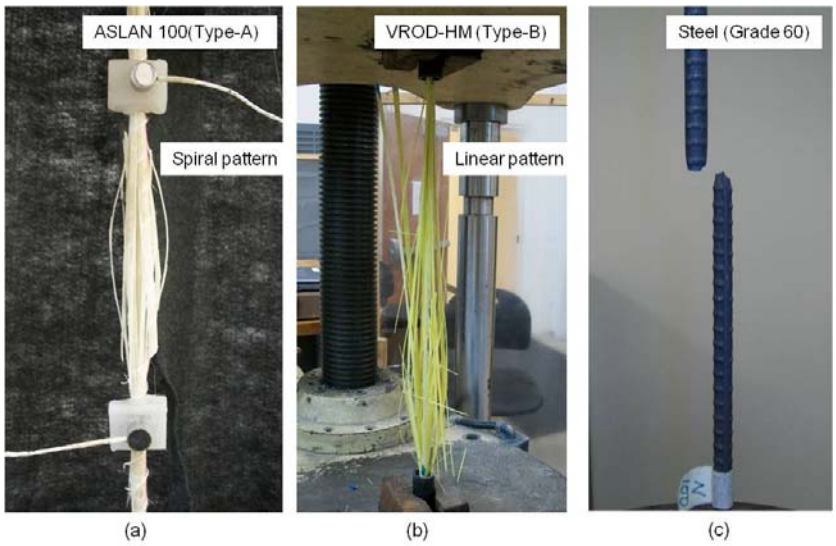

Figure 4.5 Failure modes: (a) Type-A GFRP (b)Type-B GFRP (c) Steel

4.5.2 Test results

Tensile tests were performed on the plain specimens and specimens that were incased in cement mortar paste and were conditioned in the environmental chamber with sustained loading. Tensile strength was calculated using the nominal area and measured area. The nominal area is the area of a No.3 steel reinforcing bar, while the measured area is determined from the average of the diameter measured at the top, bottom and the center of the GFRP specimen using a vernier-caliper. On the prescribed days, the specimens were removed in chambers of three and tested. Table.4.4 gives the tensile strength for unconditioned /conditioned and incased specimens.

Tensile strength and modulus of elasticity published by the manufacturer, which is calculated using the nominal area, are 110 ksi and 5920 ksi for Type-A GFRP bars(Aslan-100) and 188ksi and 8670 ksi for Type-B ones(VRod-HM) respectively. Tensile tests showed an elastic behavior until brittle failure occurred, which is the typical behavior of FRP-composites with unidirectional fibers. All specimens failed showing tensile fiber rupture. According to the

Table.4.4, Table.4.5 and Table.4.6, Type-A(ASLAN 100) rods showed a tensile strength of 143.9 ksi with a modulus of 6029 ksi for control specimens.

Table 4.4 Ultimate tensile strength after environmental exposures

Ultimate Tensile Strength of specimens-#3 bars (ksi) : RH=80% in the chamber											
Type of Exposure		No Exposure	Natural Exposure			Chamber A (79 °F:26°C)			Chamber B (115 °F:46°C)		
Duration of Exposure (days)		0	100	200	300	100	200	300	100	200	300
ASLAN 100	1	143.2	136.9	139.2	140.3	126.6	132.4	135.9	128.4	123.5	120.2
	2	143.5	146.8	144.4	143.3	142.5	127.5	121.0	128.5	129.5	121.7
	3	145.2	144.8	137.4	135.2	143.9	133.5	129.2	133.8	127.2	127.5
	Mean	143.9	142.8	140.3	139.6	137.7	131.1	128.7	130.2	126.7	123.1
	Standard Deviation	0.77	3.71	2.57	2.89	6.77	2.28	5.28	2.21	2.17	2.71
	Rate of Degradation (%)	0.00	-0.76	-2.53	-3.03	-4.36	-8.91	-10.59	-9.54	-11.96	-14.46
VROD-HM	1	164.1	163.0	155.0	156.6	161.7	153.5	150.5	147.6	153.7	132.4
	2	166.3	161.7	161.5	154.5	160.7	160.8	138.9	155.1	140.8	137.8
	3	162.5	166.5	164.4	163.8	157.5	149.9	137.2	146.5	145.4	136.6
	Mean	164.3	163.7	160.3	158.3	160.0	154.7	142.2	149.8	146.6	135.6
	Standard Deviation	1.53	2.00	3.91	4.00	1.78	4.54	5.93	3.80	5.35	2.34
	Rate of Degradation (%)	0.00	-0.35	-2.45	-3.65	-2.62	-5.83	-13.45	-8.85	-10.75	-17.47
STEEL	1	119.8	111.6	110.2	111.4	114.1	112.1	113.5	116.1	112.6	104.1
	2	116.3	125.1	124.4	119.5	116.7	121.9	110.5	114.8	113.4	100.5
	3	123.4	122.8	122.1	120.1	127.1	119.0	111.9	116.5	116.5	116.5
	Mean	119.8	119.8	118.9	117.0	119.3	117.7	111.9	115.8	114.2	107.1
	Standard Deviation	2.89	5.88	6.22	3.99	5.61	4.12	1.22	0.73	1.70	6.86
	Rate of Degradation (%)	0.00	0.03	-0.78	-2.35	-0.43	-1.80	-6.58	-3.34	-4.70	-10.65

Table.4.5 gives the tensile strain for unconditioned /conditioned and incased specimens.

Table 4.5 Ultimate tensile strain after environmental exposures

Ultimate tensile strain of specimens-#3 bars (in/in) : RH=80% in the chamber											
Type of Exposure		No Exposu -re	Natural Exposure			Chamber A (79 °F:26°C)			Chamber B (115 °F:46°C)		
Duration of Exposure (days)		0	100	200	300	100	200	300	100	200	300
ASLAN 100	1	0.0235	0.0241	0.0242	0.0241	0.0241	0.0237	0.0244	0.0239	0.0249	0.0242
	2	0.0239	0.0236	0.0240	0.0236	0.0233	0.0245	0.0239	0.0243	0.0241	0.0243
	3	0.0243	0.0241	0.0234	0.0241	0.0239	0.0244	0.0242	0.0246	0.0241	0.0241
	Mean	0.0239	0.0239	0.0239	0.0239	0.0238	0.0242	0.0242	0.0243	0.0240	0.0242
	S.D	0.0003	0.0002	0.0003	0.0002	0.0003	0.0003	0.0002	0.0002	0.0003	0.0002
	R.O.C (%)*		0.23	-0.05	0.23	-0.47	1.35	1.21	1.63	1.92	1.39
VROD-HM	1	0.0174	0.0173	0.0179	0.0182	0.0175	0.0177	0.0188	0.0178	0.0182	0.0186
	2	0.0186	0.0186	0.0181	0.0183	0.0183	0.0183	0.0173	0.0177	0.0178	0.0184
	3	0.0174	0.0167	0.0179	0.0173	0.0181	0.0180	0.0179	0.0186	0.0179	0.0177
	Mean	0.0178	0.0175	0.0180	0.0179	0.0180	0.0180	0.0180	0.0180	0.0180	0.0182
	S.D	0.0006	0.0008	0.0001	0.0004	0.0003	0.0002	0.0006	0.0004	0.0002	0.0004
	R.O.C (%)*		-1.57	0.86	0.68	0.86	1.05	1.05	1.24	0.86	2.36
STEEL	1	0.1281	0.1295	0.1285	0.1263	0.1271	0.1263	0.1242	0.1259	0.1248	0.1222
	2	0.1273	0.1278	0.1275	0.1238	0.1268	0.1264	0.1241	0.1262	0.1247	0.1219
	3	0.1325	0.1277	0.1279	0.1242	0.1270	0.1271	0.1242	0.1261	0.1251	0.1213
	Mean	0.1293	0.1283	0.1280	0.1248	0.1270	0.1266	0.1242	0.1261	0.1249	0.1218
	S.D	0.0023	0.0008	0.0004	0.0011	0.0001	0.0004	0.0000	0.0001	0.0002	0.0004
	R.O.C (%)*		-0.75	-1.03	-3.51	-1.80	-2.09	-3.97	-2.50	-3.43	-5.80

*Note : R.O.C (%)=Rate of Change

Table 4.6 Tensile test results of modulus of elasticity after environmental exposures

Modulus of Elasticity- #3 bars (ksi) : RH=80% in the chamber											
Type of Exposure		No Expo-sure	Natural Exposure			Chamber A (79 °F:26°C)			Chamber B (115 °F:46°C)		
Duration of Exposure (days)		0	100	200	300	100	200	300	100	200	300
ASLAN 100	1	6095	5681	5751	5820	5255	5585	5372	5371	4958	4966
	2	6013	6221	5868	6071	5838	5202	5063	5286	5375	5009
	3	5978	6009	5870	5609	6021	5473	5338	5440	5277	5139
	Mean	6029	5970	5830	5834	5705	5420	5258	5366	5204	5038
	Standard Deviation	60.05	272.19	68.15	231.11	400.41	196.81	169.5	76.92	218.21	90.11
	Rate of Degradation (%)		-0.97	-3.30	-3.24	-5.37	-10.09	-12.79	-11.00	-13.69	-16.43
VROD-HM	1	9426	9422	8659	8606	9242	8670	8008	8294	8447	7116
	2	8936	8695	8920	8440	8783	8509	7428	8762	7780	7490
	3	9329	9404	9182	9469	8380	8147	7537	7879	8031	7720
	Mean	9230	9174	8921	8839	8802	8442	7658	8312	8086	7442
	Standard Deviation	183.48	293.22	184.95	390.65	304.79	189.23	217.7	312.5	238.03	215.3
	Rate of Degradation (%)		-0.61	-3.36	-4.24	-4.65	-8.54	-17.04	-9.95	-12.40	-19.37
STEEL	1	30098	29286	29514	29480	29542	29230	27949	29055	28317	25777
	2	30288	29676	29746	30075	29612	29207	27972	29453	28340	25841
	3	29099	29699	29653	29978	29565	29046	27949	29009	28249	25969
	Mean	29828	29554	29638	29844	29573	29161	27957	29172	28302	25862
	Standard Deviation	451.63	163.99	82.37	225.87	25.17	70.86	9.19	172.8	33.34	68.89
	Rate of Degradation (%)		-0.92	-0.64	0.05	-0.86	-2.24	-6.27	-2.20	-5.12	-13.30

Type-A rods showed low mechanical properties, due to a low fiber content. The ultimate tensile strength was 145.2 ksi with a modulus of 5978 ksi. It was observed that tensile failure of Type-A rods specimens was accompanied by delamination of the fibers with the helical pattern,

even if the failure was always brittle. Type-B (VROD-HM) tensile specimens showed catastrophic failure, with a violent release of elastic energy that caused expulsion of the gauge length. Type-B rods showed a tensile strength of 158.9 ksi with a modulus of 9230 ksi. Ultimate tensile strengths of Type-B bars were lower than ones which the manufacturer (Pultrall Inc.) provided (the guaranteed tensile strength was 188 ksi with a modulus of 8900 ksi). Mild steel bars showed the ultimate strength was 119 ksi with a modulus of 29828 ksi.

Different values of residual tensile properties were measured on conditioned rods. The results for tensile test strength on three types of rods for different environmental treatments are shown in Tables 4.4 through 4.6. The ultimate strength showed a reduction of 9.5% after 100 days exposure and of 14.8% after 300 days exposure with the temperature of 115°F (46°C). In the case of tensile properties measured on conditioned specimens of Type-B, the ultimate strength showed a reduction of 5.8% after 100 days exposure, and of 18.1% after 300 days exposure with the temperature of 115°F (46°C). The ultimate strength of steel rods showed a reduction of 3.3% after 100 days of exposure, and of 10.7% after 300 days exposure with the temperature of 115°F (46°C) respectively. For the all unconditioned specimens exposed in outdoor tested after 300 days, strength loss observed was 3%. All rods did not show a significant decrease in mechanical longitudinal properties in the case of the outdoor exposure (DFW area).

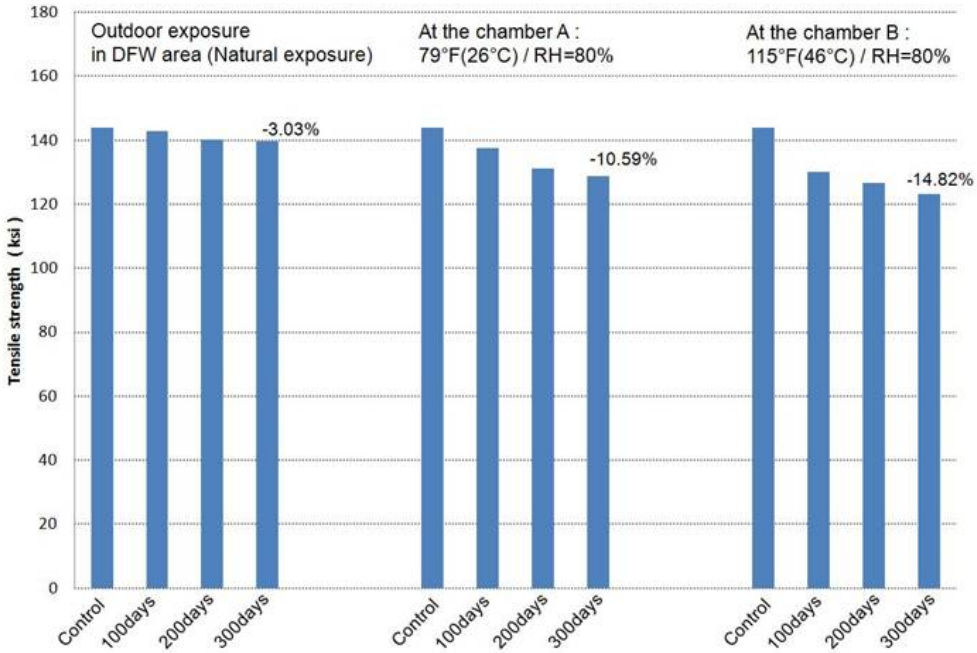

(a)

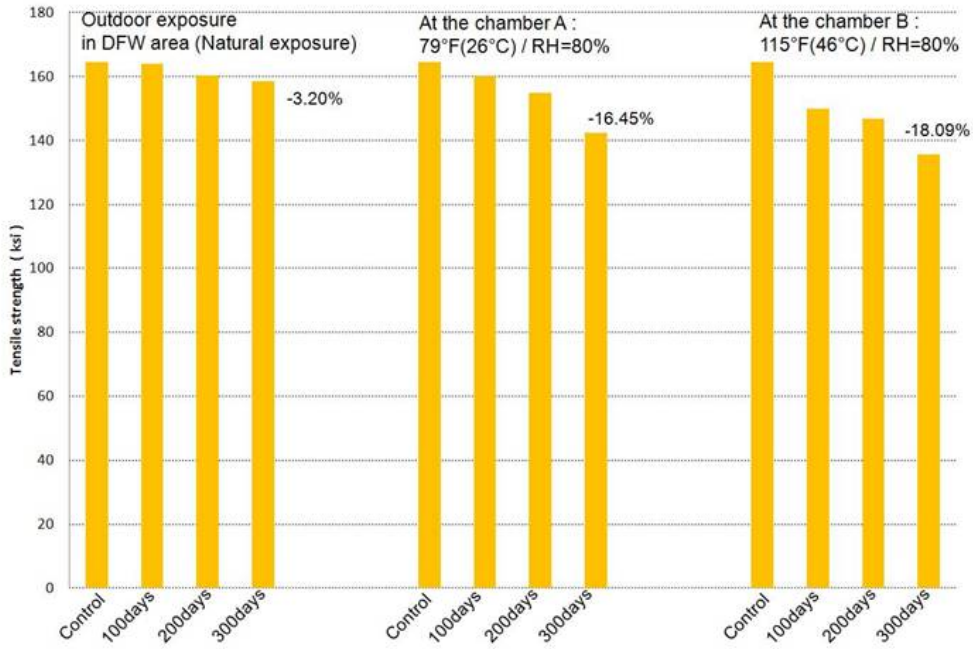

(b)

Figure 4.6 Change in strength with different environments (w/ sustained loading)
(a)Type-A (ASLAN-100) rods (b) Type-B (VROD-HM) rods

Environmental aging conditions reduced the tensile strength of both GFRP specimens since the different values as control series were measured for Type-A and Type-B exposed rods. There is a general decrease in measured strength with both the temperature of tensile testing and the duration of exposure in cement mortar paste representing the alkali condition for concrete. The strength results for Type-A and Type-B rebar and modulus data for all rebars exhibit similar trends and all data is presented in Table.4.4 through 4.6. In all cases the scatter in the results was small with coefficients of variation generally less than 10%. The reduction in strength and elastic modulus of the rebar is inevitably linked to the degradation in the properties of the glass fibers at the various conditions of testing.

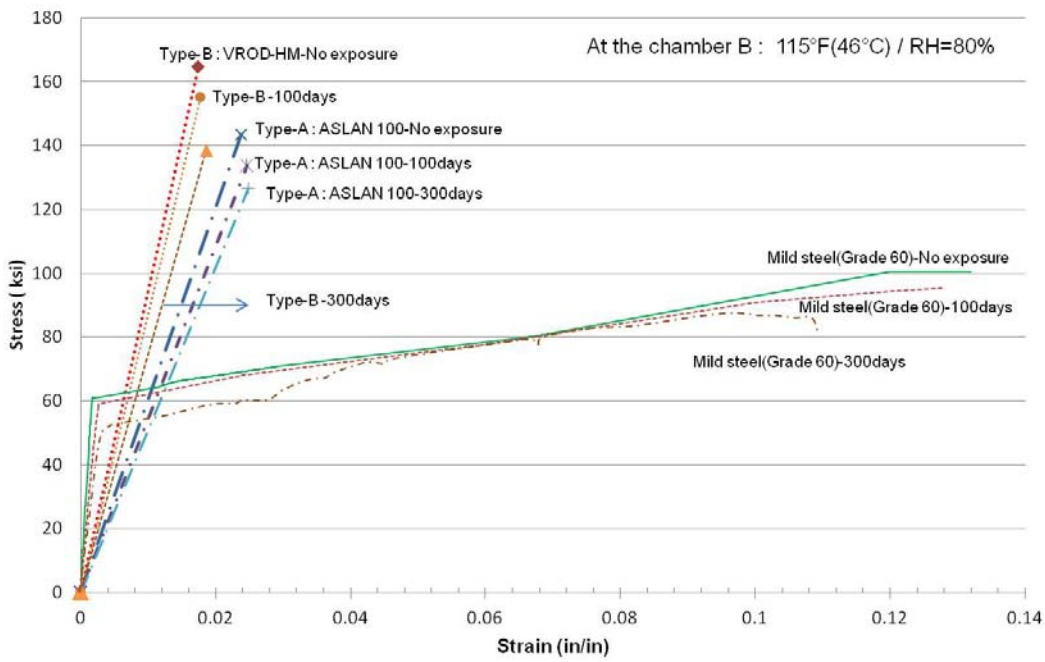

Figure 4.7 Changes of stress-strain relationship after environmental aging
(115°F / RH=8-% / with sustained loading)

The elongation of each tensile test specimen was measured using the extensometer and strain gauges. Strain was calculated using the average elongation divided by the measured

initial gage length. Typical stress-strain diagrams of each control specimen and the stress-strain diagrams for all the specimens tested during the project are shown in Figure.4.7. It illustrates that there exists linear stress-strain behaviors of GFRP bars, till failure and strength degradation after environmental treatment. Since there is still no yielding unlike steel rods, GFRP bars can be described as brittle in nature after strength/stiffness degradation by environmental aging. However, the degradation of yielding stress and decrease of strain were observed in the conditioned steel rods. The yield strength showed a reduction of 1.3% after 100 days exposure and of 18.5% after 300 days exposure with the temperature of 115°F (46°C).

Vijay (1999) reported that stiffness of both types of GFRP bars (sand coated and ribbed) did not show reduction trends observed in strength under different accelerated aging conditions such as immersion in the alkaline solution with freeze-thaw cycles. In this study, however, stiffness of both types of GFRP bars (Type-A and Type-B) showed reduction trends observed in strength under different conditioning schemes. Stiffness was affected by exposure duration. In case of Type-A GFRP rods, the modulus of elasticity showed a reduction of 11.0% after 100days and 16.4% after 300days exposure in the chamber B (115°F/ RH=80%). In case of Type-B GFRP rods, the modulus of elasticity showed a reduction of 9.9% after 100days and 19.4% after 300days exposure in the chamber B (115°F/ RH=80%). In case of steel rods, the modulus of elasticity showed a reduction of 2.2% after 100days and 13.3% after 300days exposure in the chamber B (115°F/ RH=80%). Many of the conditioned bars showed a decrease in stiffness. The decrease in stiffness associated with reduction in failure stress implies that the bar is more brittle than the unconditioned reference bar. A reduction in the stiffness associated with stress loss implies that the bar would elongate more at a given stress than the unconditioned bar. GFRP bars showed greater losses of stiffness than steel ones and Type-A specimens had a good retention of stiffness relatively compared with Type-B ones.

4.6 Correlation between actual field exposures and laboratory aging

In order to predict long-term (over 50 years) performances of FRP bars embedded in concrete, accelerated aging methodologies can be used since it is practically not feasible to expose GFRP bars in real concrete for its service life up to 50-100years. There are various models proposed for the durability of composites. However, there is no general agreement of prediction models for the long-term behaviors. The methodology used for the accelerated ageing tests is based on the Arrhenius principle, which uses high temperature as the accelerating agent for the degradation of the material in a given environment. The Arrhenius empirical model is one of the oldest and most widely used models to predict the time of failure of a material as a function of temperature. Accelerated aging tests generally include two phases. First, GFRP bars are exposed to different environmental conditions at different temperatures or to more severe conditions to accelerate the aging process. Second, long-term properties of the materials are expected to be predicted based on the accelerated aging test results.

4.6.1 Arrhenius methodology of accelerated aging

An accelerated aging methodology suggested by Litherland et al. (1981) has been used for prediction of not only the changes in the mechanical properties of FRP bars over a provided duration but also the correlation between the accelerated aging and the natural aging. In Arrhenius concept, it is assumed that there is only one dominant degradation mechanism in GFRP bars which will not change with time during the exposure but the degradation rate will be accelerated with the increase of exposure temperatures. This principle is employed to exploit the temperature dependence of polymers subjected to environmental aging consisting of several temperature levels.

$$t_f = A \times e^{(\frac{\Delta H}{kT})} = A \times e^{(\frac{-E_a}{R} \times \frac{1}{T})} \qquad \text{(Eq.4.1)}$$

Where :

t_f : the real time of failure(1/time)

k : the Boltzmann constant(8.617×10^{-5}/K)

A : the acceleration factor determined graphically from the acceleration test

ΔH : the activation energy factor of chemical reaction

E_a: activation energy

R : universal gas constant

T : absolute temperature measured in Kelvin at the time of failure

The value of ΔH, which varies from 0.3 to 1.5, depends on the failure mechanism and the type of the material used. The acceleration factor between two temperatures increases exponentially with the increase of ΔH [Benmokrane, 2005 and Chen, 2007]. Applications of their principles are summarized in the following steps [Vijay,1999]:

4.6.2 Procedures

The following procedure is used to correlate accelerated aging and natural aging [Litherland et al. 1981; Vijay and GangaRao,1999].

STEP 1

The relationship between tensile strength retention (the percentage of residual strength over original tensile strength) and exposure time can be defined as the Eq. 4.2.

$$Y = 100\exp(-\frac{t}{\tau}) \qquad \text{(Eq. 4.2)}$$

where, Y : tensile strength retention value (%)

T : the inverse of the degradation rate (1/k)

t : the exposure time

In order to obtain the coefficient τ, the data of Figure.4.8 were used by regression analysis. OriginPro7.0 was used for data analysis and curve fitting. Corresponding values of τ and coefficients of determination (R^2) are shown in Table.4.7. All regression lines had a correlation coefficient over 0.81. Using Eq.4.2, the time to reach a given tensile strength retention at a different temperatures can be calculated.

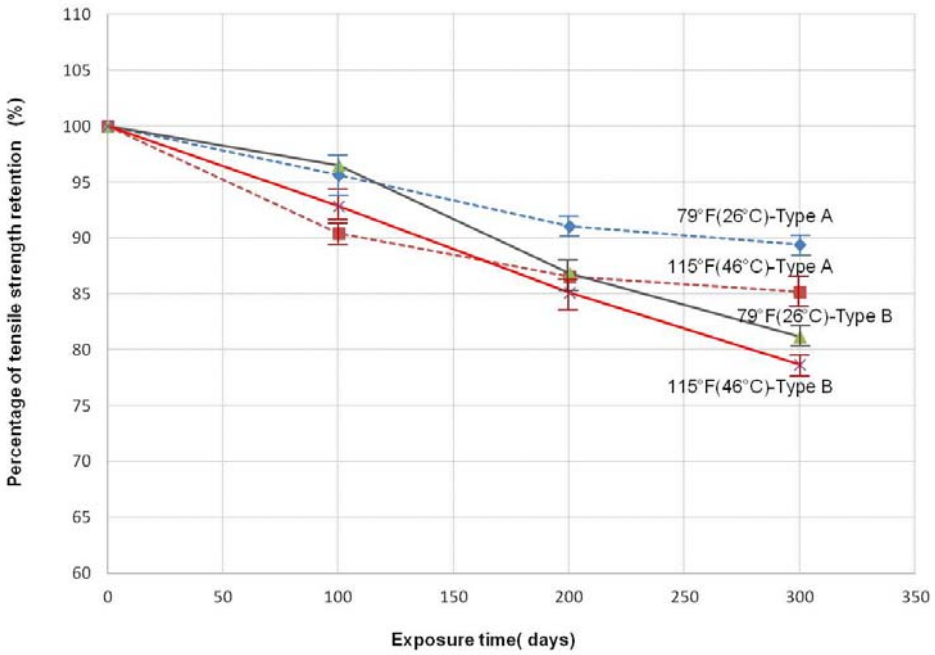

Figure 4.8 Tensile strength retention of GFRP bars

STEP 2

Plot the curves in step 1 for Arrhenius type relationship. Arrhenius equation takes the form of Eq.4.1. The data plot can be constructed in one of two ways. Time may be plotted as a function of inverse absolute temperature for various percentages of property retention, or property retention may be plotted as a function of inverse absolute temperature for various chosen lifetimes, respectively [Bank et al. 2003]. By plotting natural log of time (time to reach

particular strength retention value, i.e., 70% etc.) vs. inverse of absolute temperature (K=273 + t_0 with Celsius) in this study, the Arrhenius relationships are obtained as show in Figure.4.9 and Figure.4.10. Straight lines were fitted to the data with the assumption that the degradation rate was a function of temperatures as expressed in equation 4.1 which also fitted to the data to obtain E_a/R. The coefficients of determination for all regression analysis were close to 1.0 and straight lines in Arrhenius plots for different strength retention were parallel to each other. The slopes of straight lines are E_a/R.

Table 4.7 Coefficient of regression equation for tensile strength retention and Arrhenius plots for Type-A GFRP bars

After regression analysis (79°F with ln(t)=3.34)					
τ(1/k)	5763				
R^2 (Coefficient determination)	0.81				
Y(%) (Strength retention)	50	60	70	80	90
t (time)	3994.61	2943.89	2055.52	1285.98	607.19
ln(t)	8.29	7.99	7.63	7.16	6.41
After regression analysis(115°F with ln(t)=3.13)					
τ(1/k)	726				
R^2 (Coefficient determination)	0.91				
Y(%) (Strength retention)	50	60	70	80	90
t (time)	503.22	370.86	258.95	162.00	76.49
ln(t)	6.22	5.92	5.56	5.09	4.34

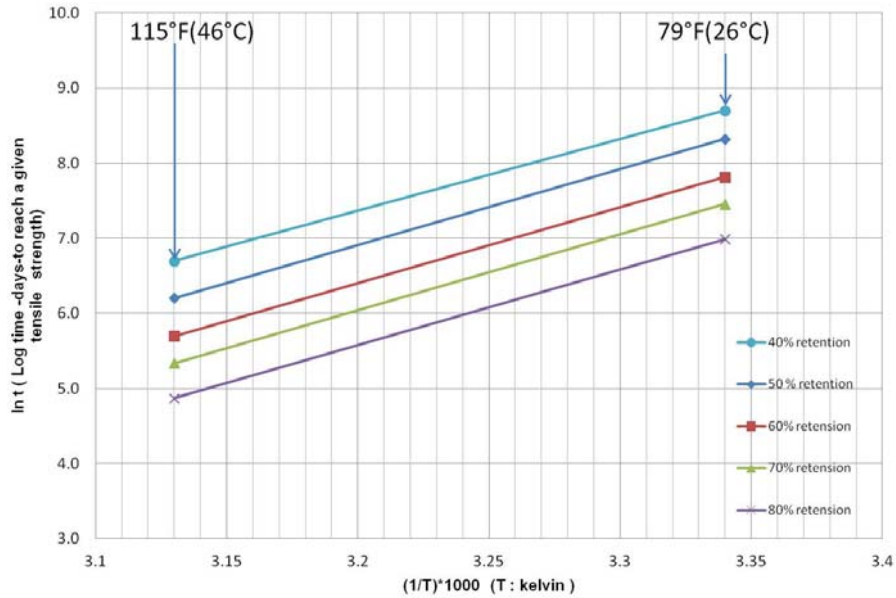

Figure 4.9 Arrhenius plots of tensile strength degradation for Type-A GFRP bars after accelerated aging

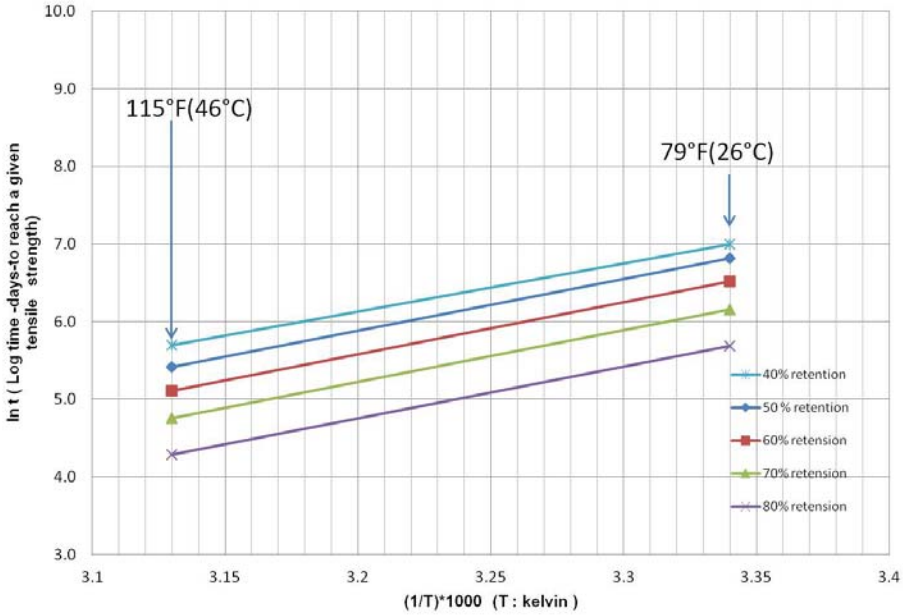

Figure 4.10 Arrhenius plots of tensile strength degradation for Type-B GFRP bars after accelerated aging

STEP 3

Based on Arrhenius relation, Dejke and Teppers (2001) proposed an approach involving time shift factors (TSF) / acceleration factor (AF) to estimate the service life of GFRP bars. The time shift factor (TSF) value between the reference temperature and any selected temperature can be written as in Eq.4.3 [Dejke ,1998]. Acceleration factors (AF) for different temperatures can be obtained by equation 4.3. Calculate the acceleration factor (AF) at two different temperatures (79°F and 115°F).

$$AF = e^{[\frac{E_a}{R}(\frac{1}{T_1}-\frac{1}{T_2})]} = \exp[11605 \times \Delta H(\frac{1}{T_1}-\frac{1}{T_2})] \qquad \text{(Eq.4.3)}$$

Where,

E_a : the activation energy of chemical reaction

R: universal gas constant (J/K/mol)

T_1, T_2: absolute temperature between accelerated test temperature (T_1 : smaller temperature)

The TSF method depends on the Arrhenius approach and requires only two accelerated data sets of different temperatures. Time shift factors are obtained by simply taking the ratio of the time values required for the specified strength loss. E_a/R is a material constant and its value is calculated using the time shift factor values based on the regression plot [Dejke ,1998]. The slopes of straight lines in the Arrhenius plot (Figure.4.9-10) are E_a/R. Then, time shift factors for other exposed temperatures of T can be obtained based as shown in Eq.4.4.

$$TSF = e^{(\frac{10095}{26+273.15}-\frac{10095}{T+273.15})} \qquad \text{(Eq.4.4)}$$

The acceleration factors (AF) with reference temperature t_0=79°F (26°C) are calculated in the Table.4.8. The result in Table.4.8 can be interpreted that one day at 46°C is equal to the 7.51 days at 26°C.

Table 4.8 Values for acceleration factors with the reference temperature of 79°F(26°C)

Temperature(°C)	E_a/R	Type-A GFRP (ASLAN 100)	Type-B GFRP (VROD-HM)
46	10095	7.51	3.89
26	6678	1.00	1.00

STEP 4

Establish the master curve not only by multiplying corresponding TSF values with exposure time at two different temperatures(79°F and 115°F) but also by plotting Arrhenius plot based on the data of both Litherland (1981) and this study(at North Texas). The time shift factors known as the acceleration factors were used to transform a time in real exposure to a time under the accelerated exposure. Regression analyses were conducted by using OriginPro7.0 in order to find the relation between the time of logarithmic scale to reach given tensile retention and the inverse of absolute temperature for each level of property retention. By using linear regression, a regression line can be fit through each set of data (one for each aging temperature)and an acceptable regression line must have an R^2 of at least 0.80 [Bank et al. 2003]. In order to fit the master curve, accelerated chamber weathering carried out in these experiments is calibrated in Figure.4.11 with respect to natural weathering at North Texas, with a mean annual temperature of 69.4°F(20.8°C). For example, for 40% retention of the tensile property (60% reduction of the one) of GFRP bars, log times to reach 40% retention take 6.7(t=812days) and 8.78(t=6502 days) at 79°F(26.1°C) and 115°F(46.0°C) respectively. This result can be interpreted that the real exposure time will take 10301 days (28.2years) at 69.4°F(20.8°C) as mean annual temperature of North Texas area if this materials degrades to 60% of its tensile strength property.

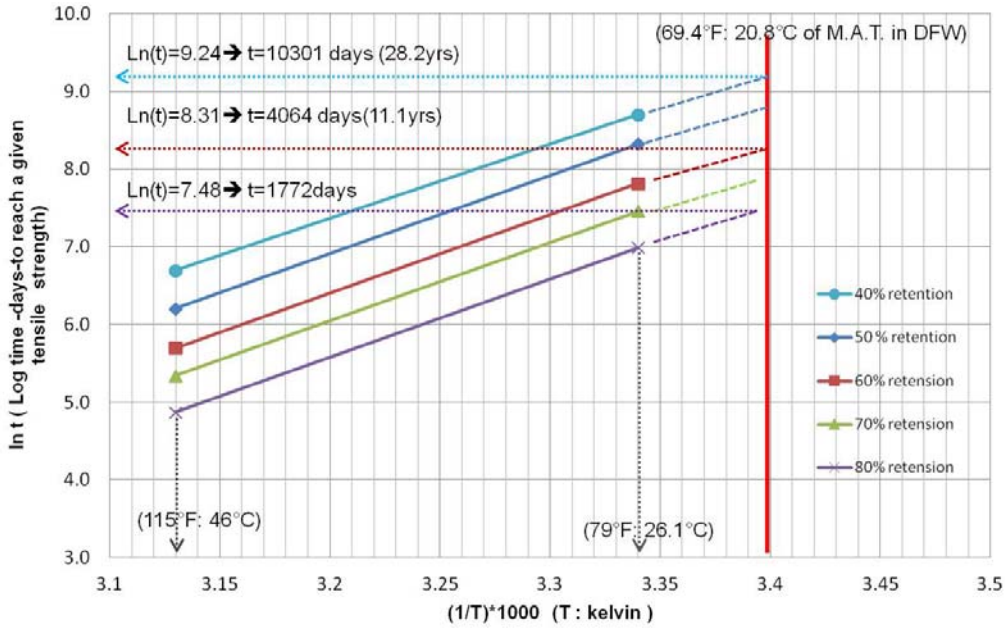

Figure 4.11 Arrhenius plots of Type-A GFRP bars for master curve fitting
With the reference temperature of 69.4°F(20.8°C)

Figure.4.12 shows calibration of North Texas data on accelerated aging and data by Litherland (1981) and a procedure of the service life prediction for FRP materials based on accelerated aging data. The test results of natural exposure and accelerated aging are plotted in the Figure.4.12 together. In terms of lines in Figure.4.12 being nearly parallel to each other , good correlation is observed between Litherland data (at 50°C) and master curve of North Texas data. The slope of the master curve by Arrhenius plot is slightly greater than the one of the master curve of Litherland (50°C). This implies that any calibration of our results with the natural weathering data given by Litherland on strength reduction is more conservative due to better resin and manufacturing techniques used in this investigation compared with glass fiber and resin used by Litherland 30-years ago. Compared with the slope of accelerated aging data, the slope of the master curve by Arrhenius plot is similar and it implies that the master curve can be used as the extension of real tested data for accelerated aging. That means that it is reasonable to compare and find out correlation between the extended line of the natural

exposure data and the master curve by the Arrhenius plot as the extension of real accelerated test data.

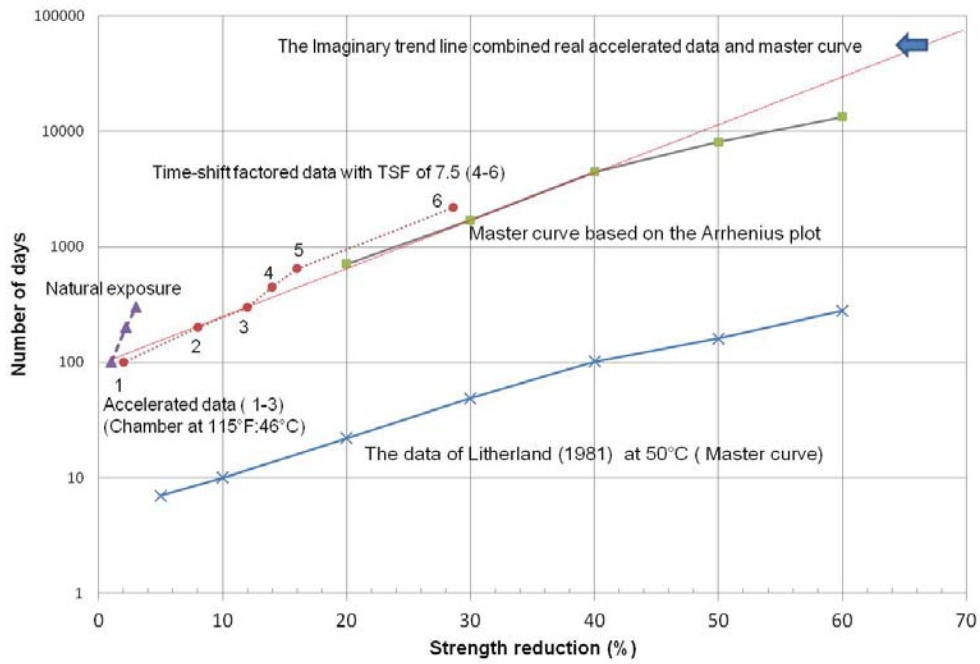

Figure 4.12 Master curves of DFW data on accelerated aging and data by Litherland (1981)

STEP 5

Using Arrhenius' principle, Vijay and GangaRao(1999) proposed a correlation formula between the accelerated ageing in the laboratory and the natural aging on the field. The formula developed for GFRP reinforcements conditioned in aqueous and alkaline solutions is as follows:

$$\frac{N}{C} = 0.098 \cdot e^{0.0558T} \qquad \text{(Eq. 4.5)}$$

Where, N is the in-service field performance in day and C is the accelerated exposure age (in day) in the laboratory with the temperature of T(°F). Another model relating accelerated ageing data to natural ageing was presented by Porter and Barnes(1998). This relationship links the

different annual average temperatures by an accelerating factor, which leads to Eq.4.6 (coefficient of correlation R^2 =0.993). Eq.4.6 was obtained using the annual average temperature of Des Moines (Iowa, USA).

$$Age = 1.025 \times e^{(0.0935T)} \qquad \text{(Eq.4.6)}$$

where T is the temperatures in Fahrenheit.

In this study, the modified correlation formula is proposed by comparison the master curve of the Arrhenius plot and the natural exposure data by regression analysis in Figure.4.13. Figure.4.13 shows correlation between accelerated aging in the chamber and natural aging in outdoor with respect to strength reduction. The form of this regression analysis is shown in Eq. 4.6 [Bank et al., 2003].

$$y = a \log x + b \qquad \text{(Eq.4.6)}$$

Where a and b are regression coefficients, x is time to reach given tensile reduction and y is property reduction value (%). To develop an accelerated aging relationship for use in this investigation with 115°F(46°C) and 80% of relative humidity, a new relationship is proposed. This relationship related the chamber temperature to the M.A.T.(mean annual temperature) for North Texas area.

According to the tests by Dejke(2001), Almusallam (2006) and Chen(2007), convergence limit was found in Figure.4.14. The master curves for different temperatures converge to constant value with the increase of exposure times for loaded specimens after 500days. The convergence occurs earlier in case of higher temperature. Simultaneously, this convergence limit is used to analyze the correlation between natural aging and accelerated aging. As the data by Aindow (1984) indicated a trend towards a stabilizing strength at the simulated 50-year age, this trend follows the behavior of specimens tested in this study after regression analysis as seen in Figure.4.13.

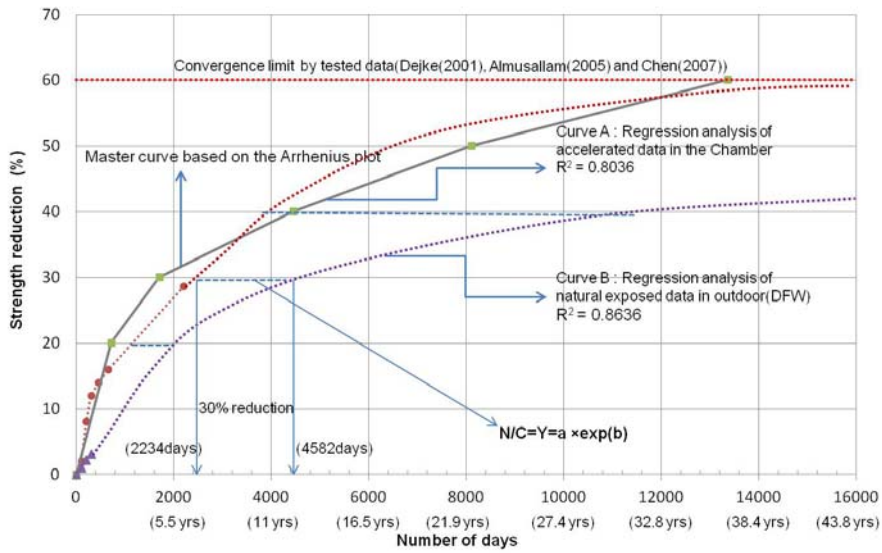

Figure 4.13 Logarithmic regression curves for converting accelerated aging to natural aging

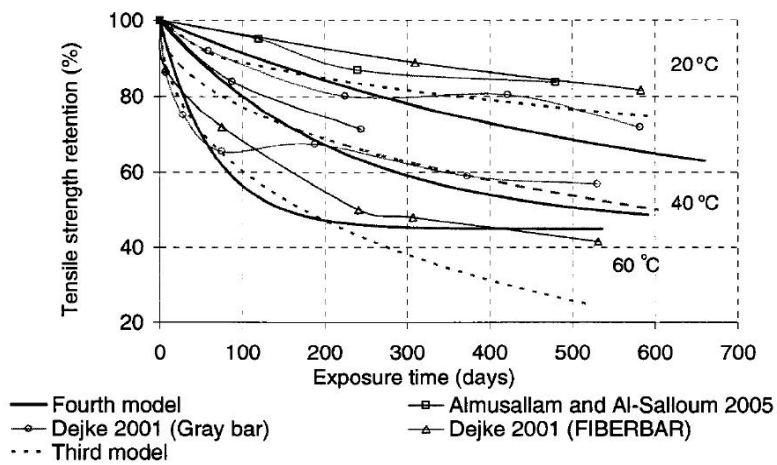

Figure 4.14 Comparisons of predictions and test results with sustained loading (Chen,2007)

As mentioned previously, logarithmic regression analyses between strength reduction and time required to reach those strength reduction were carried out to obtain the Arrhenius plots for accelerated data and natural exposed data. However, the exponential regression was used in the same way which Vijay (1999) and Porter (1998) proposed. The form of exponential

regression analysis is shown in equation 4.7. Table.4.9 shows corresponding regression coefficients.

$$y = a \cdot e^{bx} \qquad \text{(Eq.4.7)}$$

Table 4.9 Coefficient of regression equation for correlation between accelerated aging and natural aging (M.A.T=69.4°F (20.8°C))

Reference temperature (°F)	a	b	R2
115	0.0876	0.0508	0.8142

Figure.4.15 shows not only the correlation between accelerated aging(C) and natural aging (N) but also the comparison the equation of Vishay with the proposed equation. It follows that one days of the chamber exposure at 115°F (46°C) simulates 29.8days of life in an outdoor condition with an annual average temperature of 69.4°F (20.8°C) as given by the calibrated Eq. 4.8. Therefore, it can be translated that chamber weathering of 300 days in real concrete corresponds to natural weathering of 9052 days, i.e., about 24.8 years at North Texas (DFW).

$$\frac{N}{C} = 0.0876 \cdot e^{(0.0508 \cdot T)} \qquad \text{(Eq.4.8)}$$

Where, N is day(s) in natural exposure, C is day(s) in chamber conditioning and T is temperature in °F.

It can be also found from the Figure.4.15 that the proposed equation did not show good correlation compared with the equation of Vijay (1999). The accelerated aging of Vijay is more severe than of this study even though M.A.T. of Morgantown is less than the one of DFW. This difference may be due to following reasons:

- The conversion of Vijay's equation was calibrated for the specimens without sustained load while sustained loading was subjected to the specimens in this study
- Immersion into alkaline solution was used in Vijay's equation while exposure to real concrete was used in this study.

- Inaccurate assumption of creating Arrhenius plots. It is assumed that there is only one dominant degradation mechanism in GFRP bars which will not change with time during the exposure but the degradation rate will be accelerated with the increase of exposure temperatures.

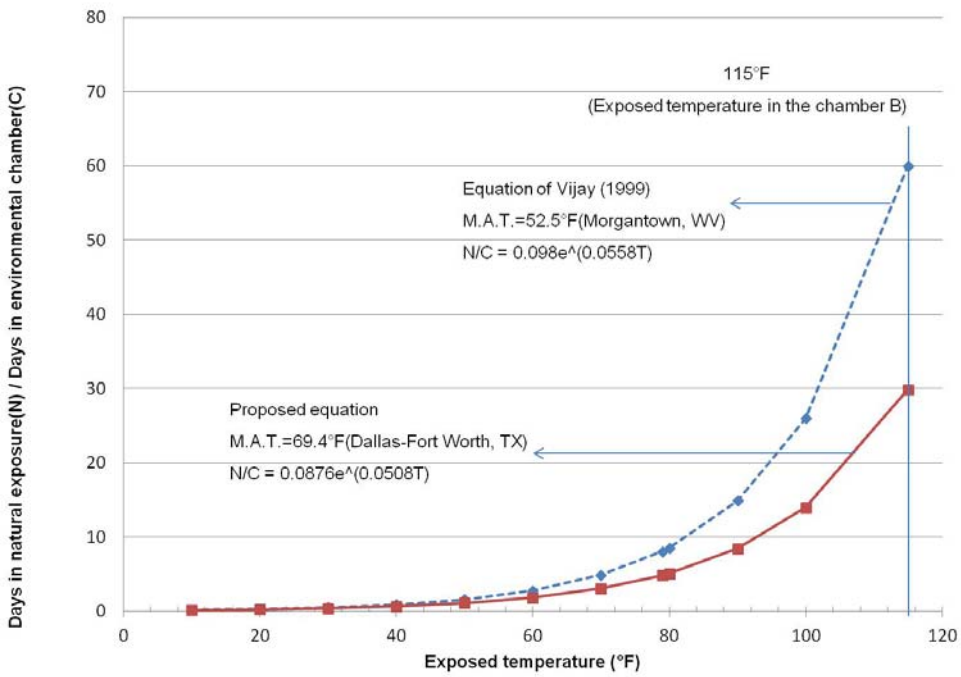

Figure 4.15 Comparison of the correlation(N/C) between Morgan town and DFW(North Texas)

4.6.3 Limitation of this study

Limitation of Litherland's approach is that it considers Mean Annual Temperature (M.A.T) as the basis for constructing normalized strength reduction curve without accounting for magnitude of precipitation and its distribution on the naturally weathered specimens [Vijay,1999]. However, the strength variations are strongly dependent on temperature, moisture, pressure and stress variations [Vijay, 1999]. Even though the above prediction approaches

provide good fundamentals for the durability evaluation of GFRP bars, there is no practical prediction approach to develop the general environmental reduction factor for GFRP bars in real reinforced concrete.

The relationship between accelerated aging methods and life in the field was the focus of several mathematical models. All models used the average ambient temperature at the geographic location of the tests as the data for the equivalency models. The elevated temperature used in the laboratory was incorporated into the model to transfer the duration of laboratory exposure to real time in the field. However, no correlation was made with the type of medium used or level of stress applied to the bars during conditioning not only in previous researches but also in this study.

4.7 Summary

In this chapter, results of accelerated aging of two different types of GFRP bars and steel rods embedded in real concrete exposed to specific humidity level, saline environment, different temperatures and sustained stress are discussed. Durability effects due to environmental exposure were studied. Concluding remarks are summarized as follows:

- The strength and modulus of GFRP and steel bars are reduced by the increase of exposure duration to cement-mortar paste at two different temperatures (79°F and 115°F).
- It is reported that the reduction in both the yield strength and the ultimate strength of steel bars ranged from 2 to 10% of the original bars.
- In terms of strain, the comparison indicates that as the exposure duration increases, the corresponding strain of the both GFRP bars before failure do not show a trend while the corresponding strain of the bar before failure decreases. This indicates that corrosion of reinforcing steel increases its brittleness.

- For Type-A rebar (ASLAN 100), maximum tensile strength reductions at 79°F(Chamber A)were 4.36%,8.91% and 10.59%, respectively, for 100, 200 and 300dyas-duration. Similarly maximum tensile strength reductions at 115°F(Chamber B)were 9.54%,13.43% and 14.82%, respectively, for 100, 200 and 300dyas-duration.
- For Type-B rebar(VROD-HM), maximum tensile strength reductions at 79°F(Chamber A)were 1.32%,8.60% and 16.45%, respectively, for 100, 200 and 300dyas-duration. Similarly maximum tensile strength reductions at 115°F(Chamber B)were 5.78%,10.26% and 18.09%, respectively, for 100, 200 and 300dyas-duration.
- For steel rebar(Grade60),maximum tensile strength reductions at 79°F(Chamber A)were 0.43%,1.80% and 6.58%, respectively, for 100, 200 and 300dyas-duration. Similarly maximum tensile strength reductions at 115°F(Chamber B)were 3.34%,4.70% and 10.65%, respectively, for 100, 200 and 300dyas-duration.
- Tensile tests showed that GFRP rods (Type-A and Type-B) had poor retentions of tensile properties of 14.82% and 18.09% after 300days-exposure compared that steel rods had 10.65% of reduction after same exposure duration. However, after 200days of environmental aging, the rate of degradation of steel rods are six times greater than the one of Type-A GFRP rebars in terms of strength and 15% greater than the one of Type-B GFRP rebars. That means, sufficient degree of reinforcement corrosion did not provided yet until 300days in environmental chamber.
- Correlation-charts developed for the stressed GFRP bars show that one days of the chamber exposure at 115°F(46°C) simulates 29.8days of life in an outdoor condition with an annual average temperature of 69.4°F (20.8°C). Therefore, it can be translated that chamber weathering of 300 days in real concrete corresponds to natural weathering of 8940 days, i.e., about 24.5 years at DFW area, Texas.
- The proposed equation did not show good correlation compared with the equation of Vijay(1999). This may be due to inaccurate assumption of creating Arrhenius plots

assumed that there is only one dominant degradation mechanism in GFRP bars which will not change with time during the exposure but the degradation rate will be accelerated with the increase of exposure temperatures. This may also be due to differences of aging conditions such as exposure to real concrete or alkaline solution.

CHAPTER 5

BOND TEST: LONG-TERM BOND PERFORMANCES OF GFRP BARS EXPOSED TO ACCELERATED AGING

5.1 General

GFRP bars are gaining popularity as reinforcement for concrete bridge deck slabs and other concrete structures owing to attractive advantages of FRP materials including light weight, corrosion resistance and high strength. However, there is still lack of information of their mechanical and structural behavior to ensure their suitability for the application of construction industry. FRP materials are an isotropic and characterized by high tensile strength only in the direction of the reinforcing fiber and the transverse coefficients of thermal expansion (CTE) controlled by the resin is up to three to six times the CTE of the concrete. This anisotropic behavior should affect the bond performance of FRP bars when embedded in concrete and these effects need to be evaluated [Masmoudi et al.2005]. The bond's long-term durability also plays a critical role in the long-term performance of concrete structures using internal FRP reinforcement [Davalos et al, 2008]

Considerable researches have been conducted on the bond behavior of FRP bars in concrete and durability performance of the bond between concrete and FRP bars. The reported results in the literature showed varied bond strengths and behaviors because of differences in material properties of FRP bars and used test methods. Porter and Barnes (1998) found that the pullout bond strength of GFRP bars did not decrease when testing bars embedded in concrete and aged in solutions at a temperature of 60°C. Bakis et al. (1998) showed that, after 28 days of immersion in a saturated $Ca(OH)^2$ solution at 80 °C followed by 5 days of drying, the ultimate bond strength of GFRP bars embedded in concrete did not decrease, although material

degradation of GFRP bars was observed. On the other hand, Robert et al.(2010) reported that the bond strength of GFRP bars decreases as the duration of immersion increases. Even at high temperature (50°C), when the environment is more aggressive, the change in bond strength remained still minor. Recently, the result that conditioning different types of GFRP bars embedded in concrete in water at room temperature and 60 °C reduced the bond by about 20% was found by Davalos et al.(2008). Clearly, FRP components and test methods significantly influence conclusions drawn about the durability of the FRP bar–concrete interface. Davalos et al. (2008) have also shown that the failure mode of bond is dependent on the profile of the surface of the bar and coating layer that is usually added to enhance the bond performance.

Even so, the general bond characteristics of FRP bar can be summarized as follows. The durability of bond properties of FRP bars with deformations of surface is evaluated to be highly influenced by the geometry of the bar surface and transverse properties of FRP bars [Bakis et al. 1998]. Pullout test is widely used, but it usually results in un-conservative bond strength values as a simple and economical solution for the evaluation of bond characteristics. This is attributed to the compressive stress induced in the surrounding concrete, which usually under tension in practical conditions and the confining action of reaction plate developed in the test specimen. The splitting of concrete during pullout testing is usually avoided by providing relative large volume of concrete surrounding the bar [Davalos et al, 2008].

5.2 Bond Mechanism of FRP rebar

The bond behavior of FRP rebars to concrete is expected to vary from that of conventional steel bars, since various key parameters that influence bond performance are different. Bond characteristics are influenced by factors such as [ACI 440R-07] : 1) size and type of reinforcement (wires or strands): 2) concrete strength: 3) surface conditions (smooth, deformed, and sand-coated): 4) concrete confinement (helix or stirrups): 5) type and volume of

fiber and matrix: 7) amount of concrete cover: 8) time-dependent effects: and 9) type of loading (static, cyclic, and impact).

Bond of plain rebars is mainly governed either by the inter-laminar shear strength between successive layers of fibers at the surface of the bar or by the adhesion between the bar surface and the surrounding concrete [Moon, 2004]. Because no tensile cracking is likely to occur along the rebar, bond failure occurs along the perimeter of the rebar is being pulled out from the concrete. The bond strength of plain rebar is normally very low and with a large variability. Therefore, only if plain bars are used together with other anchoring devices such as bends, hooks and transverse bars, they may be used as reinforcement. As shown in Figure.5.1, the bond versus loaded end slip response curve of a short embedment length subjected to pullout is used to describe the FRP rebar to concrete interaction. The specifications of each stage are summarized below from Moon (2004).

- Section OA: “At the beginning of loading, the main mechanism that resists the external load is the chemical adhesion between two materials. No measurable slip is observed at this stage”.

- Section AB: “As the load increase, adhesion breaks down and the bond mechanism changes. The slip at the loaded end of the bar gradually increases and the deformations of the bar develop bearing stresses due to reaction against the surrounding concrete. The principal tensile stress caused by bond stresses reaches the tensile strength of concrete and micro-cracks initiate at the tips of the bar deformations, which allow the bar to slip”.

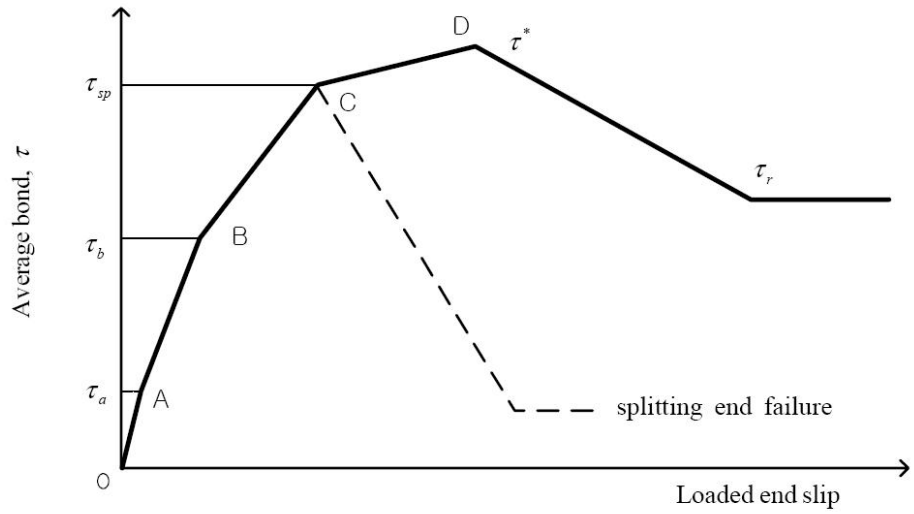

Figure 5.1 Typical average bond stress versus loaded end slip curve (Moon, 2004)

- Section BC: "At this stage, the bearing stresses from the bar deformations to the surrounding concrete increase considerably, as the slip of the increases. The splitting resistance of the concrete surrounding the rebar is decisive at this stage. The possible ultimate crack pattern giving minimum splitting resistance against the radial pressure generated by bond force determines the anchorage capacity. Confinement by the surrounding concrete mass, transverse reinforcement and pressure, applied externally to the anchorage zone, influence the splitting resistance".
- Section CD: "If sufficient resistance to splitting can be provided by the surrounding concrete, as for example in the case for short embedment in pullout cube tests, then the bond stress can reach the maximum bond strength, τ* . At this stage, both the loaded and unloaded ends of the rebar are slipping and bond stiffness is significantly decreased".
- Section DE: "After attaining the maximum bond stress, the bearing mechanism between bar deformations and concrete corbels breaks down and the bond stress decreases

considerably. The residual bond strength mainly depends on the frictional resistance (τ_r), at the failure interface. The roughness of this interface determines the magnitude of τ_r"

5.3 Bond test methods for internal FRP reinforcement

The mechanism of load transfer between FRP reinforcement and concrete is influenced by bond characteristics. Therefore, bond characteristics control the concrete crack spacing, crack width, hence, concrete cover to the reinforcement and the reinforcement development length are required. Thus, the behavior of concrete structures reinforced with GFRP bars depends on the integrity of the bond. Many test methods have been developed and conducted in order to determine the bond strength of FRP bars and rods in concrete.

5.3.1 Pullout tests

The concentric pullout test is a popular test method adopted by several researchers for comparative bond assessment for FRP reinforcement [ACI 440R-07]. In this method, an FRP bar specimen is embedded in a concrete block with the embedded length of the FRP rod typically being five times of the rod diameter (d_b). The average bond stress and bond stress versus slip at the loaded end can thus be obtained. Additional information and specimen fabrication details are given in ACI 440.3R and ACI 440R-07.

The ring test is carried out as a pullout test, where the specimen is a concrete cylinder with the studied reinforcing bar embedded along the center axis of the cylinder [Tepfers et al.1992]. This test allows for determination of the splitting tendency of the bar in all stages of loading up to bond failure by determination of the angle between bond forces and the bar axis, and the bar is pulled in tension as shown in Figure.5.2. The bond length corresponds to the height of the cylinder, which is chosen to be three diameters of the bar, so the bond stress

along the bond length becomes practically evenly distributed. The cylinder is cast in a thin steel tube (the ring), which becomes a part of the test specimen.

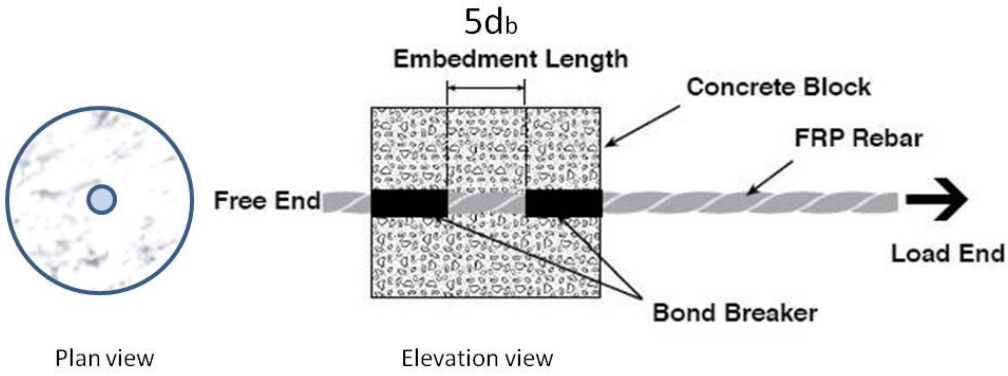

Figure 5.2 Pullout test specimens (ACI 440.3R)

However, when used for the characterization of bond, the concentric pullout test offers the advantage of simplicity but presents two disadvantages:

- At the loading face, the concrete is under compression
- The concrete surrounding the reinforcing rebar tends to split.

Several weaknesses in the use of pullout tests (cylinders or pullout specimens) have been identified in discussions in ACI Committees 408 and 440 because such tests do not sufficiently account for all types of mechanical behavior, such as the flexural curvature and the combinations of shear and flexure[ACI 440-3R and ACI 440R-07]. Many attempts have been made to find a better standard test method.

The direct pull-out test method has been considered with skepticism due to the compressive stress-field existing in the concrete near the loaded end of the rod whereas in a concrete structural element the corresponding region of concrete is under tensile stress. But it was previously concluded that the compressive stress field near the loaded end does not affect the mechanism of bond behavior of FRP rods and that the direct pull-out results are similar to those from other bond tests [Moon, 2005]. In fact, the stress field in the concrete is important in

situations such as steel-reinforced concrete where failure of the concrete governs pull-out behavior [Moon, 2005]. In FRP-reinforced concrete, FRP rod is the weak element.

One advantage of the direct pull-out test is the accessibility of the free-end of the rod which allows for measurement of free-end slip [ACI 440R-07]. The direct pullout test specimen is not bulky, so it can be easily handled during conditioning. Therefore, it is believed the direct pull-out test conveniently characterizes the FRP-concrete bond behavior. In order to investigate bond strength of GFRP reinforcement in concrete, direct pullout test has been widely used [Bakis, 1998 and Vishay,1999].

5.3.2 Flexural bond tests

Although pull-out test is extremely useful in many circumstances, pullout tests are not representative of stress field conditions in an FRP reinforced concrete beam [ACI 440R-07]. Flexural beam tests, such as the beam-end test and hinged/notched beam test, solve some of the stress field discrepancies that are present in pullout tests and offer more closely the advantages of representing the beam stress field. The beam-end test method is described in detail for steel reinforcing bars in ASTM A 944, and is specified as a test for the relative bond strength of reinforcing bars in concrete. In this method, a bar is embedded in a concrete block, and a tensile load is introduced into the bar using a special test setup as shown schematically in Figure.5.3.

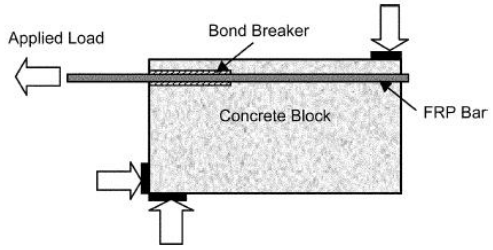

Figure 5.3 Beam-end test for bond characteristics (ACI 440R-07)

Several additional flexural test methods have been used to investigate the bond performance of FRP bars embedded in concrete.

Several of these are shown schematically in Figure.5.4, including (a) the simple beam test (Larralde et al. 1994); (b) the notched beam test (Daniali 1992); (c) the hinged beam test (Magnusson 1997) [ACI 440R-07]. If these tests are done upside down, then the effects of self-weight are practically eliminated. However, bond tests of flexural-types complicate the setup as well as the modeling of the phenomenon. Flexural-type tests can be used to determine not only bond strength but also crack width and crack spacing.

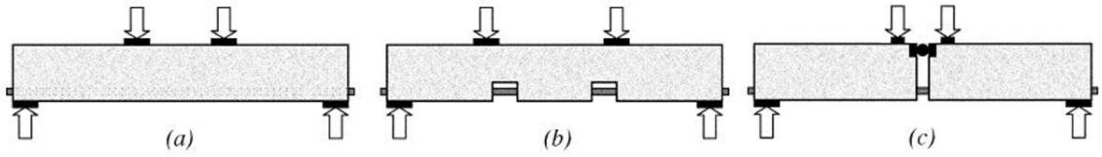

Figure 5.4 Configurations of flexural bond test set-up (a) simple beam test; (b) notched beam test; (c) hinged beam test (ACI.440R-07)

However, these flexural beam tests for bond strength were not conducted in this study based on the result by Larralde et al (1994). The load-slip behavior of the FRP bars in the beam test was slightly different from that in the pullout test. However, the test results in the beams followed the same trend as in the pullout test and the differences were not significant [Larralde et al,1994]

5.3.3 Calculation of bond strength

The transfer of axial force from a reinforcing bar to the surrounding concrete results in the development of tangential stress components along the contact surface. The stress acting parallel to the bar along the interface is called bond stress [Hadi, 2008]. For reinforced concrete to function effectively as a composite material it is necessary for the reinforcing bars to be bonded to the surrounding concrete. Bond ensures that there is little or no slip of the steel

relative to the concrete and the means by which stress is transferred across the reinforcement-concrete [Hadi, 2008].

Bond resistance is made up of chemical adhesion, friction and mechanical interlock between the bar and surrounding concrete. In the deformed bars, the surface protrusions or ribs interlocking with and bearing against the concrete key formed between the ribs contribute more positively to bond strength, and is the major reason for their superior bond effectiveness [Hadi, 2008]. Figure 5.4 illustrates the equilibrium conditions for portion of a reinforcing bar of length *dx*.

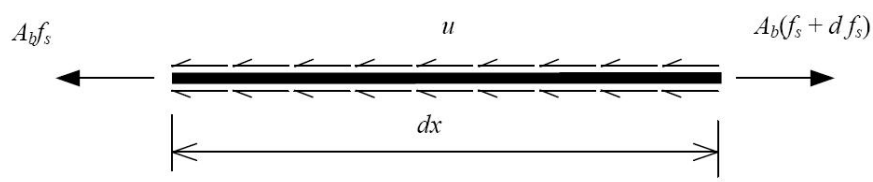

Figure 5.5 Bond stress acting on a reinforcing bar
(Hadi, 2008)

The bond stress *u* can be expressed as the change in the stress in the reinforcement over the length *dx* as follows [Hadi, 2008] :

$$u(\pi d_b dx) = A_b(f_s + df_s) - A_b f_s \qquad \text{(Eq.5.1)}$$

$$u = \frac{A_b df_s}{\pi d_b dx} \qquad \text{(Eq.5.2)}$$

where A_b is the area of bar, d_b is the bar diameter and f_s is the stress in the bar.

Bond stress is defined as the shear force per unit surface area of the bar. For a cylinder pull-out specimen with circular bar, the bond stress is given in Eq.5.3. under assumption that the bond strength was distributed equally over the embedded length of the FRP reinforcing bar[Hadi, 2008]. The bond strength was calculated from Eq.5.3.

$$\tau = \frac{F}{C_b \cdot l} \qquad \text{(Eq.5.3)}$$

where, τ is average bond stress, F is tensile force carried by the bars, C_b is equivalent circumference of FRP bar and l is bonded length. Bond strength is known to develop mainly by: (a) shearing stresses developed by adhesion along the bar surface, (b) bearing stresses developed against the face of the rib, and (c) shear stresses acting on the concrete surface between adjacent ribs. Important implication of bond is the contribution to cracking of the concrete. Better bond results in lower slip between the bar and concrete, and provides better composite action [Hadi, 2008].

5.4 Experimental program

This chapter involved bond strength after exposure to accelerated aging of GFRP reinforcing bars embedded in concrete. In terms of materials, same GFRP bars (all #3 bars of Type-A and Type-B) and concrete mix designs described in chapter-4 were used to characterize environmental impact on the interface's long-term performance. In terms of conditions of accelerated aging, specimens were cast and placed in the same chamber B with the temperature of 115°F (46°C) and RH of 80% after immersing in 3% saline solution described in chapter-4 for 300days. Only pullout test specimens with different type of rebars and exposure duration in chamber were tested.

These specimens were 12in (300mm) concrete cylinder with a single GFRP bar embedded vertically along the specimen's central axis. The bar's bonded length was five times bar diameter of 2 in. GFRP bars were prepared with bond breakers which consisted of thin aluminum tubing inserted around the bar to prevent contact of FRP with concrete in order to control the bond length. Figure.5.6. described a typical specimen. Cylinder pull-out specimens were cast with 2.0 in (50mm) bond lengths.

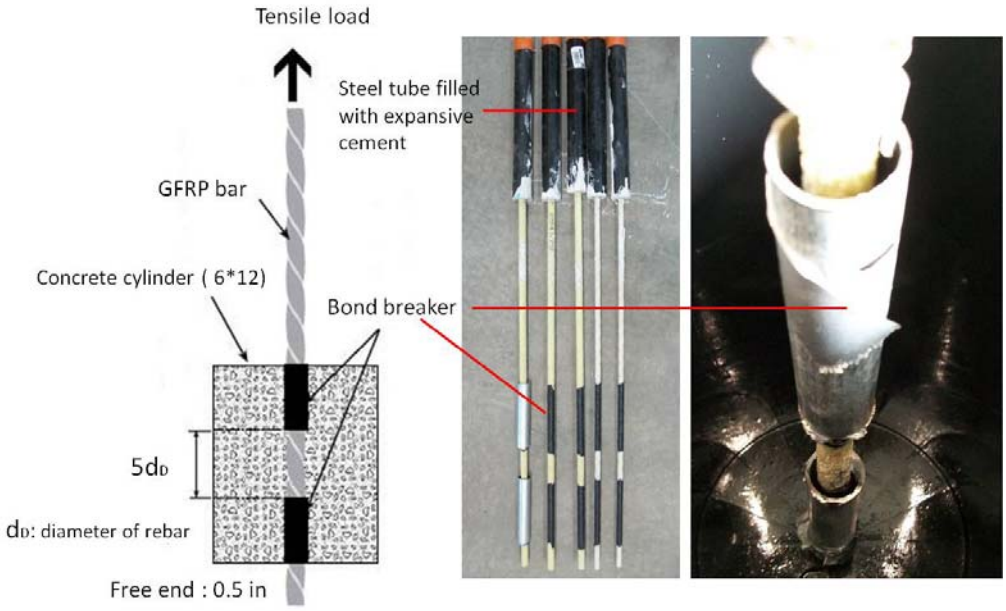

Figure 5.6 Setup for fabrication of pullout specimens

One end of the bar embedded in the concrete cylinder (6 X12) was covered with 5 in (125mm) flexible split plastic tubes of a bond breaker. Bonding length (2.0in) of the bars was located at the center of the cylinder. Positioning of the bars was conducted vertically through a wood alignment guiding frame for the fabrication of the specimens. After concrete-casting, the bond cylinder specimens were removed from the molds two days after and placed in the chamber B subjected to the environmental conditioning as described in chapter-4.

The specimens were tested as shown in Figure.5.7 for pullout testing. Two-linear variable differential transformers (LVDTs) were used to measure the slip at both the free-end and loaded-end.

The effect of axial extension of the FRP bar itself was considered from the data recorded by the second LVDT. Steel pipe grips were used as described in ASTM D7205/7205M in order to avoid premature failure. There was a 10 mm wood plate placed between the concrete cylinder and supporting steel block to prevent bending or movement by the irregularities at the contact surface of the cylinder during loading with the rate of 0.05in/min

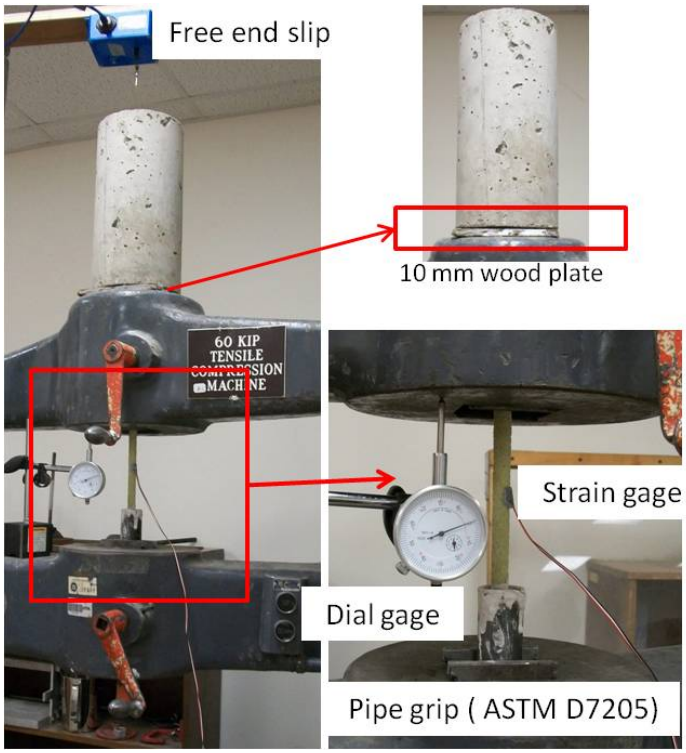

Figure 5.7 Test setup of pullout test and instrumentation

5.5 Test results and discussion

After completion of accelerated aging for 300days, specimen bond properties were measure. Accelerated aging provides information about the long-term behavior of the GRFP-bar–concrete interface by comparing their average bond stress, slippage values, and mode of failure to those of the control specimens.

Based on ACI 440.3R-04, all conditioned specimens were subjected to pulling out directly. The bond-strength results are summarized in Table.5.1. Bond stresses of the unconditioned specimens were found to be 3038 and 3219 psi for wrapped surfaced bars (Type-A) and sand coated bars (Type-B). The values of the measured bond-strength retentions were 97.5% and 94.1% for Type-A and Type-B respectively after 300 days of exposure to accelerated aging (115°F and RH=80%). The bond strength was only slightly affected by

exposure duration. Bond-strength reduction was less than 6% after 300days of complete exposure. In case of Type-A bars, the reduction was 2.5%. In case of Type-B bars, it was observed that the reduction of bond strength was 5.9%. The bond strength was slightly affected by accelerated environmental aging.

The typical relationships between bond stress and free-end slip curves are summarized in Figure.5.8 through 5.9. It can be noted that the bond-slip behaviors of FRP bars with different types of the surface were quite different. The bond failures of Type-B GFRP bar (sand-coated surface) were relative brittle compared with ones of Type-A GFRP bar (helically wrapped surface). That is, in case of the Type-B GFRP bar, the sudden free end slip was observed. Bond-slip curves after the post peak bond strength depends on characteristics of bar surface.

Table 5.1 Summary of bond strength of GFRP bars

Bar type	Average concrete strength	Increase of Concrete strength	No. of specimens			Average bond strength	Average bond strength retention
	(psi)	(%)	1	2	3	psi	%
No-exposure							
Type-A	4339	-	2916	3038	2974	2976	100
Type-B	4109	-	3094	3336	3219	3216	100
300days							
Type-A	5134	18.3	2888	2916	-	2902	97.5
Type-B	4909	19.5	2876	3179	3029	3028	94.1

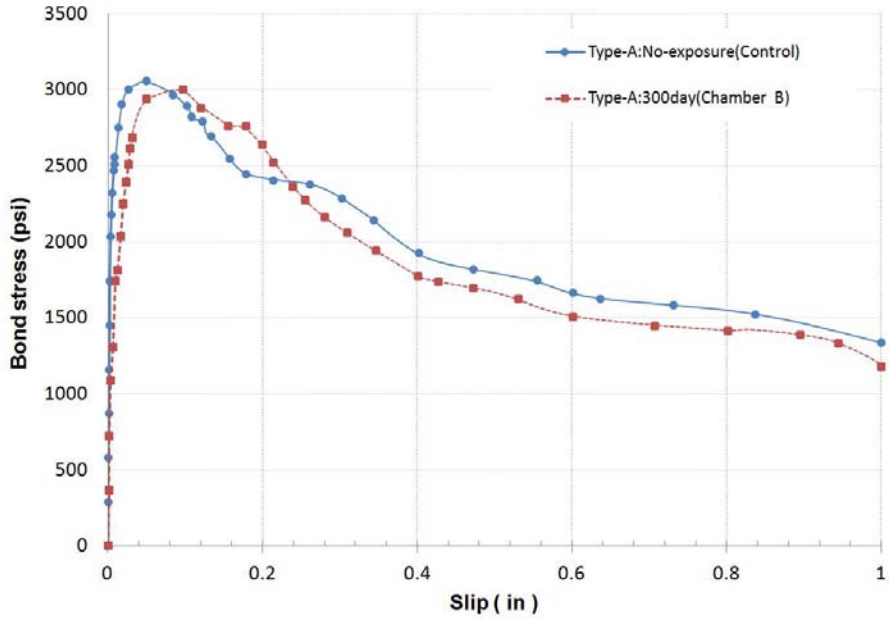

Figure 5.8 Bond stress and slip curve of pullout test (Type-A : Wrapped surface)

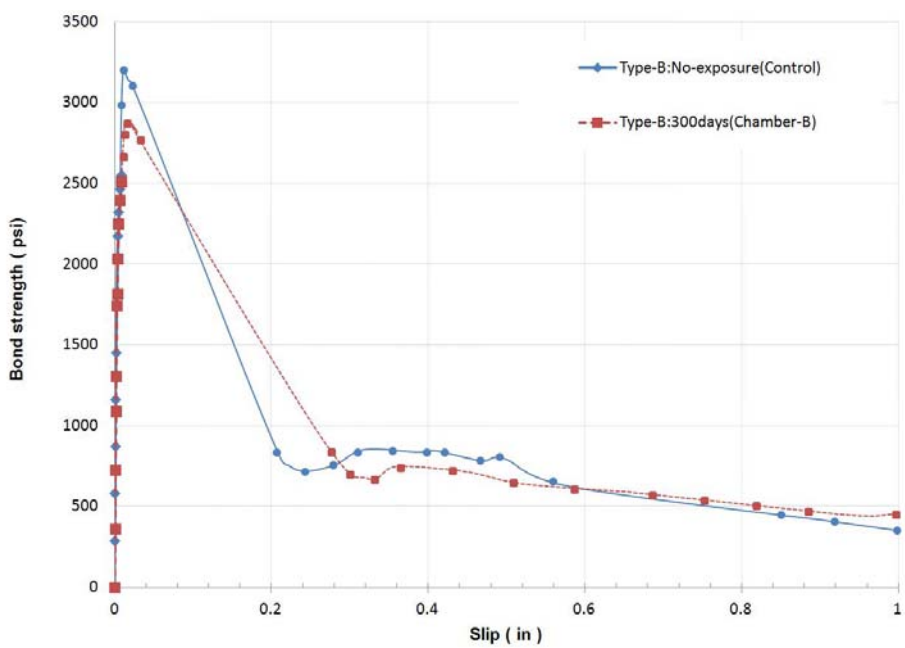

Figure 5.9 Bond stress and slip curve of pullout test (Type-B : Sand-coated surface)

In the case of Type-B GFRP bars, it can be observed not only that the sudden free-end slip was occurred but also that the post peak bond strength was about 23% of its ultimate bond strength while Type-A bars did not show post peak curves. The low post peak bond strength of Type-B bar was due to the failure of interface between the sand coating layer and core-bar during the pullout test as observed in Figure.5.9. This results show a good agreement with the results by Davalos et al. (2008).

It can be seen that all specimens tested under direct pullout tests failed exhibiting free-end slip. The unconditioned as reference and conditioned specimens exhibited the same bond failure modes. After the tests, the concrete cylinders were separated in several splitting in order to check the bond failure mode. The bond failure of Type-B bars usually occurred at the interface of the concrete and sand coating and/or at the interface of the sand coating and bar. That is, the layer of sand coating was stripped. The failure of “peel-off” of the core section was observed in the case of Type-B with perfect sand-coated surface. This results show a good agreement with the results by Davalos et al. (2008).

5.6 Summary

In this chapter, the bond strength of GFRP rebars with different types of surfaces under harsh environment was evaluated. Type-A(Aslan-100) bar is an E-Glass bar(vinyl-ester matrix), helically wrapped and sand coated partially for enhanced bonding characteristics while Type-B(VROD-HM) bar has vinyl-ester matrix and sand coated fully for enhanced bonding characteristics. Based on these experimental results, the following conclusions can be made.

- Accelerated environmental conditioning resulted in bond strength reduction of below 3% for Type-A GFRP bars and 6% for Type-B GFRP bars respectively. The effects of accelerated aging on the GFRP bars were not critical in terms of bond strength.

- The bond failure mode is dependent on the surface type of each bar which is usually made to enhance bond strength. Type-B GFRP rebar (sand-coated surface) specimens showed higher bond strength of about 8.1% compared with Type-A bars(wrapped surface).
- Type-A bars had better bond durability performance than Type-B bars. That is, rate of reduction of bond strength for Type-A was less than one of Type-B.
- Type-B specimens failed in pullout due to peeling off between sand coated surface and core section and showed relatively brittle bond behavior.
- The bond slip curve (post peak bond strength) showed different behaviors between Type-A and Type-B.

CHAPTER 6

FLEXURAL TESTS: LONG-TERM FLEXURAL BEHAVIORS OF CONCRETE BEAMS REINFORCED WITH GFRP BARS AFTER ACCELERATED AGING

6.1 General

A significant number of simulated aging tests on GFRP bars as strand alone have been conducted in the past decades and long-term performance prediction approaches have also been carried out which provided good basis for the durability evaluation and design of GFRP bars. However, few experimental approaches have been developed specifically for concrete members reinforced with GFRP bars after accelerated environmental aging. Although the number of analytical and experimental studies on long-term performances of GFRP bars has increased in recent decades, it is still lower than the number of such studies related to concrete members reinforced with GFRP bars as structural members.

This paper presents the results and discussion of an experimental program concerning concrete beams reinforced with glass-FRP (GFRP) bars after accelerated environmental aging. The main aim of the study is to evaluate the long-term flexural behavior by varying the reinforcement ratio and the exposure duration. In this study, accelerated aging tests were conducted on pre-cracked concrete beams conditioned to the environment chamber exposed to 80% relative humidity (RH), 115˚F of temperature and 3.0% salt solution for 100, 200 and 300 days similar to accelerated aging test on GFRP bars mentioned in Chapter 3. Seventy-two beams were designed with an adequate amount of longitudinal and shear reinforcement so as to make them fail by crushing of concrete in the central zone (pure bending zone). Except for the reference beams, the remaining beams were pre-cracked by simulated service loading for a

concrete strain of $800x10^{-6}$(for 2-#4) and $500x10^{-6}$(for 3-#5) respectively. Details of the specimens, materials, test setup, instrumentation and test results are described in this chapter.

6.2 Specimens, test setup and test procedure for flexure

6.2.1 Fabrication of specimens

Dimensions of seventy-two specimens, 8in×12in×83in (200mm×300mm×1800mm: Width×Depth×Length), were fabricated. For tensile reinforcement, the longitudinal reinforcement consisted of two-0.5 in (13mm: #4) or three- 0.675 in (16mm: #5) diameters for each specimen. The inclined transverse reinforcement consisted of 0.375 in (10mm: #3) diameter stirrups of steel with a yield strength of 60ksi (410MPa) spaced 5 and 7in from the end of the beam based on the ACI 318-11. Sec.11.4. A reason that inclined stirrups with an angle of 45 degree are used is the reduction of number of shear reinforcement in order to detect acoustic emission resources effectively. Conventional RC beams with equal dimension and reinforcement ratio of steel will be also fabricated for comparison. The two variables are types of GFRP bars (Type-A and Type-B with relative high modulus of elasticity), types of reinforcement (steel or GFRP), reinforcement areas (2-#4/3-#5) and environmental aging (exposure or non-exposure of temperature and humidity up to 300days). Figure.6.1 shows the variations of reinforcement ratio affecting the strength reduction factor. It is seen that minimum reinforcement of the specimen is 0.901(failure mode: FRP-rupture) and 4.759(failure mode: concrete crushing) respectively, compared GA-2-4-300 with GH-3-5-0. Reinforcement ratios of steel are less than the ones of GFRP specimens with same amount of reinforcement areas (two-#4 and three-#5). The changes of concrete compressive strength are considered to calculate the reinforcement ratio and are be tabulated in a following section. All beam specimens had a target concrete compressive strength of 4000psi with same mix design described in Table.4.1. The original mechanical properties of rebars used in this fabrication are described in Chapter 2.

The nomenclature of test specimens is as follow. The first character, “GA” or “GH” or “S”, represents the type of reinforcement for glass fiber of Type-A , Type-B(high M.O.E.) and steel respectively, the second and third characters,”2-3” or “3-5” are the rebar number and size for indicating of reinforcement ratio. For example, 2-4 represents that the reinforcement consists of two-No.4 bars and the last character varying from 0 to 300 represents the exposure duration (day). Figure.6.2 and 6.3 show the procedures for reinforcement caging and concrete casting typically.

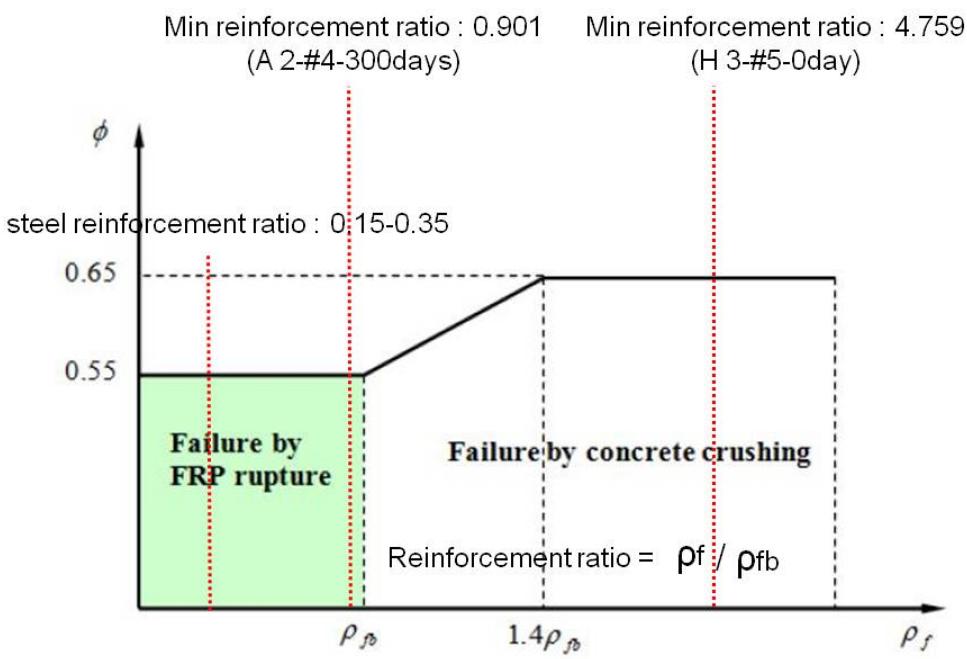

Figure 6.1 Variations of reinforcement ratio based on the change of strength reduction factors (ACI 440.1R-06).

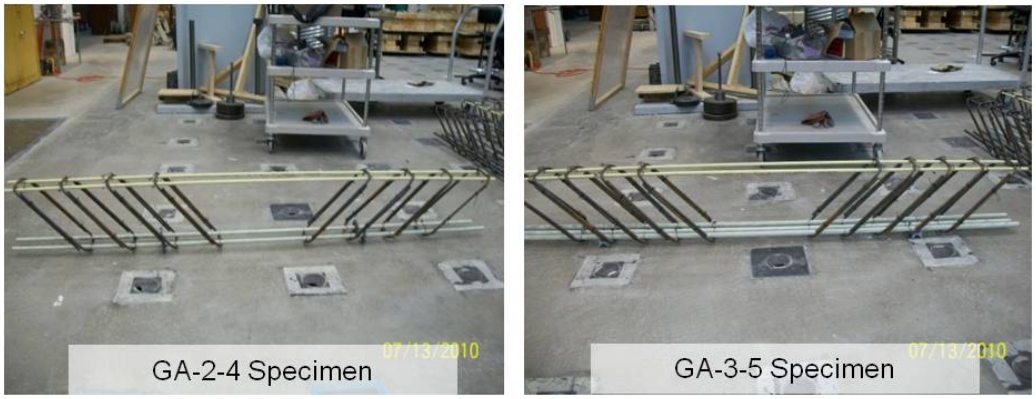

Figure 6.2 Reinforcement caging for each case (GA-2-4 and GA-3-5)

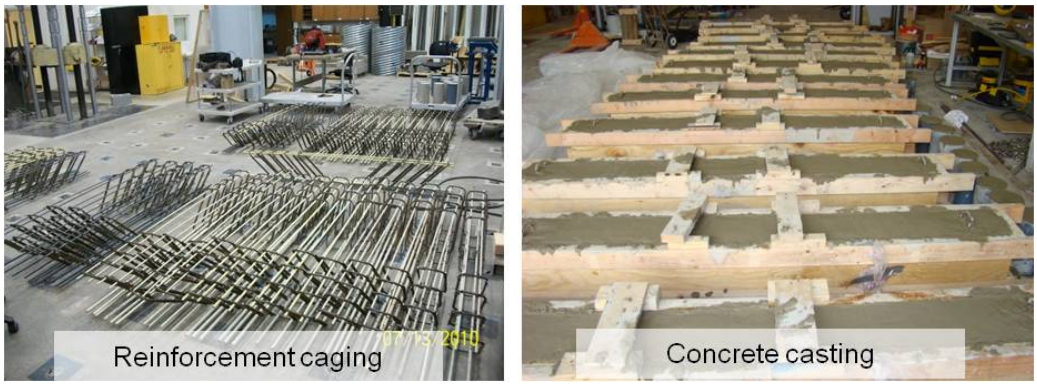

Figure 6.3 Typical caging and concrete casting

6.2.2 Sustained loading for pre-cracking of specimens

All beams were clamped in pairs using transverse steel rods at the beam end to simulate damages of cracks in service conditions. Prior to exposure in the chamber, immersion of pre-cracked specimens into 3% of saline solution and equal end moments were applied to the test beams using clamping. The sustained load level will be selected as 0.25P (25% of P) where P is the flexural load capacity of the beam reinforced with GFRP bars. Deformation constant will be used to prevent release after jacking.

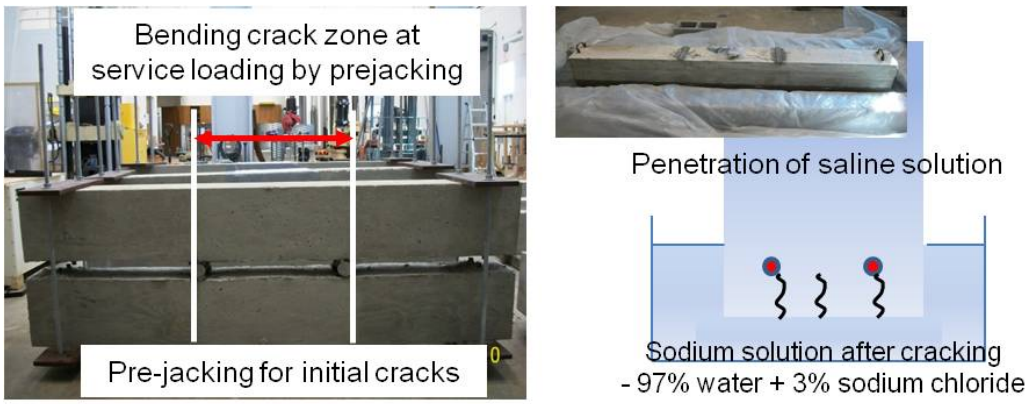

Figure 6.4 Pre-jacking for initial cracks and immersion in 3% saline solution after creating cracks simulating damages under service loading level

6.2.3 Accelerated aging method in the chamber

Accelerated weathering in North-Texas region (DFW area) is considered. The climate in DFW area is characterized by a hot summer and other humid seasons relatively with moderate seasonal variation in temperature or precipitation through the years. Also, DFW area receives not less than ten sunshine hours per day. For more aggressive environmental conditions, the test was focused on choosing average highest temperature of 115°F and average relative humidity of 80% during about last 30 years.

Table 6.1 Correlation between accelerated and real exposure in the chamber (Eq.4.8.)*

Temperature of 115°F and RH of 80%		
C (Accelerated exposure in lab.) -days	N (Equivalent-natural exposure)-days	N (Equivalent-natural exposure)-years
100	3017	8.3
200	6035	16.5
300	9052	24.8

Note* : The anticipated natural aging were calculated from $\frac{N}{C} = 0.0876 \cdot e^{(0.0508 \cdot T)}$

Where, N=Natural aging (days), C=Chamber aging (days), T=temperature (°F)

Based on the proposed equation, the Table.6.1 shows the correlation between natural exposure in the field and accelerated exposure in the laboratory. Re-jacking to simulate service

loading in the chamber and placing in the chamber are shown in Figure.6.5. Cracks by pre-jacking to simulate service stage of loading were marked and crack width and spacing were measured within the constant moment zone. Cracks induced by sustained loading also accelerate the aging effect in the chamber.

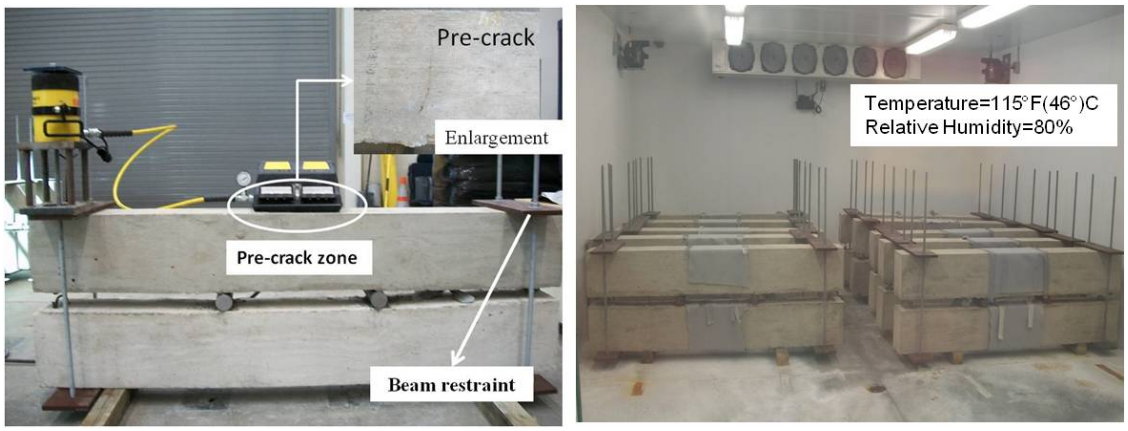

Figure 6.5 Re-jacking for simulating service loading in the chamber and placing in the chamber

6.2.4 Four-point bending test

All specimens were tested in an MTS machine controlled with Vishay software after accelerated environmental conditioning. This machine recorded the load and displacement simultaneously. All tests were displacement-controlled at a rate of 0.005in/min. Strain gauges were set up across the center of beams to check the distribution of strain. Comparative studies were necessary to investigate the various effects by the conditioning. Therefore, various comparisons were made during the test. The arrangement is as shown in the Table.6.2 below. The four variables are types of GFRP bars (ASLAN100 and V-ROD HM), types of reinforcement (steel or GFRP), reinforcement ratio (ρ_f/ρ_{fb}) and environment (exposure or non-exposure of temperature and humidity).

Table 6.2 Details of test specimens

Specimens		GA1	GA2	GA3	GA4	S1	S2
Status	Rebar type	ASLAN 100 +	ASLAN 100 +	ASLAN 100 +	ASLAN 100 +	Steel	Steel
	Exposure	exposed+	exposed+	Non-exposed+	Non-exposed+	exposed+	exposed+
	Ratio (ρf/ρfb)	1.08	2.04	1.08	2.04	0.16	0.35
Specimens		**S3**	**S4**	**VHM1**	**VHM2**	**VHM3**	**VHM4**
Status	Rebar type	Steel +	Steel +	VROD-HM +	VROD-HM +	VROD-HM +	VROD-HM +
	Exposure	Non-exposed+	Non-exposed+	exposed+	exposed+	Non-exposed+	Non-exposed+
	Ratio (ρf/ρfb)	0.16	0.35	2.28	4.76	2.28	4.76

Note : ρ_f= FRP reinforcement ratio / ρ_{fb}= FRP reinforcement ratio producing balanced strain conditions

The test set-up and the geometry of beam specimens are also shown in the Figure.6.6. The ultimate loads are defined as the maximum loads measured by the load cell used with the data acquisition (DAQ) system. A hydraulic jack applied the load to the GFRP RC beam through a spreader beam. In order to measure the deflection of the tested beam, two transducers (linear variable differential transformers LVDTs and strain gauge based transducers) were used in the mid-span section. An optical magnifier with an accuracy of 0.002 in was used to measure crack widths. Horizontal top and bottom strains were measured in the mid-span zone by five-strain gages instrumented on the surfaces of the rebars. This configuration allowed sectional rotations to be measured and the average curvature of the pure bending zone to be calculated. Two of these gauges were instrumented on the bottom longitudinal reinforcements, whereas three gauges were instrumented on the top longitudinal reinforcements as shown in Figure.6.7.

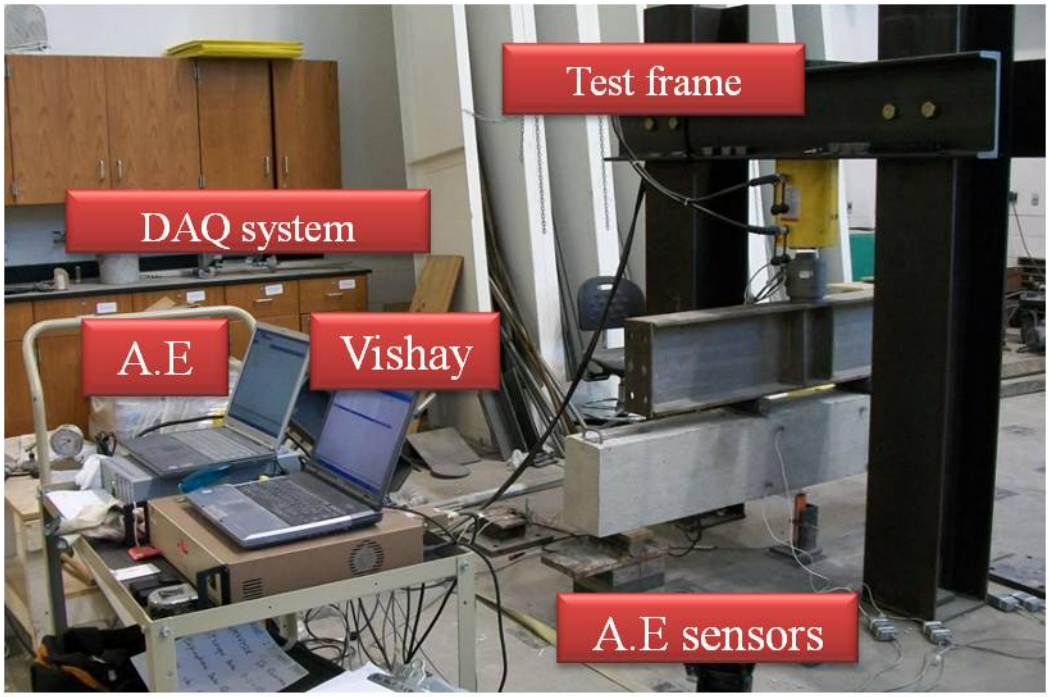

(a)

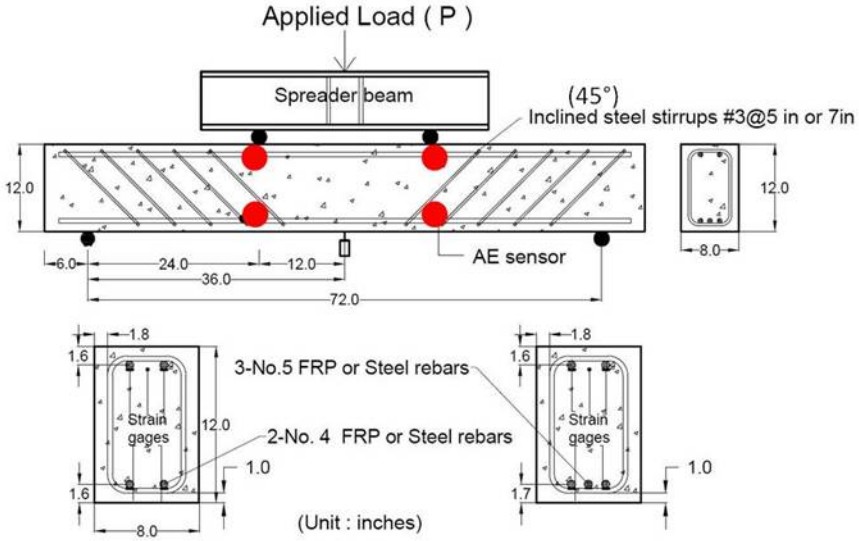

(b)

Figure 6.6 (a) Test set-up and (b) details of a specimen

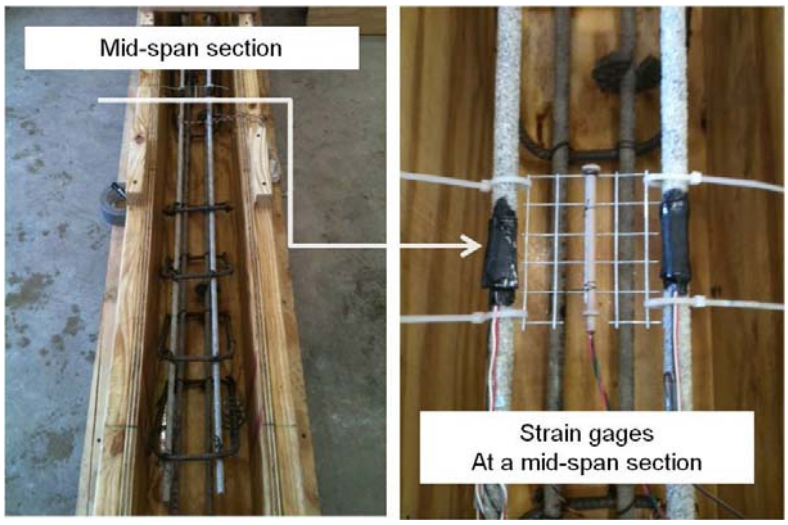

Figure 6.7 Typical instrumentation of strain gages at a mid-span section

6.2.5 Loading history

Each testing group is subjected to repeated cycles of loading and unloading until failure was reached, as shown in Figure.6.8. Energy absorption of GFRP reinforced concrete beams can be obtained in terms of area under the load-deflection curve.

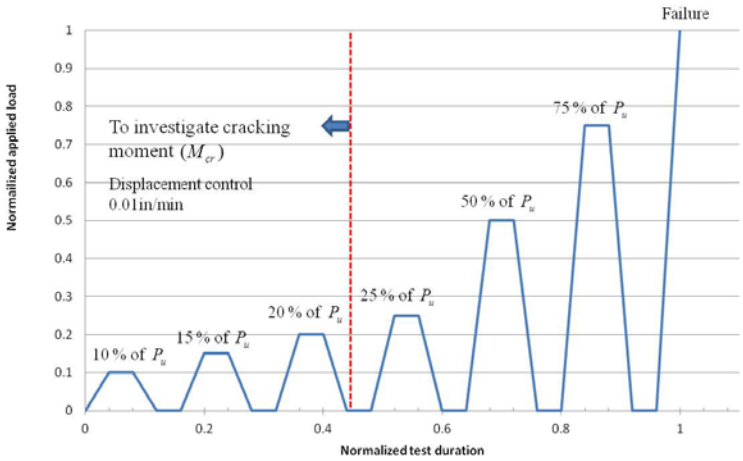

Figure 6.8 Loading history

To understand the energy absorption and AE characteristics in GFRP reinforced concrete sections, load versus deflection of each beam under progressive loading and

unloading in seven cycles was noted with each cycle resisting a higher load than the previous cycle as shown in Figure.6.8. The experimental slopes of unloading curves were recorded.

6.3 Test results and discussion

In this section, the most significant comparisons of experimental results are presented between unexposed and exposed specimens in accelerated aging conditioning up to 300days. Initially, the mid-span section is analyzed, in terms of the strain distribution along the depth of the section and the evolution of neutral axis depth with load and the moment–curvature relationship examined. Finally, a general analysis of the beam behavior is presented. In this study, both ultimate and serviceability limit states are studied by load-deflection, cracking behavior, modes of failure and ultimate load between unexposed and exposed specimens in accelerated aging conditioning. The calculations for the serviceability state were performed for loads up to 25% of the ultimate load, which is considered to be a value that covers sufficiently the usual range for GFRP RC beams [Bischoff et al, 2005].

6.3.1 Moment-curvature

6.3.1.1 Tri-linear moment-curvature relationship

The moment–curvature relation of a section is uniquely defined according to the dimensions of the concrete section and the material properties of concrete and reinforcement [He et al., 2007]. Also, the gradient of the moment–curvature relation means the elastic bending stiffness EI which includes all the section properties in a typical loading condition. In determining the theoretical moment– curvature curve for the section with flexure, the basic assumption that plane sections remain plain so that the longitudinal strain is directly proportional to the distance from the neutral axis of zero strain is used. The tri-linear moment-curvature relationship by He (2007) can be characterized by three points, point a, point b and point c as show in Figure.6.9. Point b in Figure.6.9 is the intersection point of the contour line when moment is equal to M_{cr}

and post-cracking resistance curve. The following determines the characteristic values at these points [He et al., 2007].

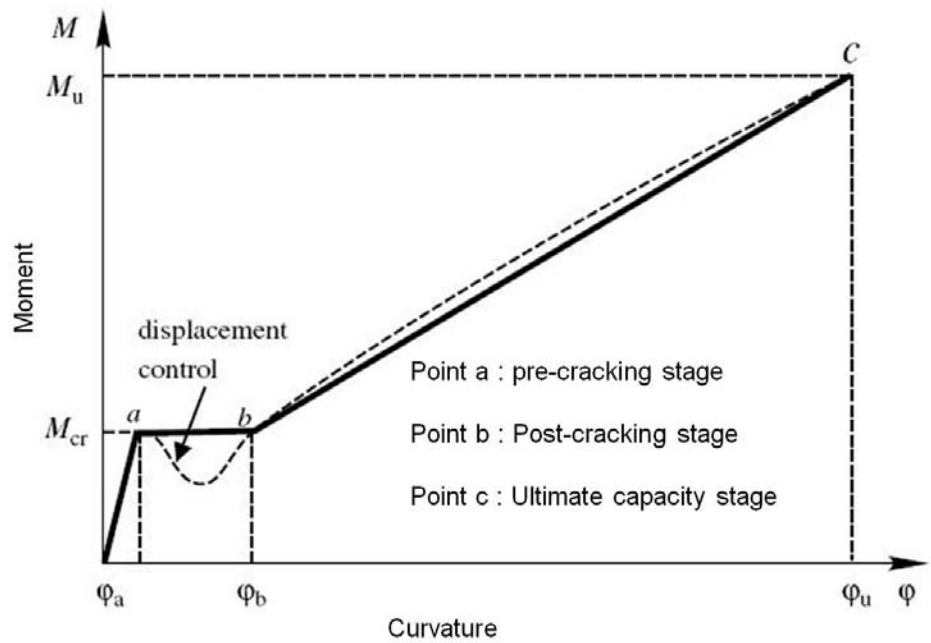

Figure 6.9 Idealized tri-linear moment-curvature relation
(He et al, 2007)

For point a, assume the compressive stress block is triangularly distributed and has a height of X_a. as seen in Figure.6.10 (a). By using static equilibrium equation, X_a and the corresponding curvatures at point a (φ_a) can be obtained as Eq.6.1 and 6.2[He et al., 2007].

$$x_a = \frac{bh^2 + 2A_f \gamma_c h_0}{2(A_f \gamma_c + bh)} \qquad \text{(Eq.6.1)}$$

$$\varphi_a = \frac{f_t}{(h - x_a)E_c} \qquad \text{(Eq.6.2)}$$

where γ_c is the ratio of modulus of elasticity of FRP reinforcement to concrete (E_f/E_c) and f_t is tensile strength of concrete [He et al., 2007].

For point b, it is still reasonable to assume the stress block for compressive concrete is triangularly distributed in that current stress level remains relatively low[He et al., 2007]. Bottom concrete has already cracked and the internal stresses have been redistributed, the curvature at this time is much bigger than that at point a, φ_a. As Figure.6.10 (b) shows, the static equilibriums can be expressed by two unknowns, sectional curvature, φ_b, and the maximum compressive strain of ε_c. as seen in Eq.6.3 and 6.4 [He et al., 2007].

$$\varphi_b = \frac{\varepsilon_f + \varepsilon_c}{h_0} = (1+\alpha)\eta \qquad \text{(Eq.6.3)}$$

$$\eta = \frac{f_t}{E_c h_o \sqrt{1 - 2\gamma_c \rho_f \alpha(1+\alpha)}} \qquad \text{(Eq.6.4)}$$

where ε_f is the strain at the level of FRP reinforcement, α is the ratio of strain of reinforcement to concrete (ε_f / ε_c) and ρ_f is reinforcement ratio (ρ_f=A_f/bh_o).

For point c of ultimate stage, it can be assumed that the tensile resistance of concrete can be ignored in calculating the flexural capacity of a beam. For over-reinforced cross-sections($\rho_f > \rho_{fb}$,), the ultimate flexural capacity, M_u can be calculated from Eq.2.7. to Eq.2.10. Then, the corresponding ultimate curvature can be obtained in Eq.6.5. Figure.6.12 (c) shows the ultimate stage at point c [He et al., 2007].

$$\varphi_u = \varphi_c = \frac{\varepsilon_{cu}\beta_1}{\overline{x}_c} \qquad \text{(Eq.6.5)}$$

where α_1 and β_1 are 0.85 for normal compressive strength of concrete.

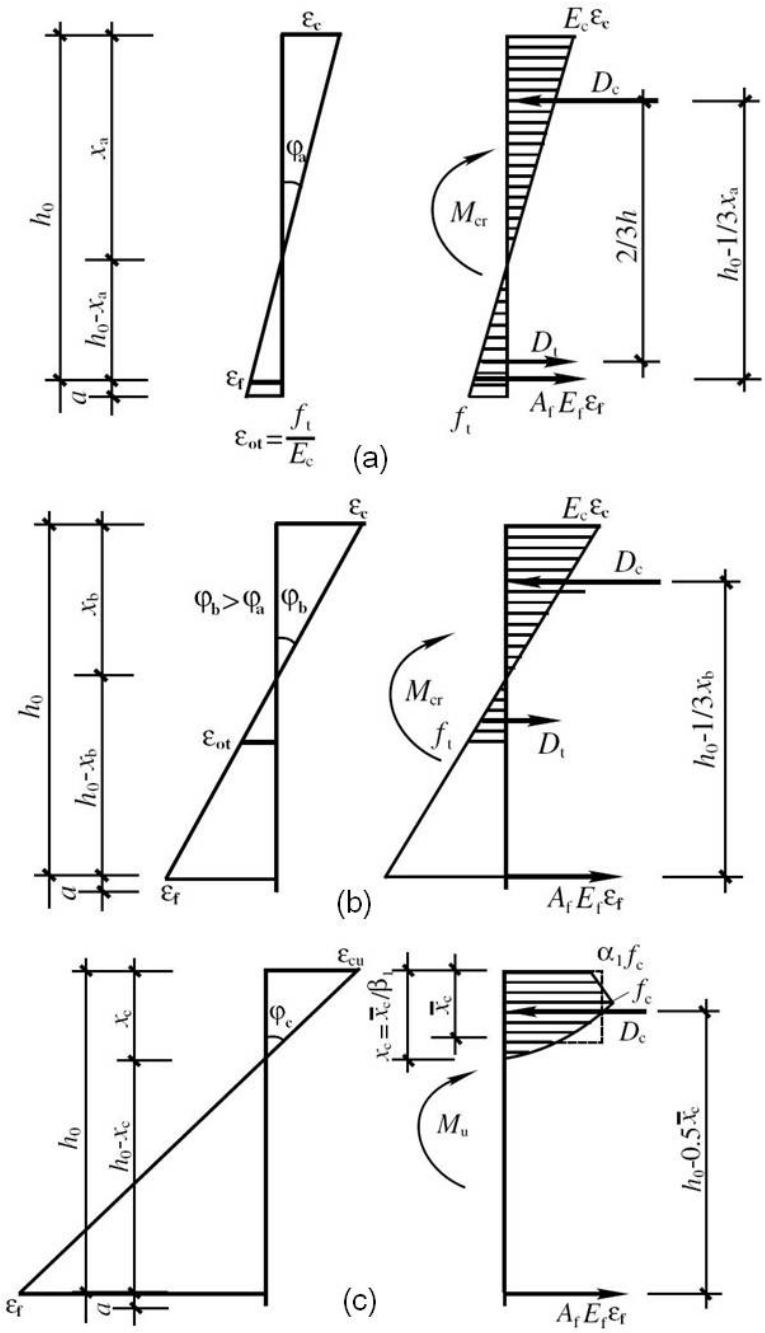

Figure 6.10 (a) Cracking state at point a (b) Cracking state at point b
(c) Ultimate stage at c (He et al, 2007)

6.3.1.2 Comparison of moment-curvature

The mean curvature of the central zone is calculated from the difference between strains (obtained from the strain gages) at the top and bottom of the beam by the corresponding distance. Moment-curvature diagrams of the beams obtained by means of the theoretical model are shown in Figure.6.11 through 6.13 and are compared with those of the experimental model.

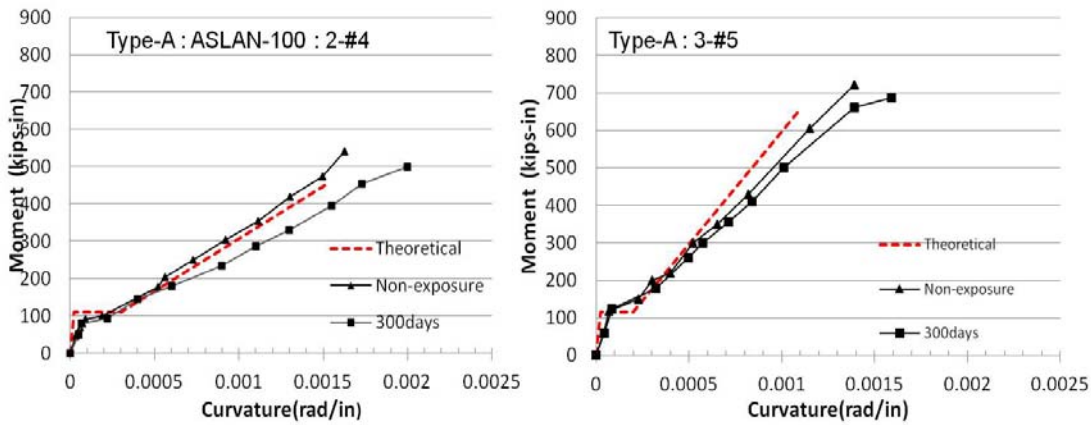

Figure 6.11 Moment-curvature of beam specimens with Type-A (ASLAN 100)

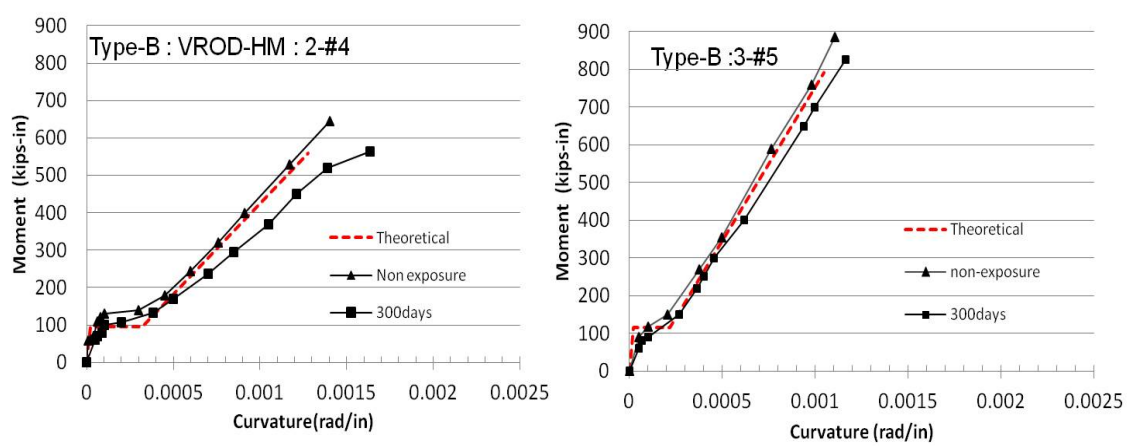

Figure 6.12 Moment-curvature of beam specimens with Type-B (VROD-HM)

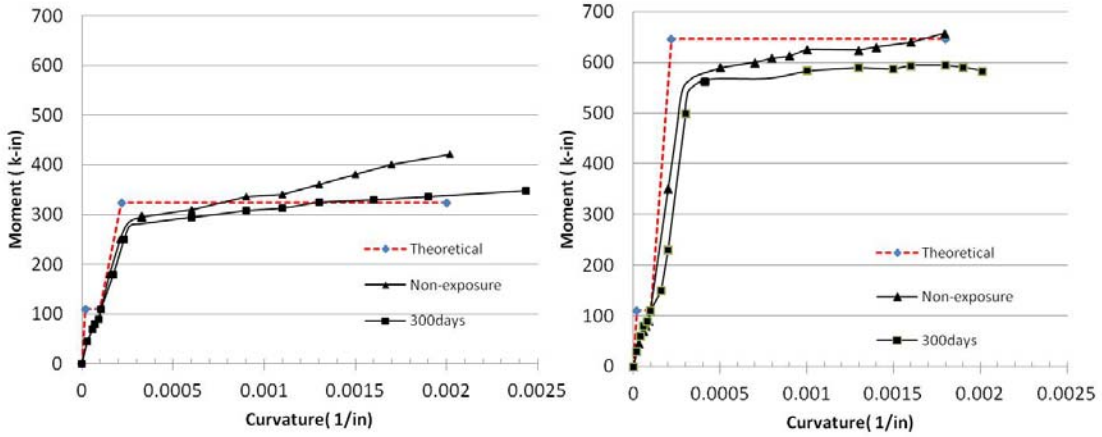

Figure 6.13 Moment-curvature of beam specimens with steel

In case of Type-A GFRP rods, ultimate curvature showed an increase of 19.8% (2-#4) and 6.9%(3-#5) after 300days exposure in the chamber B (115°F/ RH=80%). In case of Type-B GFRP rods, ultimate curvature showed an increase of 16.7% (2-#4) and 5.8%(3-#5) after 300days exposure in the chamber B (115°F/ RH=80%). In case of steel rods, ultimate curvature showed an increase of 20.7% (2-#4) and 12.0% (3-#5) after 300days exposure in the chamber B (115°F/ RH=80%). Many of the conditioned beams showed a decrease in stiffness. The decrease of flexural rigidity according to the increase of ultimate curvature is reflected. As shown in the Figure.6.11 through 6.13, the flexural rigidity has a marked reduction at the cracked and ultimate stage, following the increase of curvatures.

Figure.6.11 through 6.13 show generally not only good agreements between the unexposed experimental data (Non-exposure) and the theoretical moment–curvature calculations for each reinforcement case, but also the fact that experimental curves show less stiff cracking response before the theoretical cracked stage because the specimens were already damaged by pre-jacking. In all cases, the ultimate curvatures of the beams increase after accelerated aging for 300 days due to the higher deterioration in the strength and stiffness properties of the constituent materials. The results of experiments also show that experimental results have greater curvatures than theoretical prediction because the experimental strain in

extreme concrete fiber in compression at failure is 0.0036 while the ultimate useful strain in the analytical procedure is limited to 0.003. It is also observed that the smaller reinforcement area with two-#4 bars showed faster degradation rates than larger one with three-#5.

6.3.2 Load-rebar strain profile

Typical representations of the experimental strain profiles along the depth for different load levels are shown in Figure.6.14 (a) and (b). Because pre-cracks were occurred, the differences among them didn't increase rapidly. As expected, the maximum concrete strain in compression is reached by the top surface strain gauge depending on the position of the neutral axis. A higher reinforcement ratio eventually results in a higher depth of the concrete compression block and, therefore, more compressive strain is measured at this last strain gauge. A linear relation between the three strain values is observed, thus confirming the validity of Bernoulli hypothesis, both before and after cracking. Regardless of the exposure duration into environmental aging, the strains of unconditioned beams were similar to the ones of exposed beams at service loading stage in all cases.

The experimental position of the neutral axis was deduced from the data from the strain gauges. As can be seen in Figure.6.14 (a) and (b), the neutral axis depths did not located at the mid-height of the section due to pre-cracks and decreased as crack propagation was developed and the duration of environmental aging was increased slightly. For ultimate stages in all cases, strains of the longitudinal reinforcement increased until the maximum load is achieved. The neutral axis depth increases with the reinforcement ratio, since equilibrium of forces requires a larger compression block for the greater forces arising from larger areas of reinforcement.

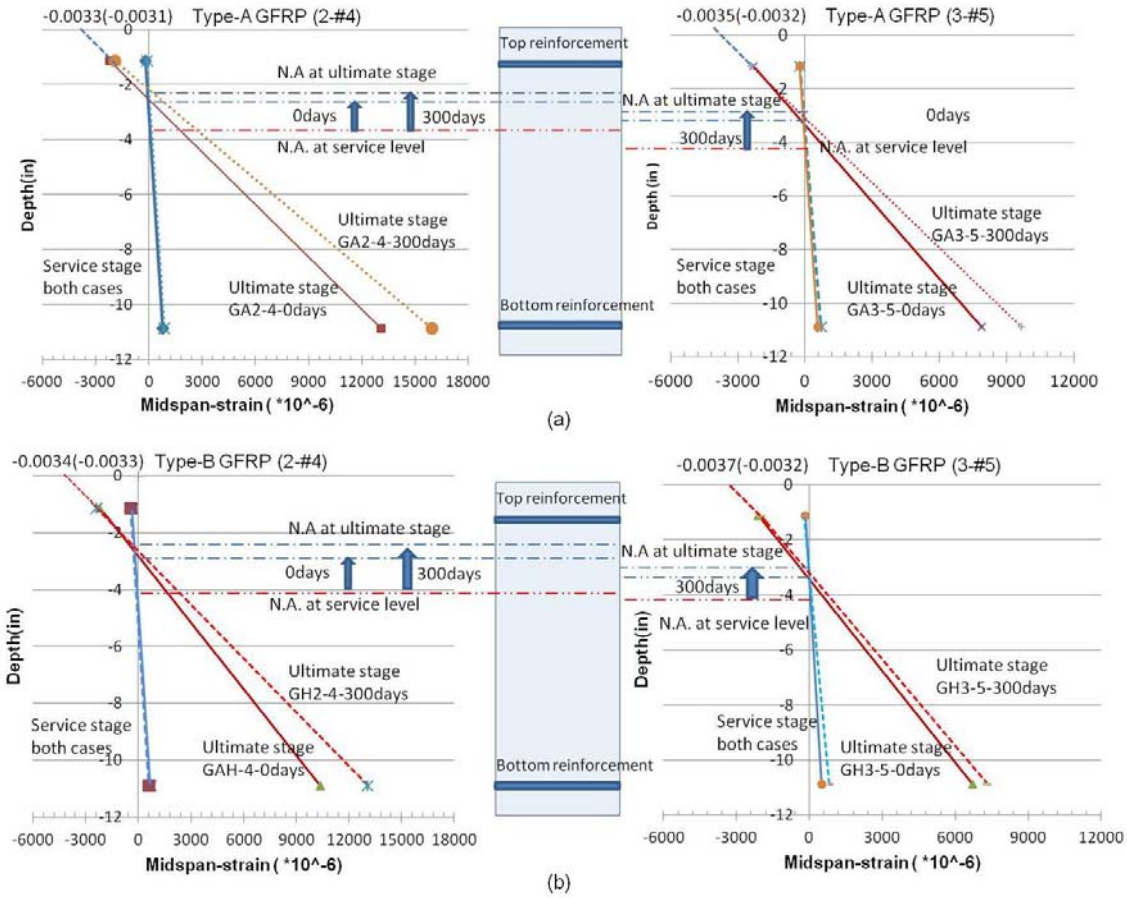

Figure 6.14 Strain along mid-span depth (a) Type-A (b) Type-B (non-exposure and 300days)

6.3.3 Failure mode

Sixty beams were designed to fail by concrete crushing, which means that failure was expected to occur when concrete reached its maximum compressive strain ε_{cu} except the case of twelve beams of GA2-4 with balanced failure. According to ACI 440.1R-06, this failure mode is obtained when the reinforcement ratio ρ_f is greater than the balanced reinforcement ratio ρ_{fb} in Eq.6.1 and Eq. 6.2.

(a)

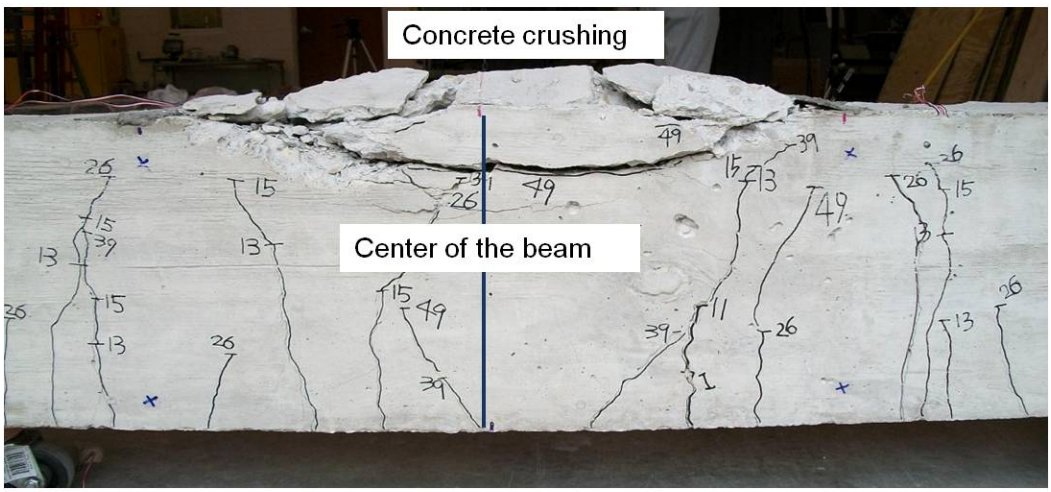

(b)

Figure 6.15 (a) Balanced failure (GA2-4) and (b) concrete crushing failure (GH2-4)

$$\rho_f = \frac{A_f}{bd} \qquad \text{(Eq.5.1)}$$

$$\rho_{fb} = 0.85\beta_1 \frac{f_c^{'}}{f_{fu}} \frac{E_f \varepsilon_{cu}}{E_f \varepsilon_{cu} + f_{fu}} \qquad \text{(Eq.5.2)}$$

where A_f is the area of FRP reinforcement, b is the width of the section and d is the effective depth in Figure.2.4. In Eq. 6.2, β_1 is the ratio of depth of equivalent rectangular stress block to depth of the neutral axis, f'_c is the concrete compressive strength, f_{fu} is the rebar tensile

strength, E_f is the modulus of elasticity of the FRP rebar, and ε_{cu} is the maximum concrete strain (0.003 for ACI provisions). Similarly, ACI 440.1R-06 suggests a minimum reinforcement area derived in Eq.6.3. In Figure.6.15, a typical concrete crushing failure and balanced failure are shown. Concrete crushing of failure was obtained for all beams except beams of GA2-4 with balanced failure.

$$A_{fb.\min} = \frac{4.9\sqrt{f_c^{'}}}{f_{fu}} b_w d \geq \frac{330}{f_{fu}} b_w d \qquad \text{(Eq.6.3)}$$

6.3.4 Cracking

All beams were initially cracked to penetrate conditions of accelerated aging into the reinforcement. When the cracking moment was reached in the pure bending zone, some cracks began to appear and existed cracks were propagated and opened. These cracks were predominantly vertical and perpendicular to the direction of the maximum stress induced by the bending moment. As the load increased, additional cracks developed in the mid span and new vertical cracks formed in the shear span.

The cracks developed in the tested specimens of RC-GFRP and RC-steel beams at the ultimate stage are shown in Figure.6.16 and 17 (a) through (c). For RC-GFRP beams, cracking started in the constant moment region with the cracks originating from bottom fibers, as the principal stresses were the greatest at these extreme fibers. These cracks were mainly vertical flexural cracks, which were perpendicular to the beam longitudinal axis since the shear stresses were absent in this zone. These initial cracks traversed quite deeply into the compression zone. The height of initial cracks was between 2.5 and 3.9 in.

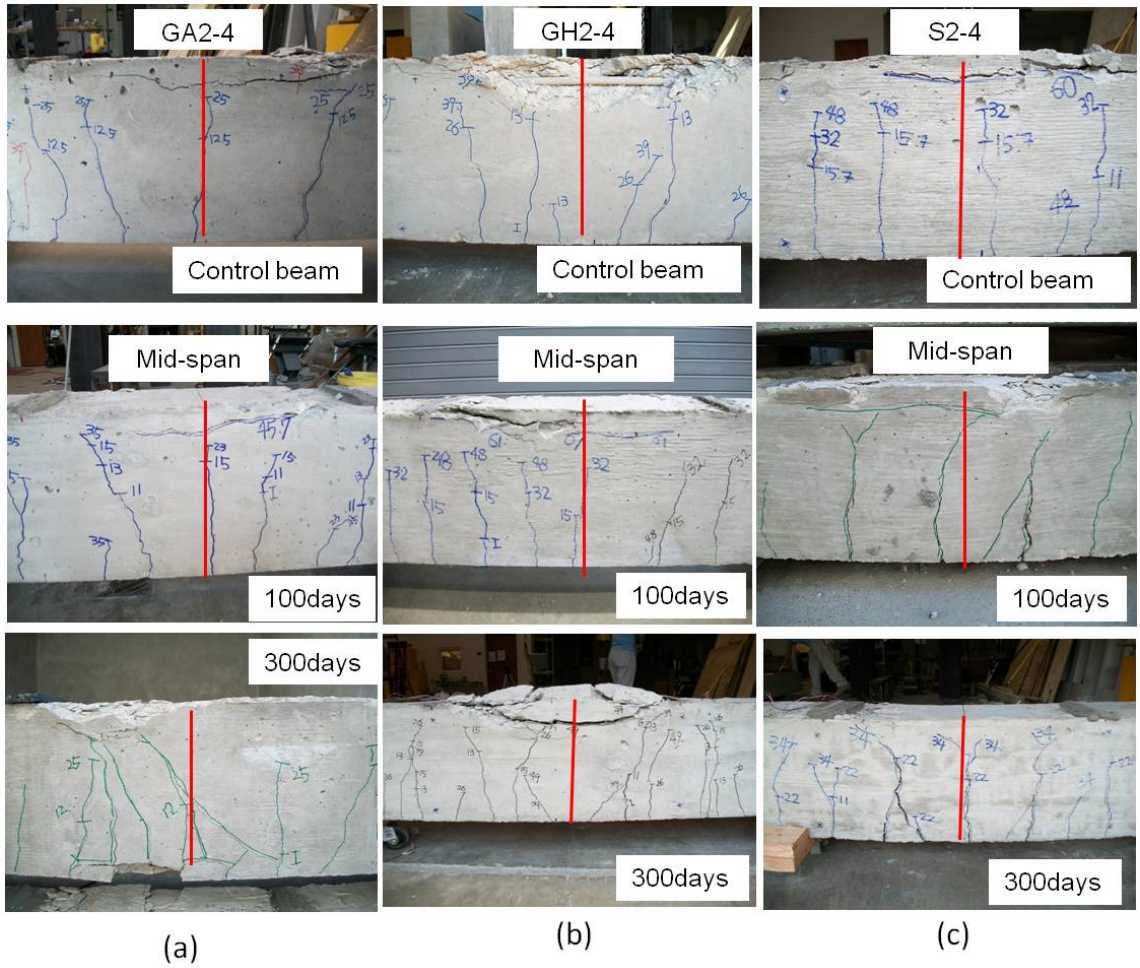

Figure 6.16 Crack pattern in tested beams (2-#4) at ultimate stage
(a) GA2-4 (b) GH2-4 and (c) S2-4

With further increase in load in steel reinforced beams (RC-steel), one of the flexural cracks in the constant moment zone extended deep into the compression zone, reducing the area of concrete in compression leading to crushing of concrete. Hence, crushing of concrete was observed in beams reinforced with steel rebar at the ultimate stage of loading. The duration of accelerated aging did not affect the change of failure mode.

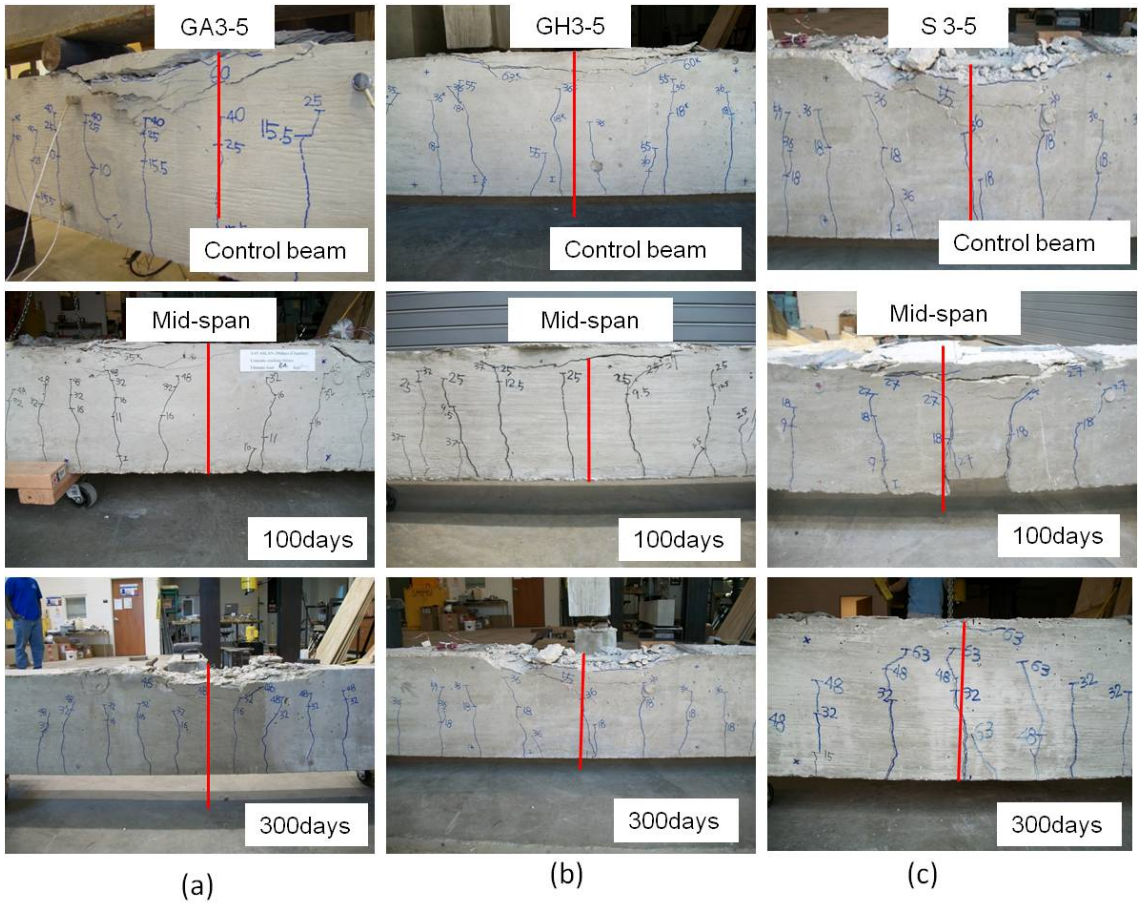

Figure 6.17 Crack pattern in tested beams (3-#5) at ultimate stage
(a) GA3-5 (b) GH3-5 and (c) S3-5

The crack spacing also decreased rapidly with the increasing load and exposure duration. However, the spacing of cracks remained approximately constant after an applied load of 35kips. Beyond this load level only existing cracks grew in length with the increase in load with almost no change in number of cracks. For RC-steel beams, similar to RC-GFRP beams, cracking in RC-steel beams also started with vertical flexural cracks in the constant moment region. However, for RC-steel beams very few cracks outside the pure bending zone turned into inclined cracks and most of these were relatively vertical as shown in Figure.6.16-17 (a),(b) and (c). These beams showed a classic reinforced concrete crack pattern involving fewer and larger

cracks. The spacing of cracks, however, decreased as the load increased. The crack formation became stabilized once again after a load of 24 kips.

The number of cracks and the average crack spacing at failure for all conditioned beams including the control beams are shown in Table.6.3. Spacing was measured with a steel rule to the nearest 0.1 in. It can be seen that both RC-GFRP and RC-steel type of beams developed almost same number of cracks at failure with similar average spacing. However, numbers of cracks were increased (i.e. decreasing of crack spacing) as the durations of accelerated aging were increased. The width of cracks at ultimate stage in RC-Steel beams was considerably narrow compared with the ones of RC-GFRP beams. This shows a good mechanical bond between Steel bars and surrounding concrete.

Also, Table.6.3 shows the average crack spacing at 25% and 100% of the flexural capacity. Crack spacing decreased not only with the increase of load but also with the increase of accelerated aging in environmental chamber. Interestingly, by comparing the crack spacing between the unconditioned concrete beams and the conditioned beams for 300days at chamber (equivalent 25 years in natural aging), the crack spacing was virtually the same at 100% of ultimate load for both the unconditioned concrete beams and the conditioned beams, while the crack spacing of the beams with Type-A was about 10% smaller than that of control concrete beams at service load (25% of ultimate load). Moreover, compared with 3-#5 reinforcement, crack spacing of specimens with lower reinforcement (2-#3) are higher. This may be attributed to relatively significant reduction of stiffness of the lower reinforcement as increase of exposes duration for accelerated aging. This shows good agreement that smaller reinforcement bar have larger reduction of strength/stiffness [Treo et al, 2009].

No horizontal crack at the reinforcement level was observed in any of the tested RC-GFRP beams while horizontal cracks at the reinforcement level were observed in RC-steel beams after accelerated aging. This may be attributed to the increased volume of steel rebars by corrosion. When the load was removed the cracks on RC-GFRP beams were observed to

close. This is due to the fact that FRP bars exhibit linearly elastic behavior up to failure. Since RC-GFRP beams failed by the crushing of concrete, GFRP bars recovered most of their deformation after the load was removed. On the contrary, no change in the crack width was observed in RC-steel beams after removal of the load as steel bars were in their irreversible strain-hardening zone once they yielded.

Table 6.3 Average number of cracks and crack spacing

Specimen I.D	No. of cracks after failure	Ave. crack spacing(s) at 25% Mu(in)	Ave. Crack spacing(s) at 100% Mu(in)	S_{300}/S_0 at 25% of Mu	S_{300}/S_0 at 100% of Mu
GA2-4-0	8	4.2	2.4	-	-
GA2-4-300	12	3.6	2.2	0.92	0.81
GH2-4-0	6	5.4	4.4	-	-
GH2-4-300	10	4.5	4.0	0.91	0.83
S2-4-0	6	5.9	4.6	-	-
S2-4-300	8	4.7	4.2	0.91	0.81
GA3-5-0	6	6.4	4.8	-	-
GA3-5-300	9	6.0	5.1	1.06	0.94
GH3-5-0	6	6.9	5.8	-	-
GH3-5-300	7	6.3	5.5	0.95	0.91
S3-5-0	6	6.9	5.9	-	-
S3-5-300	6	6.3	5.8	0.98	0.91

6.3.5 Load- deflection

6.3.5.1 Ultimate load and moment carrying capacity

Representative examples of the experimental load-deflection curves for RC-GFRP beams and RC-steel beams placed inside the accelerated weathering chamber in the mid-span section are shown in Figure.6.18 and 19. With the increasing of moment, cracks occurred in the testing region when the moment exceeded the cracking moment M_{cr}. Consequently, the flexural stiffness of the beams was significantly reduced and the curves were greatly softened. As

expected, due to the linear-elastic behavior of the FRP bars, the FRP reinforced beams showed no yielding. The curves of RC-GFRP beams went up almost linearly until the crushing of concrete. It can be seen, however, from the widening of the gap between RC-GFRP and RC-steel curves in Figure.6.18 that the rate of reduction in the stiffness of RC-GFRP beams became higher with the increase in load. This can be attributed to the low elastic modulus of GFRP bar, which is 60% less than a steel bar. The reduced stiffness of FRP reinforced beams after cracking has also been reported by various other researchers. The initial stiffness of all the weathered beams was slightly lesser than that of control beams. The last part of the curves is an indication of possible failure mechanism of the structure. As shown in Figure.6.18, both RC-steel beams showed very ductile behaviors and both beams failed at nearly the same load after undergoing considerable deformation with very small increase in the load once steel yielded.

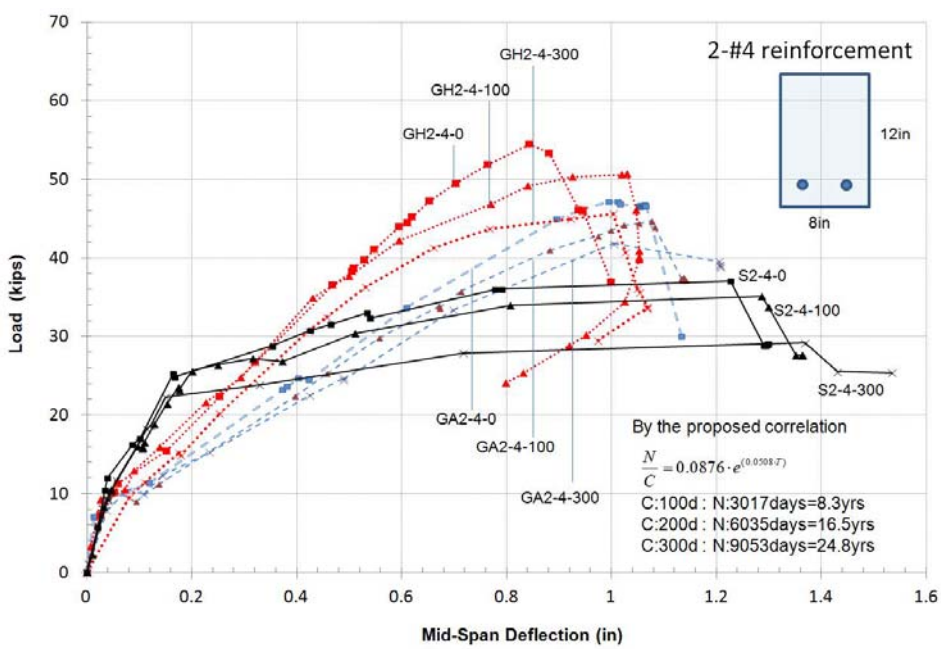

Figure 6.18 Load-vertical deflection of the tested beams(2-#4 of each case)

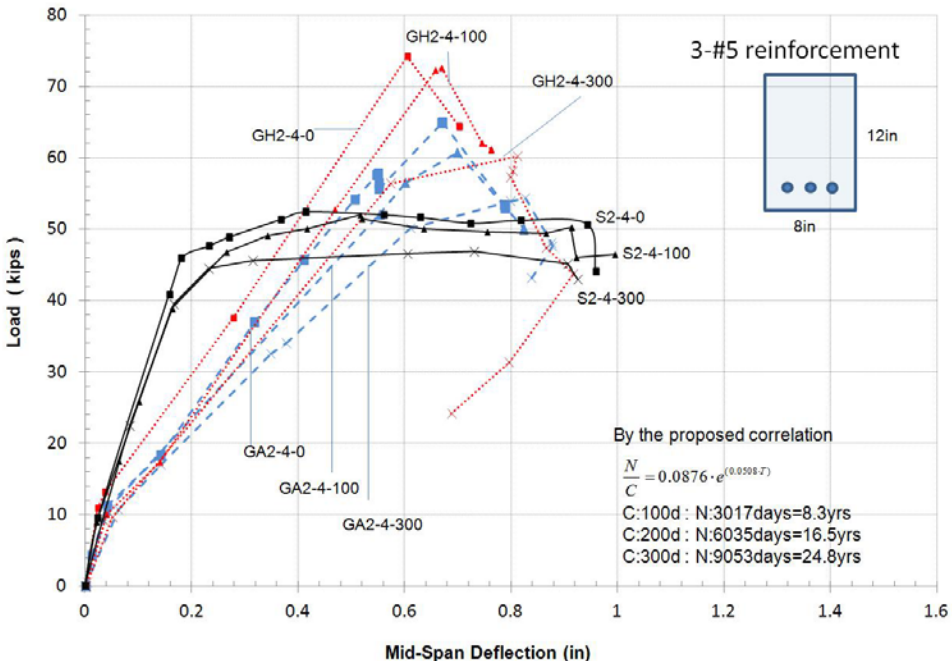

Figure 6.19 Load-vertical deflection of the tested beams(3-#5 of each case)

The reinforcement ratio and type have an effect on the stiffness of the beam specimens and, therefore, on their load-deflection behavior. As expected, larger deformations are obtained for lower reinforcement ratios, and vice versa. Moreover, for the same reinforcement ratio, beams reinforced with Type-A bars also show larger deformations due to less stiffness relatively.

For GA2-4 and GA3-5 with Type-A of reinforcement, changes of slope were at the load equal to 9.5 kips. These measured loads were about 20.5% and 15.9% of ultimate loads of beams GA2-4-0 and GA3-5-0, respectively. For GH2-4 and GH3-5 with Type-B of reinforcement, change of slope were at the load equal to 11 kips and 12.8kips, respectively. These measured loads were about 20.5% and 16.9% of ultimate loads of beams GH2-4-0 and GH3-5-0, respectively. For S2-4 and S3-5 with steel reinforcement, change of slope were at the load equal to 10.8 kips and 11.2kips, respectively. These measured loads were about 29.6% and 20.4% of ultimate loads of beams S2-4-0 and S3-5-0, respectively. It is noted that no

significant changes were observed between the unexposed RC-GFRP/Steel beams and ones placed in the chamber up to 300days for environmental exposure. In all cases, however, the moment carrying capacity decreased and the deflection increased as a function of time when exposed to accelerated aging.

Table 6.4 Summary of test results

Specimen I.D	Ratio of reinforcement[1]	Concrete strength (ksi)		Mu_{th}	Mu_{exp}	Mu_{exp}/Mu_{th}	Δu	Failure mode[2]
		At 28days	At testing day	k-ft	k-ft		in	
GA2-4-0	1.242	4.25	4.25	37.0	46.5	1.26	1.053	C.C.
GA2-4-100	1.071	4.25	4.61	37.2	44.9	1.21	1.081	B
GA2-4-200	1.026	4.25	5.04	37.8	43.8	1.16	1.088	B
GA2-4-300	0.997	4.25	5.23	38.2	41.7	1.09	1.108	Rupture
GA3-5-0	2.157	4.25	4.25	50.2	62.5	1.25	0.691	C.C.
GA3-5-100	2.024	4.25	4.83	51.1	62.0	1.21	0.742	C.C.
GA3-5-200	1.789	4.25	5.11	52.8	59.8	1.13	0.832	C.C.
GA3-5-300	1.678	4.25	5.29	53.8	57.3	1.06	0.839	C.C.
GH2-4-0	2.273	4.34	4.34	38.8	53.7	1.38	1.003	C.C.
GH2-4-100	1.981	4.34	4.98	42.0	51.1	1.22	1.020	C.C.
GH2-4-200	1.876	4.34	5.26	43.4	48.5	1.12	1.010	C.C.
GH2-4-300	1.776	4.34	5.29	44.2	46.9	1.06	1.030	C.C.
GH3-5-0	4.761	4.34	4.34	55.2	73.7	1.34	0.621	C.C.
GH3-5-100	4.149	4.34	4.98	60.1	71.4	1.19	0.669	C.C.
GH3-5-200	3.928	4.34	5.26	62.2	68.9	1.11	0.807	C.C.
GH3-5-300	3.578	4.34	5.31	62.8	64.9	1.03	0.817	C.C.
S2-4-0	0.155	4.28	4.22	20.1	36.4	1.82	1.221	S.Y.+C.C
S2-4-100	0.132	4.28	4.91	20.3	35.3	1.74	1.321	S.Y.+C.C
S2-4-200	0.124	4.28	5.22	20.4	30.9	1.51	1.419	S.Y.+C.C
S2-4-300	0.119	4.28	5.23	20.5	29.0	1.41	1.612	S.Y.+C.C
S3-5-0	0.352	4.28	4.34	44.3	54.8	1.24	0.687	S.Y.+C.C
S3-5-100	0.298	4.28	5.13	45.0	53.8	1.20	0.692	S.Y.+C.C
S3-5-200	0.287	4.28	5.29	45.1	49.9	1.11	0.909	S.Y.+C.C
S3-5-300	0.267	4.28	5.33	45.6	49.6	1.09	1.145	S.Y.+C.C

1: Ratio of reinforcement : ρ_f / ρ_{fb}
2: C.C.(Concrete crushing), B (Balanced failure), S.Y+C.C(Steel yielding and concrete crushing)
#: Mu_{th} : Theoretical ultimate moment ; Mu_{exp} : Experimental ultimate moment

Environmental conditioning had a considerable effect on the structural degradation of GFRP and steel reinforcement. GA2-4, GH2-4 and S2-4 exhibited the reduction of load-carrying capacity of approximately 12%, 13% and 21%, respectively, after 300days in environmental chamber while the increase of deflection were 20.3%, 22.1% and 25.5%. GA3-5, GH3-5 and S3-5 exhibited the reduction of load-carrying capacity of approximately 8.3%, 11.2% and 12.5%, respectively, after 300days in environmental chamber while the increase of deflection were 9.1%,8.2% and -4.2% respectively. Beams exposed in the environmental chamber showed a tendency to be less brittle in the mode of failure as compared to those not exposed.

The figures indicate that under the aggressive conditions in which the specimens were exposed, significant loss of load-carrying capacity could occur. It should be noted, however, not only that the change of load-carrying capacity in RC-steel specimens is greater than the one in RC-GFRP specimens but also that beams exposed into the environmental chamber show relatively gradual member compression failures compared with the more brittle failures of the non-exposed specimens. Moreover, relatively gradual member failure was observed in RC-GFRP beams with compression failures as accelerated aging was increased.

Theoretical and experimental characteristics of all specimens tested after various time periods of accelerated aging, are shown in Table.6.4. The theoretical ultimate loads were calculated according to ACI 440.1R-06 considering values for the ultimate concrete strain ε_{cu} of 0.0030. As can be observed in Table.6.4, all beams withstand a higher load than the one theoretically predicted by both approaches. The mean ratios of RC-GFRP and RC-steel beams between the experimental and theoretical values are 1.19 and 1.61 respectively in the case of ACI 440 provision. One possible reason for the difference between both theoretical approaches and the experimental values can be found in the value of the maximum compressive concrete strain considered, because in all the tests carried out this value was about 0.0031-0.0037 which are 3.3-23.3% higher than the one suggested by the theoretical procedures.

In general, all beams showed a reduction in strength with longer period of weathering. After 300days of accelerated aging in chamber (equivalent to 24.5 years of outdoor weathering in DFW area), the flexural strength of GA2-4 and GA3-4 beams reinforced with Type-A GFRP bars was reduced by about 11% and 8.8% respectively, that is, comparing GA2-4-0(or GA3-4-0) with GA2-4-300(or GA3-5-300) . Also, the flexural strength of GH2-4 and GH3-5 beams reduced by 12.7% and 11.9% respectively, after 300days of accelerated weathering in chamber. For RC-steel beams with ρ of 0.155, the reduction in flexural strength was about 20.9% (comparing S2-4-0d with S2-4-300d) whereas for RC-steel beams with ρ of 0.352, the reduction was 12.2% (comparing S3-5-0d with S3-5-300d) at the end of 300days of accelerated weathering (equivalent to 24.5 years outdoor weathering in DFE area). All beams still withstand a higher load than the one theoretically predicted although those were exposed to the accelerated aging chamber(115°F and R.H. of 80%) up to 300days. However, the ratios of experimental ultimate moment carrying capacity to theoretical one are become smaller as close to 1.0.

From the results, it can be observed that the rate of strength degradation of Type-B GFRP beams (GH: VROD-HM) is greater than one of Type-A GFRP beams (GA : ASLAN-100) compared RC-Type-A with RC-Type-B. This fact showed good agreement with the results of tensile tests as mentioned in chapter 4. Compared with RC-GFRP and RC-steel, the rate of strength /stiffness degradation of RC-steel is greater than the one of GFRP bars (Type-A and Type-B). It is evident that effect of weathering is lesser for beams with higher reinforcement area (3-#5). This may be due to better protection against weathering elements due to thicker FRP bars.

6.3.5.2 Deflection and effective moment of inertia

Deflection at mid-span for a simply supported beam of total length L and subjected to a four-point flexural test is given as Eq.6.4 and Figure.6.6. [Wang et al, 2005]

$$\Delta_{mid-span} = \frac{Pa}{48E_c I_e}(3L^2 - 4a^2) + \frac{Ph^2 a}{10GI_e} \quad \text{(Eq.6.4)}$$

where E_c is the modulus of elasticity of concrete and two point loads of P/2 applied at a distance a from the supports in Figure.6.6.

The first term on the right is from the flexural component, and the second term is from the shear component. In this study, testing beams had a span-depth ratio of 5.91. Based on calculation, it was found that the shear component was about 8% of the flexural component. It was, therefore, neglected for simplicity [Wang et al, 2005]. Thus, Eq.6.4 becomes

$$\Delta_{mid-span} = \frac{Pa}{48E_c I_e}(3L^2 - 4a^2) \quad \text{(Eq.6.5)}$$

$$I_e = (\frac{M_{cr}}{M_a})^3 I_g + (1 - (\frac{M_{cr}}{M_a})^3) I_{cr} \leq I_g \quad \text{(Eq.6.6)}$$

Eq.6.6 proposed by Branson (1977) was based on the behavior of steel-reinforced beams at service load levels and was developed to account for both a loss in flexural stiffness when the member cracks and variation in stiffness along the member length. This expression was adopted by ACI 318 in 1971 and continues to be used for deflection calculation of steel reinforced concrete [Bischoff et al, 2008]. It is important to note that Branson's (1977) empirical expression for I_e was calibrated for moderately reinforced concrete beams having an I_g/I_{cr} ratio less than 3. As pointed out by Bischoff (2005), deflection is underestimated when the I_g/I_{cr} ratio of the flexural member exceeds 3. The greater the I_g/I_{cr} ratio the more deflection is underestimated with Branson's expression. In other words, Branson's equation has been found to overestimate the effective moment of inertia of FRP-reinforced beams, especially for lightly reinforced beams, implying a lesser degree of tension stiffening than in comparable steel reinforced beams [Benmokrane et al. 1996a; Toutanji and Saafi 2000]. This reduced tension stiffening may be attributed to the lower modulus of elasticity and different bond stress levels for the FRP reinforcement as compared with those of steel [Bischoff et al, 2008].

In order to account for reduced tension stiffening in FRP-reinforced members, a modified expression for the effective moment of inertia is required [Gao et al, 1998] and this expression is recommended and is given by Eq. 6.7 in ACI-440. Current ACI 440.1R-06 recommends the following expressions to calculate the effective moment of inertia I_e :

$$I_e = (\frac{M_{cr}}{M_a})^3 \beta_d I_g + (1 - (\frac{M_{cr}}{M_a})^3) I_{cr} \leq I_g \qquad \text{(Eq. 6.7)}$$

where, $\beta_d = \frac{1}{5} \cdot (\frac{\rho_f}{\rho_{fb}}) \leq 1.0$

The factor β_d is a reduction coefficient related to the reduced tension stiffening exhibited by FRP-reinforced members. Research has demonstrated that the degree of tension stiffening is affected by the amount and stiffness of the flexural reinforcement and by the relative reinforcement ratio (ratio of ρ_f to ρ_{fb}) [Toutanji and Saafi 2000; Yost et al. 2003].

The approach of Toutanji and Saafi (2000) suggested in Eq.6.8 and 6.9 was also compared with experimental data. The exponent of Branson's equation is modified by adopting E_s of the steel modulus of elasticity, ρ_f is the FRP reinforcement ratio and E_f of the FRP modulus of elasticity by using their method.

For $\frac{E_{FRP}}{E_s} \rho_{FRP} < 0.3,$

$$I_e = (\frac{M_{cr}}{M_a})^{6 - \frac{10 \rho_{FRP} E_{FRP}}{E_s}} I_g + \left[1 - (\frac{M_{cr}}{M_a})^{6 - \frac{10 \rho_{FRP} E_{FRP}}{E_s}} \right] I_{cr} \leq I_g \qquad \text{(Eq.6.8)}$$

For $\frac{E_{FRP}}{E_s} \rho_{FRP} \geq 0.3,$

$$I_e = (\frac{M_{cr}}{M_a})^3 I_g + (1 - (\frac{M_{cr}}{M_a})^3) I_{cr} \leq I_g \qquad \text{(Eq.6.9)}$$

Finally, Bischoff's expression (2005) is also investigated. An equivalent moment of inertia based on the tension–stiffening effect on curvatures is adopted in Bischoff expression as seen in Eq.6.10.

$$I_e = \frac{I_{cr}}{1-(1-\frac{I_{cr}}{I_g})(\frac{M_{cr}}{M_a})^2} \qquad \text{(Eq.6.10)}$$

The experimental data of deflection with applied moment are compared with theoretical predictions obtained using ACI 440.1R-06 and proposed expressions in Figure.6.20 through 6.23. By following ACI 440.1R-06 provisions and suggested expressions, the deflection at a certain applied moment can be calculated by Eq.6.7 through Eq.6.10. It can be observed that up to the service load, both ACI 440.1R-06 approaches and proposed expression (Toutanji and Bischoff) compare reasonably well with the experimental data regardless the accelerated aging in all cases. As shown, there are no significant differences between any of the approaches for the GFRP rebars used in this experimental tests (GA2-4 and GA3-5) until service loading (25% of Mu) although the results of ACI 440.1R-06 and Bischoff methods seem to fit the experimental results better than Toutanji's model. However, for high load level, theoretical approaches of ACI-440 and Bischoff overestimate deflections and Toutanji underestimate deflection in cases of GA2-4 and GA3-5. In general, all beams showed a reduction in flexural stiffness with longer period of weathering. It is also observed that there is less difference between theoretical and experimental data as the reinforcing ratio increases. Tension stiffening (tension carried by the concrete between the cracks) decreases at the higher reinforcing ratios because the service load moment increases relative to the cracking moment when the reinforcing ratio is increased [Bischoff et al, 2005].

The deflections of GA2-4 and GA3-5 beams exposed to accelerated aging chamber were found to be more than those of control beams by about average 23% and 16% respectively at the loading level over 50% of Mu. After 300days of accelerated aging in chamber

(equivalent to 24.5 years of outdoor weathering in DFW area), the deflection of GA2-4 and GA3-5 beams reinforced with Type-A GFRP bars was increased by about average 21% and 19% respectively, that is, comparing GA2-4-0(or GA3-4-0) with GA2-4-300(or GA3-5-300). This shows the effect of accelerated aging on the deflection is larger for smaller reinforced section and the larger deflection may be due to the degradation in tensile stiffness of GFRP bars. If an environmental strength reduction factor of 0.7 were used for flexure of a member failing in compression, the ACI-440 provision is still conservative until the equivalent 24.8 years of natural exposure.

Table 6.5 Deflections at ultimate moment

Specimen I.D	Reinforcement ratio	Exp. Def.	Eq-1(ACI)	Eq-2(B)	Eq-3(T)	Eq-1/exp	Eq-2/exp	Eq-3/exp
	Af/(bd)	in	in	in	in			
GA2-4-0	0.0045 (0.45%)	0.964	1.017	1.084	0.786	1.055	1.124	0.815
GA2-4-100		1.081				0.941	1.003	0.727
GA2-4-200		1.088				0.935	0.996	0.722
GA2-4-300		1.168				0.871	0.928	0.673
GA3-5-0	0.0109 (1.09%)	0.704	0.747	0.881	0.614	1.061	1.251	0.872
GA3-5-100		0.742				1.007	1.187	0.827
GA3-5-200		0.832				0.898	1.059	0.738
GA3-5-300		0.839				0.890	1.050	0.732
GH2-4-0	0.0045 (0.45%)	0.911	0.809	0.943	0.674	0.888	1.035	0.740
GH2-4-100		0.997				0.811	0.946	0.676
GH2-4-200		1.01				0.801	0.934	0.667
GH2-4-300		1.139				0.710	0.828	0.592
GH3-5-0	0.0109 (1.09%)	0.678	0.694	0.811	0.589	1.024	1.196	0.869
GH3-5-100		0.669				1.037	1.212	0.880
GH3-5-200		0.807				0.860	1.005	0.730
GH3-5-300		0.817				0.849	0.993	0.721

1: Eq(1)=ACI 440-1R-06, Eq(2)=Bischoff equation (2005) and Eq(3)= Toutanki and Saafi (2000)
*: Experimental deflection at mid-span
Eq/Exp.=Theoretical deflection by equations / experimental deflection at ultimate stage

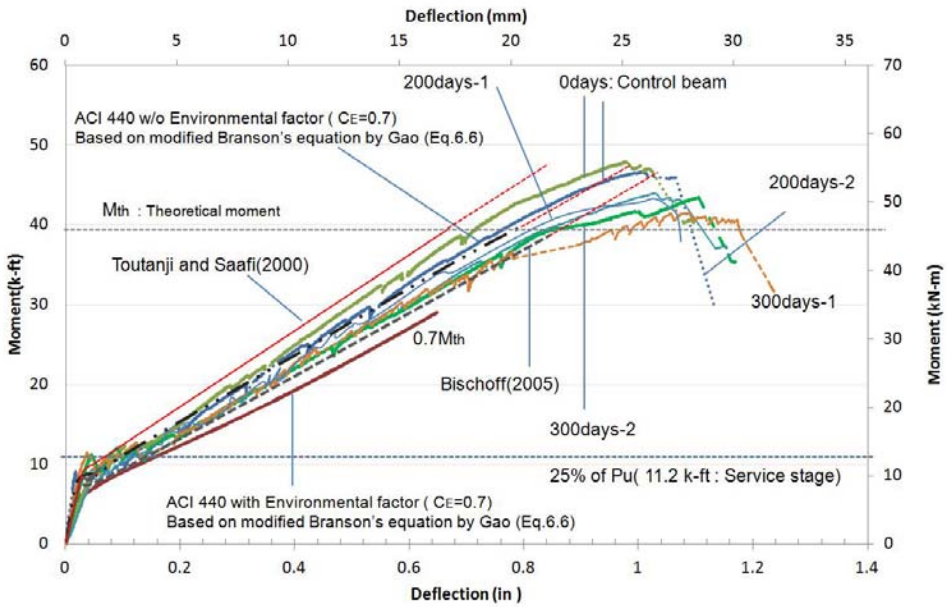

Figure 6.20 Experimental –theoretical load versus midspan deflection after accelerated aging (GA2-4)

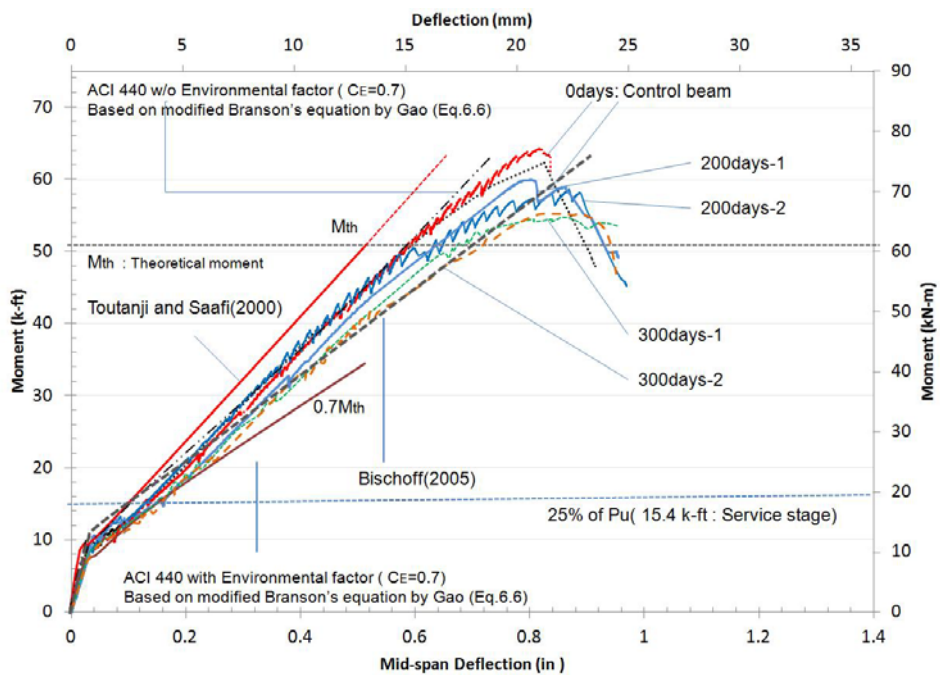

Figure 6. 21 Experimental –theoretical load versus midspan deflection after accelerated aging (GA3-5)

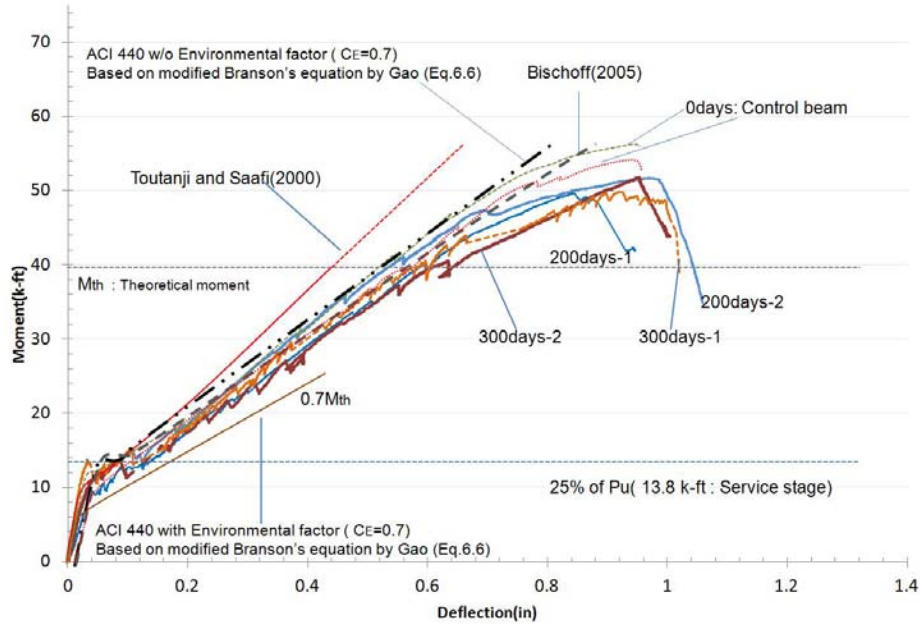

Figure 6.22 Experimental–theoretical load versus midspan deflection after accelerated aging (GH2-4)

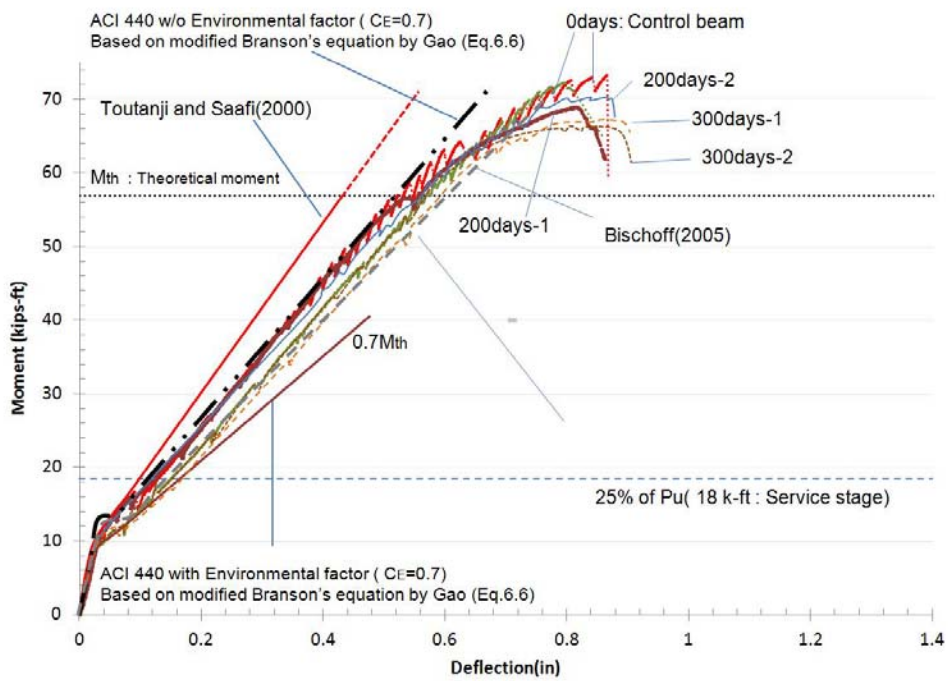

Figure 6.23 Experimental –theoretical load versus midspan deflection after accelerated aging (GH3-5)

The analytical prediction by the ACI 440.1R-06 and Bischoff(2005) predictions show conservative curves even after 300 days of accelerated aging (equivalent to 24.8 years of outdoor weathering in DFW area) while the prediction of Toutanji and Saffi (2000) is unconservative although the specimens are not exposed to accelerated aging chamber. Based on the results In Table.6.5 and Figure.6.24, the higher tension reinforcement stiffness causes higher nonlinearity in the beam compression zone leading to overestimate I_e. Accordingly, the equations underestimate the deflection at ultimate. The lower tension reinforcement stiffness causes the all predictions to overestimate I_e and underestimate the deflection and the other equations to underestimate it. Then, this rate of underestimation is increased as the duration of accelerated aging is increased.

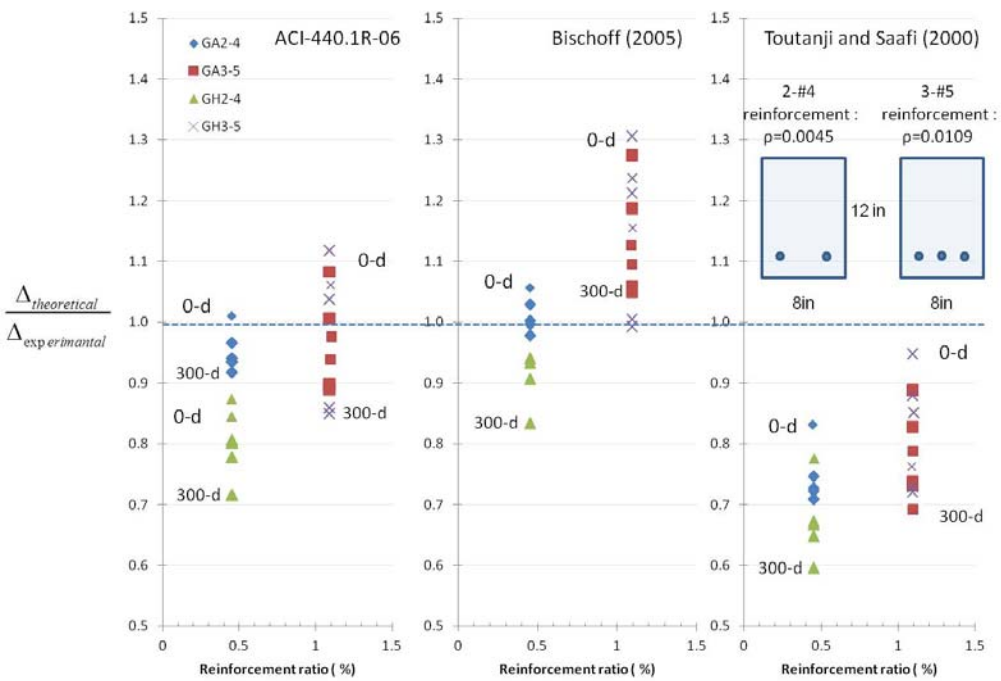

Figure 6.24 Deflection comparison at P_u using (a) ACI.440.1R-06 (b) Bischoff(2005) and (c) Toutanji and Saffi (2000)

In case of ACI-440 provisions, the prediction using the correction factor works quite well for GFRP reinforced concrete regardless of type of reinforcement and reinforcement ratio. However, ACI -440 prediction can not explain the change of aged specimens because linking the correction factor with the balanced reinforcing ratio (ρ_{fb}) does not imply a dependence on bar strength. That is, correction factor has the inherent limitation to account for stiffness/strength degradation effect providing different computed values of deflection when the strength of the bars would be changed because it came from empirical derivation. It is for this reason that the ACI 440.1R-06 approach is expected to be overestimated as the duration of environmental aging is increased.

From Figure.6.24, it is clear that Eq.6.7 of ACI 440.1R-06 gives the smallest average error closing to 1.0 of Δcal / Δexp in all cases except the case of GA2-4. Thus, it gives the best predictions for the deflections of unexposed specimens. However, the prediction becomes inaccurate as the specimens are aged (increasing of the duration of accelerated aging). It is also clear that Eq.6.9 of Bischoff (2005) gives the smallest average error in all cases for long-term performances of aged specimens. Thus, it gives the best predictions of load and deflections after accelerated aged specimens while the expression proposed by Toutanji and Saafi (2000) is not appropriate in any cases of the specimens. This approach does not work well either and underestimates deflection considerably for GFRP reinforced concrete as shown in Figure.6.24.

6.4 Summary

This chapter presents the results and discussion of flexural experiment concerning concrete beams reinforced with glass-FRP (GFRP) and steel bars after accelerated environmental aging. Accelerated weathering in North-Texas region (DFW area) is considered with average highest temperature of 115°F and average relative humidity of 80% after immersing into 3% saline solution. The correlation between natural exposure (N) in the field and

accelerated exposure (C) in the laboratory is used based on the proposed equation in Chapter 4. Both ultimate and serviceability limit states are studied by load-deflection, cracking behavior, modes of failure and ultimate load between unexposed and exposed specimens in accelerated aging conditioning. Concluding remarks are summarized as follows:

- In all cases(GA2-4,GA3-5,GH2-4 and GH3-5), the ultimate curvatures of the beams increase after accelerated aging for 300 days due to the higher deterioration in the strength and stiffness properties of the constituent materials.
- The crack spacing also decreased rapidly with the increasing load and exposure duration. However, the spacing of cracks remained approximately constant after an applied load of 0.75Pu.
- Compared with 3-#5 reinforcement, number of cracks of specimens with lower reinforcement (2-#3) is higher. This may be attributed to relatively significant reduction of stiffness of the lower reinforcement as increase of exposes duration for accelerated aging. This shows good agreement that smaller reinforcement bar have larger reduction of strength/stiffness
- Numbers of cracks were increased (i.e. decreasing of crack spacing) as the durations of accelerated aging were increased. The width of cracks at ultimate stage in RC-GFRP beams was considerably narrow compared with the ones of RC-steel beams. This shows a good mechanical bond between GFRP bars and surrounding concrete.
- No horizontal crack at the reinforcement level was observed in any of the tested RC-GFRP beams while horizontal cracks at the reinforcement level were observed in RC-steel beams after accelerated aging. This may be attributed to the increased volume of steel rebars by corrosion.

- All RC-GFRP beams demonstrated a concrete crushing mode of failure in line with design predictions except the case of GA2-4 with balanced failure. The duration of accelerated aging did not affect the change of failure mode.
- Environmental conditioning had a considerable effect on the structural degradation of GFRP and steel reinforcement. After 300days of accelerated aging in chamber (equivalent to 24.5 years of outdoor weathering in DFW area), the flexural strength of GA2-4 and GA3-5 beams reinforced with Type-A GFRP bars was reduced by about 13% and 9.8% respectively, that is, comparing GA2-4-0(or GA3-5-0) with GA2-4-300(or GA3-5-300) . Also, the flexural strength of GH2-4 and GH3-5 beams reduced by 12.7% and 11.9% respectively, after 300days of accelerated weathering in chamber. For RC-steel beams with ρ of 0.155, the reduction in flexural strength was about 20.9% (comparing S2-4-0d with S2-4-300d) whereas for RC-steel beams with ρ of 0.352, the reduction was 12.2% (comparing S3-5-0d with S3-5-300d) at the end of 300days of accelerated weathering (equivalent to 24.8 years outdoor weathering in DFE area). All beams still withstand a higher load than the one theoretically predicted although those were exposed to the accelerated aging chamber (115°F and R.H. of 80%) up to 300days.
- All the RC-GFRP beams behaved in a linear way until cracking and, due to lack of plasticity in the reinforcement, almost linearly between cracking and failure, with a greatly reduced slope. However, failure took place at relatively large displacements compared with the one of RC-steel beams
- Under the aggressive conditions in which the specimens were exposed, significant loss of load-carrying capacity could occur. It should be noted, however, not only that the change of load-carrying capacity in RC-steel specimens is greater than the one in RC-GFRP specimens but also that beams exposed into the environmental chamber show

relatively gradual member compression failures compared with the more brittle failures of the non-exposed specimens.

- It can be observed that the rate of strength degradation of Type-B GFRP beams (GH: VROD-HM) is greater than one of Type-A GFRP beams (GA : ASLAN-100) compared RC-Type-A with RC-Type-B. This fact showed good agreement with the results of tensile tests as mentioned in chapter 4. Compared with RC-GFRP and RC-steel, the rate of strength /stiffness degradation of RC-steel is greater than the one of GFRP bars (Type-A and Type-B). It is evident that effect of weathering is lesser for beams with higher reinforcement area (3-#5). This may be due to better protection against weathering elements due to thicker FRP bars.
- It can be observed that up to the service load, both ACI 440.1R-06 approaches and proposed expression (Toutanji and Bischoff) compare reasonably well with the experimental data regardless the accelerated aging in all cases.
- If an environmental strength reduction factor of 0.7 were used for flexure of a member failing in compression, the ACI-440 provision is still conservative until the equivalent 24.8 years of natural exposure.
- The higher tension reinforcement stiffness causes higher nonlinearity in the beam compression zone leading to overestimate I_e. Accordingly, the equations underestimate the deflection at ultimate. The lower tension reinforcement stiffness causes the all predictions to overestimate I_e and underestimate the deflection and the other equations to underestimate it. Then, this rate of underestimation is increased as the duration of accelerated aging is increased. Beams exposed in the environmental chamber showed a tendency to be less brittle in the mode of failure as compared to those not exposed.
- It is clear that Bischoff (2005) gives the smallest average error in all cases for long-term performances of accelerated aged specimens, while the expression proposed by

Toutanji and Saafi (2000) shows poor predictions in any cases of the specimens by underestimates deflection considerably for RC-GFRP beams

CHAPTER 7

DUCTILITY INDEX

7.1 General

Conventional definition of ductility is based on its capacity to absorb energy without critical failure and is generally related to the amount of inelastic deformation taking place before complete failure. Ductility can be expressed quantitatively as the ratio of the total deformation at failure to the deformation at the elastic limit because conventional steel reinforced beams have a distinct elastic and inelastic phase of deformation before and after yielding of steel [Naaman et al, 1995]. Ductility is an important attribute of materials in that visible deformations can occur if the loads become too large, thus providing an opportunity to take remedial action before fracture occurs. This is particularly important for the performance of structures in high seismic regions where structures must undergo large cyclic displacement without structural collapse [Mufi et al, 1999]. Because of its significance, ductility must be quantified. Unlike steel, however, FRP material is brittle in nature with linearly elastic behavior up to failure although it has advantages such as corrosion resistance, high-strength and light weight. This way of estimating ductility is inappropriate for concrete structures reinforced with FRP because the behavior of them is linear until failure steel [Naaman et al, 1995]. Since concrete flexural beams reinforced with FRP bars exhibit also substantial deformation prior to failure despite the fact that FRP does not yield unlike steel, the term of deformability was introduced by researchers as a means of assessment of displacement or curvature that occurs before failure. Although researchers have proposed several different models to estimate the deformability, there is still lack of general agreement as to how the deformability characteristics of such members may be quantified and analyzed [Au et al, 2008]. There is no general agreement on what these points should be.

Moreover, tensile strength of GFRP depends on the environmental conditions and exposure duration as mentioned in Chapter-2. This fact will affect the capacity to absorb energy named deformability without critical failure.

Objectives of this research are not only to evaluate proposed deformability indices by researchers but also to propose a modified deformability index including strength degradation after exposing specimens into environmental conditioning. This chapter accounts for a comparative study of existing deformability models for concrete beams reinforced with GFRP or steel rods by different researchers in recent years. An empirical modified deformability model has been developed to predict the full range response after accelerated aging.

7.2 Deformability factor (DF): pseudo-ductility

The concept of ductility was developed as a measure to determine the post-yielding deformational response energy absorption capacity of ductile materials. This is the conventional concept of ductility. Because of no true yield behavior of GFRP bars, ductility in its traditional sense is not appropriate when dealing with GFRP. It is for this reason that many researchers and design codes have suggested other measures which are collectively referred to as pseudo-ductility measures [Johnson, 2009]. Bakis et al. (2002) in their paper on GFRP in concrete structures identified that the major measure of pseudo-ductility is the deformability index. The index is a ratio of the ultimate deflection and the service deflection; the same can be done with curvatures as well. This index was based initially on tests conducted by Vijay and Gangarao (1997) and has formed the basis for many performance measures. The term deformability was introduced by researchers as a means of assessment of the displacement or curvature that occurs before rupture of the FRP tendons. Researchers have proposed several different models to evaluate the deformability of concrete beams with FRP rods, but there is still lack of general agreement as to how the deformability characteristics of such members may be quantified and

analyzed. In the following sections, three basic approaches which form the basis of code clauses in both the American and Canadian codes are presented.

7.3 Review of existing deformability indices

7.3.1 Energy based approach

Naaman and Jeong suggested an energy-based deformability index (the Naaman Index) to compute the ductility index of μ_e for beams reinforced or prestressed with FRP tendons as seen Eq.7.1. It is suitable for beams with steel as well as FRP reinforcement.

$$\mu_e = 0.5(\frac{E_T}{E_{el}} + 1) \qquad \text{(Eq.7.1)}$$

where E_T is the total energy which is area under load-deflection curve and E_{el} is the elastic energy which is area of the triangle formed at the failure load by a line with the weighted average slope of S as illustrated in Figure.7.1. The two initial slopes S1 and S2, corresponding to applied loads P1 and P2, of the load-deflection curve as illustrated in Figure.7.1 are weighted to define a slope S for the equivalent unloading response.

Grace et al. (1998) proposed four parameters in Eq.7.2 in order to account for the influence of type of reinforcement (main bars and stirrups), failure mode of the beam, modulus of elasticity and failure strength of the reinforcement on the slope S.

$$S = \alpha\beta\gamma \frac{E_f}{E_s} \frac{f_y}{f_{ds}} \frac{P_1 S_1 + (P_2 - P_1) S_2 + (P_3 - P_2) S_3}{P_3} \qquad \text{(Eq.7.2)}$$

where, α is stirrup factor (GFRP=0.95) ; β is failure mode factor (Compressive factor=1.0) ; γ is factor that depends on the type of reinforcement(GFRP=4.0) ; E_f is FRP modulus of elasticity ; E_s is steel modulus of elasticity ; f_y is steel yield strength ; f_{ds} is design strength of

FRP. The above energy-based deformability index is dependent on the ratio of total energy to the elastic energy at the failure state of a beam.

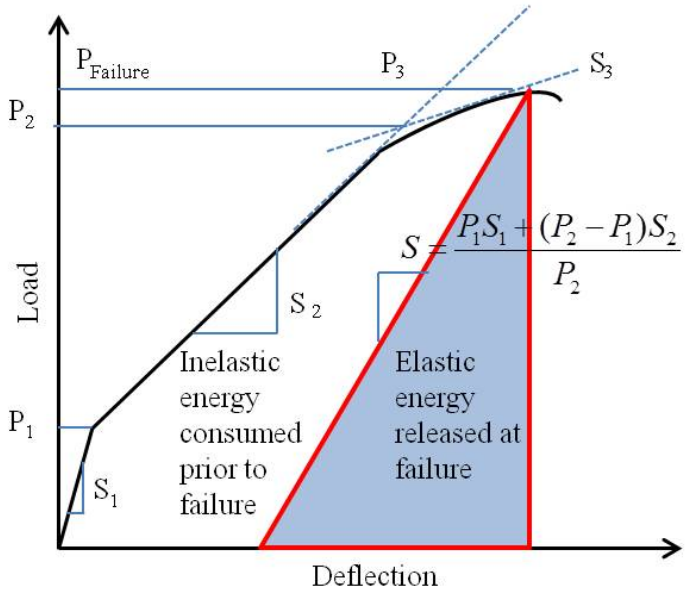

$$S = \frac{P_1 S_1 + (P_2 - P_1) S_2}{P_2}$$

Figure 7.1 New ductility index by Naaman and Jeong

7.3.2 Moment and deformation based approaches

The moment-deformation based model (the Jaeger index) was introduced by Jaeger et al. taking into account the strength effect of moment as well as the curvature (or deflection) effect on the ductility. The Jaeger index is based on a comparison of strain energy at ultimate conditions and a limiting curvature to represent service conditions but does not measure the area under the moment-curvature curve. It measures a rectangular region defined by the origin and a point of interest at opposite corners. The Jaeger index is shown in Eq.7.2 as it is found in Intelligent Sensing for Innovative Structures (ISIS-Canada). Moment and curvature at ultimate state are used as well as the moment and curvature at service state. The service limit stage corresponds to the value at concrete compressive strain of 0.001 considered as the beginning of inelastic deformation of concrete top compression fiber. It is 50% larger than the one

recommended by Vijay and Gangarao (2001). According to code requirements (ISIS), a minimum Jaeger index of 4 is required for rectangular beams while a minimum factor of 6 is required for T Beams. Those factors are meant to be very similar to those required of conventionally designed steel reinforced concrete beams [Wang et al. 2011]

$$\mu_E = \left(\frac{\varphi_u}{\varphi_{0.001}}\right) \times \left(\frac{M_u}{M_{0.001}}\right) \qquad \text{(Eq.7.2)}$$

where M_u and φ_u are the moment and curvature at ultimate stage; $M_{0.001}$ and $\varphi_{0.001}$ are the moment and curvature at service stage respectively. Curvature (φ) can be calculated using one of the expressions in Eq.7.3

$$\varphi = \frac{\varepsilon_f}{d-c} = \frac{(\varepsilon_f + \varepsilon_f)}{d} = \frac{\varepsilon_c}{c} \qquad \text{(Eq.7.3)}$$

where ε_f is the tensile strain in FRP reinforcement, ε_c is the strain in extreme concrete fiber in compression, c=the depth of neutral axis from the extreme compression fiber and d is the effective depth of the beam.

Zou proposed a deformability index (the Zou Index) defined in terms of both a moment factor and a deflection factor for FRP prestressed concrete beams. The moment part is the ratio of the ultimate moment to the cracking moment while the deflection part is the ratio of the deflection at failure to that at first cracking [Au et al., 2008]. The Zou deformability index Z appears in Eq.7-4 below.

$$Z = \mu_E = \left(\frac{\Delta_u}{\Delta_{cr}}\right) \times \left(\frac{M_u}{M_{cr}}\right) \quad \text{(Eq.7.4)}$$

7.3.3 Deflection based approach

Abdelrahman et al. (1995) established a deformability model based on deflection for beams prestressed by FRP tendons. This Abdelrahman deformability index $A_b$is expressed as the ratio of the maximum Δ_u corresponding to the failure or maximum load to the equivalent Δ_1 of the uncracked section at a load equal to the ultimate load [Au et al., 2008].

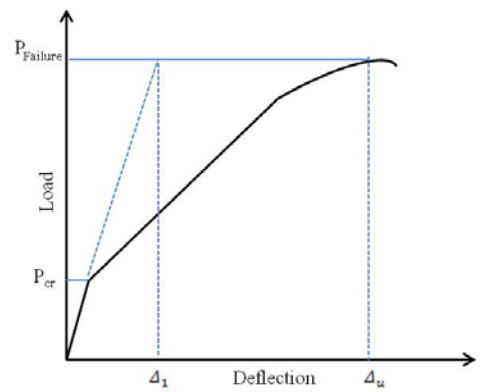

Figure 7.2 Equivalent deflection and failure deflection by Abdelrahman

$$A_b = \frac{\Delta_u}{\Delta_1} \quad \text{(Eq.7.5)}$$

This definition overestimates ductility for prestressed concrete beams with steel based on the result of Abdelrahman et al.(2000). This method represents the bilinear elastic deformation of beams pre- stressed by FRP and is different from the traditional ductility evaluation in terms of the inelastic deformation of the system prior to collapse [Au et al., 2008].

7.4 Test specimens, instrumentation and test procedure

As mentioned in Chapter 6, eighty-six beams were tested under four-point loading. The tests consisted of three categories of beams: type of reinforcement (GFRP with wrapped

surface or sand-coated surface / steel), exposure duration (No-exposure-0day,100, 200 and 300days of exposure) and reinforcement ratio(2-no.4 bars / 3-no.5 bars). Each testing group is subjected to repeated loading and unloading. Energy absorption of GFRP reinforced concrete beams can be obtained in terms of area under the load-deflection curve. To understand the energy absorption in GFRP reinforced concrete sections, load versus deflection of each beam under progressive loading and unloading in seven cycles was noted with each cycle resisting a higher load than the previous cycle as shown in Figure.7.3. The experimental slopes of unloading curves were recorded. The beams were over-reinforced to avoid possible FRP-rupture before failure by concrete crushing recommended by ACI.440. The beams were instrumented with two-LVDTs and two-inclinometers in the pure bending region (testing region) to monitor the mid-span deflection and determine the curvatures. The FRP and steel rebars were instrumented with strain gages to measure rebar deformation and curvatures. The curvatures at ultimate limit state were calculated using the maximum actual experimental concrete strain, rather than a theoretical value. In the same way, ultimate moment is given as the maximum moment recorded during the tests.

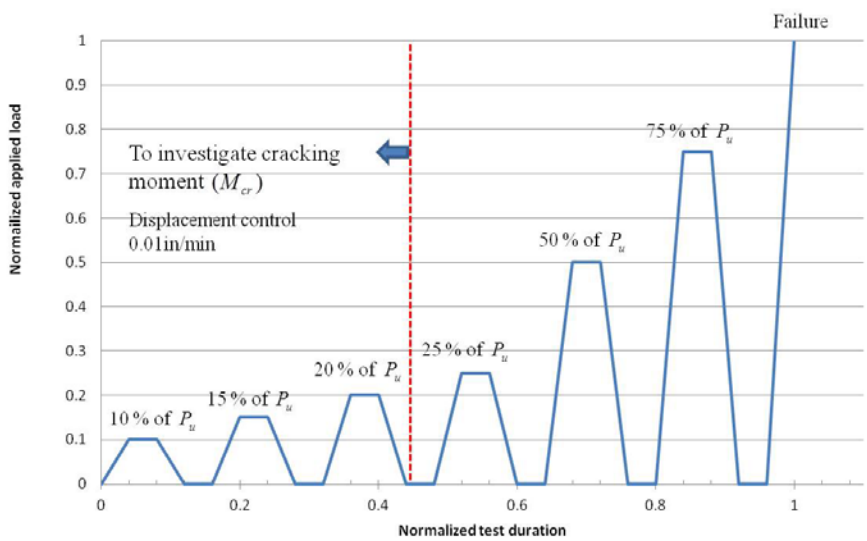

Figure 7.3 Loading history

7.5 Discussion of test results and theoretical analysis

In order to discuss the flexural ductility of the specimens quantitatively, displacements of several levels such as cracking loads or ultimate loads together with the corresponding moment levels are listed in the Table.7.1. Jaeger et al. define the service limit state as the strain state corresponding to a maximum compressive strain in concrete of 0.001. The Intelligent Sensing For Innovative Structures (ISIS-Canada) requires the deformability index (J) to be greater than 4 and 6 for rectangular sections and T-sections respectively.

As can be seen in Table.7.1, higher reinforcement allows for lower curvatures and deflections and concrete crushing of failure modes were observed except the group of GA2-4. It is obvious that GFRP reinforced beams (GA and GH-groups) have lesser values of Δ_u/Δ_{cr} than steel reinforced beams(S- group). This may be attributed to the rate of increase of deflection after accelerated aging. The increase of duration of accelerated aging could decrease the value of Δ_u/Δ_{cr} and the decrease is larger in balanced-reinforced members than the over-reinforced-members with the failure mode of concrete crushing.

The deformability factors depend on the amount of reinforcement. That is, higher reinforcement allows for lower curvatures and deformation, and thus a lower deformability factor. Although there are different ways to calculate the ductility index, there is no doubt that ductility is the ability to absorb the inelastic energy without losing the load-carrying capacity. From this standpoint, it is necessary to evaluate the change of deformability after accelerated aging for long-term performance. Table.7.2 summarizes the variation of deformability indices with different exposure durations for the six groups of beams studied respectively. The normalized deformability indices of six- groups (GA2-#4, GA3-#5, GH2-#4, GH3-#5, S2-#4, S3-#5) are plotted respectively in Figure.7.4.

Compared with beams of low reinforcement ratio (GA2-4 and GH2-4), higher DFs in compression failure of GA3-5 and GH3-5 are attributed to plastic hinge formation, significant

concrete cracking in compression zone, and stress redistribution. Comparison of the DF for compression failures of RC-GFRP and RC-steel beams indicates that the values are not similar.

Table 7.1 Experimental bending moments, displacements and curvatures of specimens at cracking, service and ultimate stages.

Specimen I.D	$M_{0.001}$	M_{cr}	M_u	$\varphi_{0.001}$	φ_u	Δ_{cr}	Δ_u	Δ_u/Δ_{cr}	Δ_1
	k-in	k-in	k-in	rad/in	rad/in	in	in		in
GA2-4-0	195.30	142.5	558.0	0.000603	0.001621	0.049	1.053	21.49	0.160
GA2-4-100	195.79	138.5	539.2	0.000628	0.001707	0.051	1.081	21.20	0.170
GA2-4-200	196.46	135.8	525.4	0.000671	0.001823	0.050	1.088	21.76	0.175
GA2-4-300	196.73	134.8	500.4	0.000685	0.001907	0.054	1.108	20.52	0.190
GA3-5-0	262.42	141.9	749.8	0.000394	0.001363	0.029	0.691	23.83	0.130
GA3-5-100	260.57	141.1	744.5	0.000409	0.001384	0.034	0.742	21.82	0.135
GA3-5-200	251.24	138.2	717.8	0.000431	0.001428	0.036	0.832	23.11	0.160
GA3-5-300	240.66	137.9	687.6	0.000448	0.001497	0.039	0.839	21.51	0.180
GH2-4-0	225.37	129.9	643.9	0.000417	0.001492	0.047	1.003	21.25	0.180
GH2-4-100	214.70	127.5	613.4	0.000461	0.001537	0.047	1.020	21.70	0.185
GH2-4-200	203.53	126.6	581.5	0.000509	0.001694	0.045	1.010	22.44	0.200
GH2-4-300	196.85	126.2	562.4	0.000535	0.001712	0.043	1.030	23.95	0.210
GH3-5-0	292.01	144.5	884.9	0.000341	0.001105	0.021	0.621	29.57	0.130
GH3-5-100	282.74	139.9	856.8	0.000371	0.001181	0.027	0.669	24.78	0.150
GH3-5-200	272.80	139.1	826.7	0.000402	0.001207	0.034	0.807	23.74	0.180
GH3-5-300	246.35	138.9	746.5	0.000418	0.001228	0.031	0.817	26.35	0.210
S2-4-0	276.23	132.8	437.0	0.000265	0.002018	0.031	1.221	39.39	0.105
S2-4-100	268.45	131.1	423.2	0.000279	0.002210	0.025	1.321	52.84	0.095
S2-4-200	261.85	125.9	370.9	0.000277	0.002387	0.024	1.419	59.13	0.095
S2-4-300	254.34	106.4	347.4	0.000294	0.002437	0.021	1.612	76.76	0.085
S3-5-0	301.12	133.9	657.4	0.000203	0.001794	0.045	0.687	15.27	0.125
S3-5-100	299.87	132.9	645.1	0.000209	0.001894	0.033	0.692	20.97	0.125
S3-5-200	298.64	131.1	598.6	0.000214	0.001951	0.029	0.909	31.34	0.105
S3-5-300	288.17	106.4	594.8	0.000238	0.002097	0.031	1.145	36.94	0.095

Note : Average values were used from each group. * : SY+CC=Steel yielding and concrete crushing

Table 7.2 Comparison of deformability indices with the increase of exposure duration between FRP reinforced concrete beams and steel ones.

Specimen I.D	Deformability factor (D.F.)					Normalized DF				
	Naaman	Grace	Zou	Jaeger	Abdelrahman	Naaman	Grace	Zou	Jaeger	Abdelrahman
GA2-4-0	2.13	1.31	84.17	7.69	6.58	1.00	1.00	1.00	1.00	1.00
GA2-4-100	1.61	1.27	88.67	7.52	6.36	0.76	0.97	1.05	0.98	0.97
GA2-4-200	1.89	1.19	89.87	7.32	6.22	0.89	0.91	1.07	0.95	0.94
GA2-4-300	1.51	0.99	79.06	7.14	5.83	0.71	0.76	0.94	0.93	0.89
GA3-5-0	1.12	0.98	125.91	9.88	5.32	1.00	1.00	1.00	1.00	1.00
GA3-5-100	0.95	0.91	123.19	9.67	5.50	0.85	0.93	0.98	0.98	1.03
GA3-5-200	0.98	0.93	127.46	9.47	5.20	0.88	0.95	1.01	0.96	0.98
GA3-5-300	0.98	0.95	112.16	9.55	4.66	0.88	0.97	0.89	0.97	0.88
GH2-4-0	1.35	1.13	124.54	10.22	5.57	1.00	1.00	1.00	1.00	1.00
GH2-4-100	1.28	1.20	123.83	9.53	5.51	0.95	1.06	0.99	0.93	0.99
GH2-4-200	1.34	1.10	122.50	9.51	5.05	0.99	0.97	0.98	0.93	0.91
GH2-4-300	1.04	1.09	126.85	9.14	4.90	0.77	0.96	1.02	0.89	0.88
GH3-5-0	1.29	1.11	181.11	9.82	4.78	1.00	1.00	1.00	1.00	1.00
GH3-5-100	1.23	1.13	184.75	9.65	4.46	0.95	1.02	1.02	0.98	0.93
GH3-5-200	1.32	1.19	150.84	9.10	4.48	1.02	1.07	0.83	0.93	0.94
GH3-5-300	1.25	1.13	156.29	8.90	3.89	0.97	1.02	0.86	0.91	0.81
S2-4-0	6.22	4.16	129.58	12.05	11.63	1.00	1.00	1.00	1.00	1.00
S2-4-100	7.82	5.33	170.59	12.49	13.91	1.26	1.28	1.32	1.04	1.20
S2-4-200	7.92	5.53	174.23	12.21	14.94	1.27	1.33	1.34	1.01	1.28
S2-4-300	7.51	5.69	250.54	11.32	18.96	1.21	1.37	1.93	0.94	1.63
S3-5-0	2.93	1.96	74.98	19.29	5.50	1.00	1.00	1.00	1.00	1.00
S3-5-100	3.08	2.06	101.81	19.50	5.54	1.05	1.05	1.36	1.01	1.01
S3-5-200	4.14	2.77	143.13	18.27	8.66	1.41	1.41	1.91	0.95	1.57
S3-5-300	4.57	3.06	206.41	18.19	12.05	1.56	1.56	2.75	0.94	2.19

RC-steel beams with a compression failure was found to have DFs of 12.1(2-#4) and 19.3(3-#5) before aging while RC-GFRP (Type-A) beams with a compression failure was found to have DFs of 7.7(2-#4) and 9.9(3-#5) before aging. This results does not show a good agreement with the results of other research by Vijay et al(1999). However, Analysis by Vijay et al(1999) on normal-strength concrete fiber reinforced beams with depths of 8 and 16 in(203 and 406 mm) indicates that the DFs are in the range of 6.70 to 13.9 found in GFRP reinforced concrete beams failing in compression. Except RC-steel with 3-#5 reinforcement, all beams have the values of DFs in the range of 6.70 to 13.9.

As shown in the Table.7.2, the ductility indices computed by five methods are quite different. Both Naaman and Grace ductility indices based on the energy-based method decrease with the increase of exposure duration. However in some cases, the changes of the indices of Naaman and Grace are found to increase rather than decrease as expected. This is apparent by comparing the change of normalized deformability indices plotted in Figure.7.4. Such results are not reasonable because these indices are not consistent by the increase of exposure duration. This inconsistent tendency is due to the sensitiveness of determination of P_2 and weighted average slope of S. It can be concluded that the energy-based method can not efficiently take into account the long-tem performance affected by the increase of the ultimate deflection and the decrease of ultimate load-carry capacity in terms of strength/stiffness degradation.

According to Park and Paulay (1975), a steel reinforced beam with a compression failure was found to have a DF over 10.2. Compared with this statement, test results show that all RC-steel specimens with a compression failure have DFs over 11.32 after 300daus of accelerated aging. However, based on the tendency of decreased DF, it can be expected that RC-steel beams will not satisfy the minimum DF requirement of 11.32. Further investigation should be needed to check this over 300days of duration.

The results show that the Jaeger and Abdelrahman indices always decrease by increase of exposure duration of accelerated aging. However, the Abdelrahman index is not as consistent in some cases. For example, Table.7.2 and Figure.7.4 provide Abdelrahman indices of 5.32 (for non-exposed specimens with f_c'=4.25ksi) and 5.50(for aged specimens during 100-days with f_c'=4.96ksi) respectively. There are no consistent tendency to show the correlation between deformability factors and exposure-durations except the Jaeger index based on the moment and deformation-based model.

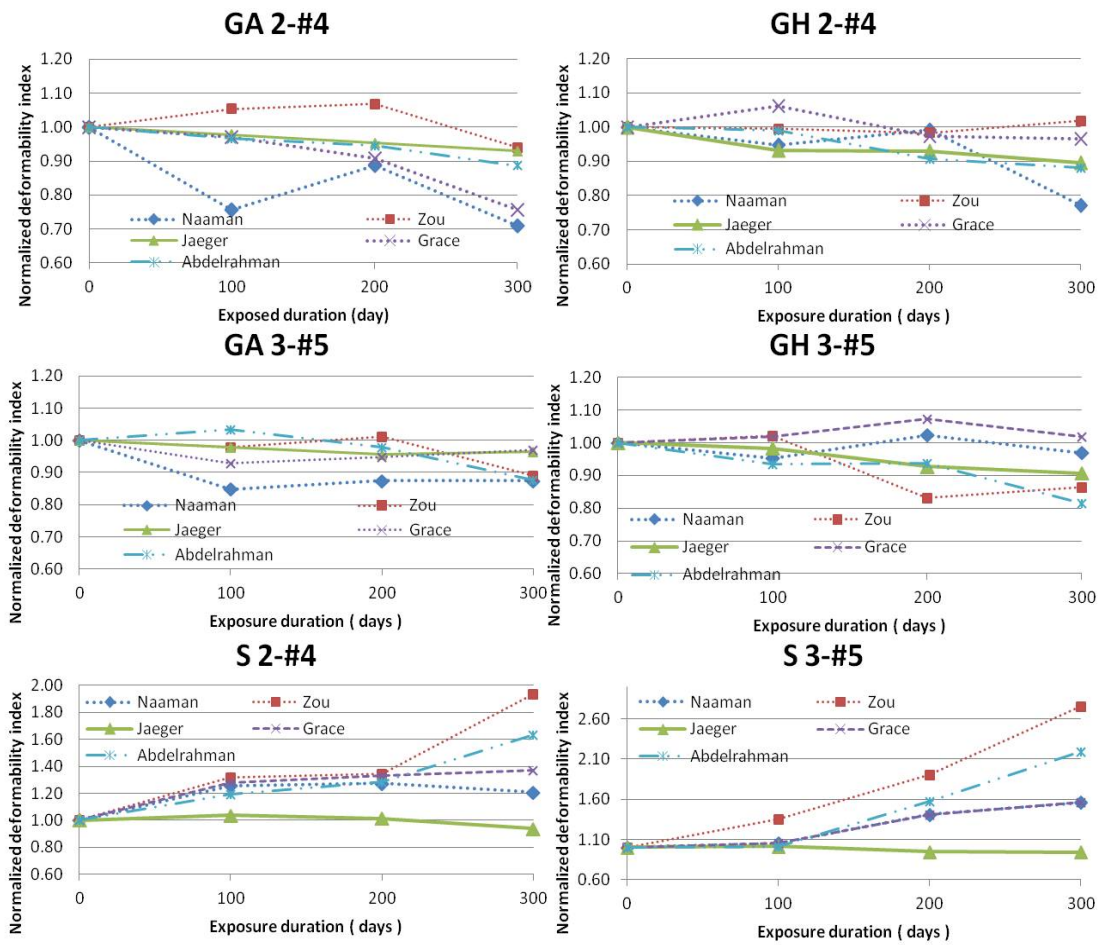

Figure 7.4 Comparison of normalized deformability indices of each test group

Comparison of DF for compression failures of RC-GFRP beams and RC-steel beams indicates that the values are not similar. In terms of the type of reinforcement, RC-Steel specimens exhibited the increase of DF as the increase of exposure duration unlike RC-GFRP ones. The values of DF in deformation-based method of Jaeger index are not similar to ones by energy-based method. Although there are differences between ways to calculate the ductility index, it can be seen that the Jaeger index shows the consistent tendency by time-dependent environmental exposure regardless of the ratio of reinforcement. Moreover, in the Jaeger index, the deformability factors were much higher than the minimum value of four as proposed in ISIS Canada design manual No.3 for RC members reinforced with FRP of the minimum requirement. The changes of DFs of the sections with type-B reinforcement (with sand-coated surface) were greater than ones with type-A of reinforcement (with wrapped surface).

In regard to the performance of the Zou index, there is not a general trend related to variation of exposure duration. Although the Zou index decreases with increase of exposure duration from 100days to 300days for beams of GH3-#5 group as shown in the Figure.7.4, inconsistent behaviors are observed for beams of GA2-#4 and GA3-#5 as shown in the Figure.7.4 as well as Table.7.2. Similar to the Naaman and Grace indices based on the energy-based model, the Zou index increase rather than decrease as expected for beams GA2-#4 and GH3-#5. These unreasonable results may be attributed to the fact that the Zou index has been developed for FRP prestressed concrete beams defined in terms of both a deflection factor and a moment factor, and whether it is applicable to concrete beams reinforced with FRP rebars needs further investigation.

7.6 Proposed weighted slope-based on energy method

Ductility may be defined as the ratio relating the elastic and total energies, based on the energy definition. Herein, the ratio of elastic to total energy is considered. This method consists of two parts. The first part is to determine the point that separates the elastic energy from

inelastic energy. The second part is to use these energies to indicate the ductility index. In the first part of this method, the unloading path is estimated by weighting the different portion of the load-deflection curve by using load weights. The second part is relied on a load-deflection curve with a hardening portion, which can be obviously observed in the case of a steel reinforced beam. Vijay et al. shows that ductility index-based on energy method is dependent on the load-level at which unloading begins. For instance, while a ductility index of 8 was calculated at 100% of the failure load for the same GFRP reinforced beams, a ductility index of 1.65 was obtained at 95% of the ultimate load. Moreover, it should be noted that these models-based on energy approach such as Naaman et al. and Grace indices do not take into consideration the degradation of strength/stiffness after aging.

7.6.1 Comparison deformability based on energy approaches

If only the weight of the load is considered such as Naaman index, the slope of the line separating the elastic energy from the total energy can be obtained as follow:

$$S = \frac{P_1 S_1 + (P_2 - P_1) S_2}{P_2} \qquad \text{(Eq.7.5)}$$

where P_1 and P_2 are loads as shown in Figure.7.1 and S_1 and S_2 are corresponding slopes. However, Figure.7.6 clearly shows that difference between the experimental unloading slopes and the calculated elastic slopes introduced by Naaman and Grace. Errors of the slopes compared with the experimental unloading path were summarized in Table.7.3.

All of the beams were loaded and unloaded with 4-cycles up to the failure load and the experimental slopes of the unloading curves were recorded. After failures, the unloading slope were extended based on the assumption that unloading slopes are linear such as other unloading slopes at other loading cycles.

Unloading slopes of beams exposed into accelerated aging chamber are not equal to ones of unexposed beams and both Naaman index and Grace index do not show a good match

between the calculated slope (s) and the experimental unloading curves regardless of exposure to accelerated aging. Weighted slope by Naaman and Jeong(1995) are greater than the slopes of the experimental unloading path as shown in Figure7.6 through 7.7 and Table7.3. This result not only leads to underestimate the elastic energy and overestimate ductility but also does not take into consideration the ratio of reinforcement and degradation of strength/stiffness

On the other hand, modified weighted slopes by Grace (1998) are less than the slopes of the experimental unloading path. This result not only leads to overestimate the elastic energy and underestimate ductility but also does not take into consideration the ratio of reinforcement and degradation of strength/stiffness.

Table 7.3 Error of the slopes compared with the experimental unloading path

	Duration	2-#4ASLAN	3-#5ASLAN
Naaman	No exposure	22%	19.80%
	300days	38%	21.50%
Grace	No exposure	-6.40%	-41.20%
	300days	-39.10%	-37.80%
Proposed slope*	No exposure	-5.10%	-3.50%
	300days	-7.60%	-5.80%

*: described in Eq.7.6

7.6.2 Modified weighted slope to calculate deformability

The following parameters were considered in order to determining the magnitudes of the elastic and inelastic energies. Eq.7.6 and Figure.7.5 shows the proposed modified slope considering degradation of strength/stiffness over time.

- Ratio of reinforcement

- Tensile strength retention value
- Acceleration factor(AF)

$$S_{weighted} = \alpha \times \rho \times Y(t) \times \frac{S_2P_2 + S_3P_3 + S_{peak}P_{peak} + S_{fail}P_{fail}}{P_2 + P_3 + P_{peak} + P_{fail}} \qquad \text{(Eq.7.6)}$$

where ρ is reinforcement ratio, α is correction factor of 0.398 based on regression analysis of empirical tested data , Y(t) (=$e^{(-t/\tau)}$) is degradation rate described in chapter.4, t= exposure time (day), τ= 1/k and k= strength degradation rate obtained from regression analysis of tensile tests data. Slopes and loads at each level used in the proposed model of weight-slope are described in Figure.7.5. It should be noted that newly defined slopes and loads at each stage are suggested empirically compared with tested data. The initial slope S1, corresponding to applied loads P1, of the load-deflection curve were not considered to establish the proposed model of the slope because it make the unloading path of weighted slope overestimated.

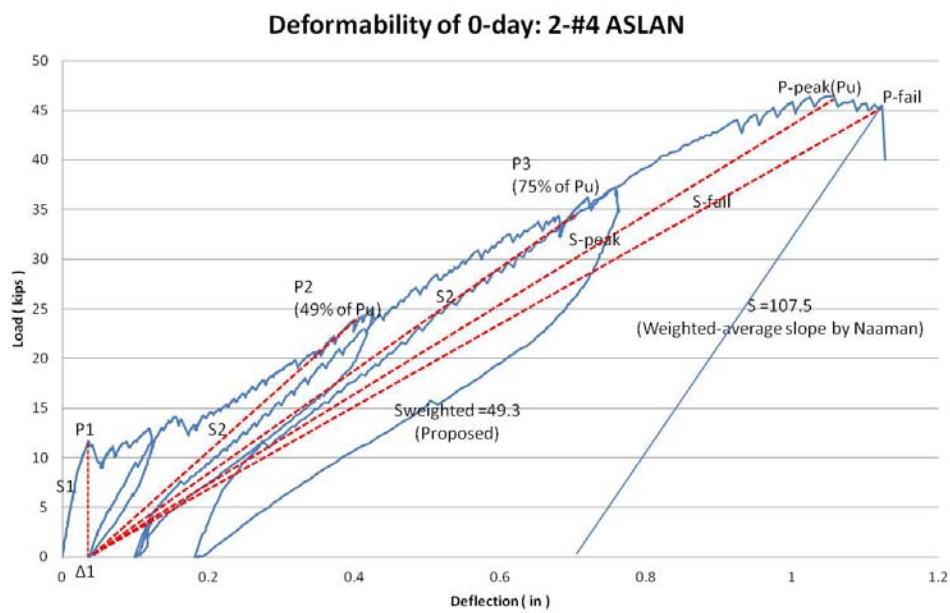

Figure 7.5 Specification of slopes and load at each level used in the proposed model of weight-slope

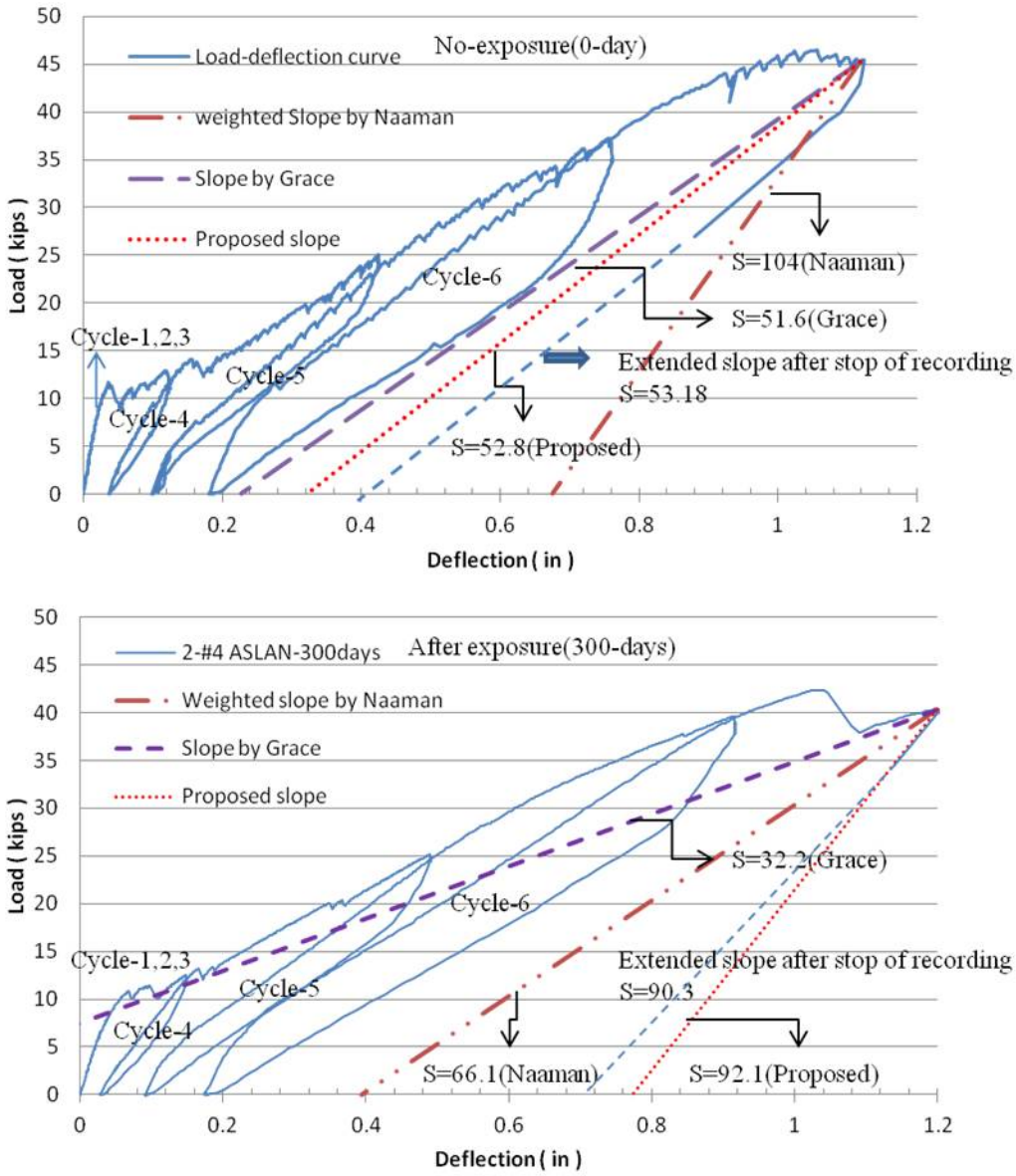

Figure 7.6 Comparison of theoretical weighted slopes with experimental unloading slopes (GA2-#4)

The slopes of the unloading pate from GA2-4-0 and G2-4-300 beams are calculated using Eq.7.6. as seen in Figure7.6. From this figures, it is evident that Eq.7.6. much closely predicts the slope of unloading curves for both unconditioned cases and conditioned ones.

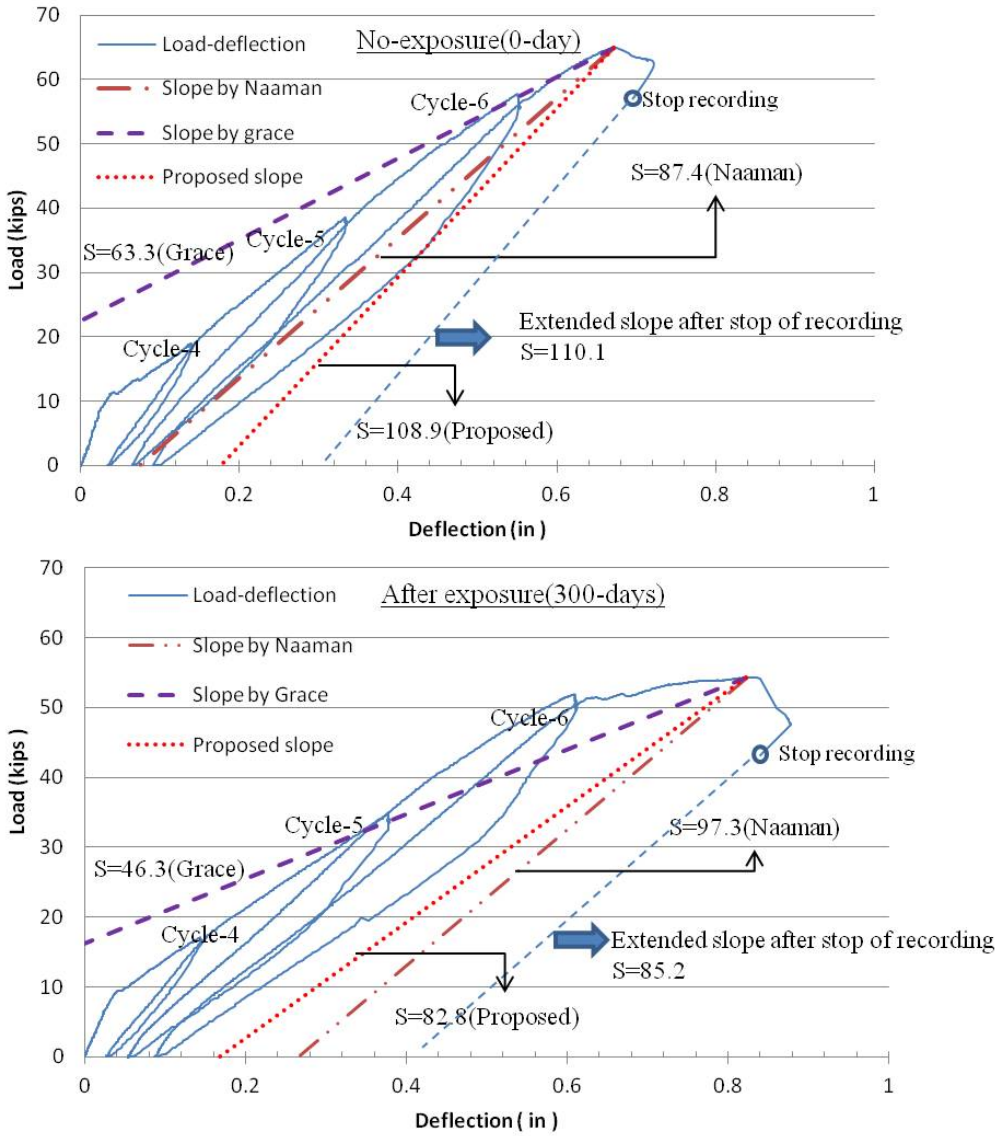

Figure 7.7 Comparison of theoretical weighted slopes with experimental unloading slopes (GA3-#5)

The same result can be drawn for GA3-5-0 and GA3-5-300 beams as shown in Figure.7.7. The suggested equation shows a reasonable rough agreement (maximum

error<7.6%) between the calculated slope S and the experimental unloading path of specimens at failure.

7.6.3 Limitation

The above energy-based deformability index is dependent on how much of the total energy is elastic and how much is inelastic. The index is also affected by the load level at which unloading begins [Vijay et al, 1996]. In order to account for level of loading-unloading cycle and stirrups(influence of shear cracks), failure mode of the beam, further parameters should be introduced.

7.7 Summary

This chapter has evaluated deformability indices for concrete beams reinforced with GFRP and steel rebars before/after accelerated aging and proposed the new defined weighted slope. A summary and relevant conclusions obtained from this chapter are given as follows:

- Higher reinforcement allows for lower curvatures and deflections regardless of duration of exposure to accelerated aging, then leads to attain higher deformability.
- Comparison of DF for compression failures of RC-GFRP beams and RC-steel beams indicates that the values are not similar. In terms of the type of reinforcement, RC-Steel specimens exhibited the increase of DF as the increase of exposure duration unlike RC-GFRP ones.
- The change of deformability in RC-steel specimens is greater than the one in RC-GFRP specimens
- For type-A, type-B and steel reinforcement, DFs were observed in the range 7.14 to 9.55, 9.14 to 11.82 and 12.05 to 19.69.

- The deformability factors of RC-GFRP showed a tendency to be decreased after accelerated aging while DFs of RC-steel increased after accelerated aging.
- No general trend can be identified except Jaeger Index related to the variation of accelerated aged duration.
- There is no general agreement on how much deformability is enough with respect to the available deformability indices. Further study is necessary to provide a scientific basis for determination of the requirement.
- The proposed model of weighted slope (Eq.7.6.) much closely predicts the slope of experimental unloading curves for both unconditioned cases and conditioned ones (Type-A reinforcement).

CHAPTER 8

ACOUSTIC EMISSION PERFORMANCE OF GFRP RODS/BEAMS WITH GFRP RODS SPECIMENS AFTER ACCELERATED AGING

8.1 General

Every structure or component in the real world always has some imperfections and can be damaged by exposure under chemical or mechanical attack. Chemical attack such as deicing salt and alkaline environment usually occurs in concrete beams reinforced with GFRP and steel bars. It can take the form of permeation, chemical changes, and dissolution of rebars. The permeation in FRP can cause blisters, swelling, debonding, and softening of resin. The chemical changes can cause softening of the resin or cracking at the surface. The dissolution removes the resin, and leaves fibers hanging down from the laminate [Niesse and Ahluwalia, 2001]. FRP material and steel are very sensitive to environmentally induced degradation in terms of environmental aging. Temperature and moisture can degrade the resin. The effect includes changing the color, initial softening and later hardening of resin [Niesse and Ahluwalia, 2001].

The damages and imperfections in a structure may or may not be harmful or visible. Therefore, nondestructive inspection (NDI) or nondestructive evaluation (NDE) or nondestructive testing (NDT) can be performed to ensure that structures can be safely operated for a certain period of time. In general, the roles of NDT are to help detect, locate, and evaluate the significance of the flaws in in-service structures [Ativitavas, 2002]. Recently several nondestructive methods have been applied to investigate damage levels of structural components. The AE technique, a nondestructive method that is relatively easy to install and is capable of predicting the damage location, is used in this study.

Acoustic emissions can be defined that “the class of phenomena whereby transient elastic waves are generated by the rapid release of energy from localized sources within a material or the transient waves so generated” [ASTM E 1316-09a, 2009]. AE is recognized as a nondestructive monitoring technique that is based on the detection of a transient sound wave that is generated by a *short and rapid release of energy*. This rapid energy release manifests itself in the form of a characteristic responds to an applied stress [ASTM E 1316-09a, 2009]. The principle of AE is illustrated in Figure.8.1. AE is generally made by a piezoelectric material, which converts physical signals to electrical signals. AE are able to determine the location of a flaw and the extent of the damage by analyzing the time of flight of the stress wave and amplitude of the signal [Promboon et al, 2000].

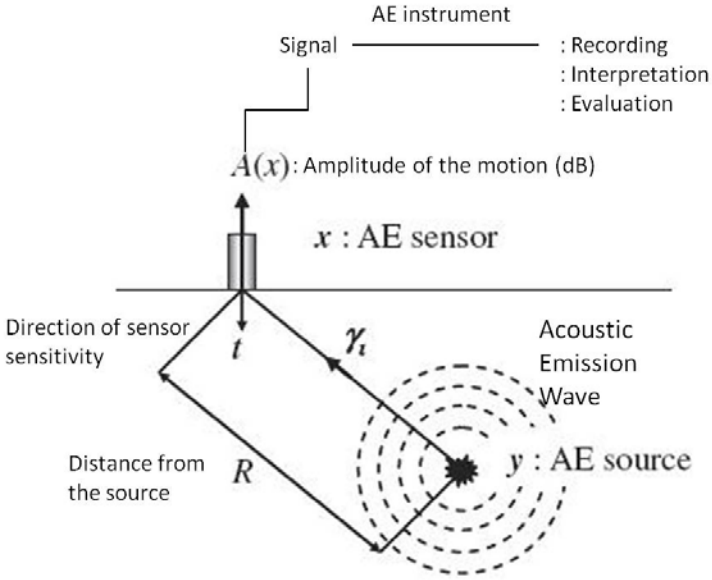

Figure 8.1 Basic of AE detection
(Ohno et al., 2010)

The purpose of monitoring AE activities is to provide beneficial information to prevent fatal fracture by correlating detected AE signals with growing deterioration and degradation of stiffness/strength. Objectives of this study to provide differences of characteristics of AE signals between unconditioned specimens and conditioned (damaged) ones.

8.2 Instruments

8.2.1 AE sensors

Acoustic emission (AE) sensors are mounted on the surface of the FRP bars and concrete beams with GFRP bars tested. “When transient waves propagate through the structure, the piezoelectric crystal in an AE sensor will resonate in response to the structure’s surface motion. The change in stress in the crystal will generate an electric current, which can be monitored” [Ativitavas, 2002]. This information will then be recorded by the acoustic emission data acquisition system (DAQ). AE sensors respond to dynamic motion that is caused by an AE event. This is detected through transducers which transform mechanical response into an electrical voltage signal. The transducer element in an AE sensor is almost always a piezoelectric crystal (PZT) [www.ndt-ed.org]. Transducers are classified into two classes- resonant and broadband. The majority of AE equipment is responsive to movement in its typical operating frequency range of 30 kHz to 1 MHz. For materials with high attenuation (e.g. plastic composites), lower frequencies may be used to better distinguish AE signals [www.ndt-ed.org]. In concrete, low frequency sensors (60 kHz) are used because the inhomogeneity of the concrete attenuates the signal (and also the background noise) more quickly than homogeneous materials [Ativitavas, 2002]. In Figure.8.2, AE sensor, pre-amplifier and AE data acquisition system used in flexural beam tests were shown.

8.2.2 Pre-amplifier

The piezoelectric crystal in the acoustic emission sensor converts the signal to a voltage. A preamplifier is required to magnify the voltage to a more appropriate range because the magnitude of the voltage is very small. Usually, the preamplifier is mounted integral in the sensor [Ativitavas, 2002].

8.2.3 AE data acquisition

After the preamplifier, the AE signal is stored to the AE data acquisition system by a cable. The DAQ system can filter unwanted signals or frequencies out and amplify the signals. It will also record, and organize the AE data. In this study, MicroDiSP was used on the Laptop using the AEwin™ software to detect AE signals.

Figure 8.2 Pre-amplifier and a sensor used for acoustic emission evaluation (www.ndt-ed.org)

8.3 AE parameters

8.3.1 Basic and modified parameters

Some of the most important parameters associated with AE as defined by the ISO12716 and ASTM E1316 [ISO 12716, Grosse et al., 2008 and ASTM E1316]. The followings will be used to account for the AE characteristics consistently and shown briefly in Figure.8.3:

Count (AE count) – "The number of times the acoustic emission signal exceeds a preset threshold during any selected portion of test"

Event (AE event) – "A local material change giving rise to acoustic emission" [ASTM E 1316].

Hit (Sensor Hit) – "The detection and measurement of an AE signal on a channel" [ASTM E1316]

Peak amplitude (AE Signal Amplitude): "The peak voltage of the largest excursion attained by the signal waveform from an emission event" [ASTM E 1316]. In other words, peak

amplitude is the highest point of the signal. It is the absolute value on either positive or negative side of a waveform. The peak amplitude is usually reported in decibels (dB) due to the wide range of typical values in voltage unit. Voltage is converted to decibels using the following Eq.8.1:

$$A = 20 \cdot \log(\frac{V}{V_{ref}}) \qquad \text{(Eq.8.1)}$$

where A is amplitude in dB, V is voltage of peak excursion and V_{ref} is reference voltage, typically 1μV (Voltage generated by 1 mbar pressure of the face of sensor).

Duration (Hit Duration) - "The time between AE signal start and AE signal end" [ASTM E 1316]. It is the time from the first to the last threshold crossing and is typically displayed in microseconds.

Risetime (AE Signal Rise Time) - "The time between AE signal start and the peak amplitude of that AE signal" [ASME E 1316]. Risetime is also measured in microseconds.

Signal Strength - The area under the envelope of the linear voltage signal. Specifically, the signal strength [Fowler et al.,1989] is:

$$S_0 = \frac{1}{2}\int_{t_1}^{t_2} f_+(t)dt - \frac{1}{2}\int_{t_1}^{t_2} f_-(t)dt \qquad \text{(Eq. 8.2)}$$

Where f_+ is positive signal envelope function, f_- is negative signal envelope function, t_1 is time at first threshold crossing and t_2 is time at last threshold crossing

Threshold (Voltage Threshold) - "A voltage level on an electronic comparator such that signals with amplitudes larger than this level will be recognized. The voltage threshold may be user adjustable, fixed, or automatic floating." [ASTM E 1316]. The threshold is set for eliminating electronic background noise, which normally has low amplitude.

Frequency – "The number of cycles per second of the pressure variation in a wave. Commonly, an AE wave consists of several frequency components" [ASTM E 1316].

Kaiser and Felicity Effects - The Kaiser effect is defined as “The absence of detectable acoustic emission at a fixed sensitivity level, until previously applied stress levels are exceeded [ASTM E 1316]. The presence of the Kaiser effect generally indicates good integrity of the structure [Fowler, 1986] The Felicity effect is described as “the presence of detectable acoustic emission at a fixed predetermined sensitivity level at stress levels below those previously applied [ASTM E 1316]. The Felicity effect is a breakdown of the Kaiser effect. That means that the structure generates emission during reloading, before the previous maximum stress is reached [Fowler, 1979]. A low Felicity ratio is generally associated with more damage in the structure [NDIS, 2000]. The Felicity ratio is an indication of the amount of damage, and is defined as the ratio of the load at which emissions occur to the previous maximum load:

Felicity ratio = load at which emissions occur / Previous maximum load (Eq.8.3)

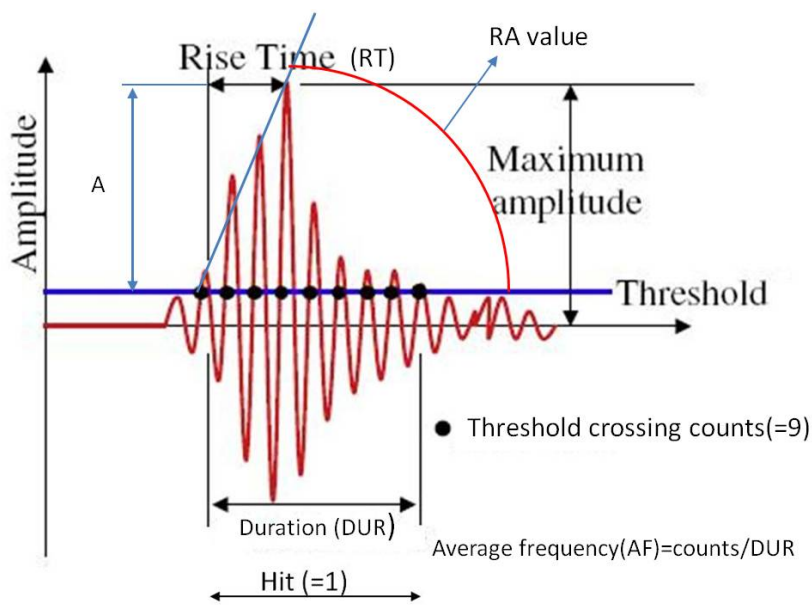

Figure 8.3 Conventional AE signal (parameter) features

Energy (AE Signal Energy) - "The energy contained in a detected acoustic emission burst signal, with units usually reported in joules and values which can be expressed in logarithmic form (dB, decibels)" [ASTM E1316]

Source (AE Source) - "The position of one or more AE events" [ASTM E1316]

8.3.2 AE parameter analysis

Amplitude vs. duration plot : The relationship of amplitude and logarithm duration plot is useful for determining whether or not the AE data is genuine. The genuine data generally creates a triangle cluster on the plot, while the no genuine hits such as mechanical rubbing and electromagnetic interference (EMI) appear in the area outside the triangle as shown in Figure.8.4. [Fowler, 1986].

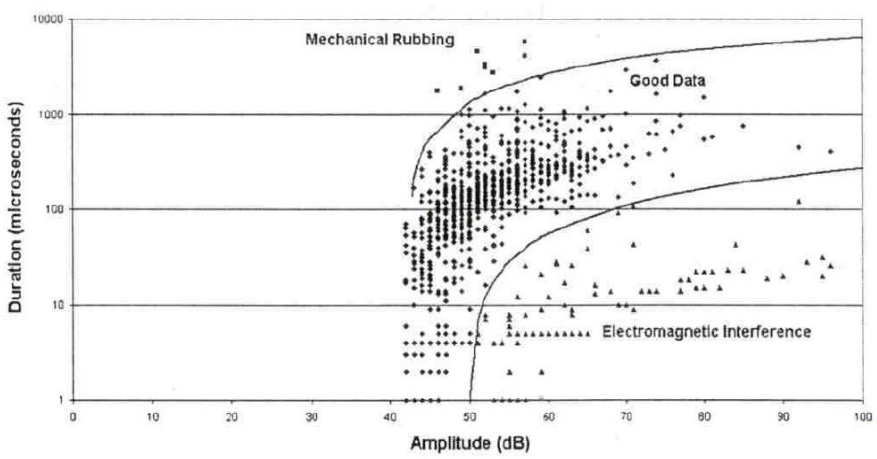

Figure 8.4 Amplitude and duration plot showing good data and two types of unexpected noise (Harvey, 2001)

Cumulative signal strength vs. Load (or Hits) plot : Some energy should be released when damage occurs in a structure under an applied load. This energy is converted into the acoustic emission. Therefore, the energy of the events is directly related with the severity of the damage [Bray and Stanley, 1997]. Thus, signal strength has become an important parameter to

evaluate AE signals. As the load increases, more damages occur, and the graph of cumulative signal strength versus load generally shows the rise of the curve. At the ultimate load, the curve usually yields the steep rise as shown in Figure.8.5 (a). The historic index is the measurement of the rate of the slope, which some researchers used it to determine the onset of significant damage [Ativitavas,2004]. AE signals generated under different loading patterns can provide valuable information concerning the structural integrity of a material as seen in figure.8.5.(b). Load levels that have been previously exerted on a material do not produce AE activity. In other words, discontinuities created in a material do not expand or move until that former stress is exceeded [Zeihl, 2000]. This phenomenon, known as the Kaiser Effect, can be seen in the load versus AE plot to the right. As the object is loaded, acoustic emission events accumulate (segment AB). When the load is removed and reapplied (segment BCB), AE events do not occur again until the load at point B is exceeded

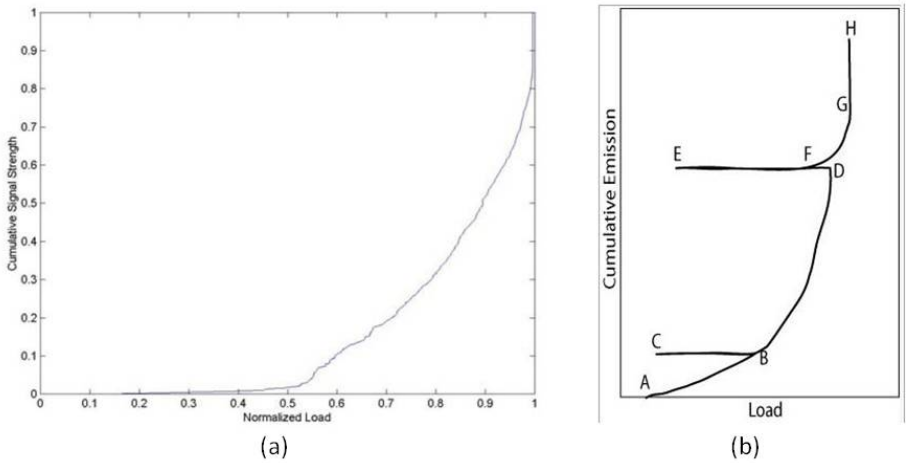

Figure 8.5 (a) Normalized cumulative signal strength and normalized load plot of fiber glass composite loaded in tension (b) Basic AE history plot showing Kaiser effect (BCB-region), and Felicity effect (DEF-region) (Bray and Stanley, 1997)

As the load exerted on the material is increased again (BD), AE's are generated and stop when the load is removed. However, at point F, the applied load is high enough to cause significant emissions even though the previous maximum load (D) was not reached. This

phenomenon is known as the Felicity Effect. This effect can be quantified using the Felicity Ratio, which is the load where considerable AE resumes, divided by the maximum applied load (F/D) [Grosse, 2008 and Ativitavas,2004]. As shown in the Figure.8.5.(b), if AE signals continue to be detected during the holding of these loads, it is likely that substantial structural defects are present. In addition, a material may contain critical defects if an identical load is reapplied and AE signals continue to be detected.

RA value vs. average frequency plot : In order to classify active cracks, AE parameters of the rise time and the maximum amplitude are applied to calculate RA value, and the average frequency is obtained from AE count and the duration time as following[Aggelis, 2011]:

RA value = the rise time/the maximum amplitude (Eq.8.4)

The average frequency = AE ring down-count/the duration time (Eq.8.5)

From these two parameters, cracks are readily classified into tensile and shear cracks as illustrated in Figure.8.6. This crack classification method is based on the JCMS-III B5706 code, of which results were confirmed under the four-point bending tests and the direct shear tests of concrete specimens. However, a defined criterion on the proportion of the RA value and the average frequency for crack classification has not been confirmed [Ohno et al., 2010].

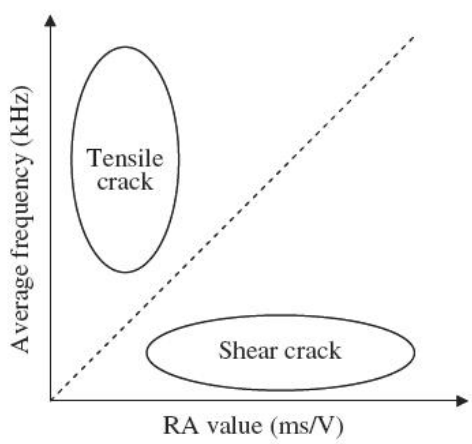

Figure 8.6 Relation between RA value and average frequency for crack classification (Ohno et al., 2010)

8.4 Experimental test program

This chapter involved the evaluation of acoustic emission performances for accelerated aged GFRP reinforcing bars embedded in concrete. In terms of materials, same GFRP bars (all #3 bars of Type-A and Type-B) and concrete mix designs described in Chapter-4 were used to characterize environmental impact on the evaluation of acoustic emission performance. In terms of conditions of accelerated aging, specimens were cast and placed in the same chamber B with the temperature of 115°F (46°C) and RH of 80% after immersing in 3% saline solution described in Chapter 4 through 6 for 300days. Two different groups of specimens were tested

- Tensile test
- Four point flexural beam tests with dimensions of 8×12in×83in (Width×Depth×Length)

The sensors used in this study were wide band sensors. Preamplifiers with a gain of 40 db were used with wide band sensors. This is interfaced with the laptop via a PC card interface slot. The output from the microDiSP was displayed on the Laptop using the AEwin™ software. After testing, the data obtained was processed and analyzed using the AEwinPost™ software.

8.4.1 Tensile test

To evaluate the acoustic emission performance of FRP bars, unconditioned and conditioned tensile specimens were tested using an Universal Testing Machine (MTS and Baldwin) of 400kips capacity based on ASTM D7205.

A 4-channel digital signal processing AE-DiSP from Physical Acoustics Corp. was utilized to measure the AE parameters in the bar as shown in Figure.8.7. AE waves were amplified with 40 dB gain by pre-amplifier. AE sensors were attached to the surface of the specimen with hot melt adhesive (HMA), so that the sensor face and the specimen surface have a good contact for the signal detection without air entrapment. To avoid mechanical noises during tests, two guard sensors were used as filters of noises. Two types of GFRP rods and two

different exposure durations of experiments (Control and 300days) were tested under the same threshold levels of 40 dB.

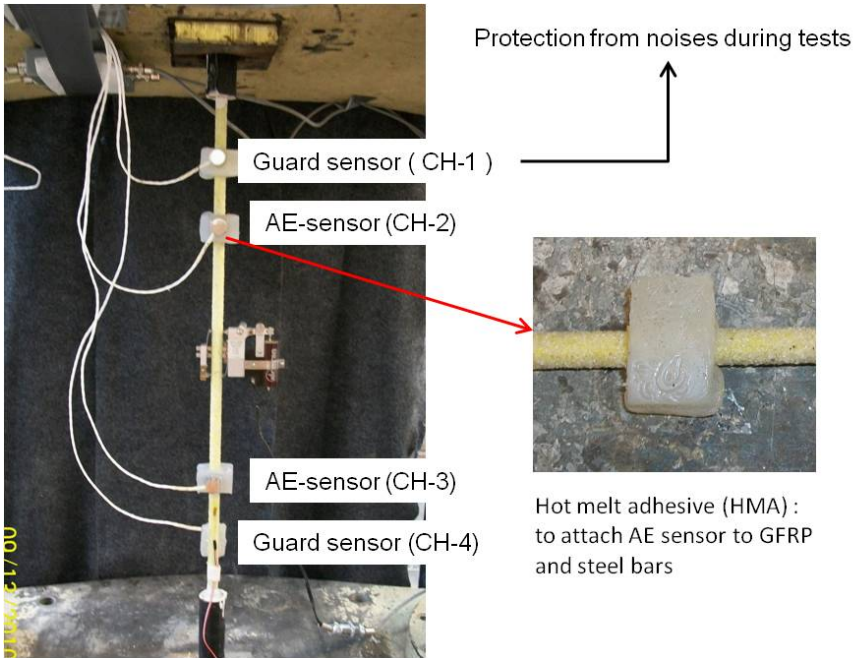

Figure 8.7 AE experimental setup of tensile specimens

8.4.2 Flexural beam test

The specimens employed for this test were equal to the tested beams in Chapter 6. For reference, RC-GFRP and RC-steel beams without exposure were also tested in advance. For each of the exposure duration (300days), three specimens were tested in bending with concurrent AE monitoring. For the purpose of the AE monitoring, four AE sensors of resonance at 300 kHz (R30S, Physical Acoustics Corp., PAC) were mounted to the side of the beams as shown in Figure.8.8. As mentioned previously, at least three sensors were required in a 2-D planar so that the optimized coordinate was selected to set the targeted span covered sufficiently. It should be noted that three sensors are a minimum numbers of sensors to capture the location of events such that more numbers of sensors generally provide more accurate

locations of events [Mirmiran et al., 2000]. Four sensors were located in shear region close to constant bending region for monitoring the AE hit rate and other major parameters where event location was not attempted. The preamplifier gain was set to 40 dB. After performing a pilot test, the threshold was also set to 40 dB in order to avoid the possibility of electronic/environmental noise.

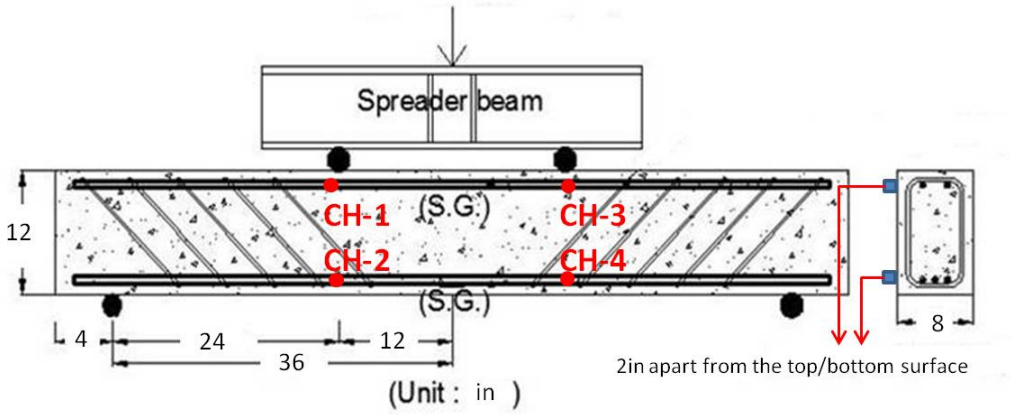

Figure 8.8 AE experimental setup of flexural beam tests

All of the beams were tested under four-point loading to investigate the AE performance of degraded specimens by accelerated aging and the degree of damage for all specimens using the AE technique as shown in Figure.8.9. The cyclic loading tests were carried out in four repeated cycles of loading and unloading at $0.25P_u$, $0.5P_u$, $0.75P_u$, and full capacity for each type of specimen. The test setup consisted of a steel reaction support beam, a 200kips high-pressure hydraulic cylinder and pump (CLRG-2006 : EnerPac Inc.) with force-control mechanism and a 4-channel digital signal processing AE-DiSP from Physical Acoustics Corp. of Princeton, NJ. Four 300-kHz sensors were used to detect the AE signals. The parameters in the hit data set included time of test, amplitude, energy, counts, duration, rise time, counts to peak, average frequency, threshold, and load parameter. The load input was attached to the pressure transducer (load-cell) and was calibrated through the parametric scaling feature of the processor and synchronized with AE parameters.

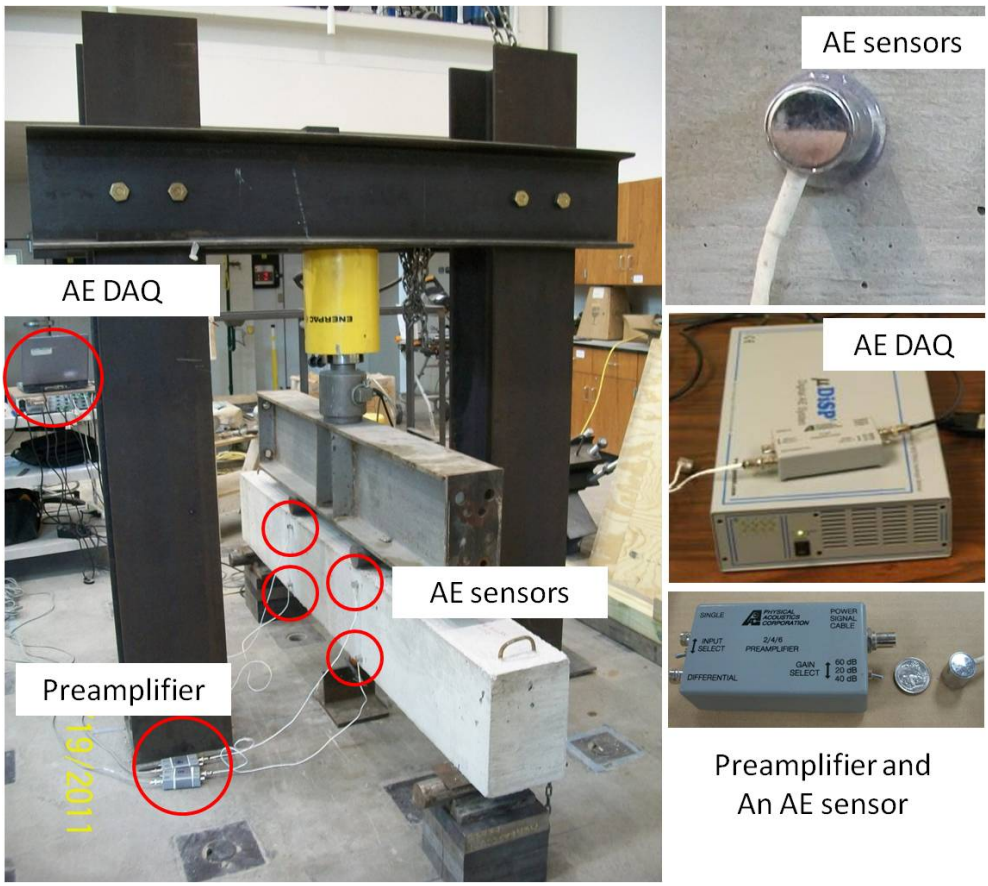

Figure 8.9 Four point bending test setup with AE monitoring instruments

8.5 Test results and discussion

8.5.1 AE activity of tensile specimens (unconditioned / conditioned specimens)

The time history of AE activity is an important index because it establishes the correlation between the load and the AE response. Since the load tests were displacement-controlled, time distributions of the loads are comparable to the load-deflection or stress-strain plots, and therefore, the AE response can be directly correlated to the extent of damages in the specimens. Behaviors of cumulative AE hits over time for all four channels and AE events during the tensile test are shown in Figure.8.10 through 8.12. For AE events, which are reasonably located inside the specimen, the number of the hits is indicated and generating

process of AE hits and AE events observed is classified into two stages. Each stage is mainly associated with a particular damage growth such as fiber/matrix failure. AE activity starts gradually to increase at the stage-1 until 82%(GA-0d),57%(GH-300d) and 84%(S-300d) of the ultimate load respectively and then rapidly increases at the stage to failure. AE activity due to the degradation of rebar is observed in the stage 2. It can be seen from the figures that higher energy levels occur near the beginning of stage-2. Considerable amount of AE activity, though at lower energy levels, was recorded during the whole test duration regardless of duration of accelerated aging.

Additionally Figure.8.10 through 8.12 shows the AE energy which exhibits its maximum at the moment of fracture while initially the energy of each AE hit was not considerable. For GA-0d specimens, it is observed that very little AE activity has taken place before about $0.82P_u$. At or near $0.82P_u$, the release of AE energy started. The rate of AE increases rapidly from $0.82P_u$ to the failure of specimen. Also, it is observed that the AE energy release is relatively less for GA-0d of control specimens when compared with that for GA-300d. Environmental conditioning had a considerable effect on AE performances of GFRP and steel reinforcement. After 300days of accelerated aging in chamber (equivalent to 24.5 years of outdoor weathering in DFW area), the rapid increases of AE hits were observed at 57%,48% and 82% of ultimate loads for GA-300d,GH-300d and S-300d respectively.

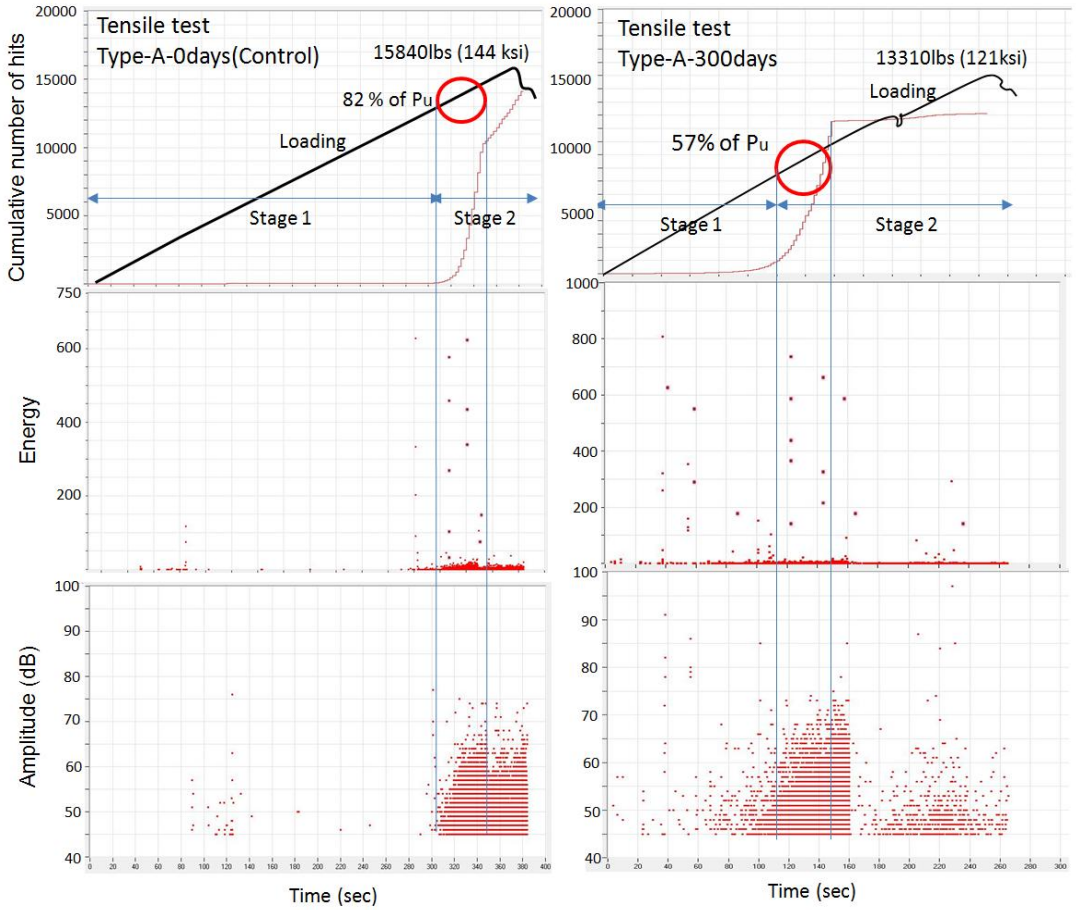

*Note : Energy(×10^2 dB)

Figure 8.10 Comparison of time history of (a) accumulated AE hits (b) AE energy and (c) amplitude(AMP) for conditioned and unconditioned specimens of Type-A GFRP bars

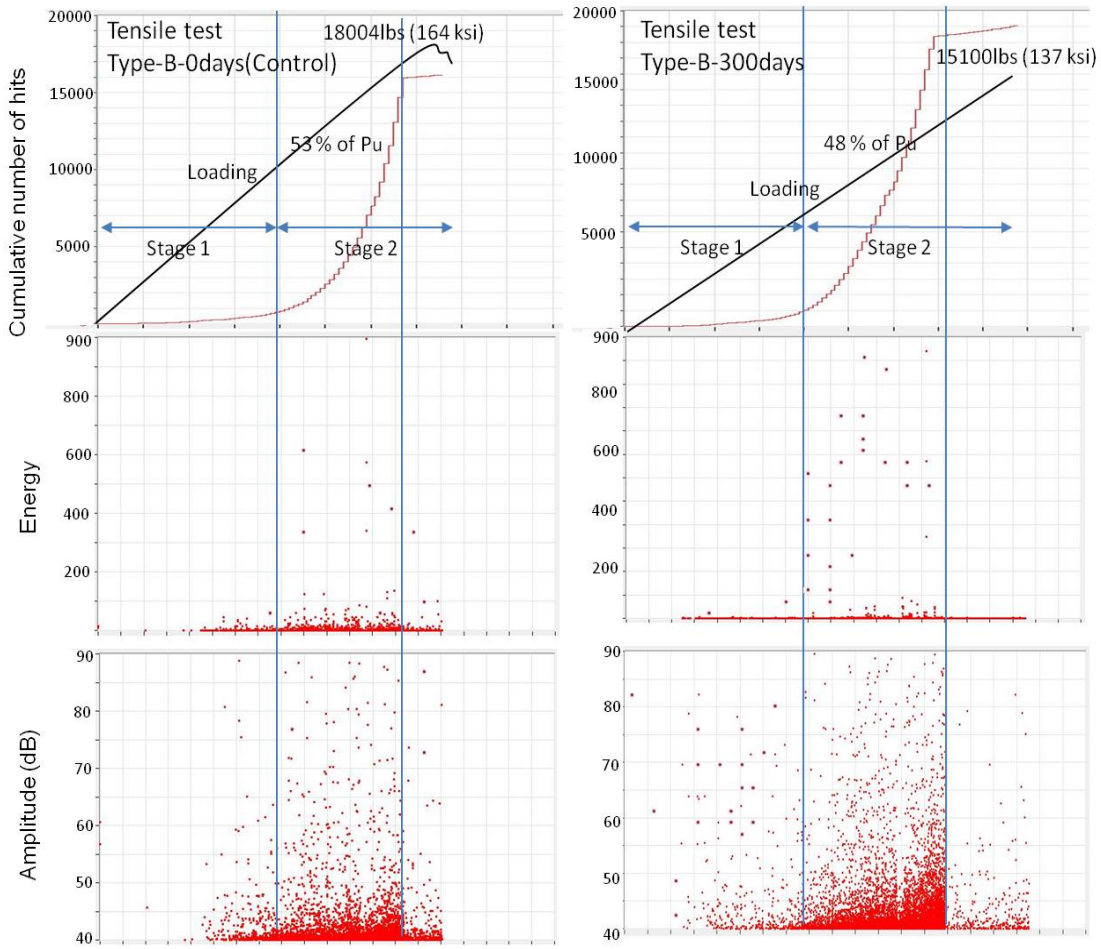

*Note : Energy(×10^2 dB)

Figure 8.11 Comparison of time history of (a) accumulated AE hits (b) AE energy and (c) amplitude(AMP) for conditioned and unconditioned specimens of Type-B GFRP bars

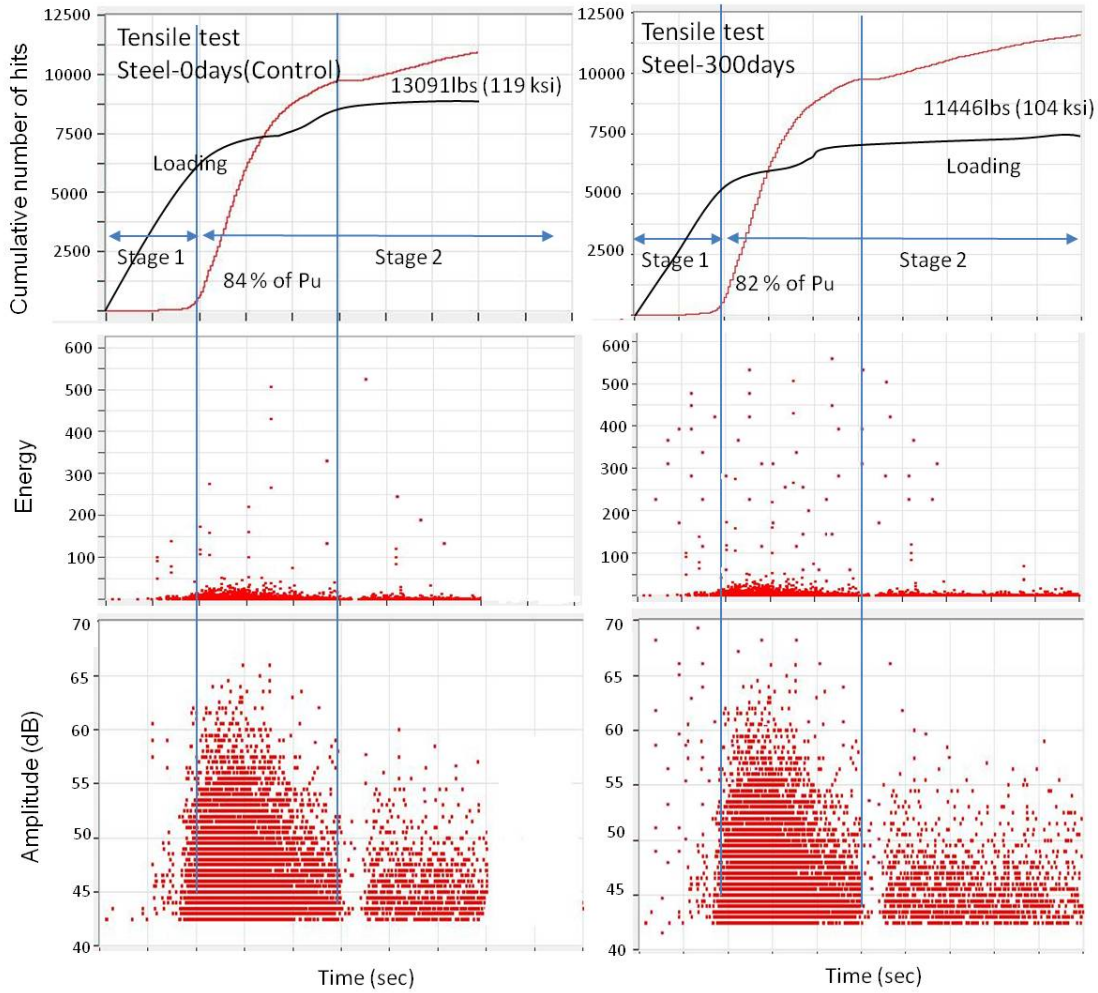

*Note : Energy(×10^2 dB)

Figure 8.12 Comparison of time history of (a) accumulated AE hits (b) AE energy and (c) amplitude(AMP) for conditioned and unconditioned specimens of steel bars

Except steel specimens of S-300d, the loading level of rapid increases of AE hits were reduced by about 42% and 26% respectively for Type-A and Type-B bars. These figures show that the GFRP specimens (GA and GH) have higher amplitudes than their steel counterparts. At the Matrix/fiber breakage stage, the energy of the hits is increased by at least twice compared to the initial. The above observations lead to some preliminary conclusions concerning the values of AE parameters corresponding to different level of damage after accelerated aging.

Amplitude (AMP)-time of plot generally tells the rates of AE hits of different amplitudes during the test. The plots of specimens GA-0d(Type-A with 0day exposure) and GA-300d(Type-A with 300days exposure) consist of two stages. However, it can be observed that the performance characteristics between 0-days specimens (GA-0d) and 300days exposure (GA-300d) were different. The first stage involves low amplitude with an increasing rate of hits. This part is found to be associated with matrix cracking. The second part involves high amplitude hits and is proved to be related to matrix cracking / debonding / delamination / fiber breakage. At the about 82% of the ultimate load, a rapid increase of high amplitude (up to 280 dB) and low amplitude hits can be seen in case of GA-0d.

Meanwhile, an increase of high amplitude (up to 280 dB) and low amplitude hits can be seen at the 30-57% of the ultimate load for GA-300d specimens. High amplitude hits in specimen GA-300d begin even earlier than in specimen GA-0d. This is due to environmental conditioning causing considerable effect on the structural degradation of GFRP reinforcement. When comparing the high-amplitude part of specimens GA-0d and GA-300d plots, it is found that number of hits from GA-300d is higher than GA-0d. This is because the conditioned specimens of GA-300d are damaged by releasing energy at earlier loading stage.

8.5.2 AE activity of four-point bending test (unconditioned / conditioned specimens)

A two-dimensional AE source location technique was carried out to monitor the crack propagation, AE parameters and the location of damage in the specimens. The AE activities and source locations were evaluated in the control beams (unconditioned) and the accelerated aged beams (conditioned) as shown in Figure.8.13. The typical failure patterns for the RC-GFRP (GA2-4) and RC-steel beams under cyclic loading are shown.

The crack patterns and failure modes for both RC-FRP and RC-steel beams were as expected. As mentioned in Chapter-6, the results of crack patterns and damage source locations by AE parameters have a good agreement with the results in Chapter-6.

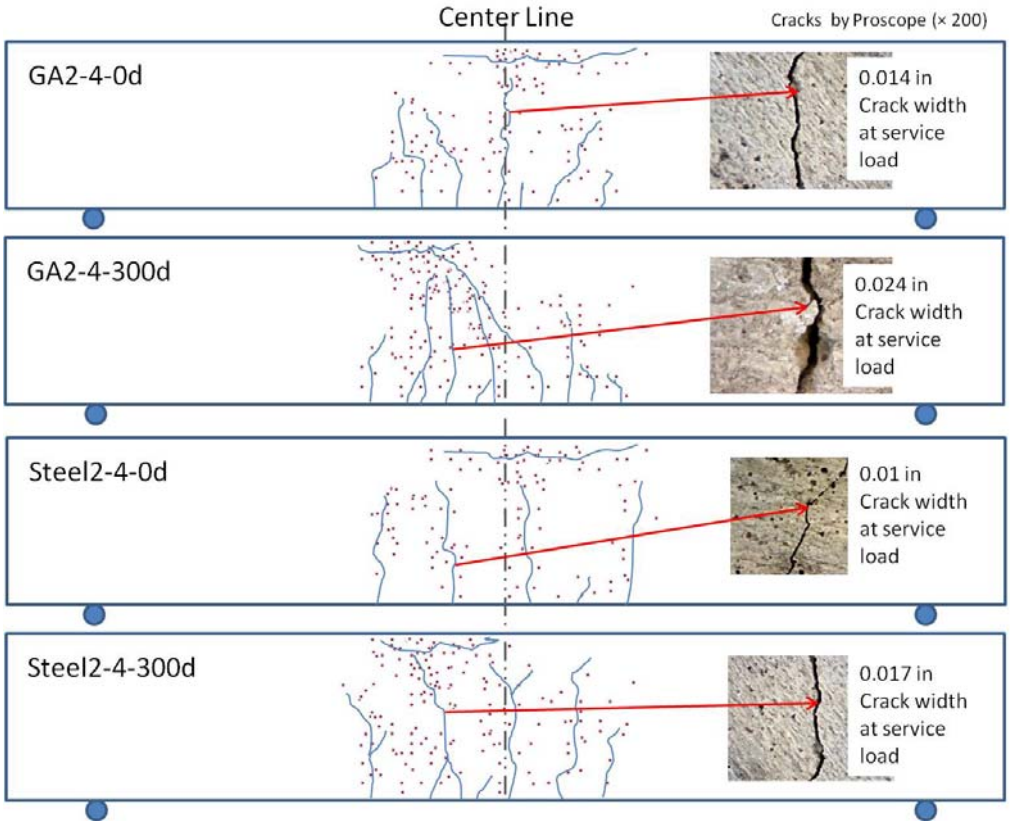

Figure 8.13 AE source location, propagated cracks and crack width at service load (GA2-4 and S2-4)

Specimens of GA2-4 showed balanced failures. On the other hand, specimens of S2-4 showed the failures of concrete crushing after yielding of steel. Also, crack openings were much less for RC-steel specimens, as they failed by crushing of concrete on the compression side under the load. The RC-steel (S2-4) beams were under-reinforced whereas the RC-FRP (GA2-4) sections were markedly over-reinforced. Generally the GA2-4 specimens showed more deflections than their counterparts of S2-4. The number of cracks and distribution of cracks in GA2-4 were much more widespread than the S2-4. For most specimens, cracks started at a small scale early in the loading process, which were then propagated and developed into major cracks. The AE sources were generated at the tension face as well as the compression face where the crack was not detected visually. These AE signals were due to the local stress

concentration of voids in the concrete at the compressive zone [Yun et al., 2010]. After the maximum loads were achieved, the AE sources were measured at the compression zone due to the crushing of the concrete in the flexural compression zone.

A summary of AE test results is shown in Table.8.1. The failure moment and the AE parameters are summarized as the average of the corresponding values for three identical samples of each type of specimen. Three distinct AE parameters are tabulated; cumulative AE hits number, average AE energy and the peak amplitude. The AE activity is not only a function of material properties and extent of damages in a structure but also depends on test duration, and in turn, strength of the specimen. Therefore, it is necessary to normalize the AE parameters [Mirmiran et al. 2000]. The best measure for normalizing the AE parameters is the failure load or strength of the beam. Therefore, as shown in Table 2, the AE parameter for each type of specimen is divided by its corresponding strength to generate a 'Specific AE Activity Ratio'(SAR) [Mirmiran et al. 2000]. The SAR, which is defined as a measure of AE activity of the section (dB/kips), provides a logical tool to eliminate the effect of different sectional strengths in comparing AE signatures for different reinforcing materials. Therefore, the fact that the RC-GFRP beams in these experiments were much stronger than the corresponding RC-steel beams would not affect the comparison of AE trends. In general, RC-FRP beams (GA and GH) emit higher AE activity than their RC-steel counterparts(S). Without exception, the SAR values of both energy and hits are higher for RC-FRP than those of RC-steel beams. Moreover, AE activities were increased as the duration of accelerated aging were increased. For the GA2-4 case, number of AE hits and average released AE energy were increased of about 26% and 28% respectively except peak AE amplitude after aged conditioning(GH2-4: 24% and 30% increase). For the S2-4 case, number of AE hits and average released AE energy were increased of about 60% and 54% respectively except peak AE amplitude. The increase of AE activities of RC-steel beams were greater than of RC-FRP beams regardless of the type of GFRP reinforcement.

Table 8.1 Tested AE parameters

Specimen I.D	Failure load	AE parameters			Specific AE parameter ratio(SAR)*		
	P_u	Total AE Hits	Average AE energy	Peak AE AMP	Total AE Hits	Average AE energy	Peak AE AMP
	kips		dB(*10^3)	dB	(1/kips)	dB(*10^3)/kips	dB/kips
GA2-4-0	48.4	98897	496	100	2045.0	10.3	2.1
GA2-4-300	43.4	111897	573	91	2580.2	13.2	2.1
GA3-5-0	65.0	75036	246	98	1154.8	3.8	1.5
GA3-5-300	59.6	84364	279	90	1415.7	4.7	1.5
GH2-4-0	55.8	90691	349	100	1625.1	6.3	1.8
GH2-4-300	48.7	98769	402	89	2026.2	8.2	1.8
GH3-5-0	76.7	70723	227	97	922.2	3.0	1.3
GH3-5-300	64.7	83684	268	89	1293.4	4.1	1.4
S2-4-0	37.9	51779	309	98	1367.0	8.2	2.6
S2-4-300	30.1	65888	382	94	2188.4	12.7	3.1
S3-5-0	57.0	30906	209	95	542.5	3.7	1.7
S3-5-300	51.6	38612	251	91	749.0	4.9	1.8

*: Specific AE parameter ratio(SAR) : Mirmiran, Amir and Philip, Salam (2000)

This phenomenon may be attributed to several factors such as bond between FRP re-bars and concrete, low stiffness of FRP that results in additional deflection and cracks of the beam and also the AE activity within the FRP composite bars themselves. No attempt was made, however, to distinguish the contributions from each of these factors. Further research in this area may be warranted.

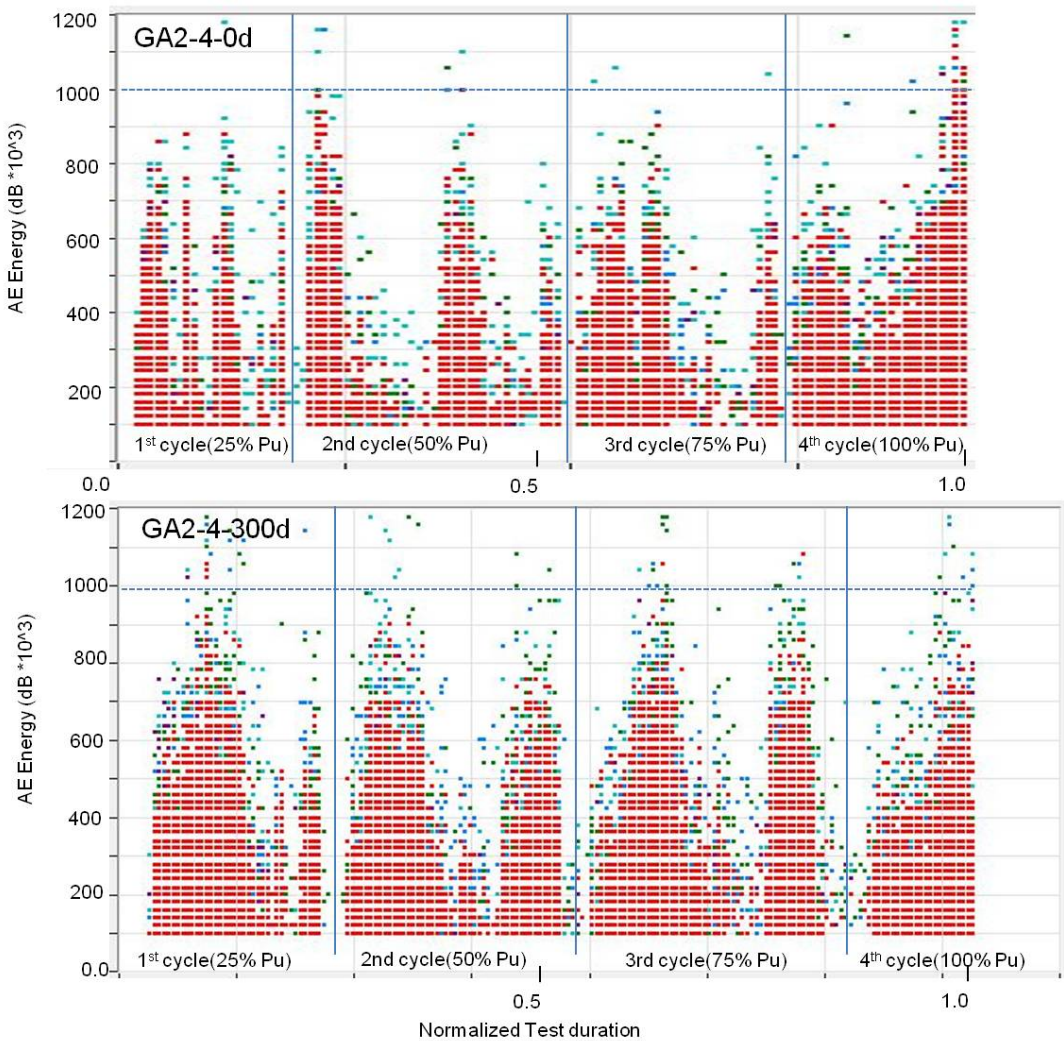

Figure 8.14 AE Energy and normalized test time plot for GA2-4 beams

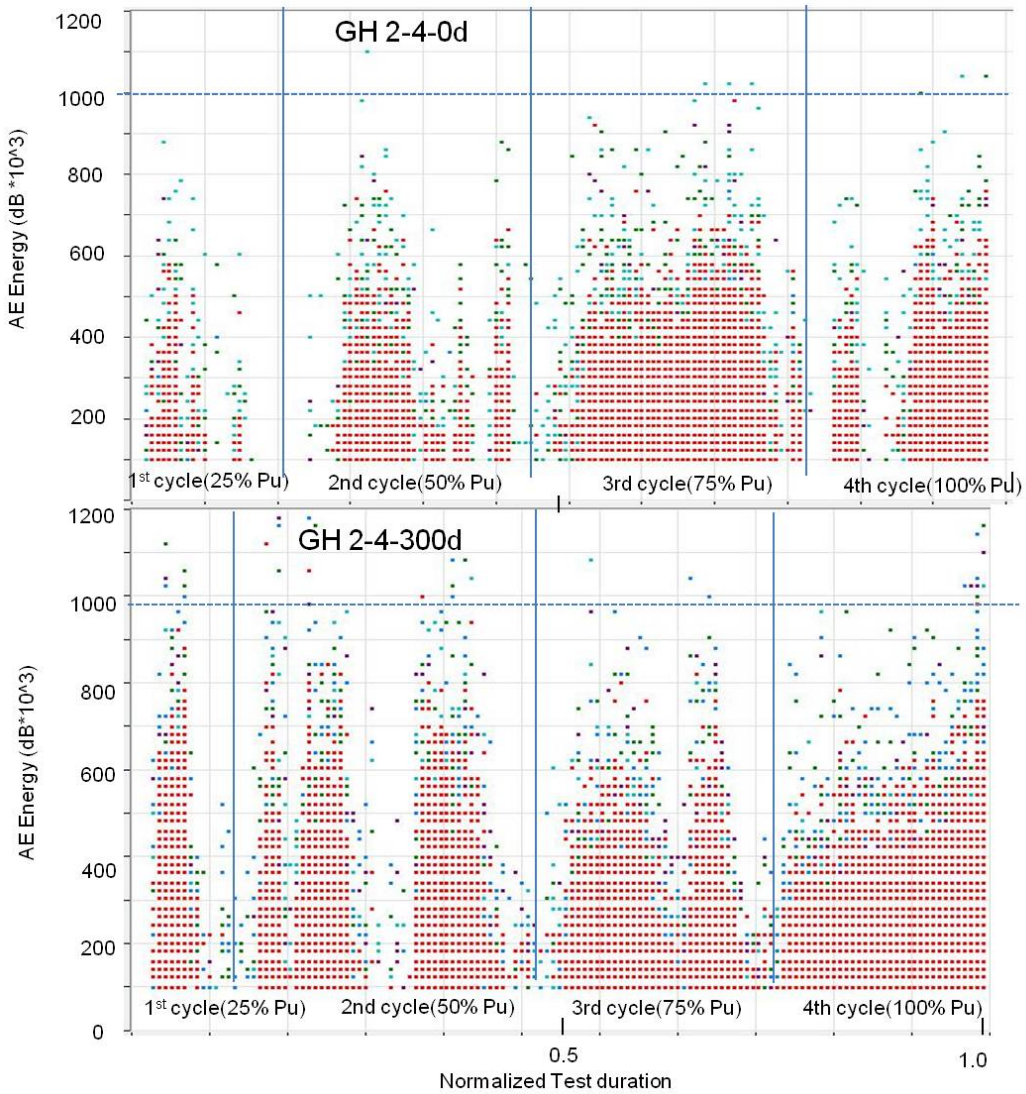

Figure 8.15 AE Energy and normalized test time plot for GH2-4 beams

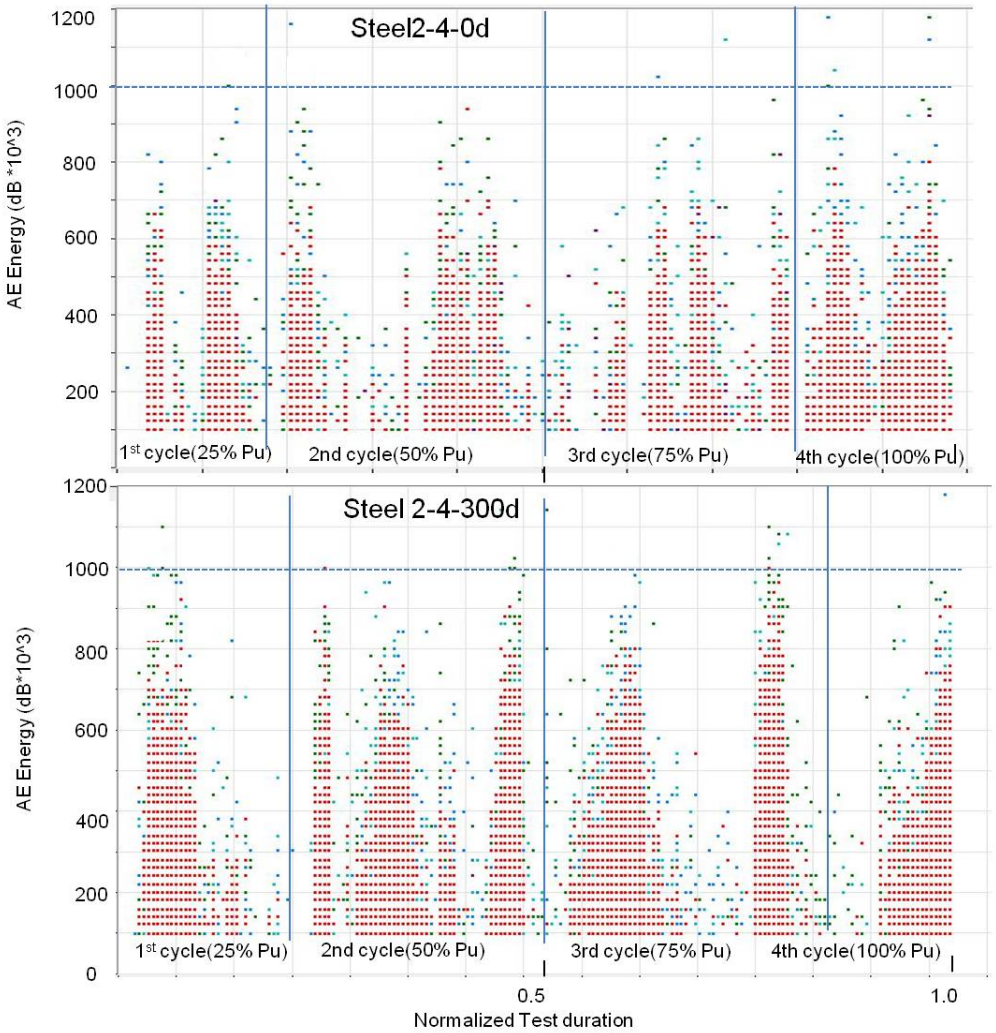

Figure 8.16 AE Energy and normalized test time plot for S2-4 beams

In addition to the AE parameters discussed above, the time history of AE activity is important index because it establishes the correlation between the load and the AE response. The same horizontal scale is used for two diagrams in each figure so as to simplify comparison between the AE signatures for cyclic loading stage in different types of specimens. That is, normalized test durations were used between 0 and 1 to show the entire test for comparisons. Time distributions of the loads are comparable to the load-deflection plots and the AE response

can be directly correlated to the extent of damages in the specimens since the load tests were displacement-controlled.

Figure.8.13 through 8.15 indicates the typical characteristics of the relationship between the released AE energy and normalized test duration of the specimen with and without accelerated aging. The released energy levels shown in these figures illustrate an interesting characteristic of the AE properties of RC beams reinforced with GFRP and steel rods. It can be seen from the figures that higher energy levels occur near the failure load or within the last loading cycle (4th cycle). Considerable amount of AE activity was recorded during the unloading process though at lower energy levels and specially RC-FRP specimens. It was observed that the RC-steel beams demonstrated lower levels of released energy.

The AE activity was found sensitive to duration of accelerated aging, type of reinforcement and reinforcement ratio. AE hits increase significantly as aged duration was increased for all cases. Additionally, the changes in released AE energy of RC-steel beams was higher after 300days of accelerated aging than ones of RC-GFRP beams although the total amount of released AE energy of RC-steel beams were less than ones of RC-GFRP beams. Higher reinforcement not only allows for lower number of AE hits and AE energy regardless of duration of exposure to accelerated aging but also leads to reduce the change of AE activities as the aged duration of specimens increased. Especially, at first cycle of loading, numerous AE sources generated at the bottom (tension face) of the beam were significantly increased, then led to release AE energy more. That is , AE energy release is relatively less for RC-steel beams compared with RC-GFRP beams and is relatively high for aged beams compared with control beams.

Another aspect of this AE study is the Kaiser and felicity effects. The Felicity effect is described as “the presence of detectable acoustic emission at a fixed predetermined sensitivity level at stress levels below those previously applied [ASTM E 1316]. The Felicity effect is a breakdown of the Kaiser effect. That means that the structure generates emission during

reloading before the previous maximum stress is reached. A low Felicity ratio is generally associated with more damage in the structure. The Felicity ratio is an indication of the amount of damage, and is defined as the ratio of the load at which emissions occur to the previous maximum load.

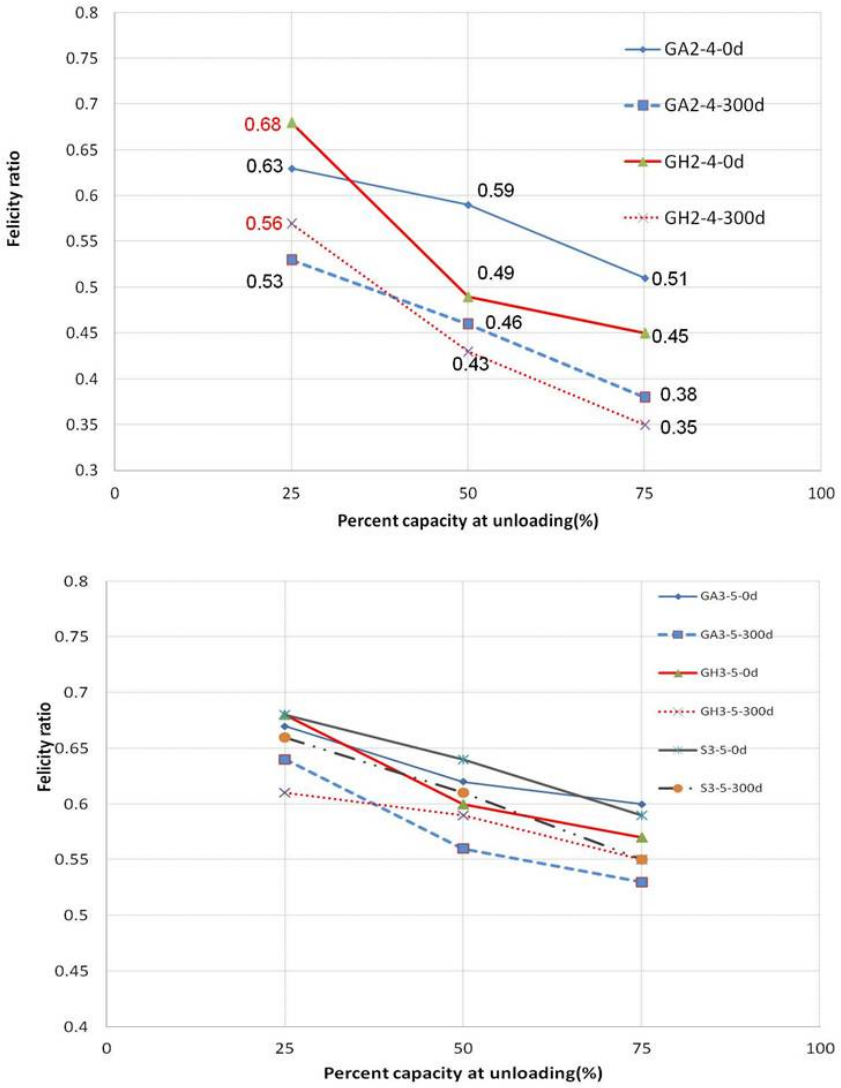

Figure 8.17 Change of felicity ratio by (a) exposure duration (b) reinforcement type and ratio

Figure.8.17 shows the felicity ratios for the RC-FRP and RC-steel beams as a function of percent of ultimate load at the time of unloading in each loading cycle. The points represent

the actual data from the various samples unloaded at different loading cycles. The first, second, and third loading cycles correspond to 25, 50, and 75% of the full capacity of the specimen, respectively. For 2-#4 (3-#5) specimens, the felicity ratios in these tests ranged between 0.35 and 0.69 (between 0.54 and 0.67) respectively. Also shown in the figure, the felicity ratios decreased as the aged duration increased. The average reductions of the felicity ratio for GA2-4 and GH2-4 were about 22 and 26% respectively after 300days of accelerated aging. In case of S2-4, the felicity ratio was increased of 10% after 300days. The average reductions of the felicity ratio for GA3-5, GH3-5 and S3-5 were about 14,17 and 19% respectively after 300days of accelerated aging.

A low Felicity ratio is generally associated with more damage in the structure. This result has a good agreement with the fact that degradation of strength/stiffness of specimens allowed more cracks, then led to damage more as the duration of accelerated aging increased. This trend, however, appears to be more pronounced for RC-steel beams when compared with the RC-FRP beams. It can be seen that felicity ratios for RC-steel beams are higher than the corresponding values for RC-GFRP beams with the same reinforcement ratio. This implies that behavior of RC-steel beams is closer to the Kaiser effect than that of RC-FRP beams. These results shows a good agreement the results by Mirmiran et al.(2000)

The relationships between the count and the amplitude beyond 40 dB of the AE elastic waves that are due to the damages of the specimens are shown in Figure.8.17 and 8.18. Figures also include a comparison for the accelerated aging duration of 300days in each reinforcement type and ratio. As can be seen in Figure.8.17, there was a tendency for the slope of counts vs. amplitude plots to increase as the aging duration increases. For the all cases of GA2-4, GH2-4and S2-4, the elastic waves are in the amplitude range 45-100db regardless of the aged duration.

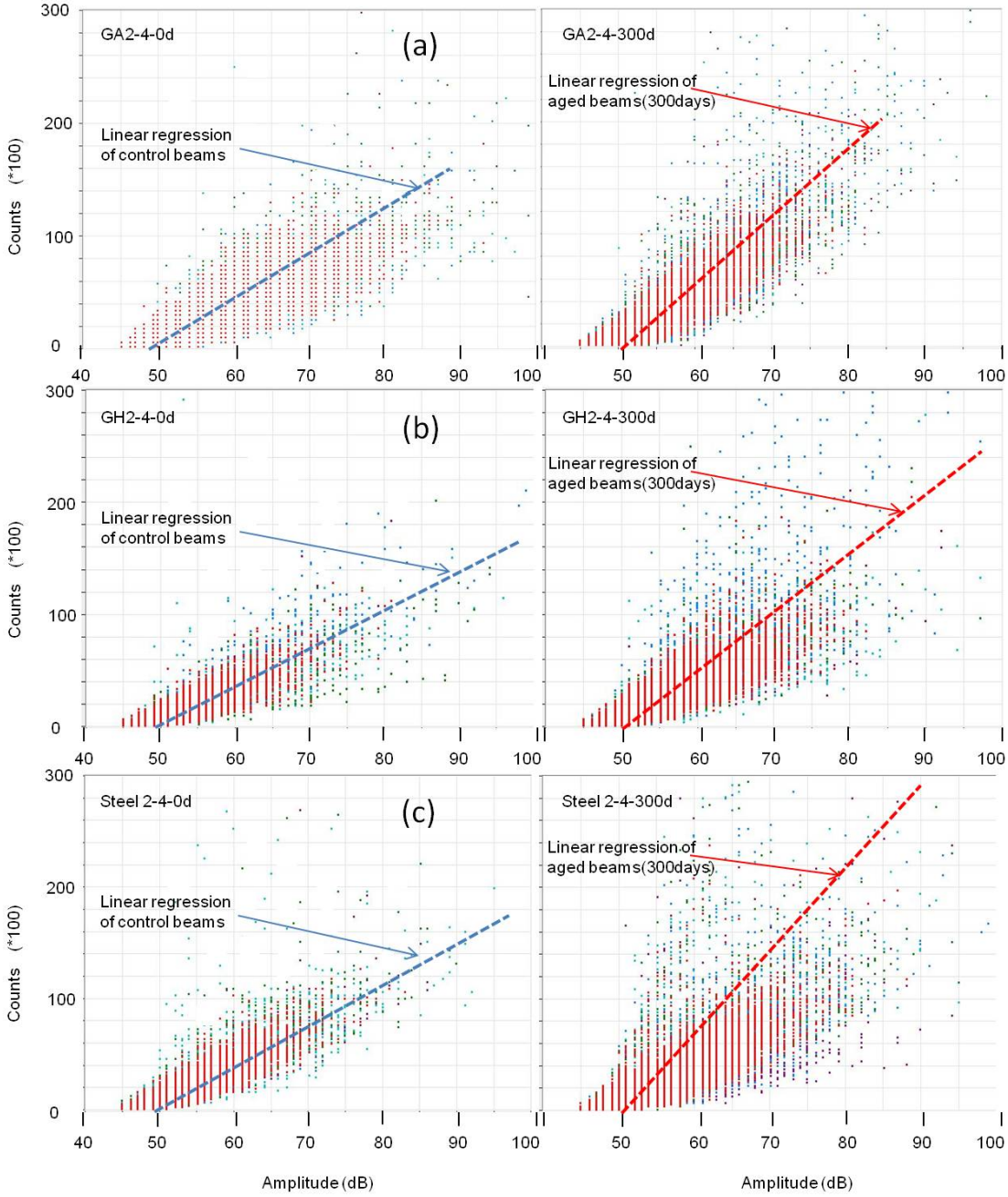

Figure 8.18 Change of the relationship between AE counts and amplitude (2-#4 group)

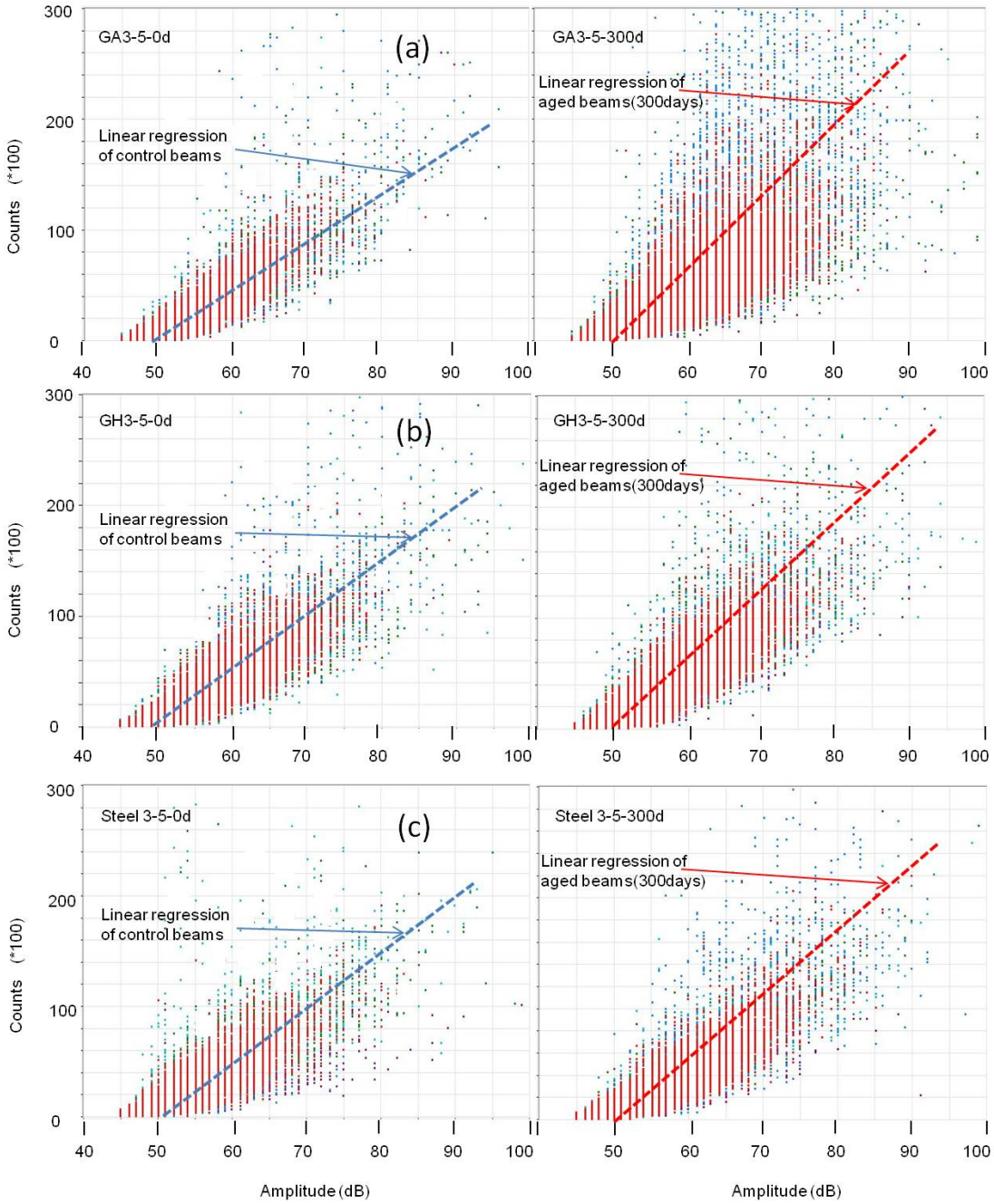

Figure 8.19 Change of the relationship between AE counts and amplitude (3-#5 group)

However, the counts of aged specimens were significantly increased and then led to increase the slope of counts vs. amplitude plots. These results showed that the slope in

amplitude and counts plot increase as the damage level increase. Change of slopes of RC-steel beams (S2-4) by increase of the aged durations was higher than ones of RC-GFRP beams. As shown in Figure.8.18, there were no significant differences between control beams and accelerated aged beams for 300days for higher reinforcement (3-#5 group) when compared with lower reinforcement area (2-#4 group). It can be conclude that lower reinforcement allows to be damaged easily by accelerated aging conditions such as temperature and humidity.

8.6 Summary

Acoustic emission of 24 tensile specimens and 48 RC-FRP and RC-steel beams with temperature, humidity and exposure to saline solution of aging conditions was monitored under cyclic four-point bending test. In AE testing technique, four sensors were used to listen to the wide range of events under various loading and unloading cycles. Each loading and unloading stage was carefully examined for Kaiser and Felicity effects in order to assess the deterioration of the specimens after accelerated aging. On the basis of the long-term AE performances after accelerated aging of beams, signal characteristics were analyzed with regards to exposure duration related to damage level. A summary and relevant conclusions obtained from this chapter are given as follows:

- For tensile tests of control specimens, AE activity starts gradually to increase at the stage-1 until 82% (GA-0d),57%(GH-300d) and 84%(S-300d) of the ultimate load respectively and then rapidly increases at the stage to failure. AE activity due to the degradation of rebar is observed in the stage 2. It can be seen from the figures that higher energy levels occur near the beginning of stage-2.
- For tensile tests of accelerated aged specimens, after 300days of accelerated aging in chamber (equivalent to 24.5 years of outdoor weathering in DFW area), the rapid increases of AE hits were observed at 57%,48% and 82% of ultimate loads for GA-

300d,GH-300d and S-300d respectively. The above observations lead to some preliminary conclusions concerning the values of AE parameters corresponding to different level of damage after accelerated aging.

- Based on the tensile tests, GFRP specimens (GA and GH) have higher amplitudes than their steel counterparts. This may be related to the Matrix/fiber breakage stage.
- Based on the tensile tests, AE performance characteristics between 0-days specimens (GA-0d) and 300days exposure (GA-300d) were different. The first stage involves low amplitude with an increasing rate of hits. This part is found to be associated with matrix cracking. The second part involves high amplitude hits and is proved to be related to matrix cracking / debonding / fiber breakage. It can be concluded that environmental conditioning gave rise to considerable effect on the structural degradation of GFRP reinforcement.
- RC-FRP beams (GA and GH) emit higher AE activity than their RC-steel counterparts (Steel). Without exception, the SAR values of both energy and hits are higher for RC-FRP than those of RC-steel beams.
- The AE activity was found sensitive to duration of accelerated aging, type of reinforcement and reinforcement ratio. AE hits increase significantly as aged duration was increased for all cases. Additionally, the changes in released AE energy of RC-steel beams was higher after 300days of accelerated aging than ones of RC-GFRP beams although the total amount of released AE energy of RC-steel beams were less than ones of RC-GFRP beams. Higher reinforcement not only allows for lower number of AE hits and AE energy regardless of duration of exposure to accelerated aging but also leads to reduce the change of AE activities as the aged duration of specimens increased.

- Felicity ratios decreased as the aged duration increased. The average reductions of the felicity ratio for GA2-4 and GH2-4 were about 22 and 26% respectively after 300days of accelerated aging.
- Degradation of strength/stiffness of specimens allowed more cracks, then led to damage more as the duration of accelerated aging increased. This trend, however, appears to be more pronounced for RC-steel beams when compared with the RC-FRP beams. It can be seen that felicity ratios for RC-steel beams are higher than the corresponding values for RC-GFRP beams with the same reinforcement ratio.
- The slope in amplitude and counts plot increase as the damage level increase. Change of slopes of RC-steel beams (S2-4) by increase of the aged durations was higher than ones of RC-GFRP beams.
- Lower reinforcement allows to be damaged easily by accelerated aging conditions such as temperature and humidity.
- Acoustic emission technique could provide a useful verification of degradation level of concrete structures reinforced with GFRP and steel rods.

CHAPTER 9

SUMMARY AND CONCLUSIONS

9.1 Summary

Change of strength/stiffness properties of GFRP bars and concrete beams reinforced with GFRP and steel bars were investigated in this study for various conditioning schemes with the application of sustained loads. Tensile strength retentions of GFRP bars were tested and considered as the indicator of durability performance. Accelerated aging procedure was conservatively calibrated with the natural weathering data to obtain real time weathering based on the Arrhenius method. Analytical analysis was also conducted to investigate the degradation of strength/stiffness. In addition, not only the change of bond strength between GFRP bars and concrete after aging, but also the durability performance concrete beams with GFRP and steel bars were investigated after exposure to specific accelerated aging conditions(115°F ,RH=80% and 3% saline solution). The evaluation of acoustic emission signatures obtained during the testing of specimens after accelerated aged with GFRP reinforcing bars embedded in concrete was also carried out. Results of different parameters investigated under this study are summarized in different sections and are provided in the following subsections.

9.1.1 Tensile test: Correlation between natural exposure time and accelerated exposure time

In Chapter 4, results of accelerated aging of two different types of GFRP bars and steel rods embedded in real concrete exposed to specific humidity level, saline environment, different temperatures and sustained stress are discussed in order to evaluate the durability performance of FRP and steel bars. The test methods for tensile properties of FRP bar can be observed in ACI 440.1R-06-Section.8 [ACI 440, 2008], ASTM D3916 and ASTM D7205/7205M. Tensile

tests were performed on the plain specimens and specimens that were encased in cement mortar paste and were conditioned in the environmental chamber with sustained loading. Tensile strength was calculated using the nominal area and measured area. The strength and modulus of GFRP and steel bars are reduced by the increase of exposure duration to cement-mortar paste at two different temperatures (79°F and 115°F) Tensile tests showed that GFRP rods (Type-A and Type-B) had poor retentions of tensile properties of 14.82% and 18.09% after 300days-exposure compared that steel rods had 10.65% of reduction after same exposure duration. However, after 200days of environmental aging, the rate of degradation of steel rods are six times greater than the one of Type-A GFRP rebars in terms of strength and 15% greater than the one of Type-B GFRP rebars. It can be translated that chamber weathering of 300 days in real concrete corresponds to natural weathering of 8940 days, i.e., about 24.5 years at North Texas, based on the Arrhenius method.

$$\frac{N}{C} = 0.0876 \cdot e^{(0.0508 \cdot T)}$$

Where, N is day(s) in natural exposure, C is day(s) in chamber conditioning and T is temperature in °F.

9.1.2 Change of bond strength

In Chapter 5, the change of bond strengths of GFRP bars with different types of the surface under harsh environment as accelerated aging was evaluated. Type-A(Aslan-100) bar is an E-Glass bar(vinyl-ester matrix), helically wrapped and sand coated partially for enhanced bonding characteristics while Type-B(VROD-HM) bar has vinyl-ester matrix and sand coated fully for enhanced bonding characteristics. Pullout test specimens were 12in (300mm) concrete cylinders with a single GFRP bar embedded vertically along the specimen's central axis. The bar's bonded length was five times bar diameter (2 in). Based on these experimental results, the following conclusions can be made. The effects of accelerated aging on the GFRP bars

were not critical in terms of bond strength. The bond failure mode is dependent on the surface profile of each bar which is usually added to enhance bond performance.

9.1.3 Long-term performance of concrete beams with GFRP and steel bars

In Chapter 6, the results and discussion of flexural experiments concerning concrete beams reinforced with glass-FRP (GFRP) and steel bars after accelerated environmental aging were represented. Accelerated weathering in North-Texas region (DFW area) is considered with average highest temperature of 115°F and average relative humidity of 80% after immersing into 3% saline solution. Dimensions of seventy-two specimens, 8in×12in×83in (200mm×300mm×1800mm: Width×Depth×Length), will be fabricated for four point flexural beam tests. For tensile reinforcement, the longitudinal reinforcement consisted of two-0.5 in (13mm: #4) or three- 0.675 in (16mm: #5) diameters for each specimen. The inclined transverse reinforcement consisted of 0.375 in (10mm: #3) diameter stirrups of steel with a yield strength of 60ksi (410MPa) spaced 5 and 7in from the end of the beam based on the ACI318-11. Sec.11.4. Both ultimate and serviceability limit states are studied by load-deflection, cracking behavior, modes of failure and ultimate load between unexposed and exposed specimens in accelerated aging conditioning. Concluding remarks are summarized as follows. (a)environmental conditioning had a considerable effect on the structural degradation of GFRP and steel reinforcement. (b)the crack spacing also decreased rapidly with the increasing load and exposure duration. (c)numbers of cracks were increased (i.e. decreasing of crack spacing) as the durations of accelerated aging were increased. (d) it can be observed that the rate of strength degradation of Type-B GFRP beams (GH: VROD-HM) is greater than one of Type-A GFRP beams (GA : ASLAN-100) and (e) the higher tension reinforcement stiffness causes higher nonlinearity in the beam compression zone leading to overestimate I_e.

9.1.4 Change of ductility indices

In Chapter 7, ductility/deformability indices for concrete beams reinforced with GFRP and steel bars before/after accelerated aging were evaluated and the proposed newly defined weighted slope was introduced. Energy based approaches, moment and deformation based approaches and deflection based approach were discussed for the evaluation of deformability indices. Relevant conclusions obtained from this chapter are (a) higher reinforcement allows for lower curvatures and deflections regardless of duration of exposure to accelerated aging, then leads to attain higher deformability; (b) the deformability factors of RC-GFRP showed a tendency to be decreased after accelerated aging while DFs of RC-steel increased after accelerated aging ; (c) no general trend can be identified except Jaeger Index related to the variation of accelerated aged duration ; (d) there is no general agreement on how much deformability is enough with respect to the available deformability indices.

9.1.5 Acoustic emission performance of GFRP bars/concrete beams with GFRP and steel bars

In Chapter 8, a non-destructive acoustic emission technique was described to assess long-term performance of concrete beams (reinforced with GFRP and steel bars) subjected to temperature, humidity and exposure to saline solution of aging conditions. Both the experimental testing and signal-processing procedures were reported in detail. Various parameters were extracted from the AE received signals, and results clearly indicated that changes in these parameters due to aging over time can be found. Based on the tensile tests, GFRP specimens (GA and GH) have higher amplitudes than their steel counterparts. This may be related to the Matrix/fiber breakage stage. AE performance characteristics between 0-days specimens (GA-0d) and 300days exposure (GA-300d) were different. It can be concluded that environmental conditioning gave rise to considerable effect on the structural degradation of GFRP reinforcement. The AE activity was found sensitive to duration of accelerated aging, type of reinforcement and reinforcement ratio.

9.2 Conclusions

The following major conclusions were drawn from this study:

- The strength and modulus of elasticity of GFRP and steel bars were reduced by the increase of exposure duration to cement-mortar paste at two different temperatures (79°F and 115°F).
- Tensile tests showed that GFRP rods (Type-A and Type-B) had reduction in tensile properties of 14.82% and 18.09% after 300days-exposure compared to that of steel rods which had 10.65% reduction after same exposure duration. However, after 200days of environmental aging, the rate of degradation of steel rods are six times greater than that of Type-A GFRP rebars in terms of strength and 15% greater than the one of Type-B GFRP rebars. That means, sufficient degree of reinforcement corrosion was not developed until 300days in environmental chamber.
- Correlation-charts developed for the stressed GFRP bars show that one day of the chamber exposure at 115°F(46°C) simulates 29.8days of life in an outdoor condition with an annual average temperature of 69.4°F (20.8°C). Therefore, it can be determined that chamber weathering of 300 days of concrete specimens corresponds to natural weathering of 9052 days, i.e., about 24.8 years at North Texas.
- The effects of accelerated aging on the GFRP bars did not appear to be critical in terms of bond strength at failure load.
- The bond failure mode is dependent on the surface profile of each bar which is usually added to enhance bond performance. Type-B GFRP rebar (sand-coated surface) specimens showed higher bond strength of about 8.1% compared with Type-A bars (wrapped surface).
- Environmental conditioning had a considerable effect on the structural degradation of concrete beams reinforced with GFRP and steel rods

- It can be observed that the rate of strength degradation of Type-B GFRP beams (GH: VROD-HM) is greater than one of Type-A GFRP beams (GA : ASLAN-100) compared RC-Type-A with RC-Type-B.
- If an environmental strength reduction factor of 0.7 were used for flexure of a member failing in compression, the ACI-440 provision is still conservative up to 300 days of accelerated aging with the equivalent 25.4 years of natural exposure.
- Results show that that Bischoff (2005) gives the smallest average error in all cases for long-term performances of accelerated aged specimens, while the expression proposed by Toutanji and Saafi (2000) does not show good predictions in any cases of the specimens by underestimates deflection considerably for RC-GFRP beams.
- The change of deformability in RC-steel specimens is greater than the one in RC-GFRP specimens.
- No general trend can be identified except Jaeger Index related to the variation of accelerated aged duration.
- There is still no general agreement on how much deformability is enough with respect to the available deformability indices.
- The AE activity was found sensitive to duration of accelerated aging, type of reinforcement and reinforcement ratio. AE hits increase significantly as aged duration was increased for all cases. Additionally, the changes in released AE energy of RC-steel beams was higher after 300days of accelerated aging than ones of RC-GFRP beams although the total amount of released AE energy of RC-steel beams were less than ones of RC-GFRP beams. Higher reinforcement not only allows for lower number of AE hits and AE energy regardless of duration of exposure to accelerated aging but also leads to reduce the change of AE activities as the aged duration of specimens increased.

- Acoustic emission technique could provide a useful verification of degradation level of concrete structures reinforced with GFRP and steel rods.

9.3 Recommendations for future works

The following areas of investigations are recommended for future research based on findings from this study.

- Sustained load factor (only 25% used)
- Longer duration (300days in the chamber B is equivalent to 24.5 years in North Texas)
- Flexural bond tests
- The behavior of a hybrid GFRP-steel reinforced beam

REFERENCES

Abbasi, A., and Hogg, PJ., “Temperature and environmental effects on glass fibre rebar: modulus, strength and interfacial bond strength with concrete”, Composites Part B: Engineering, v36, 2005,pp 394–404

Abdelrahman, A., Rizkalla, SH., and Tadros, G., ‘‘Deformability of flexural concrete members prestressed with FRP’’, Non-metallic (FRP) reinforcement for concrete structures, Proc., 3rd Int. symposium, Japan Concrete Institute, 1997, v2, pp.767–774.

Aggelis, D., “Classification of cracking mode in concrete by acoustic emission parameters”, Mechanics Research Communications, v 38,2011,pp.153–157.

Almusallam, A., ”Effect of degree of corrosion on the properties of reinforcing steel bars”, Journal of construction and building materials,2001,v15, pp361-368.

Almusallam, TH., “Load–deflection behavior of RC beams strengthened with GFRP sheets subjected to different environmental conditions”, Cement and Concrete Composites, v28, 2006, pp. 879–889.

ACI 318-11,“Building Code requirements for structural concrete and commentary”, ACI Committee 318, American Concrete Institute. Farmington Hills, 2011.

ACI 440.1R-06. “Guide for the design and construction of concrete reinforced with FRP bars”,Farmington Hills (MI), American Concrete Institute, 2006.

ACI 440.3R-04,”Guide test methods for fiber reinforced polymers for reinforcing or strengthening concrete structures”,2004.

ACI 440.R-07, “Report on FRP Reinforcement for concrete structures”,2007.

Aiello, MA., and Ombres, L., “Structural performances of concrete beams with hybrid (fiber-reinforced polymer–steel) reinforcements”, ASCE Journal of Composite Construction, 2002, v6(2), pp.133–140.

Aindow, AJ., Oakley, DR., and Proctor, BA., “ Comparison of weathering behavior of GRC with predictions made from accelerated aging tests”, Cement and concrete research, v14,1984, pp. 271-274

Alsayed, S., and Al-Hozaimy, A., “Ductility of concrete beams reinforced with FRP bars and steel fibers”, Journal of Composite Material, 1999, v33(19),pp.1792–806.

Alsayed, S., Al-Salloum, A., and Almusallam,TH.,” Performance of glass fiber reinforced plastic bars as a reinforcing material for concrete structures”, Composites B, 2000,v31,pp.555–567.

ASCE: Report card for America’s infrastructure, 2009 , pp. 75-76

Ashour, A.F.," Flexural and shear capacities of concrete beams reinforced with GFRP bars", Construction of Building Material, 2006,v20,pp.1005–15.

ASTM, ASTM E 1316, "Standard Terminology for Nondestructive Examinations," Annual Book of ASTM Standards, Nondestructive Testing, v 03, Philadelphia, American Society for Testing and Materials.

Au, F., and Du, JS., "Deformability of concrete beams with unbounded FRP tendons", Engineering structures, 2008,v30,pp.3764-3770.

Ativitavas, N., "Acoustic Emission Signature Analysis of Failure Mechanisms in Fiber Reinforced Plastic Structures," PhD Dissertation, the University of Texas at Austin, Austin, Texas, 2002

Bakis,CE., Boothby, TE., and Jia, J., " Bond durability of glass FRP bars embedded in concrete beams", Journal of composites for construction, ASCE, 2007,v11,pp.269-278.

Bakis, CE., Nanni, A., and Boothby, TE, "Analysis of bonding mechanisms of smooth and lugged FRP rods embedded in concrete", Composites Science and Technology, v58, 1998, pp 1307–1319

Bakis, CE., Nanni, A.,and Terosky, JA.,"Self-monitoring, pseudo-ductility, hybrid FRP reinforcement rods for concrete applications", Composite science and technology, v61, 2001, pp.815-823.

Bank, LC., Gentry, TR., and Barkatt, A., "Accelerated test methods to determine the long-term behavior of FRP composite structures-environmental effects", Journal of reinforced plastics and composites, v14 , 1995 ,pp. 559-587

Barnes, CA., Ramirez, G., "Acoustic Emission of Carbon Fiber Composite Offshore Drilling Risers," The Sixth International Symposium on Acoustic Emission of Composite Materials,1998

Barris, C., Torres, LI.,Turon, A., Baena, M., and Catalan, A.,"An experimental study of the flexural behavior of GFRP RC beams and comparison with prediction models", Composite structures,2009, v91,pp.286-295.

Belarbi, A., and Wang, H., "Bond splitting behavior of FRP reinforcing bars embedded in fiber reinforced concrete", In: Proceedings for the 84th transportation research board annual meeting, Washington DC, 2005.

Benmokrane, B., Chaallal, O., and Masmoudi, R.," Flexural response of concrete beams reinforced with FRP reinforcing bars", ACI Structure Journal, 1996,v91(2),pp.46–55.

Benmokrane, B., Rahman,H., Ton-That, M-T., and Robert, J-F.,"Improvement of the durability of FRP reinforced for concrete structures", 1st International Conference on Durability of Fiber Reinforced Polymer For Construction (CDCC'98), Sherbrooke, Canada, 1998,pp571–584.

Benmokrane, B., Chaallal, O.,and Masmoudi, R., "Flexural response of concrete beams reinforced with FRP reinforcing bars", ACI structural journal , v93(1), 1996 ,pp. 46-55.

Bhise,V., "Strength degradation of GFRP bars", Master thesis, Virginia Polytechnic and State University, 2002

Bischoff, PH., “Re-evaluation of deflection prediction for concrete beams reinforced with steel and fiber-reinforced polymer bars” Journal of Structure Engineering, 2005,v131(5),pp752–767.

Bischoff, PH., Gross,S., and Ospina, CE., “The story behind proposed changes to ACI 440 deflection requirements for FRP reinforced concrete”, ACI SP-264-4,2008, pp53-76.

Branson, D.E., “Instantaneous and Time-Dependent Deflections of Simple and Continuous Reinforced Concrete Beams,” HPR Report No. 7, Part 1, Alabama Highway Department, Bureau of Public Roads, AL,1965

Bray, DE., and Stanley, RK., “Nondestructive Evaluation: A Tool in Design, Manufacturing, and Service, Revised Edition”, CRC Press, New York. 1997

Carey, SA., “Acoustic emission and acousto-ultrasonic signature analysis of failure mechanisms in carbon fiber reinforced polymer materials”, Ph.D. dissertation, University of South Carolina, 2008.

Ceroni, F., Cosenza, E.,Gaetano, M., and Pecce, M., “Durability issues of FRP rebars in reinforced concrete members”, Cement and Concrete Composites ,v 28, November 2006, pp 857–868.

Chaallal, O., Benmokrane, B., “Pullout and bond of glass–fiber rods embedded in concrete and cement grout”, Material Structures, v26(3),1993, pp167–175.

Chen, HL., Sami, Z., and GangaRao, HV.,” Acoustic emission measurements of FRP bars and FRP reinforced concrete elements”, Proceedings of the 1992 ASME Winter Annual Meeting, Anaheim, CA, ASME, November 1992,pp. 93-100.

Chen, Y., “Accelerated ageing tests and long-term prediction models for durability of FRP bars in concrete”, ”, Ph.D dissertation, West Virginia University, 2007.

CSA-S6-00, Canadian highway bridge design code (CHBDC). Section 16, Fiber reinforced structures. ,b Canadian Standards Association, 2000,pp. 177.

Dai, ST., Labuz, JF., “Damage and failure analysis of brittle materials by acoustic emission” ,Journal of Mater Civil Eng, 1997,v 9(4),2005.

Daniali, S.,“Development Length for Fiber-Reinforced Plastic Bars,” Proceedings of Advanced Composite Materials in Bridges and Structures, Sherbrooke, QC, Canada, 1992, pp.179-188.

Davalos, JF., Chen, Y., Ray, I., “Effect of FRP bar degradation on interface bond with high strength concrete”, Cement and Concrete Composite, 2008,v30,pp.722–730.

Dejke V., “Durability of fibre reinforced polymers (FRP) as reinforcements in concrete structures - An update of knowledge and an overview of current research activities”, Report P-98:18, Chalmers University of Technology, Department of Building Materials,1998.

Dejke, V., and Tepfers, R., “Durability and service life prediction of GFRP for concrete reinforcement”, Proceedings of 4th International Conference on Fibre-Reinforced Plastics for Reinforced Concrete Structures FRPRCS-5, v1, University of Cambridge, 2001,pp.515–520.

Durability of Concrete Structures, Canadian Civil Engineer, May 2004.

El-Salakawy, E., Benmokrane B., and Desgagne´ G. “FRP Composites Bars for the Concrete Deck Slab of Wotton Bridge” Canadian Journal of Civil Engineering, 2003,v 30(5),pp 861–870.

Fowler, TJ, “Acoustic Emission of Fiber Reinforced Plastics”, Journal of the Technical Councils, ASCE, Vol. 105, No. TC2, December, 1979, pp. 281-289.

Fowler, TJ., “ Acoustic emission testing of process industry vessel and piping”, 5th international symposium on loss prevention and safety promotion in the process industries , 1986

Gao, D., Benmokrane, B., and Masmoudi, R., “A Calculating Method of Flexural Properties of FRP-Reinforced Concrete Beam: Part 1: Crack Width and Deflection,” Technical Report, Department of Civil Engineering, University of Sherbrooke, QC, Canada,1998.

Gerritse, A., “Durability criteria for non-metallic tendons in an alkaline environment”, Proceedings of 1st International Conference on Advanced Composite Materials in Bridges and Structures, ACMBS-I, Sherbrooke, Canada, 1992, pp.129–137.

Giernacky, RG., Bakis, CE., and Mostoller, JD., “Evaluation of concrete beams reinforced with internal GFRP bars-a long term durability study”, CDCC’02 ,pp. 39-50

Grace, NF., Soliman, AK., Abdel-Sayed, G.,and Saleh, KR., “Behaviour and ductility of simple and continuous FRP reinforced beams”, J. Composite Construction, 1998,v2(4),pp.186-194.

Grosse, CU., Ohtsu, M.(Eds.), “ Acoustic emission testing : Basics for research-Application in civil engineering”, Springer, 2008

Ha, TH.,Muralidharan,S., and Bae, JH., “Accelerated short-term techniques to evaluate the corrosion performance of steel in fly ash blended concrete”, Journal of Building and Environment, v42, 2007,pp.78–85

Hadi, M., “Bond of High Strength Concrete with High Strength Reinforcing Steel”,The Open Civil Engineering Journal, 2008, v2, pp. 143-147.

Harvey, DW., “Acoustic Emission in an Aerospace Composite”, Master’s Thesis, the University of Texas at Austin, Austin, Texas,2001

Helbling, CS., Karbhari, VM.,” Environmental durability of E-glass composites under the combined effect of moisture,temperature and stress”, CDCC’02, 2002 ,pp. 247-258

He, Z., Ou, J., and Wang, B., “ The trilinear moment versus curvature relationship of concrete beams reinforced with fiber reinforced polymer bars”, Composite structures, 2007,v77,pp.30-35.

Hollaway, LC.,” A review of the present and future utilization of FRP composites in the civil infrastructure with reference to their important in-service properties”, Construction and building materials, 2010,pp2.

Huang, J., “Durability design of GFRP bar reinforced concrete members: A new approach”, Ph.D. dissertation, Syracuse University, 2010

Intelligent Sensing For Innovative Structures, ISIS-M03-01. Reinforcing concrete structures with fibre reinforced polymers. The Canadian Network of Centres of Excellence, ISIS Canada, University of Manitoba, Winnipeg, Manitoba, Canada, 2007, 81p.

ISO 12716, “Nondestructive testing-acoustic emission inspection: Vocabulary”, ISO, 2001.

Jaeger, GL., Tadros, G.,and Mufti, AA.,” Balanced section, ductility, and deformability in concrete with FRP reinforcement”, Research report no. 2, Industry Center for Computer-Aided Engineering, Technical University of Nova Scotia,1995, pp. 29.

Jaeger, GL., Tadros, G.,and Mufti, AA., ”The concept of the overall performance factor in rectangular-section reinforced concrete beams”, In: Proc of 3rd int. symp. on non-metallic (FRP) reinforcement for concrete structures, v 2, Sapporo, Japan, 1997, pp. 551–558.

JC MS-III B5706. “Monitoring method for active cracks in concrete by acoustic emission”, Japan- Federation of Construction Materials Industries, 2003.

Johnson, D., “Investigation of glass fiber reinforced polymer reinforcing bars as internal reinforcement for concrete structures”, Master thesis, University of Toronto, 2009

Kakizawa, T., Ohno, S., and Yonezawa, T., “Flexural behavior and energy absorption of carbon FRP-reinforced concrete beams.’’ ,Rep. No. SP138-35, American Concrete Institute, 1993,pp 585–598.

Kamal, M., Safaan, M.,and Al-Gazzar, M., “Ductility of concrete beams reinforced with hybrid FRP rebars” HBRC J, Hous & Build Res Cent 2006,V2(3),pp.1–12.

Karbhari, VM., Zhao, L., Murphy, K., and Kabalnova, L., “Environmental durability of glass reinforced composites-short term effects”, 1st International Conference on Durability of Fiber Reinforced Polymer for Construction (CDCC’98), Sherbrooke, Canada, 1998,pp. 513–524.

Karbhari, VM.,” Durability of FRP composites for civil infrastructure myth, mystery or reality : Advances in structural engineering”,v 6(3), 2003 , pp.243-256.

Katsuki, F., and Uomoto, T.,” Prediction of Deterioration of FRP Rods due to Alkali Attack”, Non-Metallic (FRP) Reinforcement for Concrete Structures: Proceedings of the Second International RILEM Symposium (FRPRCS-2), Ghent, 23-25, 1995, Ed. L. ,pp.82-89.

Larralde, J., Silva-Rodrigues, R., Burdette, J., and Harris, B., “Bond Tests of Fiberglass-Reinforced Plastic Bars in Concrete,” Journal of Testing and Evaluation, 1994,V. 22, No. 4,pp.351-359.

Lee, JK., and Lee, JH., “Nondestructive evaluation on damage of carbon fiber sheet reinforced concrete” ,Composite Structure ,2002,v58,pp139–147.

Leslie, JC., "Properties and Performance Requirements", in Advanced Thermoset Composites Industrial and Commercial Applications, Margolis, J. M. (Ed.), Van Nostrand Reinhold company, New York, 1986, p. 74-107.

Lesko,J., and Cousin,T., “ Strongwell-Extren DWB design guide “, Virginia Polytechnic Institute and State University, 2003.pp.8.

Litherland, KL., Oakley, DR., and Proctor, BA., “The use of accelerated ageing procedures to predict the long term strength of GRC composites”, Cement and Concrete Research, 1981,v 11,pp. 455–466.

Mallick ,PK., “Fiber-reinforced composites, materials, manufacturing, and design”, Ph.D. Thesis, University of Michigan- Dearborn, Dearborn, Michigan, 1988, 469p.

Mallick, PK.,”Fiber Reinforced Composite Materials, Manufacturing and Design”, Marcel Dekker Inc., NY, 1993.

Hamidah, HM., Gowripalan, N. and Fadhil, NM. “Absorption of Aramid Prestressing Rods in Aggressive Solutions”, Journal of Composites for Construction, v 5, 2001, pp. 254-257.

Maslehuddin, M.,and Al-Amoudi, OSB., ”Carbonation and corrosion of rebars in salt contaminated OPC/PFA concretes”, Cement and Concrete Research, v21, 1991, pp. 38–50

Masmoudi,R., Masmoudi, A., Ouezdou, MB., and Daoud, A ,”Long-term bond performance of GFRP bars in concrete under temperature ranging from 20 °C to 80 °C ”, Construction and Building Materials ,v 25, 2011, pp 486–493.

Masmoudi, R., Zaidi, A., and Girard, P., “Transverse thermal expansion of FRP bars embedded in concrete” ACSE Journal of Composite Construction, v9,2005,pp.377–387.

Metwally, IM., ” Evaluation of existing model for predicting of flexural behavior of GFRP-reinforced concrete members” HBRC J, Hous Build Res Cent 2009,v5(1),pp. 46–58.

Mirmiran, A., Shahawy, M., and El-Echary, H.,” Characteristics of acoustic emission from FRP-confined concrete”, Journal of engineering mechanics, ASCE, 1998,v125(8),pp.899-905.

Mirmiran, A., and Philip, S., “Comparison of acoustic emission in steel reinforced and FRP reinforced concrete beams”, Construction and building materials, v14,2000,pp.299-310

Moon, DY., “Bond Behavior of Newly Developed Deformed GFRP Bars”, Ph.D. dissertation, Hanyang University, Korea, 2005

Mota, C., Alminar, S., and Svecova, D.,” Critical review of deflection formulas for FRP-RC members”, Journal of compos Construction, ASCE 2006,v10(3),pp.183–194.

Mufti, A., Onofrei, M., Benmokrane, B., Banthia, N., Boulfiza, M., Newhook, J., Bakht, B., Tadros, G. and Brett, P., “Studies of concrete reinforced with GFRP specimens from field demonstration structures”, In Hamelin P et al. (eds), 3rd International Conference on Composites in Construction, Lyon, France, 2005,pp.11-13

Mufti,A., M., Benmokrane, B., Newhook,J., Tadros, P.,” Durability of GFRP reinforced concrete in field structures”, 7th-FRPRCS,SP-230-77, 2007 ,pp.1361-1377

Mufti,A., M.,and Newhook, J., ”Deformability versus ductility in concrete beams with FRP reinforcement”, Proceedings of Adv. composite materials in bridge and structures,1996, pp 189-199.

Naaman, AE., and Jeong, SM.," Structural ductility of concrete beams prestressed with FRP tendons" In: Proceedings, 2nd international RILEM symposium, FRPRXS-2. Non-metric (FRP) reinforcement for concrete structures.,1995, pp. 379–386.

NDIS 2421, " Recommended practice for in situ monitoring of concrete structures by acoustic emission", JSNDI, Tokyo, 2000.

Nelson, W., "Accelerated testing-statistical models, test plans, and data analysis", John Wiley & Sons, New York, 1990.

Newhook, J., Ghali, A.,and Tadros, G.,"Concrete flexural members reinforced with fiber-reinforced polymer: design for cracking and deformability", Cananian Journal of Civil Eng, 2002,v29,pp.125–134.

Niesse, J., and Ahluwalia, H., "A Practical Guide to Field Inspection of FRP Equipment and Piping," MTI Project 129-99, Materials Technology Institute of the Chemical Process industries, Inc., St. Louis, Missouri, 2001

Nishizaki, I., and Meiarashi, S., "Long-Term Deterioration of GFRP in Water and Moist Environment", Journal of Composites for Construction, ASCE, v6, 2002, pp. 21-27.

Nkurunziza, G., Benmokrane, B., Debaiky, AS., and Masmoudi, R., "Effect of creep and environment on long-term tensile properties of glass FRP reinforcing bars",4th International Conference on Advanced Composite Materials in Bridges and Structures, Calgary, 2004

Nkurunziza, G., Debaiky,A., Cousin,P.,and Benmokrane, B.," Durability of GFRP bars-A critical review of the literature", Structural engineering materials , v7,2005,pp.194-209

Ohno, K.,and Ohtsu, M., "Crack classification in concrete based on acoustic emission", Constr. Build. Mater. ,2010,v24 (12), pp.2339–2346.

Ohtsu, M.,and Tomoda, Y., "Phenomenological model of corrosion process in reinforced concrete identified by acoustic emission", ACI Mater. J.,2004, v105 (2),pp.194–200.

Parish,GC., "CFRP Repair of Concrete Beams Aged By Accelerated Corrosion", Master Thesis, West Virginia University, 2008

Park, R., and Paulay, T., "Reinforced Concrete Structures", John Wiley and Sons, Inc., New York, 1975

PCI Design Handbook, Sixth Edition. U.S.A.: Precast/Prestressed Concrete Institute, 2004.

Pollack, AA, "Acoustic Emission Amplitude Distributions," Dunegan / Endevco Article 7910, International Advances in Nondestructive Testing, Volume 7, 1980.

Pollock, AA., "Acoustic Emission Amplitude Distributions," International Advances in Nondestructive Testing, Vol. 7, 1981, pp.215-239.

Porter, ML., and Barnes, BA., "Accelerated aging degradation of glass fiber composites", Proceedings of 2nd international conference on composite in infrastructure, Tucson, Arizona, 1998. pp.446–495.

Porter, ML., and Barnes, BA., ”Accelerated durability of FRP reinforcement for concrete structures”,1st International Conference on Durability of Fiber Reinforced Polymer for Construction (CDCC’98), Sherbrooke, Canada, 1998,pp191–202.

Pourbaix, M., “A comparative review of electro chemical methods of assessing corrosion and the behaviour in practice of corrodible material”, Corrosion Science, v5, 1965, pp. 677–686

Priestley, MJN., and Seible, F., “Design of seismic retrofit measures for concrete and masonry structures”, Construction and Building Materials, v9, 1995, pp. 365-377.

Prian, L., and Barkatt, A., “Degradation mechanism of fiber reinforced plastic and its implications to prediction of long-term behavior”, Journal of materials science,1999, v34, pp.3977-3989.

Promboon, Y.,“Acoustic Emission Source Location”, Ph.D. Dissertation, University of Texas at Austin, 2000.

Pultrall Inc. ISOROD Composite Reinforcing Rods. Technical Data Sheer, Pultrall Inc. Thetford Mines, PQ, Canada, 2000, 7p.

Rafi, MM., Nadjai, A., Ali, F.,and Talamona, D., ”Aspects of behaviour of CFRP reinforced concrete beams in bending”, Construction of Building Materials, 2008,v22,pp.277–285.

Ramirez, G., Monitoring and Prediction of Damage in a Filament Wound Composite Pipe under Pressure Loading,” PhD Dissertation, the University of Texas at Austin, Austin, Texas,1999

Rasheed, MA., Mansur, MA.,and Paramasivam, P., “Behavior of aramid fiber-reinforced polymer reinforced high strength concrete beams under bending”, J. Composite Construction, ASCE 2005,v9(2),pp.117-127.

Rasheed, MA.,Nayal, R., and Melhem, H., “Response prediction of concrete beams reinforced with FRP bars”, Composite structures”,2004, v65,pp193-204.

Razaqpur, AG., and Isgor, OB., “Rational method for calculating deflection of continuous FRP RC beams”,ACI SP-210-9, pp.191-208.

Robert, M., and Benmokrane, B.,”Effect of aging on bond of GFRP bars embedded in concrete”, Cement and concrete composites, 2010, v32,pp.461-467.

Sagar, RV., and Prasad, BKR., “An experimental study on acoustic emission energy as a quantitative measure of size independent specific fracture energy of concrete beams”, Construction and Building Materials, v 25, 2011, pp. 2349–2357.

Sakai, T., Kanakubo, K., and Yonemaru, K.,” Bond splitting behavior of continuous fiber reinforced concrete members” In: Proceedings, 4th int. symposium on fiber reinforced polymer reinforcement for reinforced concrete structures.,SP-188, ACI, 1999,pp. 1131–1144.

Salakawy, E.,and Benmokrane, B.,” FRP composites bars for the concrete deck slab of Wotton bridge”, Canadian journal of civil engineering, v 30(5),2003,pp. 861-870.

Shield, C., “Comparison of acoustic emission activity in reinforced and pre-stressed concrete beams under bending”, Construction of Building Matererial, 1997, v11-3,pp189-194.

Taniguchi, H., Mutsuyoshi, H., Kita, T.,and Machida, A., “Ductile behavior of beams using FRP as tendons and transverse reinforcement” ,FRP reinforcement for concrete structures. ACI SP-138., American Concrete Institute, 1993,pp. 651–70.

Tannous, FE., and Saadatmanesh, H., “Environmental Effects on the Mechanical Properties of E-glass FRP Rebars”, ACI Materials Journal, ACI, v 95, 1998, pp. 87-100.

Tepfers, R., and Olsson, PA., “Ring Test for Evaluation of Bond Properties of Reinforcing Bars,” International Conference: Bond in Concrete from Research to Practice, 1992, pp. 1-99.

Toutanji, HA., Saafi, M., “Flexural behavior of concrete beams reinforced with glass fiber-reinforced polymer (GFRP) bars”, ACI Structure J., 2000,v97(5),pp.712–719.

Trejo, D., Gardoni,P., and Kim, J.,”Long term performance of GFRP reinforcement “. Technical report (TxDot)-0-6069 , 2009.

Uomoto, T.,” Development of new GFRP with high alkali resistivity”, 4th International Conference on Advanced Composite Materials in Bridges and Structures, Calgary, Alberta, 2004.

Vedalakshmi, R., Rajagopal, K., Palaniswamy, N., “Longterm corrosion performance of rebar embedded in blended cement concrete under macro cell corrosion condition”, Construction and Building Materials, v22, 2008, pp.186–199.

Vijay, PV., “Aging and design of concrete members reinforced with GFRP bars”, Ph.D dissertation, West Virginia University, 1999.

Vijay, PV.,and Ganga Rao, HV., “Bending behavior and deformability of glass fiber-reinforced polymer reinforced concrete members”, ACI Structure Journal, 2001,v98(6),pp. 834–842.

Vijay,PV., and Gangarao, HV., “Accelerated natural weathering of glass fibre reinforced plastic bars”, Proceedings of 4th International Conference on Fibre-Reinforced Plastics for Reinforced Concrete Structures FRPRCS-4, Baltimore, USA, 1–4 November 1999,pp.605–614.

Wang, H.,and Belarbi, A., ”Ductility characteristics of fiber reinforced concrete beams reinforced with FRO rebars”, Construction and building materials, v25, 2011, pp. 2391-2401.

Wang, H.,and Belarbi, A., “Flexural behavior of fiber-reinforced-concrete beams reinforced with FRP rebars”, ACI-SP-230-51, American Concrete Institute, October 1, 2005,pp. 895–914.

Working Party 7, “Bond of Non-metallic Reinforcement, State-of-art Bulletin 10 - Bond of Reinforcement in Concrete”, Task Group of Bond Models, International Federation for structural concrete (fib),2000, pp. 322~324.

Wu, LX.,”Short-Term Effects of Sea Water on E-Glass/Vinylester Composites”,Journal of Applied Polymer Science, v 84, 2002,pp. 2760–2767.

Yun,.HD., Choi, WC., and Seo, SY., “Acoustic emission activities and damage evaluation of reinforced concrete beams strengthened with CFRP sheets” , NDT&E International, v43, 2010, pp. 615–628.

Yost, JR., Gross, SP., and Dinehart, DW., “Effective Moment of Inertia for Glass Fiber-Reinforced Polymer-Reinforced Concrete Beams,” ACI Structural Journal, v100, No. 6, 2003, pp. 732-739.

Ziehl, P.H., “Development of A Damage Based Design Criterion for Fiber Reinforced Vessels,” Dissertation of Doctor of Philosophy, The University of Texas at Austin,2000.

Ziehl, PH., and Fowler, TJ., 2001. “Development of a Damage Based Design Criterion for Fiber Reinforced Vessels”, Residual Stress Measurement and General Nondestructive Evaluation, ASME 2001, V429.

Zou, PXW., “Flexural behavior and deformability of fiber reinforced polymer prestressed concrete beams” ,Journal of Composite Construction. 2003, v, pp.275-284.

BIOGRAPHICAL INFORMATION

Yeonho Park graduated with Bachelor (B.S.) and Master (M.S.) degree in Architectural Engineering from the Kyunghee University in Suwon, Korea in 2004. Right after graduation, he had worked for Kyungjae structural consulting company as a structural engineer for two-years. In August 2006, he came to the Texas A&M University-College station to obtain a Master degree in Civil Engineering Department. In May 2008, he obtained the Master of Engineering degree at Texas A&M University. In August 2008, he entered the graduate program at University of Texas at Arlington (UTA).